# Spatial Dependence Clusters in the Estimation of Forest Structural Parameters

by

**Michael Albert Wulder**

A thesis
presented to the University of Waterloo
in fulfillment of the
thesis requirement for the degree of
Doctor of Philosophy
in
Geography

Waterloo, Ontario, Canada, 1998

## Borrower's Page

The University of Waterloo requires the signatures of all persons using or photocopying this thesis. Please sign below, and give address and date.

# ABSTRACT

In this thesis we provide a summary of the methods by which remote sensing may be applied in forestry, while also acknowledging the various limitations which are faced. The application of spatial statistics to high spatial resolution imagery is explored as a means of increasing the information which may be extracted from digital images. A number of high spatial resolution optical remote sensing satellites that are soon to be launched will increase the availability of imagery for the monitoring of forest structure. This technological advancement is timely as current forest management practices have been altered to reflect the need for sustainable ecosystem level management.

The low accuracy level at which forest structural parameters have been estimated in the past is partly due to low image spatial resolution. A large pixel is often composed of a number of surface features, resulting in a spectral value which is due to the reflectance characteristics of all surface features within that pixel. In the case of small pixels, a portion of a surface feature may be represented by a single pixel. When a single pixel represents a portion of a surface object, the potential to isolate distinct surface features exists. Spatial statistics, such as the Getis statistic, provide for an image processing method to isolate distinct surface features. In this thesis, high spatial resolution imagery sensed over a forested landscape is processed with spatial statistics to combine distinct image objects into clusters, representing individual or groups of trees.

Tree clusters are a means to deal with the inevitable foliage overlap which occurs within complex mixed and deciduous forest stands. The generation of image objects, that is, clusters, is necessary to deal with the presence of spectrally mixed pixels. The ability to estimate forest inventory and biophysical parameters from image clusters generated from spatially dependent image features is tested in this thesis. The inventory parameter of crown closure is successfully estimated from image clusters, yet the grouping of trees into clusters causes mixed results when estimating stem counts. The assignment of a cover class of each cluster is also undertaken. The knowledge of cluster cover class has also enabled the estimation of leaf area index. Further, spatial information alone may be used to estimate LAI under described conditions.

# ACKNOWLEDGMENTS

Many people have played a role in assisting my academic pursuits throughout my graduate experience. Some sources of encouragement are unmistakable, such as academic supervisor and committee, others are more subtle, such as family, friends, and colleagues. To all those who have, either put up with me, or assisted me though this graduate enterprise, I extend my gratitude.

Special thanks are offered to my graduate supervisor, Dr. Ellsworth LeDrew. Dr. LeDrew provides students with a unique combination: both the space to pursue ideas and the direction to assist in this pursuit. As a result, under the tutelage of Dr. LeDrew, it is possible to use your imagination, follow scientific leads, and still have the technical and theoretical direction to produce robust results. The insight and encouragement of Dr. Phillip Howarth while at the University of Waterloo is also very much appreciated.

Dr. Barry Boots, of Wilfrid Laurier University, has continued to be a source of academic insight and inspiration. I very much appreciate the willingness of Dr. Boots to assist me in my quarrels with data analysis and statistics.

Dr. Steven Franklin, of the University of Calgary, has provided to me, throughout my academic career, valuable encouragement and advice. Also very much appreciated is the variety of opportunities and responsibilities Dr. Franklin presented me with and encouraged me to pursue.

Sincere thanks are extended to Dr. Mike Lavigne, of the Canadian Forest Service, for sharing with me his deep understanding of the composition, structure, and functioning of forests.

# DEDICATION

To my wife Karen Laberee,

for her love, encouragement, and understanding.

# TABLE OF CONTENTS

# LIST OF TABLES

# LIST OF FIGURES

# LIST OF FORMULAS

# 1. INTRODUCTION

## 1.1. RATIONALE

Forests and woodlands are the most widely distributed vegetation ecosystem on the planet covering approximately 40% of the global land surface (Westoby, 1989). The economic importance of forests is clear, since through either consumption, or utilization of some product or service, forests affect the everyday life of most humans (van Martin, 1984). Less clear is the impact of forests upon the global environment through processes such as the regulation of the global climate, storage of carbon, conversion of carbon dioxide to oxygen, and energy exchange with the atmosphere through control of albedo (Gates, 1990). For example, it is known that deforestation and the combustion of fossil fuel contribute more than 7 billion metric tons of carbon into the atmosphere each year above the natural flux, mostly in the form of $CO_2$ (Jarvis and Dewar, 1993). Forests annually produce 70% of the net global terrestrial carbon accumulation (Peterson and Running, 1989) which results in the uptake of carbon from the atmosphere and the conversion of the greenhouse gas $CO_2$ to $O_2$ (Landsburg and Gower, 1997). While forests are necessary for the regulation of the Earth's atmosphere and climate, which requires vast tracts of forest, harvesting of forests is undertaken either due to need or for economic gain. Sustainable forest management policies have been initiated to reconcile the competing aims for the use of forests (Toman and Ashton, 1995). The responsibility of our heritage dictates a need for monitoring of forests, as anthropogenic forces are potentially responsible for significant changes in $CO_2$ levels, desertification, deforestation, and loss of biodiversity.

Canada contains approximately 10%, or 417.6 million hectares, of the global forest cover (Westoby, 1989) with Canadian forest products accounting for 18% of the world's

forest products exports, which in 1993 were valued at $27 billion (NRC, 1995). Canada's forests have been estimated to contain an estimated 2.6 x $10^{10}$ tonnes of biomass and 2.4 x $10^{10}$ $m^3$ of gross merchantable timber (Brand, 1990). This importance of forests, both environmentally and economically, has necessitated a change in Canadian forest policy. The implementation of ecosystem management shifted the emphasis from maintaining the ability to harvest a known quantity yearly, based on annual allowable cut, to the maintenance of healthy, diverse ecosystems. This change in forest management policy in Canada demonstrates the shift in global forest management priorities from stand management to ecosystem management (NRC, 1995). A key change resulting from this change in priorities is the monitoring of complete natural ecosystem areas, not only the artificial boundaries of a forest management area. Inventories under traditional forest stand management generally consisted of measures of age, species, and timber volume; yet within an ecosystem management framework, the level of detail of measures is increased, requiring information on soils, productivity, and habitat requirements. Within an ecosystem management framework, the future management goals for a forest are considered in terms of age, composition, structure, distribution, and aesthetics (Gillis and Leckie, 1993), as well as non-timber values, such as potential for employment and recreation (CCFM, 1995). The techniques utilized by forest managers and forest scientists are continuing to overlap as the need for sustainable forest management increases (Toman and Ashton, 1996).

Assessment of forests within an ecosystem management framework implies both geographic and economic advantages in applying remote sensing methods to generate data on forest extent and location. Yet, often remote sensing methods fail to capture the diversity of forests necessary for management decisions (Peterson and Running, 1989). Multi-sensor fusion (Wulder, *et al.*, 1995), multitemporal analysis (Qi, *et al.*, 1993), increased spectral

resolution (Gong, *et al.*, 1992), and increased spatial resolution (Leckie, *et al.*, 1995) may assist in providing the level of detail desired for the formulation of forest management decisions. In this thesis we are chiefly concerned with optical satellite and airborne remote sensing methods and applications for the monitoring of forest inventory and biophysical parameters. The promise of high spatial resolution sensors in satellite orbit in the near future (Aplin, *et al.*, 1997) will increase the utility of satellite data in the forest remote sensing context and will likely increase the number of users of remotely sensed data for forest management. Acknowledgment of current techniques, which have heretofore been unreliable, are important to note as these techniques may be more fruitful with the increased spatial resolution offered with the proposed sensors. A review of currently available methods and applications is provided as well as research issues and techniques which are pertinent to the high variance imagery which is collected by high spatial resolution imagery. High spatial resolution airborne remotely sensed data has permitted development of methods and applications for the assessment of forests resulting in a rich information source for potential users of high spatial resolution satellite data.

Forest structure is defined as the above-ground organization of plant materials (Spurr and Barnes, 1980). Vegetation characteristics, climate environment, and site properties combine to produce the structural characteristics of a forest stand. Mixed and deciduous forests are generally structurally complex, due to the potential for overlap between the branches and crowns of trees present. Trees of a younger age will be found suppressed beneath older, more dominant, trees. Intermediate trees are in transition between forest layers. Co-dominant trees are often found in even-aged forest stands (Sharpe, *et al.*, 1976). Tree species is also a factor in the amount of foliage overlap that may be expected; the large crowns of deciduous trees are often highly overlapped. The overlap of foliage results in

difficulties for the remote sensing of deciduous and mixed forests. Remote sensing instruments collect data in a manner which discretize a continuous surface into a grid of regularly sized and shaped pixels. As a result, when applying remote sensing to record data over a mixed or deciduous forest the pixels are often composed of the spectral characteristics from more than one element of ground cover. Even at a high spatial resolution of 1 x 1m, mixed pixels are encountered. The presence of mixed pixels diminishes the variability between pixels and creates difficulties in calibrating the spectral data to ground data. Yet, at the high spatial resolution of 1m, the variance between the pixels is still high, enabling a hybrid approach to understanding of the imagery, based upon spectral and spatial information. Acknowledgment of the manner in which remotely sensed data are collected indicates the likely presence of a spatial dependence between neighbouring pixels. The relationship between the size of the objects of interest, in this case trees, and the image resolution dictates what spatial information will be captured. If the resolution is fine enough to resolve an individual object with a number of pixels, the imagery is considered H-resolution (Strahler, *et al.*, 1986). Conversely, the L-resolution case occurs when an object of interest is found completely within a pixel. The data collected for this study are high at 1m spatial resolution, yet are not H-resolution, when considering the mixed and deciduous forests present in the Fundy Model Forest, within the Acadian forest region.

A unique set of problems are posed for analysis of a mixed forest sensed at a 1m spatial resolution:

- the data is L-resolution with mixed pixels expected, yet many pixels are nearly pure,
- the variance between the pixels is high,
- based upon the high variance and mixed pixels, cover-type, spectral signatures are variable.

The result of these conditions is an inability to use traditional remote sensing techniques to assess forests when using L-resolution data in a low-variance environment. The variance of a 30 metre Landsat pixel is low compared with 1m spatial resolution data. Wulder and Boots (1998a), studied the spatial dependence characteristics of Landsat TM imagery of a managed forest area and found the dependence to be stand-based, due to the inclusion of spectral elements in each pixel related to dominant tree species, understory, and the shadow component. The image spatial structure that arises from 1m spatial resolution data has neighbouring pixels relating the overstory, understory, and shadow component, with many pixels composing the transition between these stand elements. As a result, the spatial dependence between pixels with the 1m data is tree based as opposed to being stand-based with the Landsat data.

As evident from this discussion, techniques which were developed for analyzing different cover types or spatial resolutions are not universally transferable. Previous research in boreal coniferous forests has established that individual trees may be discriminated and classified (Gougeon, 1993, 1995a; Price, *et al.*, 1996). Within deciduous forest stands, however, species separation is limited by factors such as the variety and mixtures of species, stand density, crown closure, complex canopy structure, and spectral confusion between overstory and understory species. For deciduous and mixed forests, an alternate approach is required. The ability to cluster pixels based upon an understanding of the relationship between image spatial resolution and the vegetation objects in the forest is presented as a means to account for the mixels caused by foliage overlap, yet still enable detailed data extraction. Clustering based upon the spatial dependence between pixels enables the extraction of stand vegetation assemblages. Trees which are suppressed by more dominant trees, resulting in mixels, may be segmented into clusters.

In this thesis, we will present the pertinent background literature for the estimation of forest inventory and biophysical parameters. The theory and application of the Getis statistic is presented as a means for generation of spatial dependence values for cluster generation. Tree clusters are then generated from 1m spatial resolution *casi* data (Anger, *et al.*, 1996), through the segmentation of the Getis statistic values. Experiments are then undertaken to demonstrate the potential for the estimation of forest inventory and biophysical parameters from the image clusters. In this investigation the forest structural information that is available for mixed and deciduous forests located in the Acadian forest region of New Brunswick, Canada, when studied using remotely sensed data with a 1m pixel resolution will be determined.

## 1.2. THESIS RESEARCH OBJECTIVES

The primary research objective of this thesis is to:

- investigate alternate methods for the estimation of forest inventory and biophysical parameters based upon spatial information extraction through digital image processing of high spatial resolution multispectral imagery.

To accomplish this goal, a number of secondary objectives have been isolated:

- Present the rationale for the monitoring of forest structure in an ecosystem monitoring framework in a Canadian context. (Chapter 2)

- Provide a framework for the research through identification and documentation of the limitations of existing techniques for spatial information extraction. (Chapter 3)

- Survey existing information extraction techniques, which may be applied to discern forest structural properties at a spatial resolution of 1m. (Chapter 4)

- Propose an alternate spatial information extraction technique based upon spatial statistics, in particular the Getis statistic. (Chapter 5)

- Apply the spatial dependence data generated with the Getis statistics to partition forest stands into vegetation clusters. (Chapter 7)

- Develop and test a methodology to combine existing information extraction techniques with the Getis statistic to allow for estimation of forest inventory parameters. (Chapter 8)

- Develop and test a methodology to combine existing information extraction techniques with the Getis statistic to allow for estimation of the forest biophysical parameter leaf area index (LAI). (Chapter 9)

- Discuss issues raised through the presentation of the thesis to provide a context for the conclusions (Chapter 10).

- Synthesize the results of the combination of spectral and spatial information extraction techniques on forests of complex multi-species structure (Chapter 6) and relate these findings back to the primary thesis objective (Chapter 11) and propose a future research agenda based upon these results (Chapter 12).

# 2. FOREST STRUCTURE FOR ECOSYSTEM MONITORING AND MANAGEMENT

***Chapter Objective:*** *Present the rationale for the monitoring of forest structure in an ecosystem monitoring framework in a Canadian context*

## *2.1. INTRODUCTION*

Forest structure is the above-ground organization of plant materials (Spurr and Barnes, 1980) with the structure of a given forest being the result of competition for light, water, and nutrients at a particular location (Kozlowski, *et al.*, 1991). The growth of woody plants (trees) is controlled through hereditary and environmental processes on the plant physiology. The affected plant physiological processes include photosynthesis, carbohydrate and nitrogen metabolism, respiration, translocation, and plant water balance. Environmental processes which influence the growth and development of trees are light, water, $CO_2$ concentration, temperature, and nutrient availability (Waring and Schlesinger, 1985; Kozlowski, *et al.*, 1991). Tree growth is based upon the competition for resources; the available external environmental factors of light, water, and mineral nutrients. The amount of light available to the lower portions of trees is restricted by the level of the canopy closure. The mutual shading of trees results in differing light intensity available for interception by tree canopies. The amount of light penetrating through the canopy is inversely proportional to the number of trees per unit area. Light transmission in relation to individual stands has been quantified by stand density measures such as leaf area index, trees per unit area, crown closure, basal area, and stem density (Curran, 1980).

Forest structure may vary from homogeneous even-aged stands to heterogeneous mixed stands with multiple age classes. The greater complexity of mixed forests compared to pure

forests is a reflection of the variations among species in crown form, phenology, growth rate, longevity, and size. Accordingly, the ability to assess the structure of a forest permits insight into environmental factors such as hydrology, albedo, productivity, and soils. Understanding of the forest structure allows for the ability to monitor, model, and predict important biophysical processes, such as the interaction between the forest and the atmosphere, based upon the input of a forest structural measure to a forest productivity model (Running, *et al.*, 1994; Loveland, *et al.*, 1991). Changes in forest structure may also provide for forest inventory information related to forest vigor, harvests, burns, stocking level, disease, and insect infestations (Gillis and Leckie, 1996). As suggested, forests may be characterized in terms of inventory measures or biophysical parameters. Inventory parameters provide detailed data on the location and extent of forest resources, such as species composition, age, height, tolerance level, density, and crown closure (Gillis and Leckie, 1993).

Forest biophysical parameters provide data on the productivity, structure, and amount of forest resources. Table 2.1 presents and defines the most common forest biophysical parameters. These measures are most commonly used as they are often correlated to other measures, can be applied to any plant canopy, and may be integrated into regional scale models (Running and Hunt, 1993). Forest biophysical parameters are often an attempt to simplify the measurement of forest structure into a single measure, such as leaf area index. LAI is an important structural attribute of forest ecosystems because of its potential to be a measure of energy, gas, and water exchanges. Maximum canopy leaf area is correlated to mean annual temperature, length of growing season, mean annual minimum air temperature, and water availability (Gholz, 1982). Further, physiological processes such as photosynthesis, transpiration, and evapotranspiration are related to LAI (Pierce and Running, 1988). As an analogy, Running and Hunt (1993) present the notion of a forest canopy as a "green sponge"

with a thickness equivalent to its LAI. The collection of the detailed measures that characterize a forest inventory has previously been limited by the technical capabilities of remote sensing instruments. Current technological developments are enabling greater spectral and spatial resolution on a variety of platforms allowing for the remote measurement of inventory parameters (Leckie, 1990; Leckie, *et al.*, 1995). Forest assessment approaches which incorporate data from a variety of spectral and spatial resolutions are necessary to address the complexity of sustainable forest management with remotely sensed data.

**Table 2.1. Typical forest biophysical parameters (definitions after Bonham, 1989)**

| Parameter | Detail |
|---|---|
| LAI | leaf area index - is a measure of area of foliage per unit area of ground |
| Biomass | biomass - is the total of absolute amount of vegetation present (often considered in terms of above ground biomass) |
| NPP | net primary productivity - is similar to biomass, but has a temporal component as it is related to the amount of biomass accumulated over a given time period |

## 2.2. GLOBAL IMPORTANCE OF FOREST STRUCTURE

Geologic records demonstrate that the Earth has undergone continuous and significant change throughout its 4.5 billion year existence. The Earth's history may be viewed as a dynamic continuum, experiencing changes at various time scales. Recent research suggests that human activities may be responsible for some dramatically increased rates of change in several key components of the global system. For example, it is known that deforestation and the combustion of fossil fuel contribute more than 7 billion metric tons of carbon into the atmosphere each year above the natural flux, mostly in the form of $CO_2$. Anthropogenic forces have also been presented as responsible for significant changes in ozone levels, desertification, deforestation, and loss of biodiversity (Jarvis and Dewar, 1993).

The societal and ecological implications of human-induced global climate change and variability could be devastating. Bubbles trapped in ice cores from Greenland and Antarctica show that atmospheric $CO_2$ concentrations were relatively stable for at least 160,000 years, fluctuating between roughly 180 and 280 parts per million (ppm) (Schlesinger, 1991). Since the start of the Industrial Revolution, increased emissions have pushed this concentration to an unprecedented (in recent history) 354 ppm. This is recently observed in the excellent monthly record from Hawaii's Mauna Loa atmospheric recording station (Keeling, *et al.*, 1989). Various simulation models predicting the climate in 2 x $CO_2$ concentrations have forecasted globally-averaged warming of between 1.5 and 4.5°C (summarized by LeDrew, 1995, p. 63). Climatic simulations of increased $CO_2$ environments have shown the greatest temperature increases to occur at higher latitudes, with extremes found at the continental interiors (Gates, 1990). Such modifications in the temperature regime could alter the composition and functioning of the boreal forest (Davis and Botkin, 1985).

Gates (1990) presents the need for modeling, based upon historical and current information, to assess the response of forests to climate variability. Potential changes in forest composition and the ability of forests to adapt to changing environments may be anticipated through modeling. Through measurement of the boreal forest components the potential is presented for monitoring, modeling, and reaction. Understanding of what is expected, through modeling, at a particular location enables comparison with ground validation. The ability to accurately assess forest structure is especially important at ecotones, the boundaries between ecoregions.

In the forestry situation, changes to the boreal forest composition will be first noted at the fringes of the forest regions, such as at the northern and southern extremes of current boreal forest extent. Changes in environmental conditions may alter growing conditions and

result in a shift of boundaries, and therefore, in forest structure (Waring and Schlesinger, 1985). Gates (1990) has hypothesized that forests will undergo great changes as temperature and precipitation patterns shift. The rates of forest movement will likely be slower than climate change, resulting in the death of sensitive hardwood species. With the shifting patterns of climate and precipitation it is theorized that boreal forests will move north replacing tundra and the mixed hardwood forests may replace boreal forests. The ability to detect locational changes in forest structure is a geographical research issue that may be addressed with remotely sensed data.

## 2.3. THE CANADIAN FORESTS

Canada contains 417.6 million hectares of forested land, representing 45% of the total land base of the country, and is approximately 10% of the global forest cover (Westoby, 1989). Canada's forests have been estimated to contain approximately $2.6 \times 10^{10}$ tonnes of biomass and $2.4 \times 10^{10}$ $m^3$ of gross merchantable timber (Brand, 1990). Ninety four percent of Canadian forests are held in trust by governments (71% provincial, 23% federal), with the remaining 6% privately owned. As forest management is largely the responsibility of provincial and territorial governments, each jurisdiction has a set of forest regulations, policies, and legislation. The federal government's role in forestry relates to areas such as trade, commerce, international affairs, Indian affairs, pesticide regulation, and scientific research. Forest management and forest inventory in Canada are primarily a provincial responsibility (Gillis and Leckie, 1993).

Approximately 56% of Canadian forests are considered commercial forests (NRC, 1995), capable of producing timber and non-timber products, with nearly 28% of the potential commercial area currently being exploited. Further, approximately 12% of Canada's forest

area is protected from harvesting by policy or legislation. The sustained yield of timber from Canada's forests is currently estimated at between 2.04 x $10^8$ and 2.25 x $10^8$ $m^3$/year.

Boreal forest and Canadian forest are often considered synonymous due to the dominance of the boreal forest in Canada. In Canada's forests there are 165 different tree species, of which 63% are softwoods, 15% hardwoods, and 22% mixed woods (Gray, 1995). The majority of these stands are of even age composition due to disturbances such as harvest, fire or insect infestation.

Canada's forests, primarily due to the large area covered, are important both in a scientific and economic sense. The role the boreal forests play in the regulation of environmental processes, such as, carbon cycling, climate, hydrology, and productivity are of great interest to Canadian and foreign scientists. The history of harvesting the boreal forests is older than Canada and continues to play an important role in the Canadian economy.

### 2.3.1. Canadian Forest Coverage

For the determination of Canada's forest coverage, there are three primary classification levels, (in order of increasing detail):

1. national description of forest regions and sections (Rowe, 1977),
2. forest inventory schemes (Gray, 1995), and
3. regional and provincial site and ecoregion or biogeoclimatic zone classifications (Gillis and Leckie, 1993).

Rowe (1977) describes the forest geography of the country by region and section, with a region being roughly uniform in physiognomy and dominant tree species. Canada is divided into 10 forest regions (Table 2.2), which are further divided into 90 forest sections (Gray, 1995). The 90 forest sections are subdivided from within the forest regions based upon a further distinctive pattern of physiography and vegetation within the forest region (Rowe, 1977).

**Table 2.2. Forest regions of Canada, including area (after Gray, 1995)**

| Forest Region | Area (x1000 ha) |
|---|---|
| Boreal Forest Region, Predominantly Forest | 239,438 |
| Boreal Forest Region, Forest and Grass | 21,911 |
| Boreal Forest Region, Forest and Barren | 218,613 |
| Subalpine Forest Region | 25,139 |
| Montane Forest Region | 14,996 |
| Coast Forest Region | 12,574 |
| Columbia Forest Region | 5,456 |
| Deciduous Forest Region | 5,184 |
| Great Lakes-St. Lawrence Forest Region | 46,583 |
| Acadian Forest Region | 12,168 |
| Grassland | 30,159 |
| Tundra | 314,940 |

## 2.4. FOREST SUSTAINABILITY IN A CANADIAN CONTEXT

The long-term sustainable use of forest lands in Canada is a function of balancing a variety of interests. As a result, in 1991, the Canadian Council of Forest Ministers (CCFM), as the trustee of the National Forest Strategy, held a series of public forums to gauge public sentiment towards the management of Canada's forests. The resulting vision statement proposed that,

> "our goal is to maintain and enhance the long-term health of our forest ecosystems for the benefit of all living things, both nationally and globally, while providing environmental, economic, social and cultural opportunities for the benefit of present and future generations" (CCFM, 1995, p. *v*).

To create a management scheme which takes into account such diverse interests, detailed measurement of forest ecosystems is necessary. A commitment was made to develop criteria and indicators which would allow for such detailed measurements. A second public consultation process was embarked upon soliciting input from scientists associated will all levels of government, academia, industry, non-governmental organizations, and special

interest groups. The resulting recommendations are presented in *Defining Sustainable Forest Management: A Canadian Approach to Criteria and Indicators* (CCFM, 1995). The framework of criteria and indicators is based upon the following principles:

1. The need to manage forests as ecosystems,
2. Forest ecosystems simultaneously provide environmental, economic, and social benefits,
3. An informed and included public is necessary for implementation of sustainable forest management, and
4. Forest management is a dynamic process which should reflect the best available information.

To generate the desired criteria and indicators (Table 2.3), detailed measurements of forest inventory and biophysical parameters are necessary. For example, to assess genetic diversity, species, amounts and distributions of forest species must first be derived from forest inventory information. To assess the existing amount of biomass, a parameter such as leaf area index, may be computed. Further, to generate forest sector contributions to the global carbon budget, both inventory and biophysical parameter estimates are necessary.

**Table 2.3. Summary list of criteria and indicators for defining sustainable forest management in Canada (after CCFM, 1995)**

| **Criteria and Indicators – Ecological** |
|---|
| Conservation of biological diversity |
| • ecosystem diversity<br>• species diversity<br>• genetic diversity |
| Maintenance and enhancement of forest ecosystem condition and productivity |
| • incidence of disturbance and stress (biotic and abiotic)<br>• ecosystem resilience<br>• extant biomass (biota) |
| Conservation of soil and water resources |
| • physical environmental factors<br>• policy and protection forest factors |
| Forest ecosystem contributions to global ecological cycles |
| • contribution to global carbon budget<br>• forest land conversion<br>• forest sector $CO_2$ conservation<br>• forest sector policy factors<br>• contributions to hydrological cycles |
| **Criteria and Indicators - Socio-economic** |
| Multiple benefits to society |
| • productive capacity<br>• competitiveness of forest resource industries (timber/non-timber related)<br>• contribution to the national economy (timber/non-timber related)<br>• non-timber values (including option values) |
| Accepting society's responsibility for sustainable development |
| • aboriginal and treaty rights<br>• participation by aboriginal communities in sustainable forest management<br>• sustainability of forest communities<br>• fair and effective decision making<br>• informed decision making |

## 2.5. FOREST MANAGEMENT: FOREST INVENTORY PARAMETERS

Management of forest lands requires information describing the location and volume of timber available, and as forests are dynamic biological systems, estimates of growth are also required. Forest inventories are undertaken to accurately relate the characteristics of the forest property (Table 2.4) and these measures may also be utilized to extrapolate to future forest conditions. Forest mensuration (Section 3.2.1) is the actual collection of detailed measures on a per-tree basis, or by a statistically based sampling technique. These measures are analyzed to result in the indicators utilized by the forest manager. Forest managers may look at the site-quality of a particular stand, such as the actual volume of a stand compared against a standard for a site of similar characteristics. If the stand is found to be below the standard volume, some treatment may be prescribed (Sharpe, *et al.*, 1976). Further, the data collected for a commercial forest inventory may also be applied to predict biomass based upon empirical relationships between species, diameter (DBH), and biomass (Schroeder, *et al.*, 1997).

**Table 2.4. Indicators necessary for traditional forest management (UBC, 1983)**

| Characteristic | Indicator |
|---|---|
| Site Quality | volume<br>soil<br>lesser vegetation<br>age-height relationships (site index) |
| Stocking | crown closure<br>number of trees compared to a standard |
| Density | number of trees per hectare<br>basal area per hectare |

As forest management is primarily a provincial government responsibility, each province has a methodology for detailed inventory of forest lands (Gillis and Leckie, 1993).

Knowledgeable management of the forest resource requires basic information on the location, composition, and extent of the resource. Each province has a similar inventory technique with common elements (Table 2.5). Inventory techniques are continually evolving, especially to introduce new technologies, such as global positioning systems, geographical information systems, and remotely sensed data (Gillis and Leckie, 1996).

**Table 2.5. Typical provincial forest inventory parameters (after Gillis and Leckie, 1993)**

| Parameter | Detail |
|---|---|
| Scale | Normally 1:12,500 to 1:20,000 |
| Species | Abbreviated species or tolerance level |
| Development Stage | Development description, including elements such as cut, burn, regenerating, and mature |
| Crown Closure | Percentage classes from 10 to 30% to greater than 90% |
| Stand Indicators | Brief site description |
| Non-Forest Conditions | Non-forest characteristics, such as agricultural, mining, gravel, and cut blocks |
| Ownership | Land ownership characteristics |
| Map Symbol Legend | Explanation of the symbols used |

## 2.6. FOREST BIOPHYSICAL PARAMETERS

There is an unlimited number of combinations of vegetative arrangements found in forests; yet, to integrate forest structure into models of forest conditions a repeatable and standardized measure is necessary. The growth of individual trees may be quantified by a variety of methods (Kozlowski, *et al.*, 1991). Foresters are interested in the increment in the amount of wood produced by a stand, while ecologists are interested in dry weight increases and losses of organic matter per unit area and the partitioning of dry matter production. Changes in weight, or biomass, of forest trees are used to assess growth, nutrient cycling, and energy flow in forest stands. A common measure of forest growth is net primary productivity (NPP), that may be thought of as the difference between photosynthesis and respiration (Kozlowski, *et al.*, 1991) or as the amount of energy left to the tree for growth. NPP, is

directly related to the amount of carbon released to the atmosphere and the inversely corresponding amount is that which is incorporated by the plant. NPP is the energy base for all secondary production in the forest environment and represents the amount of potentially harvestable material or organic matter for long-term storage in soils and the forest floor (Waring and Schlesinger, 1985). The NPP of forest stands varies widely as a function of site, forest type, age of stands, species and genotype, and climate. NPP increases from arctic to tropical regions with increasing water supply, soil fertility, and also with decreasing elevation. The productivity of forest stands varies significantly between different sites. The production of dry matter (wood) is due to the capacity of trees to synthesize carbohydrates, and therefore the growth of an individual tree is often related to crown size. This allows dominant trees, with large fully exposed crowns, to produce more dry matter than may be produced by suppressed trees with small shade crowns. As a result, leaf area, as indicated by leaf area index (LAI), is directly related to the productivity of forest stands (Figure 2.1) (Running and Hunt, 1994).

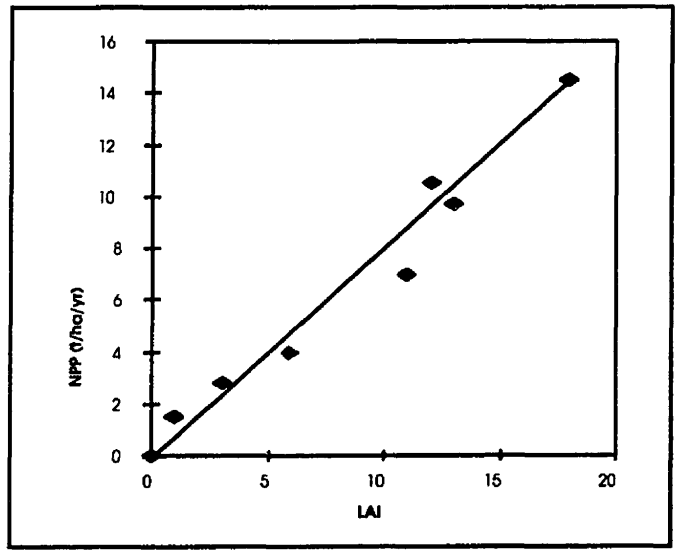


**Figure 2.1. Relationship between maximum LAI and NPP (after Waring and Schlesinger, 1985)**

The ability to measure and quantify structure is made possible through the assessment of LAI, defined as the leaf area per unit ground area, a dimensionless index usually measured with a scale that provides units of $m^2 m^{-2}$. LAI is an important structural attribute of forest ecosystems because of its potential to be a measure of energy, gas, and water exchanges. Maximum canopy leaf area is correlated to mean annual temperature, length of growing season, mean annual minimum air temperature, and water availability (Gholz, 1982). Further, physiological processes such as photosynthesis, transpiration, and evapotranspiration are related to LAI (Pierce and Running, 1988). This relationship allows for various processes to be estimated from LAI.

Absorbed photosynthetically active radiation (APAR) is important as an indication of vegetation energy requirements in forest structure studies. PAR is the solar radiation between approximately 0.4 and 0.7 μm which is consumed in the canopy photosynthetic process (Li and Moreau, 1996). The amount of absorbed photosynethically active radiation (APAR) is important in studies of forest structure due to a direct link to photosynthesis, net primary productivity, and the carbon cycle (Waring, *et al.*, 1993; Sellers, 1995). A theoretical approach is presented by Sellers (1985), for relating canopy photosynthesis and stomatal resistance to spectral reflectivity. The limits of APAR, as a structural indicator in the estimation of LAI, are demonstrated in the asymptotic relationship presented in Figure 2.2. As illustrated, a difficulty in the estimation of LAI >3 is due to the near complete absorption of PAR wavelengths related to the optical depth of a complex canopy (Sellers, 1989). The relationship between APAR and LAI and vegetation indices is also asymptotic, limiting accurate estimation to simple, single layer canopies (Baret and Guyot, 1991).

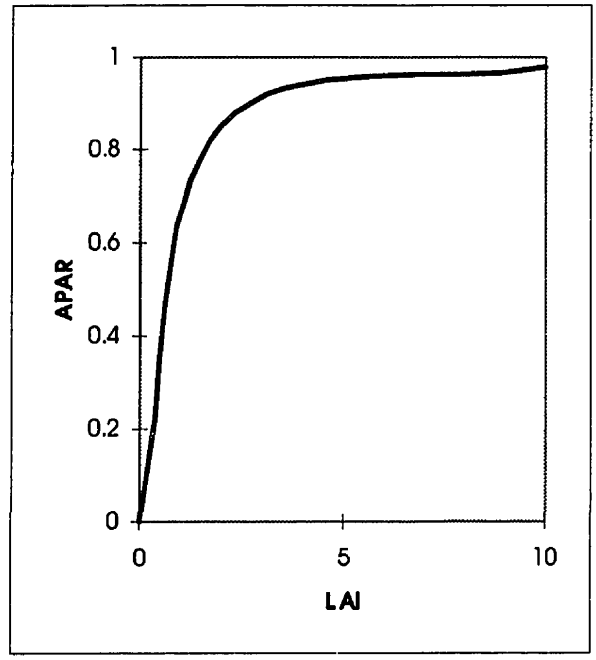


**Figure 2.2. Variation of the fraction of absorbed photosynthetically active radiation (APAR) with leaf area index (after Sellers, 1989).**

### 2.6.1. Within Stand Partitioning of LAI

A maximum potential LAI may be associated with a species and a location (Waring and Schlesinger, 1985) with overstory species having a greater potential for increasing leaf area than understory species. As a component of the Oregon Transect Terrestrial Ecosystem Research (OTTER) project, Peterson, *et al.* (1987) present the variability of LAI along a transect with variation demonstrated in a geographic nature. It was found that the coastal environment supported the growth of different species and structures than inland conditions (Peterson and Waring, 1993). Also demonstrated was the variability in stand LAI as a function of percentage of the stand which is represented by understory species (Table 2.6). In an open stand, failure to include understory species will result in an incorrect estimate of leaf area. Knowledge of the proportion of the stand represented by overstory and understory species is important through all stages of succession to properly estimate stand LAI.

**Table 2.6. Total stand LAI as a function of overstory versus understory representation (after Peterson, *et al.*, 1987)**

| Dominant Tree Species | Overstory LAI | Understory LAI | Total LAI | % of LAI of Understory |
|---|---|---|---|---|
| Western Hemlock | 15.4 | 0.71 | 16.1 | 5 |
| Sitka Spruce | 5.7 | 3.15 | 8.8 | 37 |
| Douglas Fir | 5.0 | 1.31 | 6.3 | 20 |
| Lodgepole Pine | 5.2 | 1.73 | 6.9 | 26 |
| White Fir | 5.1 | 0.02 | 5.2 | 0.4 |
| Ponderosa Pine | 3.1 | 0.04 | 3.2 | 1.2 |

The proportion of a forest stand represented by overstory and understory species is a result of the potential species assemblages and the succesional regime of the stand. Stand succession, the transition of species from less to more complex structure, generally occurs after a disturbance (Spurr and Barnes, 1980). Figure 2.3 demonstrates the succession of a forest stand, initially occupied by grasses, giving way to shrubs, then trees. The tree species will grow towards a climax forest of species that are best suited for the conditions at that location. Also demonstrated in Figure 2.3 is the increasing complexity of both vertical and horizontal structure of the forest. The vertical structure refers to tree height distribution and the horizontal distribution pertains to stand density and spatial distribution (St-Onge and Cavayas, 1995). The grasses have minimum vertical stratification and are well represented from above, in contrast to the mature forests which are poorly represented from the nadir view (Wulder, *et al.*, 1996a, 1998). Stand stratification is primarily the result of variations in time and method of establishment and growth rate of species.

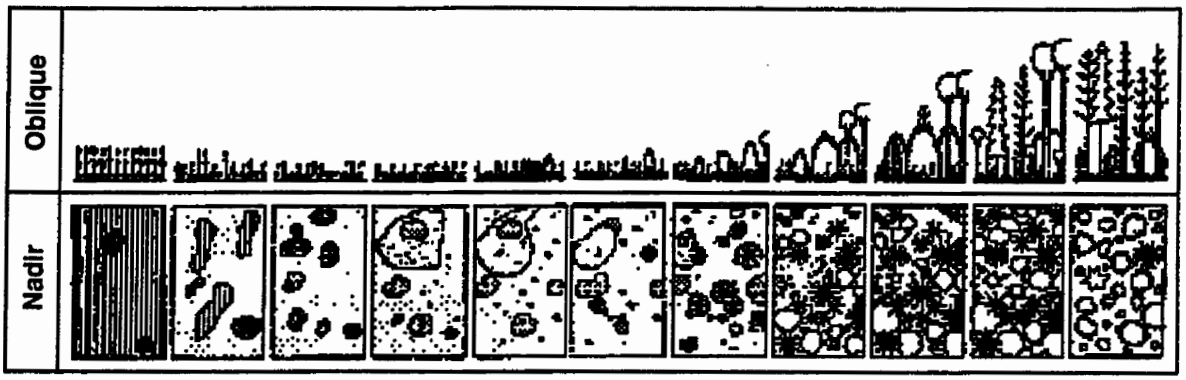


**Figure 2.3. Demonstration of vegetation succession with increasing horizontal and vertical vegetation complexity (after Falinski, 1989).**

# 3. MEASUREMENT OF FOREST STRUCTURE

***Chapter Objective:*** *Provide a framework for the research through identification and documentation of the limitations of existing techniques for spatial information extraction.*

## *3.1. INTRODUCTION*

Remote sensing, the measurement of phenomena without physical contact, enables the representation of physical realities with surrogate information. Relationships may be developed between ground-based control measurements and remotely sensed information, such as digital imaging satellites or airborne data. Studies involving remotely sensed data normally have data collection, processing, and analysis stages which relate the remote measures to the ground-based validation measures (Steven, 1987). Remote sensing is an imaging information source that can be used to assess the distribution and variability in forest structure. Approaches to the assessment of forest structure may either address forest inventory or biophysical parameters. Utilizing high spatial resolution remote sensing instruments, the forest image data may be collected at a resolution where the objects of interest are larger than the pixel size (Woodcock and Strahler, 1987). At this spatial resolution, individual stand objects, such as trees, may be reconstructed from digital image pixel values. The ability to discern individual trees, and the relationships between these trees, will allow for the estimation of both inventory parameters (Gougeon, 1995a) and biophysical parameters, such as LAI (Hay and Niemann, 1994). The suite of image processing techniques which has been developed to relate forest biophysical information to spectral information may be integrated with the newly developed object-based approaches.

Canada has been a pioneer in the research, development, and implementation of remote sensing in forestry surveys and management. Early experimentation with aerial photographs began in the 1920s, and in the 1950s Canada was the first nation to operationalize management using aerial photographic interpretation (Leckie, 1990). In the 1960s large-scale photographic sampling for aerial surveys was pioneered (Spencer and Hall, 1988). With the launch of the Landsat series of satellites in 1972, Canada began to receive and implement the use of digital satellite imagery (Leckie, 1990). New developments, such as increased spatial resolution of sensors and novel image processing techniques, have been developed which are increasing the effectiveness of remote sensing in forestry (Gillis and Leckie, 1996).

In this chapter, we will provide a summary of the development of techniques utilized to assess structure, from *in situ* stand measurements, to aerial photographs, to current state-of-the-art high resolution digital multispectral remote sensing techniques. The estimation techniques developed for the assessment of structure will also be summarized in terms of forest biophysical and inventory parameter estimation from the perspective of both satellite and airborne instruments. The satellite remote sensing section will precede the airborne multispectral section as much of the historical analysis of forest structure with multispectral methods has been undertaken with satellite data.

## 3.2. FIELD MEASUREMENT OF FOREST INVENTORY PARAMETERS

The field measurement of forest inventory parameters is an intensive and expensive process (Leckie, 1990) requiring a human presence in the forest to physically measure the trees (Gillis and Leckie, 1993; Avery and Burkhart, 1994). Forest mensuration is understood as the process by which measurement of the present and future volume, growth, and development of individual trees and stands, and related timber products are undertaken

(Sharpe, *et al.*, 1976). The field of forest mensuration is concerned with direct measurements, sampling, and prediction (Avery and Burkhart, 1994).

### 3.2.1. Forest Mensuration - Direct Measures, Sampling, and Prediction

Direct measurement of trees requires the use of appropriate instruments; for example, tree calipers or a diameter tape are utilized to make measurements of tree diameter (Spurr, 1952). Yet, as it is impractical to attempt to measure all trees of a forest stand directly, a variety of sampling techniques has been developed to scale direct measurements taken in selected locations to represent a larger area (Robinson and Wood, 1994). The techniques are generally based upon a rule for selecting sample trees within a plot, a criteria for selecting sample plots, and a method for the transformation of sample values to represent the entire area. Prediction of stand volume may be gleaned from tables that have been developed for most forest species which enable prediction of stand, or tree, volume from tree height and diameter at breast height (DBH) data.

From a nadir-viewing sensor that partitions the forest canopy into a grid of regularly sized and shaped pixels, there are limits to what may be measured. As individuals, mature trees may be discriminated in the high spatial resolution remotely sensed imagery; measures that are based upon single trees or assemblages of trees may be estimated. There appears to be promise in the application of remote sensing methods in the estimation of tree-crown diameter, canopy closure, stand density, and tree species for non-plantation forest stands of deciduous and mixed forest composition. The ground data collected for this study are typical of the measurements taken by foresters to characterize a forest stand (Cole, 1995). A forest stand is considered as a group of trees that are similar enough in characteristics to be considered as a homogeneous unit (Landsburg and Gower, 1996). Measurements made upon a sample plot in a forest stand are an attempt to characterize the trees of an area representative

of a stand, and to enable extrapolation of the measured characteristics at the plot level to the entire stand. (The suite of field data collected is presented in Table 6.1, as a component of Chapter 6.)

Estimates of site characteristics are also important. Forest site characterization is normally based upon the interaction of factors affecting the productivity of forests, such as soils, light regime, climate, and topography. Measurement of site characteristics provide the forest manager with an indication of potential productivity of forest stands, and enable a frame of reference for diagnosis and prescription (Avery and Burkhart, 1994). Site characteristics may be inferred through measurement of stand density, stocking level, basal area per hectare, and trees per hectare. As measures of site are based upon the amount and relationship of trees per unit area, high spatial resolution remote sensing methods may be appropriate for their measurement.

## 3.3. FIELD MEASUREMENT OF FOREST BIOPHYSICAL PARAMETERS

The measurement of forest structure may be undertaken at a variety of scales, with accuracy inversely related to the size of the area assessed. *In situ* field methods for the estimation of forest structure are expensive and time consuming, yet the most accurate. The trade-off when utilizing airborne or satellite remote sensing methods to estimate forest structure is the large spatial area of coverage and repeatability of measurement. *In situ* measures of forest structure will always be necessary for the calibration and validation of remotely sensed measures of forest structure.

### 3.3.1. *In situ* Assessment of LAI

In forestry the high labor intensity of direct measures of LAI has been an impediment to LAI measurement and as a result many indirect measures have been devised. Direct

measurement of forest LAI involves destructive sampling of representative trees and assessing the dry weight to live weight ratio of all constituent components of the sample tree. The individual tree leaf areas calculated are summed for the plot and divided by the plot area to calculate the $m^2$ leaf area per $m^2$ ground area (Kaufmann and Troendle, 1981). Indirect measurements of LAI are often related to the amount of light penetrating the canopy (light interception) and degree of canopy closure (see Table 3.1 for a summary of methods).

**Table 3.1. Summary of the research related to direct *in situ* estimation of LAI**

| Detail | Description | Reference |
|---|---|---|
| Allometric equations | computation and assessment of the relationship between leaf area and sapwood cross-sectional area | Kaufmann and Troendle, 1981 |
| Pipe model theory | explanation and demonstration of pipe model theory | Waring *et al.*., 1982 |
| Non-linear relationship | a non-linear relationship is found for trees of increasing size | Dean and Long, 1986 |
| Effect of stand density | stand density is demonstrated to have an effect upon the ratio of foliage area to sapwood cross-sectional area | Hungerford, 1987 |
| Unbiased estimates | methodology for estimates unbiased by stand density and site index | Long and Smith, 1988 |
| Hemispherical photography | hemispherical photography are assessed to determine plant area index and geometry of a forest stand | Chen, *et al.*, 1991 |
| Comparison of direct and indirect | LAI estimates derived from allometric and light interception methods are compared; found to be poorly related | Smith, *et al.*, 1991a |
| Error assessment | bias and error assessment in LAI estimation from sapwood cross-sectional area | Woods, *et al.*, 1991; Dean, *et al.*, 1988 |
| Comparison of prediction techniques | Predictions based upon sapwood cross-sectional area are found to provide the most accurate | Lavigne, *et al.*, 1996 |

### 3.3.1.1. Direct *In situ* LAI Estimation

Tree stems are generally composed of bark, cambium, and heartwood. Bark is the protective outer layer of trees, the cambium is where tissue formation is initiated, sapwood conducts water and nutrients from the roots to the leaves, and the heartwood contains cells which no longer function physiologically but act as the supportive skeleton of the tree. Most of the sapwood cells are dead but are able to conduct water. The pipe model theory is based upon the concept that a unit weight of tree foliage is serviced by a specific cross sectional area of conducting sapwood in the crown. Below the crown component of a tree, a large fraction of the tree stem may be non-conducting tissue (heartwood), so therefore the sapwood area would have to be known to estimate foliage (Waring, *et al.*, 1982; Grier and Waring, 1974). Lavigne, *et al.*, (1996) assessed a variety of predictor variables in allometric estimation of LAI and found that estimates computed with sapwood cross-sectional areas at breast height as the most reliable independent variable. As a result, knowledge of the sapwood cross sectional area of a tree may be applied to predict LAI (Kaufmann and Troendle, 1981; Lavigne, *et al.*, 1996). Sapwood cross-sectional area is calculated from the radius provided from the DBH measurement, bark width, and sapwood width. The standard guidelines for assessment of tree leaf area are detailed in Aldred and Alemdag (1988). Allometric relationships are stand specific, based upon the local plant/environment interaction, potentially resulting in a need for the derivation of new relationships for each studied stand. Less expensive and more timely estimation methods are necessary based upon the prevailing plant/environment conditions found at the particular location (Chen and Cihlar, 1995).

### 3.3.1.2. Indirect *In situ* LAI Estimation

Indirect *in situ* methods for the assessment of forest structure have been developed to provide a less expensive and faster technique for the derivation of ground validation data (Steven, 1987) for the remote sensing of forest structure. Indirect *in situ* estimation of forest structure is based upon the theory that leaf material may generally accumulate to a magnitude in relation to the amount of solar irradiance received. The commonly used techniques to estimate LAI consider the canopy as accumulated layers of foliage through which solar radiation is absorbed exponentially as the amount of leaf area increases (see Table 3.2). Foliage area may be expressed as the LAI representing the upper surfaces of the leaves (single sided LAI) projected downward to a unit area of ground beneath the canopy. The penetration of radiation through the leaf layers approximates the Beer-Lambert Law,

$$\ln \frac{I_z}{I_o} = k \sum \text{LAI} \qquad [1]$$

where, $I_z$ is the intensity of light below the canopy, $I_o$ is the intensity of visible light above the canopy, $k$ is an extinction coefficient (the slope of the relationship), and $\Sigma$LAI is the cumulative amount of projected leaf area measured in square meters of foliage area per square metre of ground area. The extinction coefficient ($k$) is normally a species specific value based upon the amount of vegetation overlap and crown shape (Waring and Schlesinger, 1985).

**Table 3.2. Summary of the research related to indirect *in situ* estimation of LAI**

| Detail | Description | Reference |
|---|---|---|
| Review of measurement methods | fisheye photography, a "crownmeter", and a "pasture probe" are assessed by as additional methods to obtain gap fraction measurements | Welles, 1990 |
| All vegetation included in computation | light interception techniques cannot distinguish between foliar interception and that intercepted by plant woody tissues; also reviews measurement methods | Fassnacht, *et al.*, 1994 |
| Underestimation of LAI | indirect measures are often found to underestimate LAI especially in stands where the assumption of random distribution of foliage is violated, such as conifer stands | Gower and Norman, 1991 |
| Effect of sun angle | recommend caution as the sun angle has an effect upon the results when using gap fraction methods | Nel and Wessman, 1993 |
| TRAC method | a technique based upon repeated hemispherical sampling and calculation of gap fraction which provides ground truth LAI values through assessment of foliage angular distribution and foliage spatial distribution | Chen and Cihlar, 1995 |

Chen and Cihlar, (1995) have developed a method of LAI estimation which is an attempt at accounting for both the amount of light penetrating the canopy and the non-random arrangement of foliage elements. The leaf area measured with gap fraction is the effective leaf area as all leaf and woody matter are included. Gap fraction methods are based upon the assumption that the foliage distribution are random (Chen and Black, 1992) although foliage is non-random in distribution at the stand, species, tree, and branch levels (Whitehead, *et al.*, 1990; Kuuluvainen and Pukkala, 1989; Oker-Blom and Kellomaki, 1983). The Chen and Cihlar (1995) technique is based upon repeated hemispherical sampling and calculation of gap fraction which provides ground truth LAI values through assessment of foliage angular distribution (LI-COR LAI-2000) and foliage spatial distribution (TRAC - Tracing Radiation and Architecture of Canopies). This method addresses the two key problems with light penetration gap fraction methods by assessing both the distribution of foliar elements and the

below canopy penetration of light at a number of sample points to calibrate the hemispherical penetration characteristics. Ground measurements are labor intensive and cover small sampling areas, yet the values derived at local sites may be utilized as training data for larger scaled remotely sensed measurements.

## 3.4. FACTORS WHICH AFFECT THE REMOTE SENSING OF FORESTS

Optical remotely sensed data is a the result of a complex series of interactions between the electromagnetic radiation emitted by the sun reflected off Earth's surface and received by a sensor. In the forestry context, this complex series of interactions encompasses factors such as the optical properties of the stand, spatial resolution (scale), stand object relationship to scale, and spatial aggregation.

### 3.4.1. Spectral Response of Forest Canopies

The interpretation of remotely sensed data of forest canopies requires knowledge of the factors affecting their optical properties (Guyot, *et al.*, 1989). The factors affecting the forest canopy may be internal or external to the forest stand. External factors that have an affect on the reflectance of forests are the size of the viewed area, orientation and inclination of the view axis, sun elevation, wind speed, and clouds or other potential atmospheric interference (nebulosity). Factors internal to the stand that have an effect on reflectance are row orientation, optical properties of the background, and canopy geometry (Guyot, *et al.*, 1989). Terrain also has an effect upon stand reflectance (Craig, 1981; Civco, 1989) resulting in variations in reflectance based upon the sun / surface / sensor geometry (Schaaf, *et al.*, 1994). Knowledge of the potential factors affecting the spectral response of forest canopies assists in the application of the most appropriate image analysis technique.

### 3.4.2. Scale in Remote Sensing

The spatial resolution of a remotely sensed measurement is determined by the sensor's instantaneous field of view (IFOV), the area of the target which is viewed by a sensor in an instant of time. With imaging sensors, this quantity is normally expressed as a pixel size. Using this definition, spatial resolution is analogous to scale (Woodcock and Strahler, 1987). Scale is a fundamental concept in remote sensing and plays an important role in determining the type and quality of information that can be extracted from an image. Unfortunately this concept is poorly understood, likely because an image is a regular, comprehensive representation of the ground surface which creates the illusion of strong and predictable correlations between the measured radiance at each pixel and the surface features of interest (Woodcock and Strahler, 1987). The appropriate scale for analysis is the subject of debate (Table 3.3) with the cover type often playing a key role in the result. In the analysis of geographic spatial phenomena, the difficulty relating to spatial scale and scale changes is because the size of the phenomena decide the scale (Meentemeyer, 1989) and that the phenomena of interest are variable in size across a landscape.

**Table 3.3. Studies addressing the issue of the selection of appropriate scale for analysis in remote sensing**

| Detail | Description | Reference |
|---|---|---|
| Information content and measures | information extraction measures based upon assessment of local entropy present as a function of resolution | Wong and Vogel, 1977 |
| Effective resolution | for urban examples the minimum resolution at which unique surface objects are resolvable is assessed | Welch, 1982 |
| Simulated scene | use of geometrical optical models to simulate forest scenes in order to estimate optimal resolution | Li and Strahler, 1985 |
| Internal class variability | as the resolution decreases (more coarse) the internal class spectral variability decreases improving the ability to classify homogeneous areas | Cushnie, 1987 |
| Sensor dependent information content | assessment of the spatial variability captured as a function of resolution; the effect upon classification and information extraction | Irons, *et al.*, 1985; Chavez, 1992; Johnson and Howarth, 1987 |
| Landscape ecology | the effect of changing spatial scale on the spatial patterns present, concepts such as grain and extent; concept of the land unit as a homogeneous tract at the utilized scale | Zonneveld, 1989; Turner, *et al.*, 1989 |
| Effect of resolution up variograms | variograms are often used to relate the range of spatial structure of a scene; this paper assess the effect of initial spatial resolution upon variogram results | Ramstein and Raffy, 1989 |
| Decrease in variance with increase in spatial resolution | the scale and spatial aggregation problem is demonstrated and illustrated in a forestry context; the effect of scale changes upon classification accuracy is also demonstrated | Marceau, *et al.*, 1994a |
| Sampling grid to correspond to cover type | the scale and aggregation characteristics of the cover type should dictate the spatial sampling grid interval; determined with minimum spectral variance | Marceau, *et al.*, 1994b |
| Variogram assessment | use of semivariogram analysis on digitized aerial photographs at a variety of scales to determine spatial dependency to derive optimal resolution; Hyppanen provides an example for boreal forests | Woodcock and Strahler, 1987; Hyppanen, 1997 |
| Local variance and variogram support | utilization of the variogram to select appropriate resolution for analysis | Atkinson and Curran, 1997 |

### 3.4.3. The Nature of Models in Remote Sensing

The relationship between the spatial resolution and the forest objects of interest influences the information content as the elements which comprise an image are represented in detail as a function of the scale. Strahler, *et al.*, (1986) propose the concepts of H-resolution and L-resolution to characterize scene models based on information content. The H-resolution case occurs if the objects of interest in the scene are larger than the image resolution. The L-resolution case occurs when the resolution cells are larger than the objects resulting in an inability to resolve individual elements. The terms high and low resolution often carry an absolute connotation of a pixel size, not of information content. Differing abilities for analysis exist depending on the initial image data content. The availability of H-resolution imagery has blurred the distinction between biophysical and inventory approaches in the remote sensing of forests as the information content of the imagery is no longer a limiting factor.

### 3.4.4. Scale and the Representation of Geographic Data

Remotely sensed instruments typically discretize a continuous natural surface into a uniform grid of equally sized and shaped pixels (Fisher, 1997; Jupp, *et al.*, 1988). This arbitrary sampling of grid units by remote sensing instruments does not provide a suitable model for nature, and as a result there is no intrinsic geographical meaning to the spectral measures recorded by remote sensing systems (Marceau, *et al.*, 1994a). This problem is demonstrated as the difficulty in extracting accurate, reproducible information from images of varying resolutions, and in this respect is similar to a phenomenon understood to human geographers as the modifiable areal unit problem (MAUP) (Openshaw, 1984). The MAUP is two sets of interacting problems which are related to the spatial scale of the data and any need for aggregation of the spatial data. There are two primary problems within the MAUP,

• a variety of different results may be computed for the same data as it is increasingly aggregated (scale problem), and

• the data may also be aggregated in a variety of ways (aggregation problem).

The scale problem refers to the variation of results that can be obtained when the same areal data are combined into progressively larger units of analysis, and indicates a failure to discriminate the objects of geographical inquiry. The aggregation problem arises from the large number of ways in which these areal units can be combined, and reflects a failure to understand the processes at work between scales. The integrity of the analysis is dependent upon the knowledgeable integration of the data during analysis through an understanding of the geographical phenomenon taking place and the scale of the initial data collection. Further, the scale of the map or image dictates the level of detail that may be represented (Table 3.4). The required scale for analysis or model input will dictate the detail of data acquisition.

**Table 3.4. Levels of plant recognition in forestry to be expected at selected image scales (after Avery and Berlin, 1992)**

| Type or Scale | General Level of Plant Discrimination |
|---|---|
| Earth Satellite Images | Separation of extensive masses of evergreen versus deciduous forests |
| 1:25,000 to 1:100,000 | Recognition of broad vegetative types, largely by inferential processes |
| 1:10,000 to 1:25,000 | Direct identification of major cover types and species occurring in pure stands |
| 1:2,500 to 1:10,000 | Identification of individual trees and large shrubs |
| 1:500 to 1:2,500 | Identification of individual range plants and grassland types |

The amount of variance that is captured is a function of the scale and the accuracy of any modeled results will be a function of properly representing the original variance (Marceau, *et al.*, 1994a). The scale of the geographic data implies a region of representation and an associated level of variance (Levin, 1993). Point data are often physically collected and scaled to represent a larger area (Norman, 1993) which implies broad homogeneity of the collected characteristics. The ability of the point data to capture the characteristics of a larger region gives rise to issues of spatial scale and aggregation. Collection of structural

information at a number of locations within the larger area at the local scale enables the assessment of the appropriateness of the data collected to represent a larger area. Utilization of estimates made at the local level with high spatial resolution data may be integrated with data collected at lower spatial resolutions to increase the accuracies of regional estimates of spatially varying phenomena (Wulder, *et al.*, 1996c).

## 3.5. AERIAL PHOTOGRAPHY

Aerial photography is the oldest and most frequently utilized form of remote sensing, originating with the merging of a photographic camera and a balloon platform in 1859. The spatial resolution of aerial photographs is very high and is limited mainly by film properties. The spectral resolution of panchromatic is defined as the range from 0.25 to 0.7 μm, with the potential for collection of other spectral ranges (Avery and Berlin, 1992). For forestry applications the spectral range from 0.5 to 0.7 μm is most commonly used. Aerial photography is the most frequently utilized remote sensing tool for the assessment of forests (Gillis and Leckie, 1996). The use of aerial photographs in the estimation of biophysical parameters is infrequent in the literature in comparison to usage in forest inventory (Table 3.5).

### 3.5.1 Aerial Photography for Forest Inventory and Biophysical Parameters

The photogrammetric interpretation of aerial photographs in forestry is normally an analog process involving three stages:

1. photo reading,
2. photo measuring, and
3. answer deduction (Watts, 1983).

Photo reading is the recognition of familiar objects, such as roads or trees; photo measuring is the application of photogrammetric methods in the measurement of tree heights, crown

diameters, or topographic contours; and, answer deduction is the derivation of information not directly obtainable from the photograph, such as tree species or tree condition (Watts, 1983). Estimation of inventory and biophysical parameters is undertaken as a potential component of the answer deduction phase. The technology to allow for the digitization of aerial photographs is a relatively recent development, with the analog approaches being better established and more diverse.

**Table 3.5. Summary of the research related to the use of aerial photography in the estimation of forest inventory parameters**

| Detail | Description | Reference |
|---|---|---|
| Analog Methods | | |
| Texts; manuals | the analog field of air photo interpretation is beyond the scope of this study; referred to are a selection of texts and manuals related to the aerial photograph of forests | Watts, 1983; Avery and Berlin, 1992; Sayn-Wittenstein, 1978 |
| Stem counts | manual interpretation of 35-mm aerial photographs to count stems and determine species; greatest success found for dominant species | Needham and Smith, 1987 |
| History, present, and possibilities | good survey of remote sensing technologies in a Canadian context; from aerial photography to current and potential future remote sensing techniques; presents costs of different techniques | Leckie, 1990 |
| Map production | summary of forest inventory in Canada with an emphasis on actual map production; photo acquisition timing, quality, scales, interpretation, organization, procedures and accuracy are presented | Leckie and Gillis, 1995 |
| Digital Methods | | |
| Digitization of aerial photographs | scanning, digitizing, georectification or orthorectification of aerial photographs, to enable registration to GIS based forest inventory maps | Leckie, 1990; |
| Classification of digitized air photographs | a method is outlined to account for topographic effects, lens falloff, and hot-spot effects of digitized air photographs | Dymond, 1992 |
| Applied geostatistics | compared semivariance and root mean square texture information; root mean square provided similar results with less computation needed; processed digitized aerial photographs | Lark, 1996 |

## 3.6. SATELLITE REMOTE SENSING OF FOREST STRUCTURE

With the launch of the first Landsat satellite in 1972 systematic, synoptic, repetitive, mid-resolution (80 m) multispectral images of the Earth's surface were available from space. Data capture, transmission, storage, and analysis technologies have increased substantially since the first Landsat, with a wide variety of spectral, spatial, and temporal options available to users of satellite image technology (Table 3.6).

**Table 3.6. Most frequently utilized Earth resource satellite systems (Avery and Berlin, 1992)**

| Sensor | Spectral Range (μm) | Number of Spectral Bands | Spatial Resolution (m) | Temporal Resolution (days) |
|---|---|---|---|---|
| Landsat | | | | |
| Multispectral Scanner (MSS) | 0.5-0.6 | 4 | 80 | 16 |
| | 0.6-0.7 | | 80 | |
| | 0.7-0.8 | | 80 | |
| | 0.8-0.11 | | 80 | |
| Thematic Mapper (TM) | 0.45-0.52 | 7 | 30 | 16 |
| | 0.52-0.60 | | 30 | |
| | 0.63-0.69 | | 30 | |
| | 0.76-0.90 | | 30 | |
| | 1.55-1.75 | | 30 | |
| | 2.08-2.35 | | 30 | |
| | 10.4-12.5 | | 120 | |
| SPOT | | | | |
| HRV (XS) | 0.50-0.59 | 3 | 20 | 26 |
| | 0.61-0.68 | | 20 | |
| | 0.79-0.89 | | 20 | |
| HRV (P) | 0.51-0.73 | 1 | 10 | 26 |

The use of satellite data in the estimation of forest structure has been directed at the estimation of biophysical parameters and the accurate estimation of forest inventory parameters. The L-resolution sensors which have been available up to this point have not provided the high accuracy inventory information required by forest managers (Gillis and Leckie, 1996). The ability to estimate biophysical parameters and inventory information from satellite digital multispectral remote sensing systems is addressed in the next sub-section.

### 3.6.1. Satellite Estimation of LAI

The utility of remotely sensed data in the estimation of LAI has been widely recognized and studied (Table 3.7). Remotely sensed data provides the ability to assess LAI in a synoptic, digital, and repeatable manner, at a variety of scales, allowing for mapping and modeling at regional and global scales (Loveland, *et al.*, 1991; Running, *et al.*, 1994). In the estimation of LAI from above the canopy two general approaches are the most frequently and successfully applied:

1. empirical studies involving spectral reflectance values, and
2. stochastic or deterministic canopy radiation models

Complex canopy radiation models have been developed (Li and Strahler, 1985; Wu and Strahler, 1994) to assess the structure of forest canopies which take into account the effects of solar elevation, diffuse and direct radiation, and spectral quality (Waring and Schlesinger, 1985). In comparison, empirical spectral studies are normally based upon the relationship between vegetation indices, such as the normalized difference vegetation index (NDVI) and LAI (Chen, 1996). The relationship between LAI and NDVI is asymptotic resulting in poor estimation above LAI of approximately 4 (Figure 3.1) due to the overlapping of vegetation as both stand structural complexity and LAI increase (Running, *et al.*, 1986; Franklin, 1986; Spanner, *et al.*, 1990; Baret, *et al.*, 1988; Baret and Guyot, 1991; Asrar, *et al.*, 1984; Spanner, *et al.*, 1994; Smith, *et al.*, 1991b).

**Table 3.7. Summary of the research in estimation of LAI from above the forest canopy with satellite instruments or spatial physical data stored in a GIS**

| Detail | Description | Reference |
|---|---|---|
| Canopy radiation models | stand models based upon the relationship sunlit and shaded portions of the canopy; assessment of the effect of mutual shadowing, crown shape, topography | Li and Strahler, 1985; Li and Strahler, 1992; Wu and Strahler, 1994; Li, *et al.*, 1995; Schaaf, *et al.*, 1994 |
| Spectral channels and ratios | assessment of empirical relationships between spectral values, band ratios and LAI | Peterson, *et al.*, 1987; Spanner, *et al.*, 1990; Chen and Cihlar, 1996 |
| Optical/SAR fusion | multi-source remote sensing through the fusion of optical and SAR data for the empirical estimation of LAI | Wulder, *et al.*, 1995; Franklin *et al.*, 1994 |
| Seasonal LAI from NDVI | estimation of the seasonal variability of LAI | Curran, *et al.*, 1992 |
| MIR correction for canopy closure | applied a rated MIR to correct NDVI for the level of canopy closure | Nemani, *et al.*, 1993 |
| LAI from existing information | the determination of LAI may be based upon previously mapped data and known relationships stored and assessed in a geographic information system | Franklin, 1995; Franklin and Stephenson, 1996 |
| Semivariance of simulated images | scene semivariance has also been demonstrated to contain a direct relationship with canopy structure | St-Onge and Cavayas, 1995 |
| Evaluation of vegetation indices | comparison of the ability vegetation indices to estimate LAI; introduction of a modified simple ratio | Chen, 1996 |
| Pixel decomposition | an attempt to discern the spectral contents of a pixel, in conjunction with geometrical optical modeling has also been applied to the estimation of forest structural characteristics | Hall, *et al.*, 1995; Peddle, *et al.*, 1997 |
| LAI from vegetation indices | estimation of hardwood and mixed conifer-hardwood forest LAI from a variety of vegetation indices | Fassnacht and Gower, 1997 |

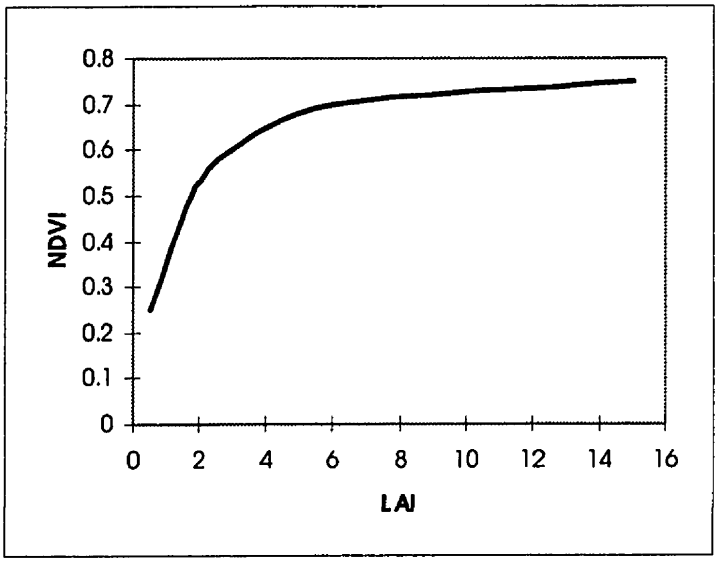


**Figure 3.1. Simulated relationship between LAI and NDVI (after Spanner, *et al.*, 1990). Demonstrated is the saturation of NDVI response due to vegetation overlap as stand structural complexity increases.**

Current analysis techniques and understanding of satellite data have provided relatively poor estimates of forest structure due to limitations of sensor spatial, spectral, and temporal resolution. No better information source is currently available for regional and global assessment of forest biophysical parameters.

### 3.6.2. Satellite Estimation of Inventory Parameters

The forestry community is the largest market for satellite data in Canada of any application field, accounting for approximately 22% of the annual sales of satellite imagery (Leckie, 1990). The satellite estimation of inventory parameters offers the potential for large area estimation of forest stand parameters at a low cost (Table 3.8) enabling inventory and change detection analyses to be undertaken (Danson, 1987).

Human visual assessment of aerial photographs continues to be the remote sensing inventory method of choice. Conventional methods of interpretation are both time consuming and costly and results may vary between analysts. The development of inventory techniques

based upon image processing of multispectral satellite imagery increases the potential for reduced costs and automation. Table 3.9 presents a summary of studies which have attempted to assess forest inventory parameters, most of which are empirically related to ground measures (Danson, 1987; Franklin, 1994). (Airborne simulations of satellite sensors are also included in this summary.)

**Table 3.9. Summary of the research in estimation of inventory parameters from above the forest canopy with satellite instruments**

| Detail | Description | Reference |
|---|---|---|
| Landsat MSS | a test case for operational mapping with the mid-resolution Landsat MSS; good agreement at scale of analysis | Bryant, *et al.*, 1980 |
| Landsat TM | volume estimation; assessment of empirical relationships between forest stand parameters and reflectance data | Franklin, 1986 |
| Landsat and ancillary data (DEM) | automated system for forest classification and inventory; use of MSS reflectance, texture, and digital elevation model | Franklin, *et al.*, 1986 |
| PCA of Landsat TM | poor estimation of stand density; principal components analysis used to select bandsets for softwood discrimination | Horler and Ahern, 1986 |
| SPOT-1 HRV inventory | SPOT-1 correlation study between reflectance data and DBH, canopy closure, height, density, and age; | Danson, 1987; De Wulf, *et al.*, 1991 |
| SPOT and TM | volume estimation; estimation of coniferous forest volume with correlation and regression relationships; significant relationships were found between softwood volume and the log of reflectance data | Ripple, *et al.*, 1991 |
| Multi-sensor | experiment to estimate crown closure from spectrally un-mixed classified imagery | Gong, *et al.*, 1993 |
| Landsat TM | visually assisted species identification; digital enhancements to assist analog interpretation; use of PCA and linear band combinations | Beaubien, 1994 |
| Volume estimation | accuracy of volume estimates found to be within 25% of field estimates; effects of forest cover, terrain, and scale assessed upon timber volume estimation with thematic mapper data in a rocky mountain site; reflectance not related to volume | Gemmel, 1995 |

## 3.7. NEW GENERATION OF COMMERCIAL HIGH RESOLUTION SATELLITES

The knowledge acquired from the analysis of airborne high resolution data will soon be applicable to a new suite of proposed high spatial resolution satellites. In the near future, high spatial resolution satellites will provide spatial data at a resolution of approximately 4 m multispectral and 1 m panchromatic. A complete discussion of the high resolution satellite systems is beyond the scope of this thesis, but a summary listing of proposed sensors is provided to indicate the types of systems which will be available (Table 3.10). The ability to perform forest inventory and structural analysis from a stable satellite platform with an image footprint of greater than 10 km should soon be possible (Fritz, 1996).

**Table 3.10. Specifications and proposed launch dates of a selection of high resolution satellites (Aplin, *et al.*, 1997)**

| Country | Program | Scheduled Launch | Resolution in Meters | | No. of Bands |
|---|---|---|---|---|---|
| | | | Pan-chromatic | Multi-spectral | |
| France | Spot 5B | 2004 | 5 | 10 | 4 |
| Japan | ALOS | 2002 | 2.5 | 10 | 4 |
| France | Spot 5A | 1999 | 5 | 10 | 4 |
| U.S. | GDE | 1998 | 1 | | |
| U.S. | OrbView | 1998 | 1, 2 | 8 | 4 |
| U.S. | Space Imaging | 1998 | 1 | 4 | 4 |
| U.S. | Eyeglass | 1997 | 1 | | |
| U.S. | Earth Watch (QuickBird) | 1997 | 1 | 4 | 4 |
| U.S. | Earth Watch (EarlyBird) | 1997^ | 3 | 15 | 3 |
| U.S. | TRW Clark | 1997 | 3 | 15 | 3 |
| U.S. | CTA Lewis | 1997* | 5 | 30 | 384 |

~Table contents created from review of press releases, Internet documentation, and Fritz (1996)
^Launched December 24, 1997, as of December 28/97 communication with the satellite has been sporadic, satellite now in uncontrolled orbit
*Launched August 23, 1997, technical failure resulted in re-entry September 27, 1997

The availability of ≈1m spatial resolution data is of relevance as the image processing that is undertaken in this thesis is upon 1m spatial resolution data (Section 6.3.1). The methods and applications developed may provide insights to ability estimate forest structural parameters from the ≈1m spatial resolution satellite data. Small changes in the spatial resolution of high resolution imagery have a significant effect on image information content. For example, the parameter tree crown size may be distinguishable at 0.5m but no longer at 1.0m (Lévesque and King, 1995). These results are consistent with the findings of St-Onge and Cavayas (1995) who could no longer estimate crown diameter once simulated imagery was degraded from 0.36m to 2.16m. A simulation study assessing the change in image texture as a function of image resolution, as indicated by image semivariance, also illustrated the change of information content at differing image spatial resolutions (Bruniquel-Pinel and Gastellu-Etchegorry, 1998). The information content at a given spatial resolution, in conjunction with the size of the trees in the scene, result in unique image structural conditions relating forest structural information of a particular size regime.

## 3.8. HIGH SPATIAL RESOLUTION AND AIRBORNE MULTISPECTRAL REMOTE SENSING

Airborne remote sensing provides a flexible operational and experimental tool. The ability to remotely sense the surface of interest at a desired time, with the chosen technical specifications, is the key feature of airborne remote sensing. Sensors such as the compact airborne spectrographic imager (*casi*) provide high spectral and spatial resolution (see Table 3.11 for *casi* technical specifications). Airborne remote sensing has limitations due to the instability of the platform, resulting in the need to correct for image attitude (Anger, *et al.*, 1996). The high resolution data collected creates an H-resolution environment with the associated increase in variance over present satellite systems. The increase in variance results

in problems in the application of traditional remote sensing techniques, such a multispectral classification (Gougeon, 1995b). Due to low flying altitudes, high resolution, and sensor engineering, airborne multispectral remote sensing instruments often have a narrow image width (footprint) resulting in the need for mosaicking.

**Table 3.11. Technical specifications of the compact airborne spectrographic imager (*casi*) (from Wulder, *et al.*, 1996d)**

| Parameter | Summary |
|---|---|
| Spatial coverage | 512 pixels, 37.8° field of view across track (May be optimized to 44.7° with a motorized aperture lens.). Ground resolution governed by aircraft speed, altitude, and sensor configuration time. Typically one to ten meters.* |
| Spectral coverage | 545 nm spectral range within 400 nm to 1000 nm. Using 288 channels; 2.2 nm spectral resolution, with 1.9 nm sampling interval. |
| Spatial mode | Full spatial (512 pixels) resolution across 37.8 across track field of view for up to 19 user selected bands. |
| Spectral mode | Full spectral (288 pixels) resolution for up to 39 look directions across the 37.8• field of view. Includes a single band, full spatial resolution scene recovery channel. |
| Enhanced spectral mode | Full spectral (288 bands) resolution for up to 101 look directions. Charge summation increases spatial coverage if spectral resolution is reduced (511 look directions, 48 contiguous bands at a spectral resolution of 11.4 nm). |

* In all modes, data are digitized to a precision of 12 bits.

### 3.8.1. Estimation of LAI with Multispectral Airborne Instruments

Estimation of LAI from airborne instruments is a relatively new application and is currently addressed by applying image processing techniques initially developed to assess imagery from satellite systems (Smith, *et al.*, 1991b). In general, the approaches in the estimation of LAI from airborne data have been empirical relationships between ground validated LAI and airborne vegetation indices (Table 3.12). The high variance environment requires additional information to increase the accuracy of LAI estimates. Texture has been combined with a vegetation index in the multivariate regression estimation of LAI with promising results (Wulder, *et al.*, 1996a, 1998).

**Table 3.12. Summary of the research in estimation of LAI from above the forest canopy with high resolution airborne instruments**

| Detail | Description | Reference |
|---|---|---|
| *casi* estimates of LAI | use of a ceptometer to generate validation LAI values; assessment of the relationship between LAI and NDVI; resolution from 1.58 to 2.34m | Smith, *et al.*, 1991b |
| High resolution hyperspectral | Hyperspectral *casi* collected at 5m resolution was found to be strongly related to 8 pine stands with a LAI range of 0 to 3.0 | Gong, *et al.*, 1992 |
| Multi-platform estimation of LAI, including *casi* | *Casi* estimates of LAI were included as a portion of the OTTER project; comparatively larger standard errors with the *casi* attributed to increased spectral variance | Spanner, *et al.*, 1994 |
| *casi* estimates of LAI, spectral and textural | Addition of texture to regression based relationships between vegetation indices and LAI; resolution 2 m and 1 m | Wulder, *et al.*, 1996a, 1998 |
| Digital frame camera estimates of LAI, spectral and textural | Use of spectral and second order textural information to estimate LAI; regression estimates with spectral data are improved with textural information; LAI range of 1.2 to 4.9; 0.25m digital frame camera imagery | Olthof and King, 1997 |
| Multivariate spectral estimates from shadow fractions | Estimates of LAI from three spectrally unique shadow fractions; reported $R^2$ of 0.9 with standard error of 0.34 over an LAI range of 1.12 to 4.92; 0.25m digital frame camera imagery | Seed and King, 1997 |

### 3.8.2. Estimation of Inventory Parameters with Airborne Instruments

The use of airborne multispectral instruments in the estimation of forest inventory parameters is the logical progression from aerial photographs and large scale digitized aerial photographs. Aircraft attitude correction systems (Schwarz, *et al.*, 1993), GPS (Gibbons, 1992), and image analysis techniques are being developed to the point that operational applications are possible in forestry (Table 3.13). Leckie, *et al.* (1995) present a summary of the application of airborne multispectral remote sensing to forest inventory mapping, including an operational framework consisting the following steps:

1. collection of high resolution digital multispectral imagery (≈ 0.70 m resolution),
2. calibrate the data,
3. correct the imagery for atmospheric influences,
4. correct for remaining illumination-viewer geometry effects (BRDF),
5. geometrically correct the imagery to a base map,
6. apply enhancements to help discern species,
7. visually interpret the forest stands, and
8. transfer stand boundaries with a quality control step to produce an inventory map stored on a GIS.

The ability to digitally process imagery is not yet developed enough for full automation of processing, but progress is being made with an increased ability to discriminate between individual conifer trees (Gougeon, 1995a; Price, *et al.*, 1996), classify individual trees (Gougeon, 1995b), and to estimate stand volume (St-Onge and Cavayas, 1995). Although visual interpretation is currently still a necessary component of operational forest inventory (Leckie and Dombrowski, 1984; Beaubien, 1994) the advances mentioned will soon make components of an inventory eligible for automation.

**Table 3.13. Summary of the research in estimation of inventory parameters from above the forest canopy with high resolution airborne instruments**

| Detail | Description | Reference |
|---|---|---|
| Advances in remote sensing for forest management | the current state-of-the-art in remote sensing technologies for forest surveys and mapping applications; costs, platforms, technologies, and future potential | Leckie, 1990 |
| Stem counting | a crown-following approach to the automatic delineation of individual tree crowns in high spatial resolution aerial images; multi-pass valley following approach | Gougeon, 1993; Gougeon, 1995a |
| Estimation of stand age with *casi* | L-resolution data hyperspectral data; analysis found a poor relationship with digital data and age classes; assessed red edge, derivative spectra, and band ratios | Niemann, 1995 |
| Forest inventory mapping | a summary of processing and techniques involved in the current level of operational use of multispectral data for forest inventory mapping | Leckie, *et al.*, 1995 |
| Empirical approach estimates of forest parameters | a regression based empirical approach was taken in the estimation of forest stand parameters; limited by lack of proper image correction and L-resolution (5 m resolution) | Baulies and Pons, 1995 |
| Semivariance and geometrical optical models | use of semivariograms to estimate height and stocking of forest stands; analysis of MEIS and simulated scene created utilizing geometrical optical models | St-Onge and Cavayas, 1995 |
| Classification of sub-metre data | trees as image objects; demonstration of classification techniques for variance rich environment; tree color line approach | Gougeon, 1995b |
| Use of the *casi* as an inventory tool | stem counts, individual tree crown areas, mean crown spectra, individual tree crown spectra are demonstrated in a forest management context | Price, *et al.*, 1996 |
| Semivariance on multi-resolution imagery | 0.25, 0.5, and 1.0 m spatial resolution pixels of forested area sensed with a digital frame camera illustrate change in forest structural content with decrease in image resolution | Lévesque and King, 1996 |
| Texture analysis in classification of inventory elements | an object specific image texture approach is developed and presented; the ability to place inventory parameters in proper class is increased with object specific texture of H-resolution imagery | Hay, *et al.*, 1996 |

## 3.9. OTHER TECHNOLOGIES IN THE ESTIMATION OF FOREST STRUCTURE

The remote sensing of forests is undertaken with more technologies than those rigorously presented in this paper. Development has been undertaken on passive and active remote sensing systems (see Table 3.14 for a summary). Digital frame cameras, are an alternative to pushbroom scanners and imaging spectrometers that also provide detailed spatial and spectral information. Digital frame cameras acquire multispectral imagery similar to a digitized aerial photograph, often with one camera per wavelength range requiring multiple camera systems for multispectral imagery. Digital camera sensor technology is flexible in allowing many configurations, such as multiple single cameras with filters, single cameras with a filter wheel or optical beam splitting, and low cost imaging spectrometers using a spatially variable filter or grating (King, 1995). Imaging spectrometers provide spectral information for a large number of narrow spectral bands for each pixel resulting in a full spectral curve for each pixel (Vane and Goetz, 1993). However, the spectral channels collected are highly correlated, resulting in much redundant spectral data. The strength of imaging spectrometer data is in applications such as spectral curve analysis, end member collection for spectral mixture analysis, and for the identification of sub-sets of critical bands. Active remote sensing systems are becoming more prevalent as laser and radar technology are applied to forestry studies. Airborne laser systems emit a laser signal and time the response to create a profile of the top of the tree canopy (Leckie, 1990). Radar systems emit microwave energy and record the signal that is scattered back to the sensor. In addition, spatial information technologies are being developed to provide for new options for storage and analysis of collected data with geographical information systems (Ehlers, *et al.*, 1989).

**Table 3.14. Brief summary of new technologies in the estimation of forest structure**

| Detail | Description | Reference |
|---|---|---|
| GIS integration with remote sensing | review papers demonstrating the synergy between remote sensing and GIS; Trotter focuses on GIS in natural resource management. | Ehlers, *et al.*, 1989; Davis and Simonett, 1991; Trotter, 1991 |
| Radar literature review | thorough survey of radar remote sensing applications for forestry applications; literature review; commissioned for CCRS | Werle, 1989 |
| Airborne lasers systems | survey of airborne laser systems, demonstrated an ability to discern canopy closure, tree height, ground elevation and stand density | Leckie, 1990 |
| GPS | global positioning systems may provide for improved placement of sample plots and integration of physical data to remote sensing and GIS analysis | Gibbons, 1992 |
| Imaging spectrometry | introduction to special issue on terrestrial imaging spectrometry; review of technology and progress in imaging spectrometry based upon AVIRIS data | Vane and Goetz, 1993 |
| Radar investigations of forests | biomass relationship to SAR data; forest backscatter characteristics; backscatter models related to forest cover | Kasischke, *et al.*, 1994; Sun, *et al.*, 1991; Hoekman, 1985 |
| Digital frame cameras / Videography | excellent survey of the history, development, technology, and application of digital frame cameras; full summary of the use of airborne videography | King, 1995 |
| GIS storage and analysis of forestry data | integration of GIS and a classified remotely sensed image to improve estimates of LAI by decomposing polygons; improvement of classifications for model input; NPP estimation and assessment | Franklin, *et al.*, 1997a, 1997b; Wulder, 1998a; Wulder, *et al.*, 1997c |

## 3.10. CHAPTER SUMMARY

The history and techniques for the measurement of forest structure from *in situ* observations to state-of-the-art high spatial resolution multispectral airborne imaging spectrometers were presented in this chapter. Direct and indirect ground based measures of LAI provide the ground validation data for remote sensing projects. The information content in relation to the image spatial resolution was also presented. The ability to extract information from remotely sensed imagery is often limited by the technology available.

Advances in instrument technology, both in airborne and satellite areas, promise a rich information source for the study of forest landscapes.

The spatial resolution available for analysis in this present study, at 1m spatial resolution, enables the extraction of detailed forest information. Yet, even at 1m spatial resolution the spatial structure of the imagery, which results from the discretization of the continuous forest landscape, is at the limit of tree discernment and beginning to relate to stand level characteristics. The foliage overlap which occurs in deciduous and mixed forests further confounds the analysis of the forest upon an individual tree basis. The information content of the imagery requires development of a technique which takes into account the spatial structure of the imagery. Current image analysis techniques, presented in the next chapter (Chapter 4), generally operate at a tree or stand level. To maximize the information content of the imagery available in this study, and upon forthcoming satellite sensors, a void in the image processing techniques may be addressed. The approach undertaken in this thesis proposes to make a contribution to the maximization of data extraction at a 1m spatial resolution sensed over deciduous and mixed forests. Subsequent chapters (Chapters 5, 7, 8, and 9) address the shortcomings of existing image processing techniques and present an alternate approach. The generation of tree clusters based upon the spatial dependence between pixels is an approach to extract detailed forest inventory and biophysical data from available remotely sensed imagery.

# 4. IMAGE ANALYSIS TECHNIQUES FOR THE EXTRACTION OF FOREST STRUCTURE

***Chapter Objective:*** *Survey existing information extraction techniques, which may be applied to discern forest structural properties at a spatial resolution of 1m.*

## *4.1. INTRODUCTION*

The change in Canadian forest management policy, stressing ecosystems over stands, has blurred the traditional lines between forest science and forest inventory. Successful assessment of forest structure with high spatial resolution instruments may borrow from the established L-resolution satellite techniques and develop new techniques suited to the properties of the new technology. The data collected by multispectral remote sensing instruments is in a digital form, allowing for mathematical analyses and manipulations. The information content of remotely sensed data is enhanced by the ability to apply image analysis techniques to extract subtle structural information. Image processing provides the ability to assess the interrelationships between pixel location and values. Following is an assessment of the image analysis techniques which are appropriate for the extraction of forest structural information from high spatial resolution digital imagery. For a full review of image analysis techniques for the extraction of forest structural information see the review paper by Wulder (1998c).

As mentioned in Section 3.4.3, the relationship between image spatial resolution and the objects of interest is paramount to what type of forest information may be extracted. The 1m spatial resolution imagery of mixed and deciduous forests available for this study are at the transition between H- and L-resolution. The existing imagery analysis techniques for the

extraction of forest structure were not developed with consideration specifically to the image structure present in the images available for this study. The survey of related image processing techniques in this chapter will demonstrate which image processing techniques may be appropriate while also exhibiting which techniques are not, providing the rationale for the selection of the tree clustering technique based upon pixel spatial dependence.

## 4.3. VEGETATION INDICES

Characteristically, green plants strongly absorb visible electromagnetic radiation and strongly scatter near-infrared radiation (Curran, 1980). This is as a result of pigments, especially chlorophyll, which absorb visible wavelengths, while the air-water interfaces between the intercellular spaces and cell walls cause multiple refraction, resulting in high net reflectance values in the near-infrared wavelengths (Gausman, 1977). Vegetation indices have been developed to emphasize the difference between the absorption in the visible and reflectance in the infrared through mathematical processing of multispectral bands, such as ratioing and differencing. The normalized difference vegetation index is a commonly used vegetation index, calculated from the red (R) portion of the visible and near infrared (NIR) radiation, in the form of,

$$NDVI = (NIR-R) / (NIR+R) \qquad [2]$$

initially developed as a measure of green leaf biomass (Tucker, 1979). NDVI has also been demonstrated to assist in compensation for changing illumination conditions, surface slopes, and viewing aspects (Avery and Berlin, 1992). Canopy interception dictates the upper limit for vegetation to utilize available sunlight for photosynthesis which further drives production (Law and Waring, 1994). NDVI captures information relating to the amount of radiation absorbed in the visible (Red) and reflected in the infrared (NIR) by vegetation.

Vegetation indices, such as NDVI, may be viewed as a surrogate for scene vegetation content and are applied in an attempt to relate to physical measures of vegetation, such as LAI. Other vegetation indices may be utilized with some success, such as RVI, demonstrated by Spanner, *et al.*, (1994) to be well related to LAI. Nemani, *et al.*, (1993) utilized the middle infrared of the Landsat sensor to apply a correction for the effects of changes in the level of canopy closure on the computation of NDVI. There are many different vegetation indices which may relate to particular characteristics in a given case (Huete, 1988; Chen, 1996; Myneni, *et al.*, 1995). Chen and Guilbeault (1996) found that in relationships between a vegetation index and LAI, that the indices based upon simple ratios of two bands were best correlated with ground measurements of LAI and the fraction of photosynthetically active radiation (FPAR). Limiting the effectiveness of vegetation indices in the estimation of forest structure is that relationships are frequently non-linear and reach an asymptote at an LAI value of approximately 4 (recall Figure 2.2, p. 21) (Running, *et al.*, 1986; Franklin, 1986; Spanner, *et al.*, 1990; Baret, *et al.*, 1988; Baret and Guyot, 1991; Asrar, *et al.*, 1984; Spanner, *et al.*, 1994; Wulder, 1996b).

By definition, NDVI is a function of infrared and red reflectance values (Formula 2). Table 4.1 is a mathematical illustration of the lack of variability in NDVI values for a series of infrared and red reflectance values which result from a diversity of image features. The spectral conditions which result in the same NDVI could be the result of differing vegetative and forest structural conditions or from non-vegetated features. Variability in forest structural characteristics, such as stand density, crown closure, or species composition could be accounting for the variability in infrared and red reflectance. Surface conditions which result in low infrared and red spectral values, such as a sandy loam soil (Avery and Berlin, 1992), may result in an NDVI value which causes confusion with vegetation. Conversely, high

infrared and red values, while physically unlikely, could also produce a NDVI value expected for vegetation. The presentation of the mathematical argument is intended largely to illustrate that spectral vegetation indices, while useful, must be applied with caution. As a result, an attempt to incorporate ancillary information to assist NDVI in the assessment of forest structure is indicated.

**Table 4.1. Variability in NDVI with changing infrared (IR) and Red reflectance values**

| IR | Red | NDVI | IR / Red |
|---|---|---|---|
| 10 | 2.5 | 0.60 | 4 |
| 20 | 5 | 0.60 | 4 |
| 30 | 7.5 | 0.60 | 4 |
| 40 | 10 | 0.60 | 4 |
| 50 | 12.5 | 0.60 | 4 |
| 60 | 15 | 0.60 | 4 |
| 70 | 17.5 | 0.60 | 4 |
| 80 | 20 | 0.60 | 4 |
| 90 | 22.5 | 0.60 | 4 |
| 100 | 25 | 0.60 | 4 |

## *4.3. TEXTURE IN THE CONTEXT OF FOREST STRUCTURE*

The preceding section demonstrated the shortcoming of NDVI in the estimation LAI due to an asymptotic relationship for LAIs greater than 3. The vegetation index values saturate as a function of being derived from a remote platform which may only view the vertical expression of a stand. As LAI values increase, the horizontal complexity of the stand also increases, proving difficult to measure from a vertical viewing remote platform. For example, stands with differing horizontal levels of complexity may appear the same to a vertical viewing sensor (recall Figure 2.3, p. 23). Accordingly, stands with varying vegetation composition and structure may have similar vegetation index values due to a similar vertical expression.

The introduction of spatially sensitive image texture variables in the estimation of LAI increases the accuracy of LAI values obtained remotely in relation to field collected data,

especially for LAI values greater than 3 (Wulder, *et al.*, 1996a). The variation in texture is related to changes in the spatial distribution of terrestrial vegetation. Texture derivatives are supplemental to the image data, and, accordingly, provide an accessible, low cost, additional information source. Image tone alone is of limited utility in the estimation of LAI. The addition of texture, representing the spatial variation in tones, will add structural information to the empirical prediction of LAI. The textural values act as surrogates for the actual physical canopy composition. Texture has been demonstrated to add structural information to the spectrally derived vegetation indices and improve estimates of LAI (Wulder, *et al.*, 1996a, 1998). Texture has been utilized in remote sensing as ancillary information in multispectral classifications of L-resolution imagery of vegetation cover (Franklin and Peddle, 1990; Frank, 1984) and H-resolution of forest structure (Table 4.2).

**Table 4.2. Summary of texture in H-resolution analysis of forest structure**

| Detail | Description | Reference |
|---|---|---|
| Development of textural signatures for MEIS forest scene | the development of textural signature to compare to spectral signatures to assist in region growing segmentation of MEIS forest imagery | Gougeon and Wong, 1986 |
| Object-specific imager texture analysis | an object-specific image texture analysis of H-resolution forest imagery improve the ability to place forests into structural classes based upon the texture created by the inter-relationship between mature conifer trees | Hay, *et al*, 1994; Hay, *et al.*, 1996 |
| Comparison of texture measures in the empirical estimation of LAI | first order, second order, and a newly developed semivariance moment texture are compared for ability to estimate LAI; a spectral dependency is found between species heterogeneity, texture derivative, and predication ability | Wulder, *et al.*, 1997b |
| Digital frame camera estimates of LAI, spectral and textural | Use of spectral and second order textural information to estimate LAI; regression estimates with spectral data are improved with textural information; LAI range of 1.2 to 4.9; 0.25m digital frame camera imagery | Olthof and King, 1997 |
| Texture combined with NDVI | texture is combined with NDVI to provide an increase in empirical ability to estimate LAI over NDVI alone | Wulder, *et al.*, 1996a, 1998 |

### 4.3.1. Texture and NDVI in the Estimation of LAI

Texture has been demonstrated to be valuable in the statistical estimation of LAI (Wulder *et al.*, 1996a). Yet, many texture measures are limited by subjective user based decisions, such as the texture measure to apply and the size of window. In this example, digital image semivariance is computed to assess the mean spatial dependence within image sample plots to dictate customized window sizes (Franklin, *et al.*, 1996) for the derivation of first and second order texture measures. First-order texture is a representative statistical value for the central cell of a fixed moving window which is passed over the image (Jensen, 1986). Second-order texture measures are not computed directly from the image values but rather from the statistical distribution of local properties in the spatial domain. An example is the calculation of second-order statistics from pixel relationships stored in a gray level co-occurrence matrix (Haralick, *et al.*, 1973). A hybrid spatial measure is also presented in this example, semivariance moment texture, or SMT (Wulder *et al.*, 1998). SMT is derived from the semivariance response found at each pixel. At each pixel semivariance response is computed and significant locations of the semivariance response are utilized as spatial descriptors. The nugget, sill, range, mean semivariance between nugget and sill, and the slope of the semivariance response between nugget and sill, are the values which may be derived for each pixel with SMT.

The work of Wulder *et al.* (1996a, 1998) is an exploration of the relationship between LAI, NDVI, and texture. A summary of the findings of Wulder *et al.* (1998) demonstrates the potential of a variety of texture measures in the estimation of LAI from airborne spectrometer data. The relationship between LAI and NDVI is important to provide the vegetative characteristics of a stand. The relationship between LAI and NDVI is weak when considered over a variety of stands simultaneously, due to spectral variation between stands. Within

stands, the species heterogeneity will also diminish the relationship with LAI and decrease the strength of the relationships. The spectral and structural variability between stand types dictates the need for stratification between stand types for analysis. For hardwood stands, a strong initial relationship between LAI and NDVI may be found based upon broad canopy elements and species spectral similarity. In hardwood stands, primary texture measures and SMT values are found to be best related to LAI. Primary texture measures are most successful for the estimation of homogeneous cover types. SMT measures are sensitive to the spatial characteristics of the stand such as crown closure and density and as a result are useful in the estimation of a variety of cover types. Multivariate estimation of LAI from NDVI and two texture measures resulted in an increase of coefficient of variation to 0.61 from an initial 0.42 between LAI and NDVI. An assessment of softwood plots demonstrated the need for stratification between regeneration regimes. In plantations the tree planting pattern results in a strong textural component to the softwood stands. Mixed wood plots, containing both deciduous and coniferous species, consequently contain spectral variability based upon both species and vegetation distribution. As a result, texture proved significant in increasing the ability to estimate mixed forest LAI.

Based upon these encouraging results, further investigation of image spatial information in the estimation of forest structure will be pursued. Some conclusion which may be drawn from these previous studies are,

- first- and second-order texture are capturing different information based upon factors such as species spectral response and density,
- SMT is generating data related to the distribution of vegetative elements of a stand and the spectral response of these elements, and
- the performance of the texture measures in the predictive equations of LAI is found to be dependent upon forest cover type. Accordingly, in the spectral

estimation of LAI, a specific texture measure may be required as input on a species specific basis.

As described above, in the summary of the work by Wulder *et al.* (1996a, 1998), spatial information was incorporated into empirical models for the estimation of LAI with promising results. One problem with the empirical estimation of LAI from image spectral and spatial values is the selection of pixels from which to extract the reflectance information.

## 4.4. DIGITAL TREE CROWN DELINEATION

The ability to digitally delineate tree crowns of a forest allows for improved estimation of inventory elements such as density, volume, and canopy closure. Forest stand density estimation has been attempted on L-resolution data with an accuracy too low for inventory usage, but high enough for regional density characterization (Franklin, 1994; Wu and Strahler, 1994). Methods are being developed to estimate forest structure directly through the delineation of the actual objects of interest. Once delineated, trees may be classified, separated from the understory, or spectrally assessed (see Table 4.3). An international forum on the *Automated Interpretation of High Spatial Resolution Imagery for Forestry* (Leckie and Hill, 1998) demonstrated several current approaches to the delineation of tree crowns, such as valley following (Gougeon, 1998), radiance peak filtering (Niemann and Adams, 1998; Walsworth and King, 1998), edge finding (Pinz, 1998), template matching (Pollock, 1998), morphology (Barbezat and Jacot, 1998), and clustering (Culvenor, *et al.*, 1998; Wulder, 1998b).

An example of the valley following approach to stem counting and classification has been demonstrated upon H-resolution MEIS multispectral scanner data of conifer forests. Image processing techniques are applied for the isolation of conifer tree species (Gougeon, 1995a), and subsequent classification schemes for the crowns delineated on the H-resolution

imagery (Gougeon, 1995b). The tree delineation approach outlined by Gougeon (1995a) considers the dark understory areas between trees as "valleys" and attempts to join together the comparatively low valley digital numbers. An iterative approach to the joining of valley pixels results in nearly delineated trees requiring further sharpening with a rule-based strategy. The rule-based classification is based upon spatial discrimination of the trees considered as objects, and applying techniques borrowed from manual aerial photo interpretation.

A stem isolation approach based on radiance peak filtering has been presented by Hay, *et al.* 1996. Radiance peak filtering is based upon the premise that each tree in an H-resolution scene has a bright pixel which represents the apex of the tree. Passing a filter over the image and seeking the highest digital number within the filter kernel provides an estimate of tree stem locations (Dralle and Rudemo, 1997). Normally a kernel of a fixed size is passed over the image which does not account for the presence of trees of a variety of sizes. Hay, *et al.* (1996), used semivariance to customize the kernel size for the extraction of the radiance peaks. Daley, *et al.* (1998), dynamically allocated the kernel size for each pixel location based upon the local scene structure. The problem common to radiance peak filtering is a large number of pixels indicated as trees that are not. The problem of false positives has been investigated by Burnett, *et al.* (1998), through the introduction of spatial autocorrelation and spectral directionality. To account for false positive identification based upon multiple radiance peaks for an individual tree crown upon high spatial resolution digitized aerial photography, Walsworth and King (1998) compare a cumulative pixel transversal, or cost surface, to a local maxima filter. Among the results indicated is the ability of a double aspect technique of image decomposition which provides information relating changes in tree size, density, and illumination conditions.

Edge finding techniques for the isolation of tree crowns often work in conjunction with a radiance peak filter. Once the radiance peak is isolated the edges to the image object may be delineated based upon an iterative search approach (Pinz, 1998). Template matching approaches are based upon the spectral characteristics found within an image scene compared to synthetic image templates. The synthetic image templates are generated based upon known stand characteristics which may be matched to image scenes to indicate the crown distribution present in the imagery (Pollock, 1998; Larsen, 1998). The morphology of digitized airphotos has also been presented as a means to extract tree crowns (Barbezat and Jacot, 1998).

The overlap of foliage common to deciduous species results in difficulty in the delineation of individual stems. The foliage of co-dominant species are found to overlap, while suppressed trees growing beneath the more dominant trees result in spectral confusion. Wulder (1998b), has approached the problem through generation of clusters based upon spatially dependent groups of pixels. On 1m spatial resolution imagery of a deciduous forest the clusters represent either a large single tree or a cluster of spectrally similar trees. The clusters of trees may be spectrally classified, provide clues to crown closure, and also indicate the stand level structure. Culvenor, *et al.* (1998), demonstrate an approach to clustering based upon identification of maxima and minima pixels, of an infrared image channel, to represent crown centroids and crown edges. A user defined parameter is used to calculate a threshold value for acceptance or rejection of a pixel's membership to the crown under consideration.

The interest by the forestry and ecological communities to possess an accurate accounting of all trees within a management unit or an ecosystem is illustrated by the variety of tree crown delineation approaches. Factors which affect the remote sensing of forest canopies also have an effect on the efficacy of the tree crown delineation approaches. The relationship between the image resolution and the tree size is important, as the ability to

reconstruct trees with a number of individual pixels is often required. Cover type is also important as conifers are generally more readily delineated than deciduous species. The difficulty in finding an automated approach to tree crown delineation that is robust to all forest conditions indicates the utility of a system which pairs the automated crown detection approaches with a photointerpretation approach (Leckie, *et al.*, 1998).

**Table 4.3. Summary of stem counting in analysis of forest structure**

| Detail | Description | Reference |
|---|---|---|
| Multiple pass valley following, plus rule based improvements | a crown-following approach to the automatic delineation of individual tree crowns in high spatial resolution aerial images; complete and thorough outline of methodology and rationale; initially a valley following approach is implemented then a rule based stage improves the initial delineation | Gougeon, 1993; Gougeon, 1995a |
| Bright pixel as the crown centre | through implementation of an object specific texture measure Hay created tree objects from H-resolution imagery; the highest NDVI value (bright spot) was found to correspond with tree crowns | Hay, *et al.*, 1996 |
| Use of the *casi* of a forest management tool | implementation of Gougeon's techniques; demonstrated an ability to delineate trees, compute stem counts, stand density, canopy closure, and estimation of broad classes of DBH and height | Price, *et al.*, 1996 |
| Cellular automata and Markov transition matrices | Radiance peak filter applied to isolate individual tree locations; transitions between computed Markov transition matrices demonstrate differing forest structural information content for pixel based and neighborhood based estimates | Walsworth and King, 1997 |
| Automated interpretation of high spatial resolution imagery for forestry | An international workshop on techniques and applications related to the processing and analysis of high resolution imagery in a forestry context; example techniques are valley following, radiance peak filtering, edge finding, template matching, morphology, and clustering (summaries in text above) | Leckie and Hill, 1998 (*in press*) |

## 4.5. SPATIAL DISCRIMINATORS

The ability to discern individual conifer trees has been demonstrated in the previous section, based upon spectral differences between the overstory and understory and the implementation of rule-based procedures. The rule-based procedures which are implemented

attempt to introduce techniques utilized in the visual interpretation of aerial photographs based upon shape, size, and distribution (Gougeon, 1995a). Fournier, *et al.*, (1995) developed a catalogue of spatial discriminators for future implementation of a rule-based delineation procedure. Discrimination of stems was undertaken on 40 cm MEIS data by a photogrammetrist to assess the utility and validity of the spatial discriminators. The accuracies found from visual interpretation of the MEIS imagery based upon the classification rules was found to be within the range of accuracies expected for interpretation of aerial photographs. The 40 cm resolution data were found to be at the limit for the assessment of tree outlines and a need was expressed to apply the technique to higher spatial resolution imagery. Unfortunately, the resolution of the imagery being available for this thesis research is of too low a resolution to attempt shape detection.

## 4.6. HIGH RESOLUTION IMAGE CLASSIFICATION

Once trees have been delineated through the application of digital methods, further information is available based upon the digital numbers found within each crown. Spectral information may be extracted from each individual tree crown to enable classification to species types based upon the observed spectral response. Traditional classification tools, successfully applied to L-resolution data (Robinove, 1981; Congalton, 1991) assume pixels to be independent and normally distributed, which is not the case with the delineated tree objects. Gougeon (1995b) presents a comparison of possible multispectral classification schemes for individually delineated coniferous plantation tree crowns. Seven differing multispectral representations for the tree crowns are extracted for comparison by Gougeon (1995b):

1. mean digital number,
2. mean of sun lit crown,

3. highest digital number (brightest pixel),
4. tree color line - slope, (slope signature derived from relationships between all the bands compared individually with the infrared),
5. tree color line - mean vector and first principal component, (mean vector of tree color line in multidimensional space)
6. tree color line - mean vector, first principal component, and eigen values, (as with number 5, with the addition of the eigen values to describe the spread of the distribution), and
7. mean and covariance matrix, (the mean and covariance matrix of the distribution of pixels in multispectral space for each tree crown.

The tree color line is an attempt to generate a single value to represent the relationships found with principal components analysis (Gougeon, 1995b). A single summary value may be incorporated into the tree classification schemes. Similar maximum likelihood classification accuracy results are found for each technique with the greatest classification success demonstrated with the "mean of sun lit crown" digital number representing the spectral response of the crown.

## 4.7. IMAGE SEMIVARIANCE IN THE CONTEXT OF FOREST STRUCTURE

A variogram describes the magnitude, spatial scale, and general form of the variation in a given set of data (Matheron, 1963). Variograms have been the tool used to link models of ground scenes to spatial variation in images (Woodcock, *et al.*, 1988a). Semivariograms are a graphical representation of the spatial variability, and provide a means of measuring the spatial dependency of continuously varying phenomena (Curran, 1988; Cohen, *et al.*, 1990; Rossi, *et al.*, 1994; Brown and Bara, 1994). The semivariogram also displays the average change of a property with increasing lag, although the true variogram is continuous (Oliver, *et al.*, 1989). Semivariance is the variance per site when sites are considered as profiles or areas of pixels, and is developed from the theory of regionalized variables (Matheron, 1963, Curran, 1988; Webster, *et al.*, 1989; Cohen, *et al*, 1990; Woodcock, *et al.*, 1988b). In a remote

sensing context the sites are pixels, and the semivariance is the variance found between a pair of pixels (Lévesque and King, 1996).

### 4.7.1. Semivariance Computation

A remotely sensed image may be processed for semivariance through the computation of the relationships between pixel pairs. In the case of a transect passing across a remotely sensed image, the digital numbers $z$ of pixel transect $x$ are extracted at regular intervals (where $[x = 1, 2, \ldots, n]$). The relationship between a pair of pixels found $h$ pixels apart, or the lag distance, is recorded as the average squared difference between all pixel pairs. The semivariance, $\gamma(h)$, between pixels is half of the value of the average squared difference between pixels, and is computed as follows for pixels found $h$ lags apart is (Curran and Atkinson, 1998):

$$\gamma(h) = \tfrac{1}{2}E[Z(x) - Z(x - h)]^2 \qquad [3]$$

In each transect of values there will be $m(h)$ pairs separated by the same lag distance $h$. The value $\gamma$ is an estimate of the semivariance $\hat{\gamma}$ and is understood as a measure of dissimilarity between pixels spatially separated (Jupp, *et al.*, 1988). As a result, the semivariogram function $\hat{\gamma}(h)$ may be used to display the average semivariance at each lag in a graphical manner. For each transect there are $m(h)$ observational pairs all separated by the same lag $h$. For a given lag $h$, the semivariogram is calculated using the following formula:

$$\hat{\gamma}(h) = \frac{1}{2m(h)} \sum_{i=1}^{m(h)} [z(x_i) - z(x_i - h)]^2 \qquad [4]$$

In Figure 4.1 we present a theoretical semivariogram based upon the commonly found spherical shape model (Curran, 1988). As the example semivariogram illustrates, through the low semivariance values found between locations at the initial lags, the pixels found close together are more closely related than those located further away. The semivariance

computed for lag 0 is an estimate of the intra-pixel variability and provides an indication of the level of noise in the data, it is termed the *nugget.* As the distance between pixels increases the semivariance between the pixels also increases which results in a rise of the semivariance curve. The semivariance curve will rise until reaching the *sill,* which indicates the maximum variability between pixels. The *range* is the lag taken for the semivariance to reach the sill (Curran and Atkinson, 1998). The range provides an indication of the region of spatial dependency, the values at the lag locations greater than the range are spatially independent of the pixel from which the computation transect was initiated (Lévesque and King, 1996).

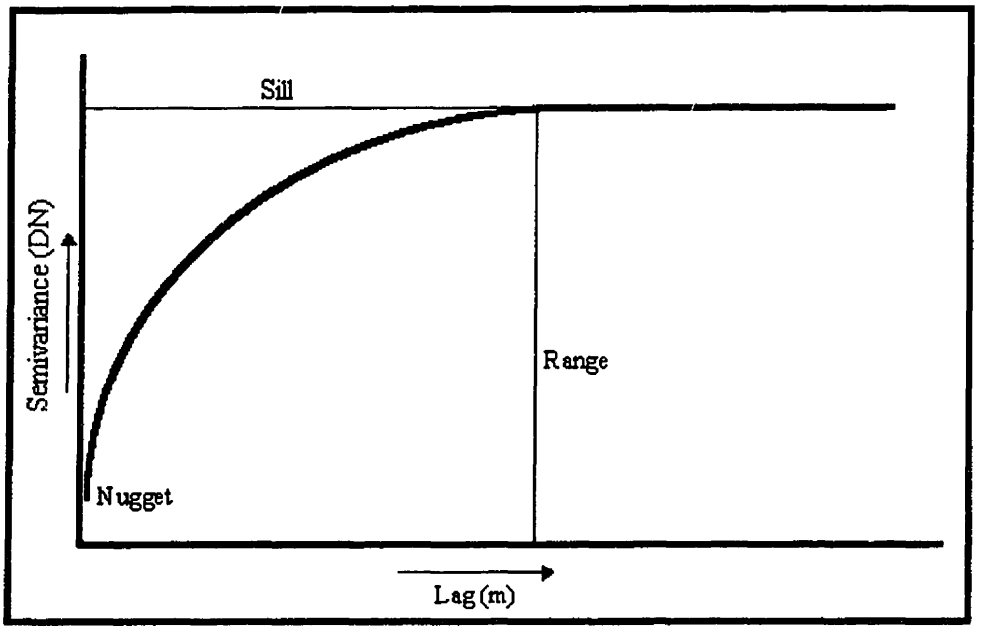


**Figure 4.1. Example spherical semivariogram showing nugget, sill, range, and curve form.**

The curve forms generated are related to the relationship between image resolution and the spatial extent of a surface cover. The form of the semivariogram is dependant upon the size and spacing of sample points or the ground resolution elements, also known as the *support.* The support is defined as the area and shape of the surface represented by each

sample point (Curran, 1988). As a result, high spatial resolution imagery is often required to fully capture the fine detail of spatial dependence characteristics present. The differing information content with varying resolution is presented in a forestry context (Lévesque and King, 1996) and urban, agricultural and forestry contexts (Woodcock, *et al.*, 1988b).

The shape of the semivariance curve is dependent upon factors such as the aforementioned support, and additional factors such as, the ground surface cover, the spectral resolution, and the orientation of the sampling transect. The heterogeneity of the ground surface cover will have an impact upon spectral distinctiveness of the support and the variance inherent to that ground cover. The impact of spectral resolution is limited as spatial features are found to be consistent for gross spatial features (Curran, 1988). The orientation of the sampling transect is important due to the often anisotropic nature of remotely sensed imagery, which results from factors such as sun elevation and planting patterns. Curran (1988) presents six semivariance curve forms common to remotely sensed imagery. The curve forms are the result of the image characteristics such as spatial resolution, support, transect direction, and surface cover. The two primary groups for the possible models are bounded and unbounded. Bounded models reach a sill, while unbounded models do not reach a sill (Oliver, *et al.*, 1989). Patterns to the relationship between the image characteristics and curve form allow for curves to be fit to modeled data (Woodcock, *et al.*, 1988a) and image data (Woodcock, *et al.*, 1988b).

In this research, semivariogram analysis is undertaken utilizing specifically developed C computer language code (Franklin, *et al.*, 1996) that computes semivariance for each pixel location within an image that is found to be within a buffer of 30 pixels from the image edges. The 30 pixel limit is invoked as that is the length of the semivariance computation transect. To account for the potential effects of image anisotropy, the image semivariance may be

computed in the Queen's case around each pixel, with the average of the eight results stored in an image channel, or in a Rook's case where 4 directions are averaged and stored. Within this thesis the semivariance range is utilized as an indicator of spatial dependence (as discussed above), and is stored as an 8 bit integer value, which may be converted to a window size (Franklin, *et al.*, 1996) or analyzed as an indication of texture (Wulder, *et al.*, 1998). The use of 8 bit integer values rather than 32 bit real values saves storage space with little loss of information. Computing a range value for each eligible pixel in the image reduces problems which arise when attempting to select a transect origin. The automated process for computing range values did so by computing semivariance for each of the Queen's case directions radiating from the central pixel. Once it is determined that a pixel is eligible for processing based upon being within the edge buffer, each direction is treated like an individual transect. For each transect the semivariance at each lag is stored in an array until the semivariance values cease to increase. The highest value, understood to be the sill, indicates the lag number to be written to an array to represent the range for that direction. This procedure is followed for all eight directions. The eight range values are then extracted from the array and averaged. The average range value is written to file and the processes is resumed for the next pixel. With this methodology a bounded semivariogram model is assumed. If an unbounded model is encountered the range is set at the maximum allowable lag location. The maximum allowable lag location is set as one third of the total transect length as the reliability of semivariance ($\gamma(h)$), decreases with increasing lag ($h$) (Curran, *et al.*, 1988).

### 4.7.2. Semivariance Application

A recent review paper by Curran and Atkinson (1998) provides: an introduction to use of semivariance in remote sensing, computation, statistical rationale, summary of application, and some examples using semivariograms, and an indication of future applications. The

summary provided by Curran and Atkinson (1998) is not application specific. The emphasis of the following summary of applications is upon forestry applications, and especially those undertaken with high spatial resolution imagery.

Image semivariance has been used extensively in the assessment of L-resolution forest structure (see Bowers, *et al.*, 1994; Cohen, *et al.*, 1990 for examples). In analysis of H-resolution forest imagery each pixel represents near pure spectral characteristics of an object. Image semivariance has been demonstrated to represent image structural information (Franklin and McDermid, 1993). St-Onge and Cavayas (1995) have utilized the information inherent in the directional variogram as a method to estimate the stocking and height of forest stands, both strongly related to LAI. Semivariance response has also been exploited in the multivariate estimation of LAI as an image textural indicator based upon extraction of discrete points from the semivariance response curve (Wulder, 1996; Wulder, *et al.*, 1997b, 1998). At a high image spatial resolution small changes in image resolution have an effect on the accuracy and ability to estimate forest biophysical parameters (Bruniquel-Pinel and Gastellu-Etchegorry, 1998; Lévesque and King, 1996). Lévesque and King (1996) present a multi-scale analysis illustrating the relationship between information content and image semivariance. For example, in the measurement of crown closure the semivariance range was found to have a 0.80 correlation with crown closure with 0.25 metre resolution imagery; with a decrease in correlation between range and crown closure to –0.16 with 0.5 metre resolution imagery.

## 4.8. CHAPTER SUMMARY

The image analysis techniques presented in this chapter provide an indication of the current state-of-the-art tool box for processing digital images of forests. Vegetation indices provide an indication of the vegetative characteristics of a particular location. Texture values provide an indication of the forest structure, based upon the spatial variability in image tones that is related to discretization of the forest by the remote sensing instrument. Digital tree crown delineation has proved successful upon conifer plantations. The ability to spectrally classify the conifer stands has also been promising. The use of spatial discriminators to digitally characterize tree crown outlines requires imagery of less than 40 cm in spatial resolution, even for the more predictable conifer vegetation arrangements. The utility of image semivariance provides an argument for continued research based upon the spatial dependence between pixels. The following chapter presents the Getis statistic as a means to characterize the spatial dependence between the pixels and we discuss how this type of information is appropriate for 1m spatial resolution imagery of deciduous and mixed forests.

# 5. THE GETIS STATISTIC

***Chapter Objective:*** *Propose an alternate spatial information extraction technique based upon spatial statistics, in particular the Getis statistic.*

## *5.1. INTRODUCTION*

To enable data collection by remote sensing instruments, the Earth's continuously varying surface is regularized into a grid of consistently sized and shaped pixels (Schowengerdt, 1997). Remotely sensed data, as a result, are often highly spatially autocorrelated. The characterization and quantification of spatial autocorrelation can provide a valuable source of information for both theoretical and applied studies in remote sensing. Consequently, various techniques have been developed to assess the spatial dependence characteristics of remotely sensed imagery. Typically such techniques yield summary measures which enable the identification of distinctive regions of spatial dependency within the image. In contrast, local indicators of spatial association (LISA) measures, focus upon variations within the regions of spatial dependence. In this chapter we provide an introduction to one such LISA measure, the Getis statistic, and indicate how it may be used in the analysis of high spatial resolution digital imagery of deciduous and mixed wood forests. The Getis statistic provides a measure of spatial dependence for each pixel while also indicating the relative magnitudes of the digital numbers in the neighbourhood of the pixel. Knowledge of the spatial dependence between pixels will permit the generation of clusters based upon the discretization of a forest landscape.

## 5.2. GETIS STATISTIC BACKGROUND

Considered generally, spatial autocorrelation arises when the value of a variable $x$ recorded at a location on the Earth's surface is related to values of the same variable at nearby locations. Thus, the measurement of spatial autocorrelation involves the simultaneous consideration of both locational and attribute information (Goodchild, 1986). In the case of remotely sensed images, the locations are pixels and the attribute data are the spectrally derived digital numbers. Positive spatial autocorrelation is said to occur when similar values of $x$ are found in spatial juxtaposition while negative spatial autocorrelation occurs when neighbouring values of $x$ are dissimilar. In general, the degree of spatial autocorrelation is not independent of the scale at which the data are analyzed, with negative spatial autocorrelation being more sensitive to scale changes (Chou, 1991). As remote sensing methods regularize continuous landscapes into a grid of equally sized and regularly spaced data in the form of pixels (Fisher, 1997), it is anticipated that there will be some degree of dependency between pixels, most likely in the form of positive spatial autocorrelation. Such dependence has potentially a dual impact on the analysis of image data. On the one hand it is a source of nuisance and error when traditional statistical techniques involving independence assumptions are applied, while on the other hand it represents information which may be exploited as an image characteristic.

The spatially autocorrelated nature of imagery was identified early in the assessment of remotely sensed data (Craig, 1979) and its effect upon traditional classification techniques was noted by Campbell (1981). Later, studies of image spatial autocorrelation examined pixel inter-relationships using a scanline technique (Labovitz and Masuoka, 1984). This approach, however, only allows spatial dependency to be assessed in a limited number of directions. A more flexible approach is provided by semivariance analysis which permits both the scale and

pattern of spatial variability in an image to be identified (Jupp, *et al.*, 1988; Franklin *et al.*, 1996). Semivariance may be computed in a given direction along a transect (Curran, 1988) or in a non-directional fashion, sometimes utilizing mean variograms (Marinda and Carr, 1994) or structure functions (Wald, 1989). Table 5.1 summarizes representative examples of this work. Note that the usual focus of semivariance analysis is on summary values which identify distinctive regimes of spatial dependence within the image. Only occasionally are values generated for an individual pixel or its immediate vicinity. Such exceptions are Woodcock and Strahler (1987) who used the local variance within a (3x3) window as an aid to determining scale effects and Marinda *et al.* (1992) who compute the semivariance in a (7x7) moving window for each pixel in a training mask. However, in the latter case it is the means and standard deviations of the semivariances so obtained which are actually used.

Spatial dependency has also been explored using spatial autocorrelation statistics such as join-counts and Moran's $I^*$ and Geary's c (Goodchild, 1986) (see Table 5.1 for examples). However, such approaches yield a single summary measure which may be unrepresentative if the nature and extent of spatial autocorrelation varies significantly over the image. To overcome these limitations, local indicators of spatial association (LISA) have been developed (Anselin, 1995). In contrast to existing methods, LISA measures focus on local variations *within* patterns of spatial dependence (Table 5.2 summarizes such work). Thus, they have the potential to uncover discrete spatial regimes which might be overlooked by existing techniques.

---

* For example, Moran's *I* may be computed in the software package IDRISI to generate a value to represent the entire image or within a sub-region defined by a binary mask. As a result, to generate an image of Moran's *I* values within the first lag an individual binary mask with a 3x3 sub-region defined for each pixel of the image is required (Votour, 1998).

**Table 5.1. Summary of a selection of techniques utilized in the assessment and application of autocorrelation in the remote sensing literature**

| Detail | Description | Reference |
|---|---|---|
| Assess autocorrelation by row and column | spatial autocorrelation presence demonstrated in this early study to assess the appropriate use of statistics upon Landsat TM imagery; spatial autocorrelation was assessed directionally along image scan lines or along image columns | Craig, 1979 |
| Sources of image autocorrelation; scanline processing | present sources of variation of autocorrelation in Landsat TM imagery; effects such as surface cover, terrain, instrument specifications, and Sun angle | Craig and Labovitz, 1980; Craig, 1981; Craig, 1984 |
| Areal mean and variance changes over season | spatial correlation effects upon accuracy of supervised classification of land cover are assessed through analysis of the means and variances of a series of kernels over six growing season dates | Campbell, 1981 |
| Assessment of autocorrelation on a scanline basis | demonstrate the effect of autocorrelation in training data upon spectral signatures; autocorrelation of signatures causes the appearance of false anomalies | Labovitz and Masuoka, 1984 |
| Semivariance as an image processing technique | spatial filtering, spatial registration, and image restoration, are demonstrated utilizing the semivariance values of Landsat TM imagery | Carr and Myers, 1984 |
| Join count statistics to assess classification errors | use of join count statistics to assess the errors in maps generated from remotely sensed data | Congalton, 1988 |
| Semivariogram structure functions | demonstration of the semivariogram as a structure function which may linked to Fourier transform for assessment of periodicity of autocorrelation | Wald, 1989 |
| Semivariance theory and application in remote sensing | the relationship between pixels of a regularized surface is presented in terms of semivariance, and then applied to simple model images | Curran, 1988; Jupp, *et al.*, 1988; Jupp, *et al.*, 1989 |
| Semivariogram textural classifier (STC) | semivariogram textural classifier (STC) demonstrated to exploit pixel inter-relationships relationship to vegetation cover types on radar imagery | Marinda, *et al.*, 1992; Marinda and Carr, 1994; Marinda, *et al.*, 1996 |
| Scale dependence of semivariograms | the scale dependence of semivariograms is demonstrated for soil and vegetation; semivariograms assessed in reference to theoretical models | Lacaze, *et al.*, 1994 |

**Table 5.2. Summary of literature related to local indicators of spatial association with reference to computation or application of the Getis statistic**

| Detail | Description | Reference |
|---|---|---|
| Second-order neighbourhood analysis | heterogeneity of the forest as a function of the scale of analysis; use of the Getis model (circa 1984) to influence data sampling methodologies | Getis and Franklin, 1987 |
| Demonstration of standardized $G_i^*$ | demonstration of $G_i^*$ in applications; statistic derivation and distribution described and demonstrated | Getis and Ord, 1992; Ord and Getis, 1995 |
| Demonstration of Getis statistic upon remotely sensed imagery | spatial dependence and heterogeneity of remotely sensed data are demonstrated on a small (8x8 pixel) Landsat TM image sub-sample, implications to studies of scale effects, model specification, sampling procedures, data storage, and segmentation | Getis, 1994 |
| Summary of LISA statistics | presentation of local indicators of spatial association as a new class of statistics; describes decomposition of global measures to assess contribution of each observation; valuable to indicate pockets of nonstationarity, identify outliers, and to assess locational influence of values upon global statistics | Anselin, 1995 |
| Determination of a minimum sample size | the authors state that computation of the *G* statistic is normally distributed with a minimum sample size of 8 | Griffith, *et al.*, 1996 |
| Snow cover and atmospheric patterns | examination of patterns of spatial of snow water equivalent (SWE) values; hemispheric patterns of spatial dependence found to be related to atmospheric circulation | Derksen, *et al.*, 1998ab; |
| Radiance peak filtering | semivariance is applied to dictate optimal window size for radiance peak filtering with Getis statistic values used to screen out false positives | Burnett, *et al.*, 1998 |
| Getis statistic in relation to TM imagery | a relationship is found between level of Getis statistic and Landsat TM image channels and digitally classified species | Wulder, *et al.*, 1997a; Wulder and Boots, 1998a |

One set of LISA measures is the *G* statistics developed by Getis and Ord (Getis and Ord, 1992: Ord and Getis, 1995). Although these statistics were initially developed for the analysis of point data, Getis (1994) has demonstrated their potential to identify significant spatial dependency in remotely sensed imagery. One Getis statistic, $G_i^*$, yields a standardized value which indicates both the degree of autocorrelation in the values of the digital numbers centered on a given pixel and the magnitude of these values in relation to

those of the entire image. Wulder and Boots, (1998b) introduced the rationale and presented a methodology for the $G_i^*$ to the remote sensing community. Wulder and Boots (1998a) have also applied $G_i^*$ in the assessment of a Landsat Thematic Mapper (TM) image of a managed forest region. Study results indicate a strong Landsat TM channel and cover type dependence to local spatial autocorrelation measured by the $G_i^*$. The following section will provide an overview of the Getis statistics and illustrate the computation and interpretation of $G_i^*$ values.

## 5.3. COMPUTATION OF THE GETIS STATISTIC

In general, LISA measures evaluate the extent and nature of concentration in the values of a variable $x$ in a local region within the study area. The Getis statistics achieve this by expressing the sum of the weighted variate values within a specified distance of a particular observation $i$ as a proportion of the sum of the variate values for the entire study area. This value can be compared with the statistic's expected value under a hypothesis of no local spatial autocorrelation to indicate if the degree of clustering of $x$ values in the vicinity of $i$ is greater or less than chance would dictate (Getis, 1994).

There are two versions of the Getis statistic, $G_i$ and $G_i^*$. In the former, the value of $x$ at $i$ is excluded from the local sum, while in the latter it is included. $G_i^*$ seems more appropriate for remote sensing applications since it allows for the computation of the statistic with a window of user-defined dimensions and so it is this statistic which we describe below.

Formally, the statistic $G_i^*(d)$ for some distance $d$ is defined (Getis and Ord, 1992) as

$$G_i^*(d) = \Sigma_j w_{ij}(d)x_j \;/\; \Sigma_j x_j \qquad [5]$$

where $\{w_{ij}(d)\}$ is a spatial weights matrix. Here we consider symmetric binary weights, with ones assigned to all locations within distance $d$ of observation $i$, including $i$ itself (i.e., $w_{ii} = 1$),

and zero otherwise. In the remote sensing context, a window can be defined around an observation $i$ by specifying an appropriate value of $d$.

Ord and Getis (1995) provide steps to derive a standardized version of $G_i^*$ which are summarized in the context of application to remote sensing digital images. We begin by calculating the mean and variance of $x$ for the entire image as follows

$$\bar{x} = \Sigma_j x_j / n \quad \text{and} \quad s^2 = \Sigma_j x_j^2 / n - \bar{x}^2 \qquad [6]$$

The expected value of $G_i^*$is,

$$E(G_i^*) = W_i' / n \qquad [7]$$

with a variance of

$$\text{Var}(G_i^*) = \frac{W_i^* (n - W_i^*)}{n^2 (n - 1)} \left[ \frac{s}{\bar{x}} \right]^2 \qquad [8]$$

resulting in the following standardized form,

$$G_i^* = \frac{\Sigma_j w_{ij}(d) x_j - W_i^* \bar{x}}{s[W_i^*(n - W_i^*) / (n - 1)]^{1/2}} \qquad [9]$$

where $W_i^* = \Sigma_j w_{ij}(d)$. The values of $G_i^*$ given by (5) are in $Z$ score standardized form. Griffith *et al.* (1996) suggest that if a minimum of 8 values are used for the computation of $G_i^*$, the resultant distribution of $G_i^*$ values is normal. Significant positive values indicate clustering of high variate values while significant negative values indicate clustering of low variate values. In consideration of remotely sensed imagery, the $G_i^*$ values measure the extent to which a pixel is surrounded by a cluster of high or low values of a particular variable, such as image digital number (DN) values. Large positive $G_i^*$ values denote a cluster of high DN values; large negative $G_i^*$ values denote a cluster of low DN values. In addition, computing $G_i^*$ within a series of windows of increasing windows and noting the distance at which the largest absolute value of $G_i^*$ occurs allows for an assessment of the size of the region of association

around an individual pixel, noted as the maximum $G_i^*$ distance (MGD). A small window size (distance) indicates that spatial dependency is confined to a very localized region while a large distance value indicates more spatially extensive spatial dependence. Yet, the interpretation of the MGD values should be done with caution. A MGD of 1 could mean that the region of association is small, or that the region of association is large and that $G_i^*$ is maximized between neighbouring pixels. Assessment of the difference between $G_i^*$ at maximum and minimum values provides insights to such situations. A weakness of the $G_i^*$ statistic, which it shares with other LISA measures (Tiefelsdorf and Boots, 1997), is that it cannot be used to identify clustering of medium values since mid-range values of $G_i^*$ (i.e., values around zero) can result from either this situation or an absence of clustering of similar variate values.

Computer code was developed to process remotely sensed imagery for spatial dependence characteristics. $G_i^*$ is computed within four different window sizes representing four differing distances ($d$) measured in terms of pixels, from an initial distance of 1 (a 3 by 3 window) up to distance of 4 (a 9 by 9 window). The largest absolute standardized $G_i^*$ value computed for any window represents a maximization of local association. These maximum $G_i^*$ and the MGD at which they occur are written to an image file for numeric and visual assessment.

## 5.4. POTENTIAL OF $G_i^*$ FOR PROCESSING OF HIGH SPATIAL RESOLUTION IMAGERY

Measures of spatial dependence, such as semivariograms, have proven valuable in digital image processing of remotely sensed imagery. Local indicators of spatial association are complementary to semivariograms while also providing some information not detectable in semivariogram analysis which allows for an improved understanding of image spatial structure. Knowledge of the magnitude of autocorrelated values is valuable supplementary

information available through the assessment of digital imagery. Further investigation of local indicators of spatial association in the context of remotely sensed digital imagery may:

- allow for assessment of clusters to assist in up-scaling of digital data,
- provide unique magnitude information related to image clusters,
- act as ancillary data in multispectral image classifications,
- allow for the creation of fuzzy boundaries around image objects,
- provide information for the delimitation of regions of similar spatial structure,
- assist in development of appropriate sampling schemes, and
- provide criteria to assist in the creation of statistically valid class signatures.

LISA statistics, specifically the Getis statistic, provide information based on the spatial structure of digital images. The ability to assess the strength of inter-pixel relationships, as well as the magnitude of the autocorrelated data, may prove valuable when the values computed from semivariance, as a positive valued function, prove inadequate for a particular objective. For imagery collected over a forest at a spatial resolution of 1m, spatial dependence information helps account for the foliage overlap and the inability to delineate trees by providing values from which clusters may be generated.

## 5.5. RELATIONSHIP BETWEEN OBJECTS OF INTEREST AND RESOLUTION WHEN PROCESSING WITH $G_i^*$

The spatial dependency information computed upon remotely sensed imagery is based upon the synthesis of image spatial resolution with the size of the objects of interest. In the case of forest inventory trees are the objects of interest. The size of the tree crown in relation to the resolution dictates the type of spatial dependency information that will be generated. Figure 5.1 presents a binary example of a tree crown with a 3 metre radius with a series of simulated image spatial resolutions. At the highest simulated resolution (0.5m) many pixels compose a single tree crown; yet, as the resolution decreases the number of pixels which compose an object decreases. The number of pixels which compose an object relates the type of spatial dependency information that will be generated. At the higher spatial resolution

levels the spatial dependency information computed as $G_i^*$ relates the within-crown spectral variability. As the resolution decreases, spatial dependencies relating the spectral differences between crown, understory, and shadow spectral components are generated. A decrease in resolution to the point that a single pixel contains an entire tree, or trees, results in the generation of spatial dependency values which relate stand level characteristics. As mentioned, this is a generalized binary example, in contrast to the complex tree crown objects represented by the spectral values collected with an airborne multispectral scanner. Tree crowns are complex spectrally due to forest architectural and structural considerations such as within crown variation in reflectance, irregular shading patterns, and tree overlap.

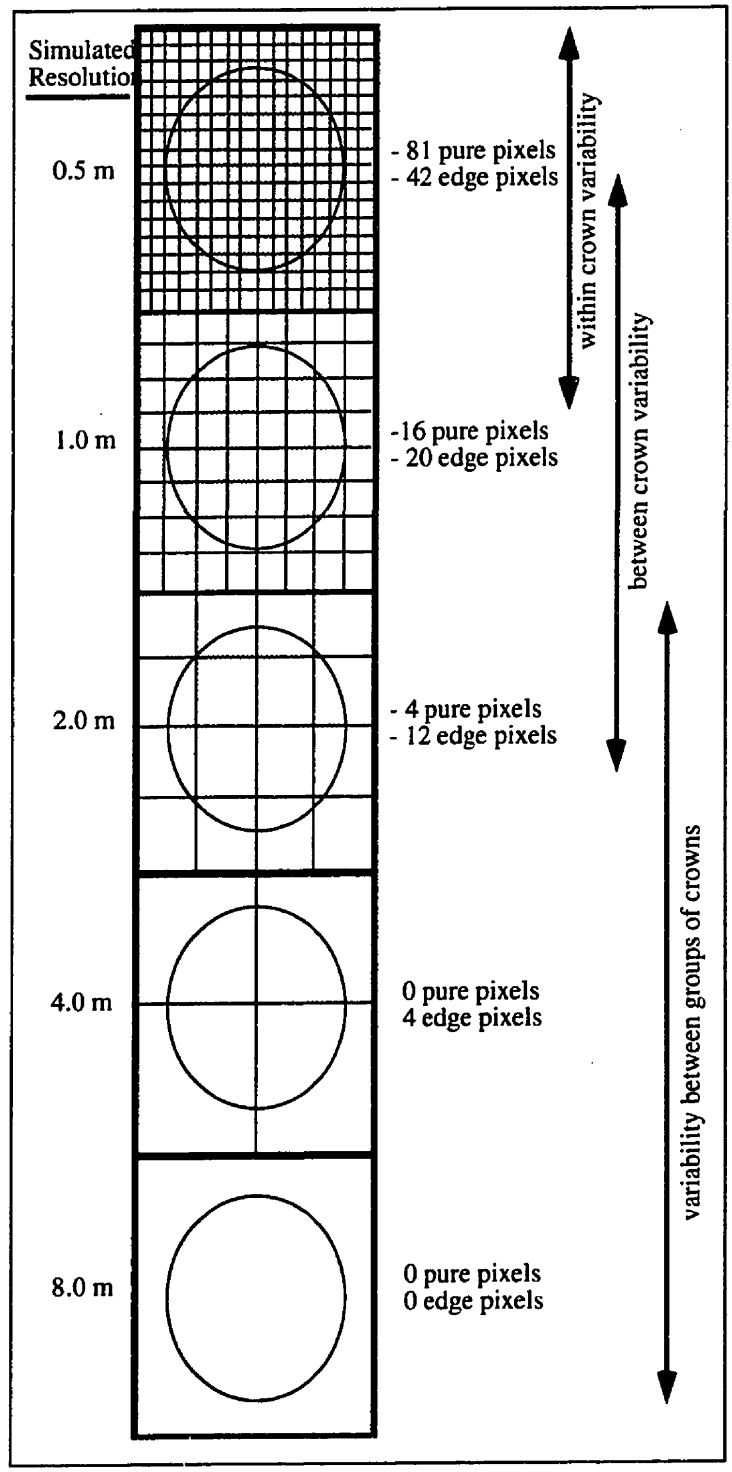


**Figure 5.1. Idealized binary illustration of the relationship between image resolution, object resolution, and the computation of spatial dependency. Simulated image object has a 3m radius.**

## 5.6. RELATIONSHIP BETWEEN DIGITAL IMAGE SEMIVARIANCE AND THE GETIS STATISTIC

In the near future, ≈1m spatial resolution panchromatic (450-900nm) data may be available from the proposed high spatial resolution satellite sensor QuickBird (Aplin, *et al.*, 1997). To explore the forestry potential of such imagery, 1m panchromatic data collected with the *casi* are assessed in the following example. The panchromatic image data were processed to generate an image of semivariance range values. Semivariance was computed in Rook's case, 4 directions, for each pixel with the results averaged to represent the pixel (Woodcock, *et al.*, 1988a). (Refer to Section 4.7.1 for semivariance computation details.) As noted in Section 4.7.1, the transect length for computation of semivariance for each direction of the Rooks case is 30 pixels, which is larger than the image objects of interest, while also allowing for a sufficient number of pixels for pair-wise processing at the size of the support. The support, representing the size of the sampling unit, in the case of remotely sensed data is indicated as the pixel size.

Figures 5.2a-d numerically illustrate the spatial dependence characteristics within the semivariance range computed upon a subset of *casi* panchromatic image data (Wulder, 1998b). The central number outlined is the pixel of reference for this example. The initial panchromatic digital numbers (Figure 5.2a) represent a cluster of four deciduous trees, two of which have canopy radii in excess of 3m. The semivariance range values, denoted in bold in the four computation directions, illustrate the pixels which resulted in a range value of 4 to result for the pixel of interest (Figure 5.2b). The strength of the relationship between neighbouring pixels, within the range of 4 computed with semivariance, is illustrated in Figure 5.2c. As noted in Figure 5.2d, this $G_i^*$ value was found to be at a maximum at a distance of one. The 3x3 window in which the $G_i^*$ was found to be at maximum is also noted in bold type. The local spatial dependency is found to be at a maximum at the central point of the cluster. The high level of autocorrelation between the pixels within the tree cluster is demonstrated by the low distance values in which the $G_i^*$ value is maximized. The

complementary nature between the semivariance generated range and $G_i^*$ allows for the extraction of image information that increases the utility of semivariance measures. Elsewhere in the illustration high distance values are seen to relate to regions of transition. The relationship between spectral transitions and the nature of the pattern of distances at which $G_i^*$ is maximized relates well to stand density. To enable comparison, Figure 5.3a-d graphically illustrates the spatial dependence characteristics of the same image subset used for demonstration in Figure 5.2a-d. With 1m spatial resolution, as stand density increases, the amount of change of distance values within an area also increases.

**Figure 5.2a. Sub-set of image panchromatic *casi* data**

| | | | | | | | | | | |
|---|---|---|---|---|---|---|---|---|---|---|
| 38 | 32 | 29 | 28 | 28 | 24 | 26 | 26 | 25 | 25 | 25 |
| 29 | 27 | 26 | 29 | 32 | **27** | 26 | 28 | 27 | 26 | 25 |
| 27 | 31 | 32 | 29 | 30 | **32** | 29 | 27 | 26 | 26 | 24 |
| 30 | 34 | 34 | 30 | 30 | **34** | 27 | 24 | 25 | 27 | 28 |
| 26 | 33 | 34 | 35 | **33** | **36** | **34** | 34 | 33 | 32 | 36 |
| 24 | **28** | **34** | **35** | **37** | **37** | **37** | **36** | **37** | **32** | 32 |
| 26 | 28 | 29 | 31 | **36** | **35** | **33** | 34 | 36 | 28 | 33 |
| 32 | 25 | 23 | 21 | 29 | **32** | 31 | 30 | 34 | 31 | 29 |
| 28 | 24 | 20 | 20 | 26 | **28** | 26 | 29 | 32 | 30 | 27 |
| 21 | 20 | 19 | 15 | 19 | **26** | 27 | 28 | 31 | 30 | 29 |
| 15 | 11 | 9 | 6 | 9 | 18 | 26 | 29 | 28 | 24 | 22 |

**Figure 5.2b. Semivariance range values computed for each pixel using Rooks case**

| | | | | | | | | | | |
|---|---|---|---|---|---|---|---|---|---|---|
| 3 | 4 | 4 | 4 | 5 | 4 | 4 | 3 | 4 | 4 | 4 |
| 3 | 3 | 4 | 4 | 4 | **3** | 3 | 3 | 4 | 4 | 4 |
| 3 | 4 | 4 | 4 | 4 | **4** | 3 | 4 | 4 | 4 | 4 |
| 3 | 3 | 3 | 4 | 4 | **4** | 3 | 3 | 4 | 4 | 4 |
| 4 | 5 | 4 | 4 | **4** | **4** | 4 | 4 | 4 | 5 | 5 |
| 4 | **4** | **3** | **4** | **4** | **4** | **4** | **3** | **4** | **4** | 5 |
| 3 | 4 | 4 | 5 | **4** | **4** | **4** | 3 | 4 | 4 | 4 |
| 5 | 4 | 4 | 4 | 4 | **4** | 5 | 4 | 5 | 4 | 5 |
| 4 | 3 | 3 | 4 | 4 | **3** | 3 | 4 | 5 | 5 | 5 |
| 3 | 4 | 3 | 4 | 3 | **3** | 4 | 3 | 5 | 5 | 5 |
| 4 | 4 | 4 | 5 | 4 | 5 | 3 | 3 | 4 | 4 | 5 |

**Figure 5.2c. Getis statistic values computed for each pixel**

| | | | | | | | | | | |
|---|---|---|---|---|---|---|---|---|---|---|
| 1.38 | 1.16 | 1.11 | 0.94 | 0.84 | 0.76 | 0.65 | 0.50 | 0.37 | 0.33 | 0.09 |
| 0.91 | 0.98 | 1.01 | 0.99 | 0.92 | **0.69** | 0.56 | 0.49 | 0.43 | 0.33 | 0.34 |
| 0.91 | 0.91 | 1.00 | 1.01 | 0.96 | **0.87** | 0.86 | 0.80 | 0.72 | 0.66 | 0.63 |
| 0.86 | 1.07 | 1.23 | 1.17 | 1.18 | **1.13** | 1.06 | 0.96 | 0.89 | 0.86 | 0.92 |
| 0.76 | 1.01 | 1.30 | 1.37 | **1.44** | **1.41** | **1.33** | 1.16 | 1.06 | 1.09 | 1.24 |
| 0.78 | **0.81** | **1.16** | **1.40** | **1.56** | **1.60** | **1.57** | **1.54** | **1.37** | **1.33** | 1.30 |
| 0.75 | 0.67 | 0.75 | 0.99 | **1.24** | **1.44** | **1.41** | 1.46 | 1.31 | 1.23 | 1.28 |
| 0.73 | 0.42 | 0.40 | 0.54 | 0.74 | **1.00** | 1.10 | 1.13 | 1.11 | 1.07 | 1.16 |
| 0.40 | 0.09 | -0.27 | -0.20 | 0.15 | **0.54** | 0.73 | 0.89 | 0.99 | 0.96 | 0.82 |
| -0.23 | -0.55 | -0.88 | -0.89 | -0.55 | **0.34** | 0.44 | 0.72 | 0.79 | 0.67 | 0.62 |
| -0.62 | -0.97 | -1.38 | -1.52 | -1.25 | -0.57 | 0.40 | 0.60 | 0.64 | 0.56 | 0.48 |

**Figure 5.2d. Distance value at which Getis statistic value is maximized**

| | | | | | | | | | | |
|---|---|---|---|---|---|---|---|---|---|---|
| 1 | 1 | 2 | 3 | 4 | 4 | 4 | 4 | 1 | 1 | 1 |
| 4 | 2 | 3 | 3 | 4 | **1** | 1 | 1 | 1 | 1 | 4 |
| 4 | 1 | 2 | 2 | 1 | **1** | 4 | 4 | 4 | 3 | 3 |
| 4 | 1 | 1 | 2 | 1 | **1** | 2 | 2 | 3 | 2 | 2 |
| 4 | 1 | 1 | 1 | **1** | **1** | **1** | 1 | 1 | 1 | 1 |
| 2 | **2** | **1** | **1** | **1** | **1** | **1** | **1** | **1** | **1** | 1 |
| 2 | 2 | 2 | 1 | **1** | **1** | **1** | 1 | 1 | 1 | 2 |
| 1 | 1 | 2 | 2 | 1 | **1** | 2 | 1 | 1 | 2 | 2 |
| 1 | 1 | 1 | 1 | 1 | **1** | 1 | 1 | 1 | 1 | 2 |
| 1 | 1 | 1 | 1 | 1 | **4** | 1 | 1 | 1 | 1 | 4 |
| 1 | 1 | 1 | 1 | 1 | 1 | 4 | 1 | 1 | 2 | 4 |

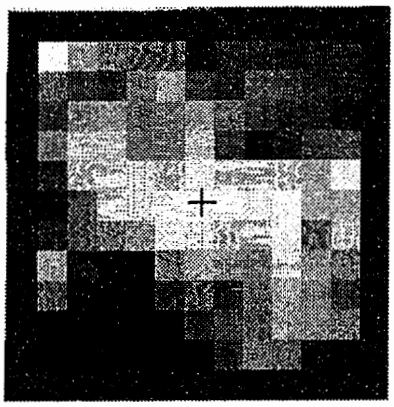

**Figure 5.3a. Sub-set of panchromatic *casi* digital image data**

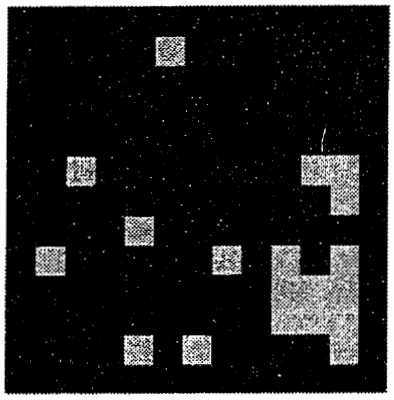

**Figure 5.3b. Semivariance range values computed for each pixel using Rooks case**

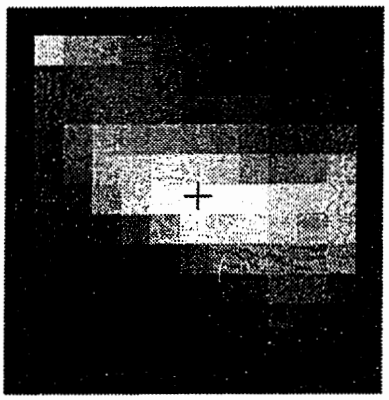

**Figure 5.3c. Getis statistic values computed for each pixel**

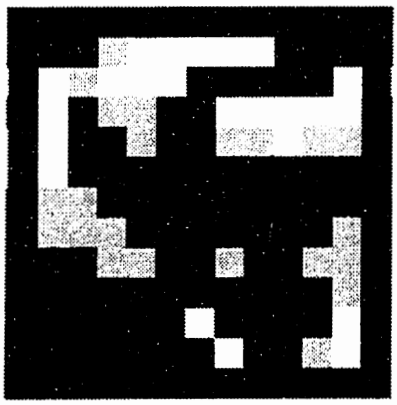

**Figure 5.3d. Distance value at which Getis statistic value is maximized**

## 5.7. CHAPTER SUMMARY

The Getis statistic provides information related to the spatial dependence between pixels within the semivariance range. The ability to quantify the strength of spatial dependence between pixels is a function of the relationship between image resolution with the size of the objects of interest on the landscape. High spatial resolution imagery partitions a continuous surface into a grid of regularly sized and shaped pixels. The Getis statistic provides a metric for assessing the strength of the relationships between the pixels which result from the discretization of a continuous forest surface. In the case of mixed and deciduous forests where there is overlap between the foliage of adjacent and suppressed trees a spatial resolution of 1 x 1m is insufficient to extract image objects. The spatial dependence data generated by the Getis statistic provides a means to group trees together based on the strength of the inter-relationships between pixels.

The spatial information content of the Getis statistic is complementary with semivariance. The range of the semivariogram indicates a region of spatial dependence. The Getis statistic provides an indication of the strength of the spatial dependence *within* the range of semivariance. Spatial information sources provide a means to assess forest structure based upon the image spatial structure which is processed; where the image spatial structure is a function of image spatial resolution and the forest objects of interest.

# 6. RESEARCH CONTEXT, STUDY AREA, AND DATA DESCRIPTION

***Chapter Objective:*** *Present the context for the analysis based upon the physical characteristics of the study area and the image and field data collected.*

## *6.1. STUDY AREA DESCRIPTION*

The Fundy Model Forest (FMF) is a 420,000 hectare working forest in southeast New Brunswick, Canada (Figure 6.1). The model forest is located in the Acadian forest region (Figure 6.2) and is composed of a variety of broadleaf deciduous and coniferous species and include a wide range of forest conditions (Rowe, 1977) with stand ages ranging from regeneration to old growth. The Acadian forest region is characterized by a wide variety of forest species. Coniferous tree species are predominantly jack pine (*Pinus banksiana*), white spruce (*Picea glauca*), balsam fir (*Abies balsamea*), and red spruce (*Picea rubens*). The predominant deciduous species are red maple (*Acer rubrum*) and white birch (*Betula papyrifira*), with stands also including beech (*Fagus grandifolia*), striped maple (*Acer pensylvanicum*), trembling aspen (*Populus tremuloides*), long tooth aspen (*Populus grandidentata*), and sugar maple (*Acer saccharum*) (Wulder, 1996). The study area was centered near Sussex at 45° 43' North and 65° 31' West, with data collected immediately north and south of the town site. Stands were selected for inclusion in the study to represent a range of forest types, crown closures, stand densities, tree species, and LAI values.

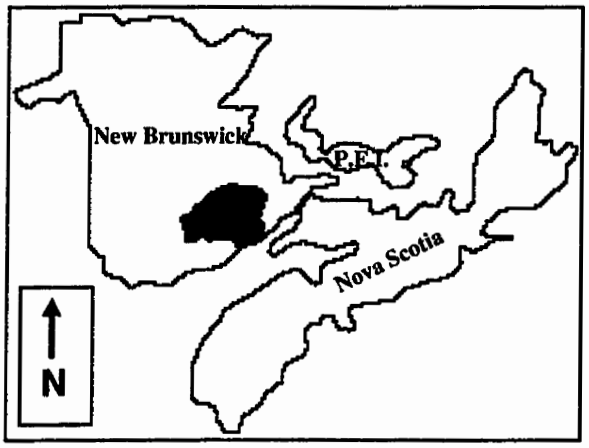


**Figure 6.1. Location of the study area in the eastern Canadian Maritime region, of New Brunswick, Nova Scotia, and Prince Edward Island, with the Fundy Model Forest study area shaded.**

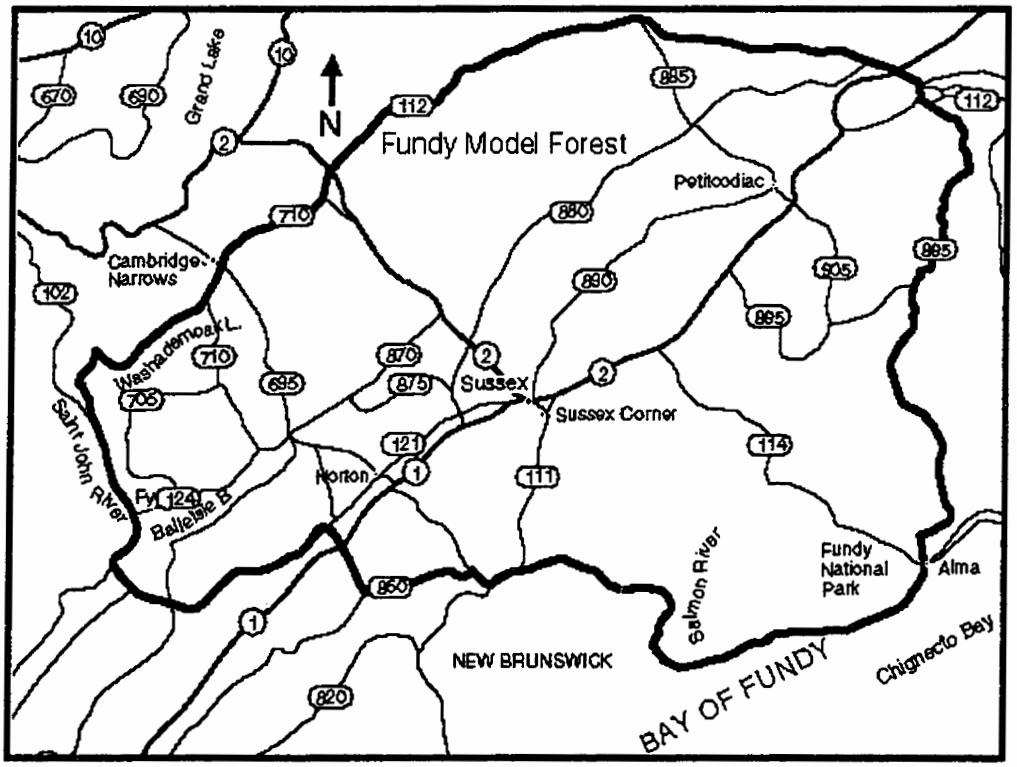


**Figure 6.2. The Fundy Model Forest study area presented in detail, with Sussex located at 45° 43' North and 65° 31' West (NRC, 1994).**

## 6.2. GROUND REFERENCE DATA

The ground reference data are the result the combination of a summary survey, that required collection of a representative set of parameters for every tree in each sample plot, with an intensive survey that measured a selection of trees in detail (Table 6.1). All plot locations were referenced, in metres from the south east corner of the plot. Sap wood width was measured using a tree core sample extracted with an increment borer at breast height (1.37 m above ground). The tree core once extracted was held up to allow the opaque area of the sap wood area to stand out in contrast to the heart wood area. The opaque sap wood area was then measured using a ruler with a millimetre scale and recorded. The bark width was also measured from this same tree core. Errors may be introduced through biases introduced by different individuals making the measurements. Total tree height was measured in metres using a Abney level (Avery and Burkhart, 1994). The inclinometer provides the angle at which the instrument is held. With knowledge of the distance that the person holding the Abney level was standing away from the tree, while pointing the instrument at the tree top and to the tree base and recording the angles, the tree height may be computed using trigonometry. Similarly the base-to-live crown area was measured. The base-to-live crown is the distance from the ground up to the point where the tree bole is predominately foliated. Errors may result from irregular landscape, different individuals making the measurements, and dense foliage obscuring the view of the tree tops. Crown widths are measured using a measuring tape and two people. One person holds the tape to the bark of a tree while the other person walks out backwards from under the tree crown foliage looking up to see where the outer edge of the tree branches occurs. The point at which the tree being measured ends was recorded as the crown radius (Cole, 1995). The crown radius was measured in two directions, one in the

same direction as the intended flight line, the other perpendicular to the flight line. Crown radius measurements are difficult in densely foliated areas.

Tree species and DBH were measured for every tree found entirely within the plot area; this is considered as the summary sample. All of the trees which were found entirely within the plot were provided with a reference number. In the field the measurement crew assessed the breakdown of tree species and the total number of trees. To reduce the amount of time necessary for field sampling bivariate regression relationships were generated between DBH and the intensively surveyed parameters which allows for extrapolation of the characteristics of interest to all trees in the summary sample (Table 6.2). A random sample of the trees within each species was selected from random number tables to select the trees for the intensive survey within the 20 x 20m plot. A minimum number of 3 trees was required for any given species within a stand. If there were fewer than 3 trees of a particular species within a stand, all trees of that species are measured. In the case of plot 9 all trees were measured due to the small total number of trees. For species with greater than 3 available samples, a minimum of 40% of the trees of that species are sampled. The means and standard errors are provided for the estimates of sap wood width, bark width, total tree height, base-to-live crown, and crown radius in two directions from the summary sample of DBH values (Table 2). In many cases all trees of a particular species were measured.

**Table 6.1. Ground reference data sampled for each plot (* denotes parameters measured in both summary and intensive survey)**

| |
|---|
| plot number |
| slope |
| Aspect |
| stand type |
| Date |
| tree number* |
| species* |
| diameter at breast height (DBH)* |
| location 1 (X)* |
| location 2 (Y)* |
| crown class (C.C.) (C = co-dominant, I = intermediate, S = suppressed, D = dominant) |
| sapwood width (SapW) |
| bark width (bark) |
| total height (TotHt) |
| base to live crown (BLC) |
| crown width one (with flight line) |
| crown width two (perpendicular to flight line) |

**Table 6.2. Results of bivariate regressions between DBH and intensively sampled field parameters (* "m" denotes all trees measured in field, no need for estimation)**

| | | | | Sapwood (mm) | | Bark (mm) | | Height (m) | | Base to live crown (m) | | Crown width 1 (m) | | Crown width 2 (m) | |
|---|---|---|---|---|---|---|---|---|---|---|---|---|---|---|---|
| Plot | species | total stems | Intensive sample | Mean | SE | Mean | SE | Mean | SE | Mean | SE | Mean | SE | Mean | SE |
| 5 | Be | 5 | 3 | 14.0 | 6.02 | 2.3 | 0.65 | 6.5 | 1.23 | 3.6 | 0.25 | 2.6 | 0.46 | 3.1 | 0.73 |
| | rM | 35 | 10 | 39.1 | 7.52 | 5.7 | 0.88 | 15.1 | 2.47 | 9.7 | 1.85 | 5.4 | 1.33 | 4.2 | 1.09 |
| | rS | 1 | 1 | m | m | m | m | m | m | m | m | m | m | m | m |
| | sM | 4 | 3 | 56.7 | 24.07 | 5.0 | 1.83 | 16.7 | 0.88 | 11.8 | 0.21 | 7.1 | 0.22 | 6.3 | 2.91 |
| | stM | 3 | 3 | m | m | m | m | m | m | m | m | m | m | m | m |
| | wB | 4 | 3 | 48.0 | 14.47 | 5.7 | 1.17 | 14.6 | 1.58 | 8.8 | 0.58 | 5.9 | 0.00 | 7.0 | 0.33 |
| | yB | 15 | 6 | 32.2 | 8.62 | 4.8 | 0.79 | 14.7 | 1.06 | 6.4 | 1.99 | 5.7 | 1.33 | 5.4 | 1.56 |
| | Total | 67 | 29 | | | | | | | | | | | | |
| 6 | bF | 15 | 10 | 38.6 | 12.06 | 4.7 | 0.70 | 11.9 | 1.59 | 4.3 | 1.42 | 3.8 | 0.61 | 4.0 | 0.72 |
| | rM | 19 | 10 | 53.4 | 14.84 | 7.3 | 2.29 | 18.7 | 2.23 | 12.6 | 1.59 | 5.8 | 1.24 | 5.7 | 1.65 |
| | rS | 3 | 3 | m | m | m | m | m | m | m | m | m | m | m | m |
| | wA | 1 | 1 | m | m | m | m | m | m | m | m | m | m | m | m |
| | wB | 4 | 4 | m | m | m | m | m | m | m | m | m | m | m | m |
| | Total | 42 | 28 | | | | | | | | | | | | |
| 7 | Be | 10 | 8 | 42.1 | 11.43 | 8.1 | 3.09 | 8.4 | 3.83 | 4.4 | 0.91 | 5.7 | 1.13 | 5.3 | 0.75 |
| | bF | 1 | 1 | m | m | m | m | m | m | m | m | m | m | m | m |
| | eH | 1 | 1 | m | m | m | m | m | m | m | m | m | m | m | m |
| | rM | 7 | 3 | 34.3 | 4.37 | 7.3 | 2.61 | 13.3 | 0.29 | 8.0 | 0.34 | 3.5 | 0.83 | 4.9 | 0.09 |
| | rS | 9 | 6 | 49.5 | 17.13 | 6.7 | 1.86 | 14.9 | 2.67 | 6.5 | 3.70 | 5.0 | 1.24 | 5.5 | 1.03 |
| | stM | 2 | 2 | m | m | m | m | m | m | m | m | m | m | m | m |
| | wB | 10 | 8 | 58.9 | 11.99 | 8.8 | 1.94 | 16.8 | 2.00 | 11.7 | 1.47 | 5.8 | 1.07 | 5.5 | 0.80 |
| | Total | 40 | 29 | | | | | | | | | | | | |
| 8 | Be | 1 | 1 | m | m | m | m | m | m | m | m | m | m | m | m |
| | rM | 11 | 7 | 42.3 | 12.74 | 4.7 | 0.98 | 12.9 | 1.46 | 5.9 | 2.48 | 5.7 | 0.88 | 4.8 | 1.28 |
| | rS | 8 | 4 | 45.3 | 16.04 | 5.8 | 0.84 | 11.5 | 3.33 | 2.8 | 1.05 | 21.2 | 2.27 | 21.2 | 2.07 |
| | stM | 1 | 1 | m | m | m | m | m | m | m | m | m | m | m | m |
| | wB | 31 | 10 | 51.2 | 11.94 | 5.7 | 1.21 | 16.0 | 1.45 | 9.6 | 0.91 | 4.1 | 0.71 | 4.3 | 0.78 |
| | bF | 2 | 2 | m | m | m | m | m | m | m | m | m | m | m | m |
| | Total | 54 | 25 | | | | | | | | | | | | |
| 9 | ltA | 1 | 1 | m | m | m | m | m | m | m | m | m | m | m | m |
| | rM | 19 | 19 | m | m | m | m | m | m | m | m | m | m | m | m |
| | rS | 2 | 2 | m | m | m | m | m | m | m | m | m | m | m | m |
| | tA | 2 | 2 | m | m | m | m | m | m | m | m | m | m | m | m |
| | wB | 3 | 3 | m | m | m | m | m | m | m | m | m | m | m | m |
| | Total | 27 | 27 | | | | | | | | | | | | |
| 10 | rM | 14 | 7 | 45.1 | 15.74 | 6.1 | 1.67 | 14.3 | 1.59 | 8.6 | 1.59 | 4.3 | 0.62 | 4.8 | 1.36 |
| | stM | 1 | 1 | m | m | m | m | m | m | m | m | m | m | m | m |
| | jP | 2 | 2 | m | m | m | m | m | m | m | m | m | m | m | m |
| | wB | 34 | 10 | 49.7 | 10.24 | 6.7 | 1.02 | 15.3 | 1.97 | 9.7 | 0.87 | 4.2 | 0.49 | 4.0 | 0.71 |
| | Total | 51 | 20 | | | | | | | | | | | | |

Note: for species abbreviations see Table 6.4.

**Table 6.3. Dubee Settlement flight line plot summaries, including species, number of stems per species and total, and LAI**

| plot no. | stand type~ | species (number of stems) | total stems | LAI |
|---|---|---|---|---|
| 5 | IH -TH over | Be(5), rM(35), rS(1), sM(4), stM(3), wB(4), yB(15) | 67 | 4.93 |
| 6 | MW over, light HW under | bF(15), rM(19), rS(3), wA(1), wB(4) | 42 | 5.87 |
| 7 | HW - SW over, MW under | Be(10), bF(1), eH(1), rM(7), rS(9), stM(2), wB(10) | 40 | 6.88 |
| 8 | HW -SW over, HW -SW under | Be(1), rM(11), rS(8), stM(1), wB(31), bF(2) | 54 | 5.25 |
| 9 | HW over, SW under | ltA(1), rM(19), rS(2), tA(2), wB(3) | 27 | 3.28 |
| 10 | IH over, TH under | rM(14), stM(1), jP(2), wB(34) | 51 | 4.30 |

* all plots $20m^2$
~Stand crown class/type:
IH - intolerant hardwood,
TH - tolerant hardwood,
HW - hardwood,
SW - softwood,
MW - mixed-wood.
(for species abbreviations see Table 6.4)

Based upon the plot information generated from the field data plot maps are created. The plot maps have been degraded to a regular 1m grid to allow for comparison to the 1m spatial resolution remotely sensed data. The plot maps are created from the field data held in a GIS. To generate the digital field plot maps, information relating tree height, crown size, and tree crown class was integrated with a specifically developed C program (Figure 6.3). Tree height information is available for each tree based upon the field sampling and regression results. Crown size is a term to describe the estimate of the two-dimensional radial extent of the tree crown from the estimates of crown width recorded in the field and estimated through regression. To enable comparison of continuous measurements made in the field to discrete digital image data, the plot maps are a probability map. As the radial extent of a tree cannot be captured in 1m spatial resolution gridded data, the likelihood of tree presence at a particular location is recorded. At the centre of a tree the likelihood of the tree being captured on the imagery is high, yet the amount of a pixel which is composed of tree materials decreases with movement from the centre of the tree. As a result, 3 classes of tree presence

are generated, tree pixels (centre of tree), tree extent pixels, and suppressed/tree extent pixels. Treitz, *et al.*, (1992), explore the problems associated with the collection of field data for

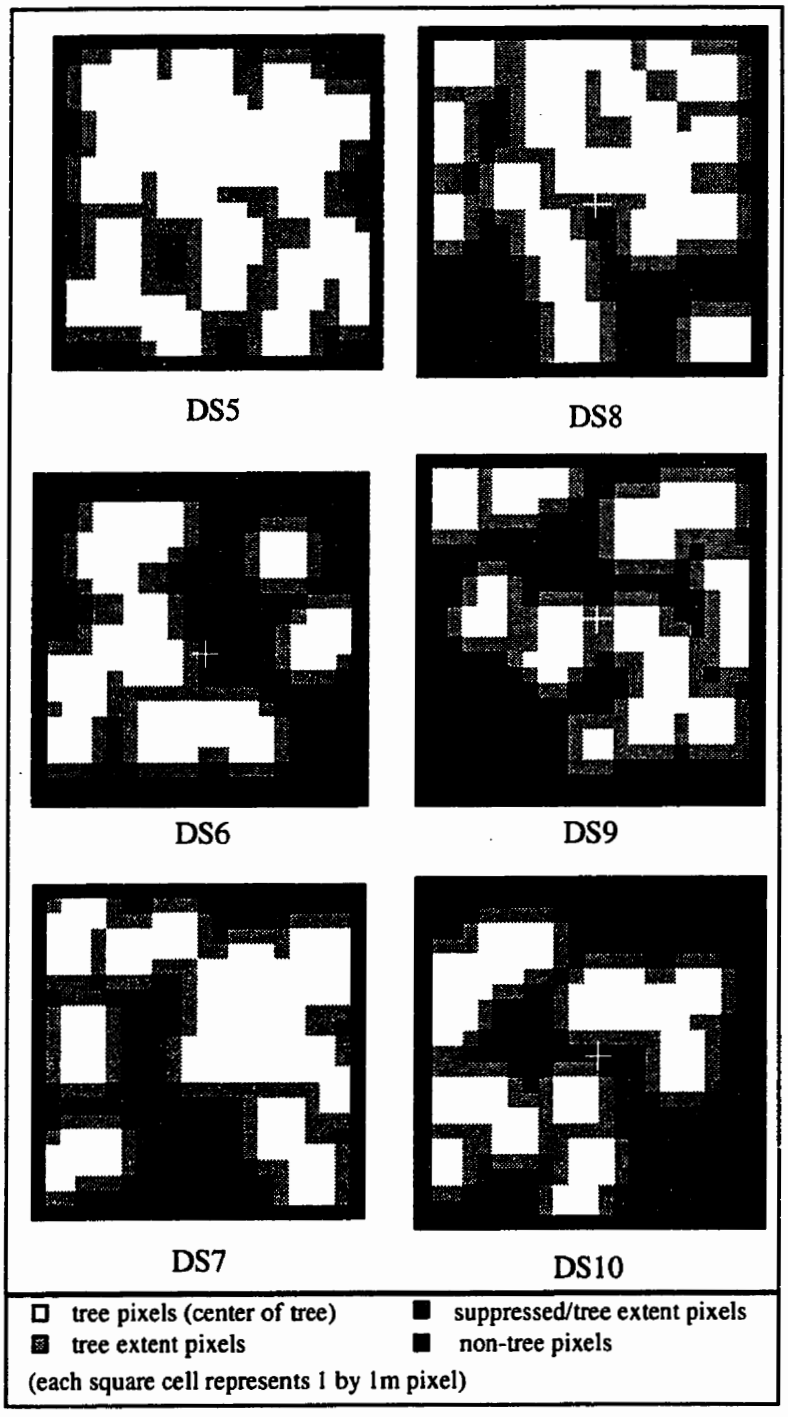


**Figure 6.3. Field data plot maps for each study plot and image.**

classification with high spatial resolution imagery (5x5 m pixels), finding that the more spectrally diverse a class the lower the classification accuracy. These results illustrate the difficulty in capturing the original forest variance in the remotely sensed imagery.

For the purposes of analysis the stands have been stratified into hardwood, softwood, and mixed-wood species (Table 6.4). Where the hardwoods are the combination of all pure deciduous species, softwoods are all the coniferous species, mixed-woods are the stands which are a combination of hardwood and softwood species.

**Table 6.4. Forest stand species composition and abbreviations**

| | | |
|---|---|---|
| hardwood class species | | |
| Be | beech | *Fagus grandifolia* |
| rM | red maple | *Acer rubrum* |
| sM | sugar maple | *Acer saccharum* |
| stM | striped maple | *Acer pensylvanicum* |
| wB | white birch | *Betula papyrifira* |
| yB | yellow birch | *Betula alleghaniensis* |
| gB | gray birch | *Betula popufolia* |
| eH | eastern hemlock | *Tsuga canadensis* |
| ltA | long tooth aspen | *Populus grandidentata* |
| tA | trembling aspen | *Populus tremuloides* |
| wA | white aspen | *Populus glauca* |
| softwood class species | | |
| jP | jack pine | *Pinus banksiana* |
| wP | white pine | *Pissodes strobus* |
| rS | red spruce | *Picea rubens* |
| bF | balsam fir | *Abies balsamea* |
| wS | white spruce | *Picea glauca* |

The heterogeneous species composition of the FMF study area required a variety of allometric equations to compute field based estimates of LAI (Table 6.5). To ensure confidence in the allometric estimation of LAI, new equations were developed for white birch, red maple, and trembling aspen, the most commonly occurring species in the study region, from destructive samples, following the approach outlined and demonstrated by Singh (1982).

For species which occur infrequently in the study region, expensive destructive sampling was avoided by using, or adapting, existing equations.

**Table 6.5. Allometric equations applied to derive leaf area (LA) of study plots ***

| Species | Equation | Source |
|---|---|---|
| wB | LA = 0.04121 SA^1.325 | Wulder, *et al.*, 1998 |
| rM | LA = 0.6964 SA^0.8472 | Wulder, *et al.*, 1998 |
| tA | LA = 0.1418 SA^0.9921 | Wulder, *et al.*, 1998 |
| bF | LA = (163.05 SA^1.4081)/ ( 202.16^1.4081 + SA^1^4081) | adapted from Lavigne, *et al.*, 1996 |
| rS | LA = .1746 SA^1.266 | adapted from Robichaud and Methven, 1992 |
| wS | use the equation for rS | |
| jP | LA = 0.25 SA | adapted from Hungerford, 1987 |
| sM | use the equation for rM | ---------- |
| stM | use the equation for sM | ---------- |
| Be | use the equation for sM | ---------- |
| eH | use the equation for bF | ---------- |
| ltA | use the equation for tA | ---------- |

*SA is sapwood area at breast height in $cm^2$, LA is leaf area in $m^2$.

## 6.3. REMOTELY SENSED DATA

### 6.3.1. Remotely Sensed Airborne *casi* Imagery

On July 31, 1995, at 13:00 local time, compact airborne spectrographic imager (*casi*) imagery was acquired from a Cessna 310 aircraft at an elevation of 700 m and at a speed of approximately 55 knots utilizing the standard *casi* 12.5 mm focal length (Anger *et al.*, 1996). This configuration was selected to scan 1x1 m resolution imagery with five user selected spectral bands (Table 6.6), to characterize significant locations on a vegetation spectral response curve (Figure 6.4). The sample spectral response curve presented in Figure 6.4 is of a single Maple leaf as sensed with a spectroradiometer (Analytical Spectral Devices, 1993) in the study area. Spectral signatures of any species occur within an envelope of maximum and minimum likely response. The spectral signature illustrated may, as a result, not be completely representative of all deciduous tree spectral response. The intention of providing a sample spectral response curve is to provide the reader with an indication of the general form

of the spectral response expected. The illustrated spectral response curve has a steep red edge, the rise in reflectance from the red to infrared wavelengths, that is not common. As a result, the selection of 750 nm to represent the infrared requires additional justification. When deciding upon the wavelength range to represent the infrared two considerations were paramount, sufficient distance from the red wavelengths and red edge and not too far into the outer range of the *casi* spectral sensitivity as instrument noise increases near the edges of the approximate 400 to 900 nm range. The 750 nm wavelength centre was decided upon as appropriate due to the satisfaction of the two aforementioned restraints. The azimuth of the data acquisition flight lines is approximately towards the sun to reduce changing illumination conditions and view angle effects. The sky was clear and the relative humidity was low reducing the effects of the atmosphere upon the imagery (Wulder, *et al.*, 1996d). See Appendix 1 for a complete summary of pre-, during, and post flight data acquisition activities.

**Table 6.6. Fundy Model Forest *casi* imagery spectral wavelength channel summary**

| Channel and Spectral Location | Bandwidth(nm) | Centre (nm) | Width (nm) |
|---|---|---|---|
| channel 1 (green) | 560.5 to 569.4 | 565.0 | 8.9 |
| channel 2 (red) | 640.9 to 649.8 | 645.4 | 8.9 |
| channel 3 (red well) | 660.6 to 669.6 | 665.1 | 9.0 |
| channel 4 (red edge) | 707.4 to 714.6 | 711.0 | 7.2 |
| channel 5 (infrared) | 748.8 to 752.4 | 750.6 | 3.6 |

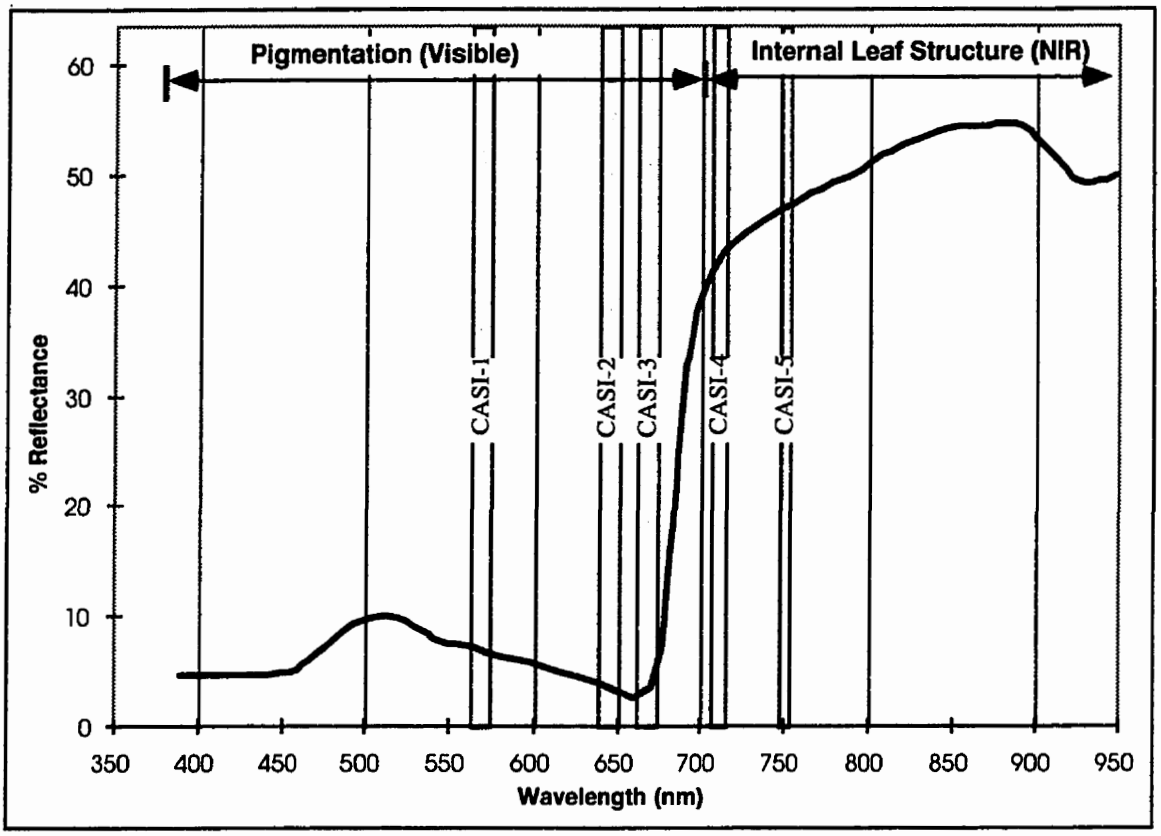


**Figure 6.4. Sample vegetation spectral response curve with user selected *casi* channels superimposed. Also noted are the characteristic regions of wavelength sensitivity, where the spectral response in the visible wavelengths are related to vegetation pigmentation, and in the near infrared where spectral response is a function of internal leaf structure.**

To enable insight to the type of forestry information that may be extracted from 1m panchromatic imagery that is expected to be included upon high spatial resolution satellite sensors in the near future (recall Table 3.11), a simulated panchromatic channel has be computed from the *casi* spectral data. As panchromatic literally means "sensitive to light of all colors" (Avery and Berlin, 1992) there is variability in what may be considered as panchromatic. The SPOT panchromatic range spans 510 to 700 nm (Avery and Berlin, 1992) while the panchromatic range of the proposed 1m spatial resolution instrument on board the OrbView and the 0.82m spatial resolution QuickBird satellites is 450 to 900 nm (Aplin, *et al.*,

1997). Based upon the data available, and the flexibility in consideration of the panchromatic range, the five *casi* spectral channels available for this study were summed and averaged to represent data which would be similar to remotely sensed panchromatic data. The regular distribution of *casi* channels at important spectral locations on portions the vegetation spectral response curve allowed for averaging without potential error being incorporated through a weighting of the channels.

### 6.3.2. Atmospheric Correction of Image Data

Utilized in this field campaign was an ASD spectroradiometer (Analytical Spectral Devices, Inc., 1993) which collects data from approximately 400 to 900 nm at a 1.8nm recording interval. Collection of spectral data *in situ* enables characterization of the spectral characteristics of a sample object free of atmospheric interference between the object surface and the sensor (Milton, 1987). This characterization enables the comparison of spectra which are, in theory, undisturbed by the atmosphere between the sensor and surface and the airborne collected data which is subject to atmospheric interference. Objects which are present in remotely sensed imagery and *in situ* spectral calibration data act as pseudo-invariant features (PIFs) for use in atmospheric correction of image data (Freemantle, *et al.*, 1992). Spectral information were recorded in the field concurrent with the *casi* over-flight to enable atmospheric correction of the *casi* data. Paved roads, which intersect the flight lines at a number of known locations, are used as PIF targets.

The spectroradiometer was operated using the procedure recommended by Peddle, *et al.*, (1995), utilizing Kodak gray cards to calibrate the incoming irradiance. The date, time, and geographic location, in terms of latitude and longitude, are noted during spectral sample collection to enable the computation of the solar zenith angle. Spectral and angular computation are based upon the provided sun angle/location/time/date combination, which

yield a panel bi-directional reflectance factor (BRF) specific to the solar zenith angle present. Reflectance values may then be computed from the panel and target reflectance values with a panel calibration BRF specific to the solar zenith angle.

### 6.3.3. Radiometric and Geometric Processing of Digital Image Data

Image preprocessing of the *casi* data is performed to radiometrically correct the data for the effects of scattered light, to remove instrument offsets, and to convert the digital numbers to standard radiometric units (Anger *et al.*, 1995). General correction techniques which address visible and near infrared image radiometry are often required for successful application of aerial and satellite remote sensing (Hall, *et al.*, 1991; Franklin and Giles, 1995). Accordingly, an initial bundle adjustment was undertaken to correct for the non-systematic airborne imaging effects of roll, pitch, and yaw . Correction of image radiometry, especially reflectance, is of most importance for studies incorporating temporal analysis. Image radiance and reflectance are strongly linearly related allowing for the option of not undertaking a radiometric to reflectance calibration for single time period studies, such as this research. Collection of global positioning system (GPS) ground data and flight locational data enabled differential correction and geometric adjustment of the airborne imagery. The aircraft position and angular orientation was recorded for each scanline using the onboard GPS receiver and a two-axis vertical gyro. The geometric correction process utilized this aircraft attitude information and placed each pixel of the image on a georeferenced UTM grid (Cosandier *et al.*, 1992; Schwarz *et al.*, 1993). The base station GPS receiver unit, located at a known geographic point, was used to correct the imagery acquired by the airborne GPS unit (Hoffman-Wellenhof, *et al.*, 1992). For this study locational data were collected with L1 Carrier Phase Novatel GPS receiver units at a 5 second epoch rate, allowing for a positional error of less than 10cm based upon 10km baseline length and a 15 minute observation time.

### 6.3.4. Image Data: Context and Subject

The collection rationale and processing procedures have been presented to demonstrate the integrity of the data under consideration. Six sample images have been sub-set for processing in this study and are presented here to illustrate the *context* of the image analysis. As the Getis statistic is derived including the global mean and variance (Formula 4) knowledge of the entire scene contents is important to understanding the spatial dependency results. The *subject* of the analysis, the field sampled plots, are also considered in relation to this global data, which has an influence upon the data which is extracted from the sample plots. As each field sample plot is geographically located in a different area, six images were subset from a larger image for analysis. As a result, each field sample plot under consideration has an associated image (Figure 6.5a to f).

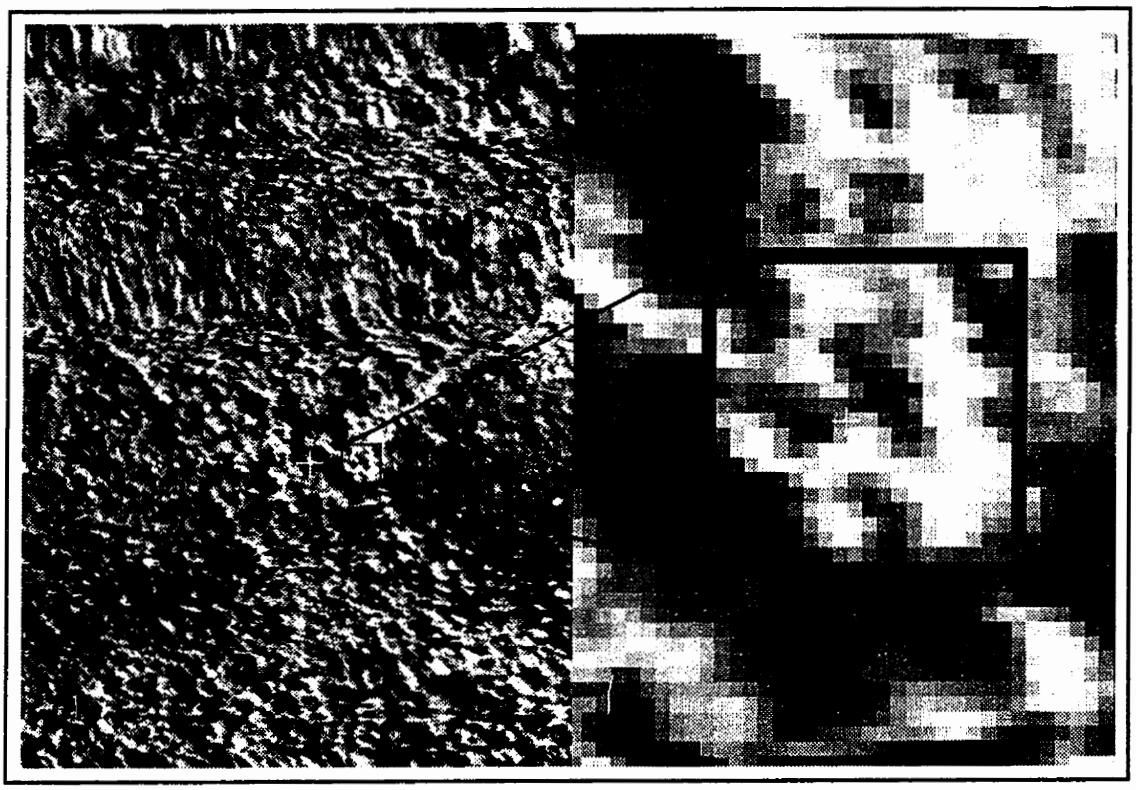

**Figure 6.5a. DS5 infrared full image sample (x1) and plot zoom (x8), illustrating a plot with a mature intolerant/tolerant hardwood overstory.**

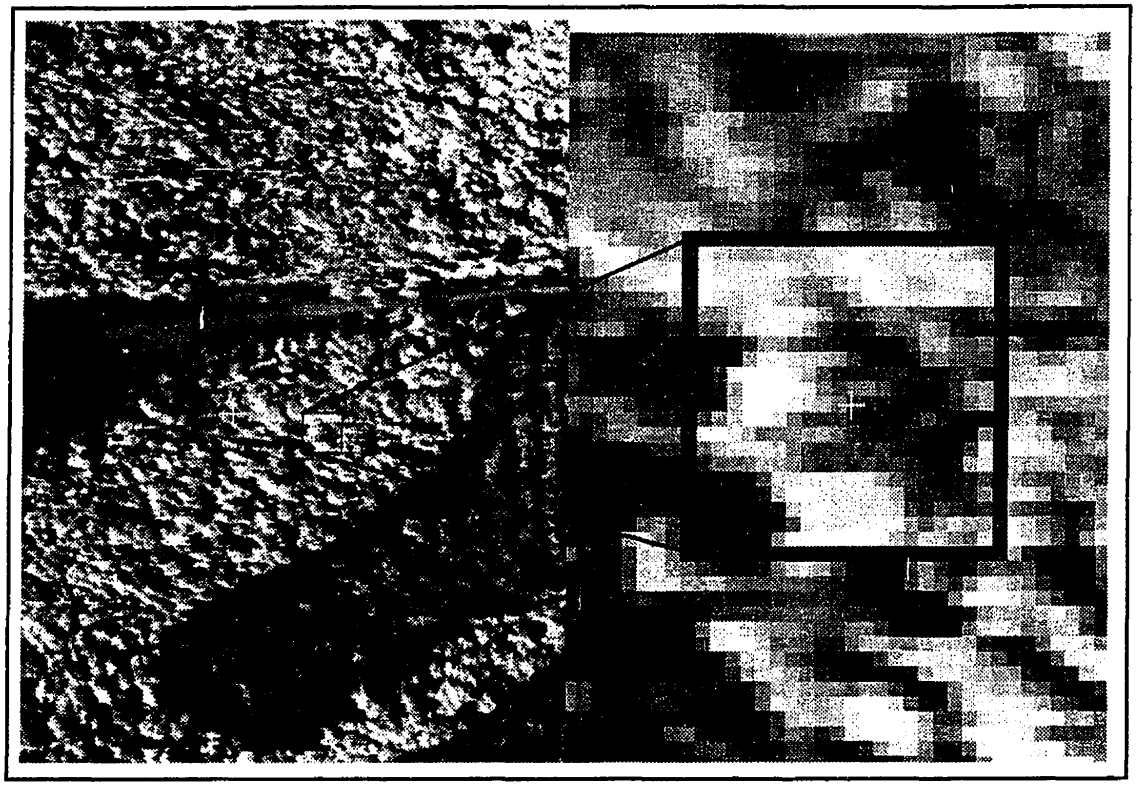

**Figure 6.5b. DS6 infrared full image sample (x1) and plot zoom (x8), illustrating a plot with a mixed wood overstory and a light hardwood understory.**

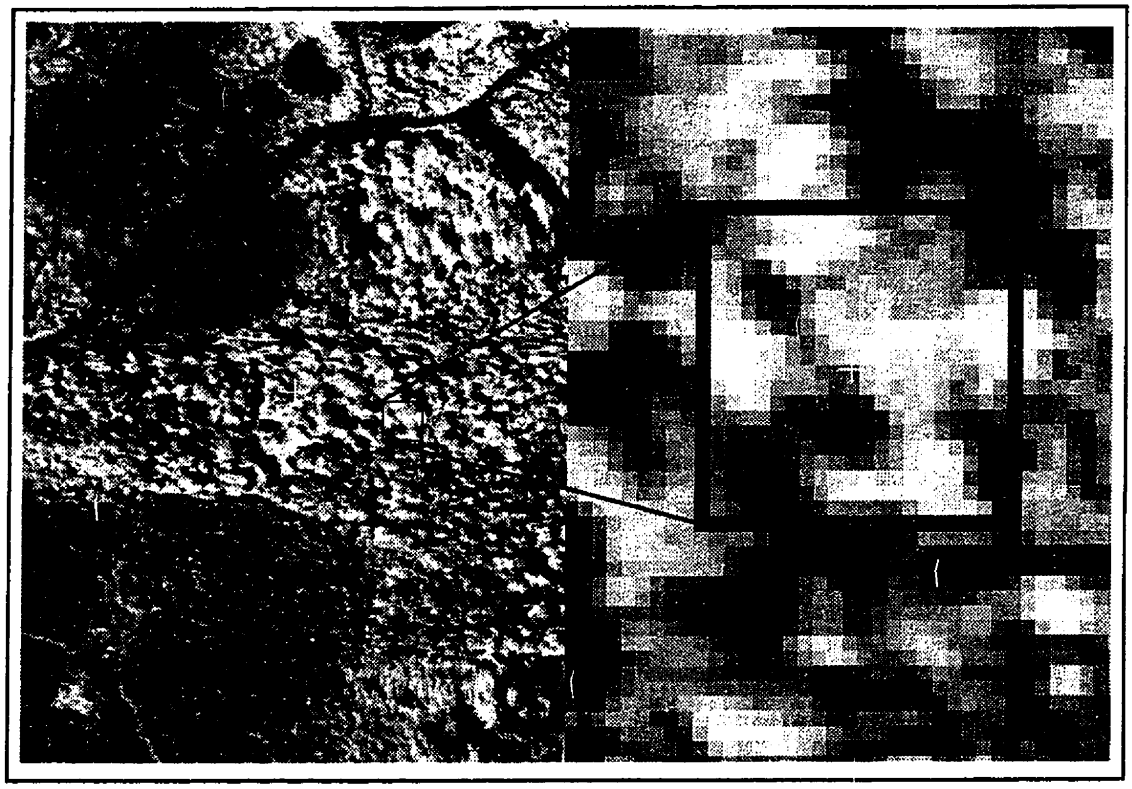

**Figure 6.5c. DS7 infrared full image sample (x1) and plot zoom (x8), illustrating plot with a hardwood/softwood overstory and a mixed wood understory.**

**Figure 6.5d. DS8 infrared full image sample (x1) and plot zoom (x8), illustrating a plot with a hardwood/softwood overstory and understory.**

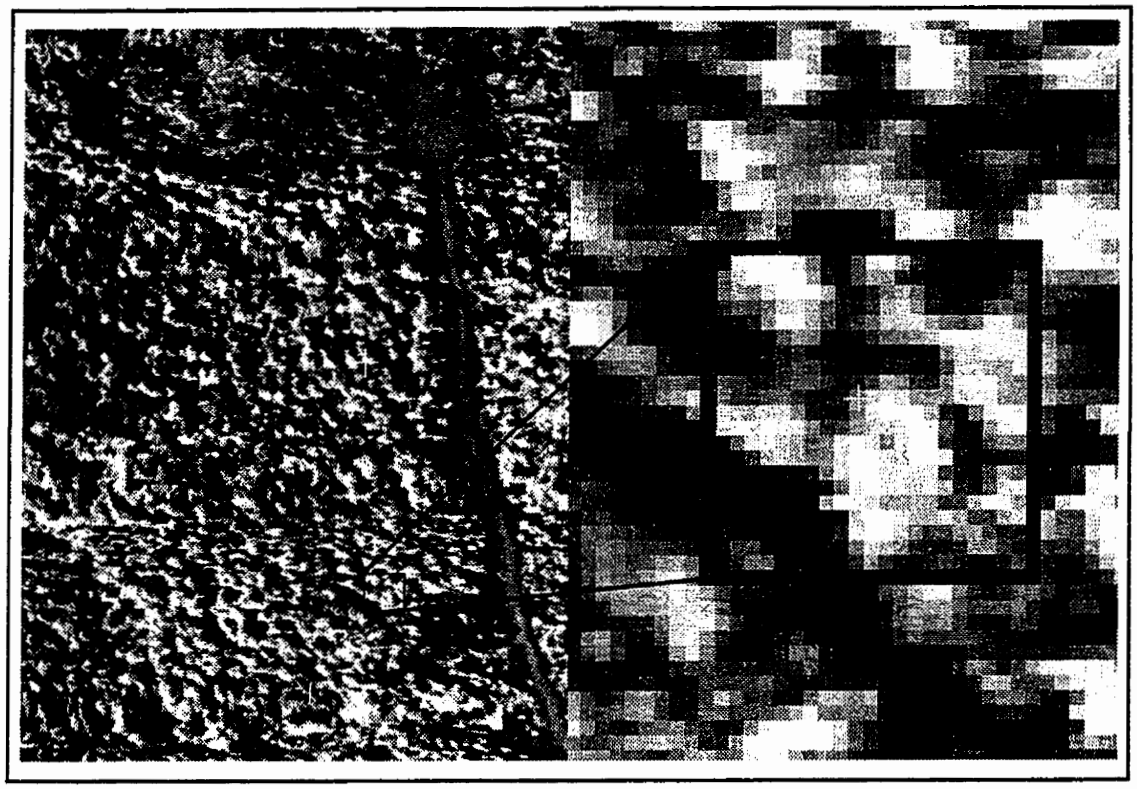

**Figure 6.5e. DS9 infrared full image sample (x1) and plot zoom (x8), illustrating a plot with a hardwood overstory and a softwood understory.**

**Figure 6.5f. DS10 infrared full image sample (x1) and plot zoom (x8), illustrating a plot with an intolerant hardwood overstory and a tolerant hardwood understory.**

# 7. GENERATION OF IMAGE VEGETATION OBJECTS

***Chapter Objective:*** *Apply the spatial dependence data generated with the Getis statistics to partition forest stands into vegetation clusters.*

## *7.1. INTRODUCTION*

This chapter demonstrates the problems and potential related to the partitioning of forest vegetation based upon image spatial information for 1m spatial resolution imagery collected over deciduous and mixed forests. The Getis statistic ($G_i^*$) is presented as a means to generate clusters of forest vegetation. The image spatial resolution of 1m is too coarse to allow for a situation where many pixels make up a single tree object. The image spatial resolution limitations present in this study encourage the examination of a new approach for the assessment of image structural information. The use of image spatial autocorrelation, as represented by the Getis statistic ($G_i^*$), allows for the generation of image objects based upon pixel associations related to the forest structure. Digitally generated image objects, or clusters, are a representation of the trees which are discernible at a spatial resolution of 1m. The clusters which are generated may be composed of a single or multiple species, which is a shortcoming of this approach. Further, the clusters may also be related to the presence in the forest of a multitude of structural situations, such as a single large dominant tree, groups of co-dominant trees, or a dominant tree in association with suppressed trees.

Techniques exist for very high spatial resolution data, such as 3cm, which discern characteristics at the individual *within* tree level, such as branch architecture (Brandtburg, 1997) which enable techniques such as tree vectorization (Landry, *et al.*, 1997). Techniques appropriate at the 1m spatial resolution discern *between* tree variability. In reference to the 1m spatial resolution data available for analysis in this study; large solitary trees may be

discernible, yet trees which overlap, or are of varying height, are difficult to discern at the one metre level. Tree cluster information may be analyzed to provide information related the characteristics of forest stands which are potential discernable with the 1m spatial resolution imagery available for this study.

To enable a comparison between ground measured tree data and the remotely sensed prediction of forest vegetation from image objects, spatial dependency values, in the form of the Getis statistic ($G_i^*$), are generated for each pixel. As the generation of $G_i^*$ values in remote sensing is a new technique (Wulder and Boots, 1998b), before a prediction of forest structural parameters may be made, the behavior of the $G_i^*$ values is assessed. A prudent assessment of both the reflectance values and resultant $G_i^*$ values generated for the images processed for this study prior to integration of the image and field data is undertaken to allow for an increased understanding of the behavior of the Getis statistic in a variety of situations. The data generated in this chapter are to be further analyzed in subsequent chapters for a relationship to forest inventory (Chapter 8) and biophysical parameters (Chapter 9). Once the behavior of the $G_i^*$ values generated in this study is established, the image objects are generated. This will allow for an assessment of the agreement between the plot maps created from the ground collected and the remotely sensed data.

## 7.2. ASSESSMENT OF IMAGE SPATIAL AND SPECTRAL DATA

To allow for comparison between the distribution of reflectance and $G_i^*$ data for the entire image area with the portion of the image found within the study area a random sample of 400 DNs was extracted from the entire image area. The spatial dependency values generated for the entire image area were related to the distribution of initial reflectance data based upon the

physical vegetation properties which dictate the reflectance in each channel. As a result, factors such as high values for non-vegetated areas will alter the results of clusters.

### 7.2.1. Spectral Data Summary

The relationship between spatial resolution and the dominant ground cover dictates the spectral signal which is received at the sensor. At a spatial resolution of 1m, over a region dominated by forest cover, the spectral response largely resembles that expected for vegetation, with the anthropogenic features, such as roads, having some effect on the mean image spectral response. Understanding of the spectral response for each image utilized in this study is important as the global mean and variance values are included in later analysis to generate Getis statistic values.

Table 7.1 presents the summary statistics for the spectral data present in each study image randomly selected from the entire image area. (Recall Table 6.6 for the wavelength range occupied by each image channel.) As expected for a vegetation spectral response curve (see Figure 6.4) the values in the green spectral range have a higher reflectance than the red channels and the infrared channels have the highest mean reflectance values and greatest range. As each image is sampling unique ground cover, distinct patterns to the spectral response for each study image are also expected. The complexity of the gross image spectral characteristics preclude definitive statements on the rationale for the resultant image spectral characteristics. General statements may be made, such as in reference to the red spectral channel, that the presence of roads likely increases the mean red reflectance. The *casi* panchromatic simulation channel is moderated by the wide spectral bandwidth including a variety of spectral characteristics.

A degree of variability has been illustrated for the overall image spectral characteristics above. The field plots, with the sample restricted to a single area, have a distribution of

values which relate the spectral characteristics found within each plot area. In Table 7.2 we present the spectral characteristics found within the image areas corresponding to the field plots. As the spectral signal of roads and other non-vegetation surface covers are not included in the plot areas, the spectral resemblance to a vegetation spectral response curve is further accentuated. Indicators have been placed in Table 7.2 to demonstrate the change in spectral response between the overall image values and those found exclusively within the plot areas. In general, the red (C2) reflectance is lower in the plots than in the remainder of the image. Also, the NIR (C5) reflectance is higher than that found outside of the sample plot. The lower reflectance in the red and increased reflectance in the infrared is indicative of vegetation dominated spectral response.

**Table 7.1. Summary statistics for random sample of *casi* spectral data, measured in percent reflectance, for each image which contains one of the surveyed sample plots**

| | *casi*-1 | *casi*-2 | *casi*-3 | *casi*-4 | *casi*-5 | *casi*-PAN |
|---|---|---|---|---|---|---|
| DS-5 Image Sample Summary statistics | | | | | | |
| Minimum | 4 | 1 | 1 | 3 | 8 | 3 |
| Maximum | 40 | 18 | 16 | 56 | 85 | 38 |
| Range | 36 | 17 | 15 | 53 | 77 | 35 |
| Mean | 18.2 | 6.4 | 4.8 | 25.2 | 45.2 | 19.5 |
| Median | 18 | 6 | 5 | 25 | 46 | 20 |
| Standard Deviation | 6.2 | 2.6 | 2.0 | 10.4 | 15.0 | 6.8 |
| DS-6 Image Sample Summary statistics | | | | | | |
| Minimum | 6 | 2 | 1 | 4 | 6 | 4 |
| Maximum | 87 | 87 | 86 | 82 | 84 | 79 |
| Range | 81 | 85 | 85 | 78 | 78 | 75 |
| Mean | 25.6 | 15.3 | 13.8 | 31.8 | 41.9 | 25.3 |
| Median | 23 | 9 | 7 | 32 | 41.5 | 25 |
| Standard Deviation | 12.2 | 14.4 | 14.8 | 12.7 | 15.9 | 10.8 |
| DS-7 Image Sample Summary statistics | | | | | | |
| Minimum | 6 | 2 | 1 | 5 | 2 | 4 |
| Maximum | 53 | 48 | 46 | 62 | 84 | 45 |
| Range | 47 | 46 | 45 | 57 | 82 | 41 |
| Mean | 23.7 | 11.0 | 9.0 | 28.9 | 43.2 | 22.7 |
| Median | 23 | 9 | 7 | 29 | 42 | 23 |
| Standard Deviation | 8.4 | 7.0 | 6.8 | 11.8 | 15.1 | 7.9 |
| DS-8 Image Sample Summary statistics | | | | | | |
| Minimum | 6 | 2 | 1 | 5 | 2 | 6 |
| Maximum | 53 | 48 | 46 | 62 | 84 | 68 |
| Range | 47 | 46 | 45 | 57 | 82 | 62 |
| Mean | 23.7 | 11.0 | 9.0 | 28.9 | 43.2 | 24.7 |
| Median | 23 | 9 | 7 | 29 | 42 | 25 |
| Standard Deviation | 8.4 | 7.0 | 6.8 | 11.8 | 15.1 | 8.3 |
| DS-9 Image Sample Summary statistics | | | | | | |
| Minimum | 5 | 1 | 1 | 3 | 4 | 3 |
| Maximum | 80 | 79 | 78 | 74 | 82 | 71 |
| Range | 75 | 78 | 77 | 71 | 78 | 68 |
| Mean | 19.8 | 10.3 | 8.9 | 24.2 | 37.0 | 19.6 |
| Median | 18 | 7 | 6 | 24 | 36 | 19 |
| Standard Deviation | 11.1 | 11.5 | 11.5 | 12.7 | 15.0 | 10.3 |
| DS-10 Image Sample Summary statistics | | | | | | |
| Minimum | 5 | 2 | 1 | 4 | 7 | 4 |
| Maximum | 85 | 85 | 83 | 81 | 95 | 77 |
| Range | 80 | 83 | 82 | 77 | 88 | 73 |
| Mean | 24.8 | 13.2 | 11.4 | 31.2 | 44.1 | 24.5 |
| Median | 23 | 8 | 6 | 31 | 44 | 24 |
| Standard Deviation | 11.7 | 13.2 | 13.5 | 12.5 | 15.2 | 10.3 |

**Table 7.2. Summary statistics for the *casi* spectral data corresponding to the field plots, measured in percent reflectance, for of the surveyed sample plots**

| | *casi*-1 | *casi*-2 | *casi*-3 | *casi*-4 | *casi*-5 | *casi*-PAN |
|---|---|---|---|---|---|---|
| DS-5 Plot Summary Statistics | | | | | | |
| Minimum | 7 ↑ | 1 = | 1 = | 6 ↑ | 19 ↑ | 6 ↑ |
| Maximum | 34 ↓ | 23 ↑ | 21 ↑ | 53 ↓ | 89 ↑ | 37 ↓ |
| Range | 27 ↓ | 22 ↑ | 20 ↑ | 47 ↓ | 70 ↓ | 31 ↓ |
| Mean | 20.6 ↑ | 6.8 ↑ | 4.9 ↑* | 30.6 ↑ | 57.4 ↑ | 23.6 ↑ |
| Median | 21 ↑ | 7 ↑ | 5 = | 32 ↑ | 59 ↑ | 25 ↑ |
| Standard Deviation | 5.87 ↓ | 2.93 ↑ | 2.46 ↑ | 10.60 ↑ | 14.90 ↓ | 6.86 ↑ |
| DS-6 Plot Summary Statistics | | | | | | |
| Minimum | 8 ↑ | 2 = | 2 ↑ | 9 ↑ | 18 ↑ | 9 ↑ |
| Maximum | 36 ↓ | 12 ↓ | 12 ↓ | 55 ↓ | 85 ↑ | 39 ↓ |
| Range | 28 ↓ | 10 ↓ | 10 ↓ | 46 ↓ | 67 ↓ | 30 ↓ |
| Mean | 21.1 ↓ | 7.0 ↓ | 5.2 ↓ | 30.4 ↓* | 54.4 ↑ | 23.2 ↓ |
| Median | 21 ↓ | 7 ↓ | 5 ↓ | 31 ↓ | 56 ↑ | 24 ↓ |
| Standard Deviation | 5.82 ↓ | 2.07 ↓ | 1.57 ↓ | 10.03 ↓ | 15.07 ↓ | 6.65 ↓ |
| DS-7 Plot Summary Statistics | | | | | | |
| Minimum | 7 ↑ | 2 = | 1 = | 5 = | 14 ↑ | 6 ↑ |
| Maximum | 43 ↓ | 15 ↓ | 13 ↓ | 61 ↓ | 89 ↑ | 41 ↓ |
| Range | 36 ↓ | 13 ↓ | 12 ↓ | 56 ↓ | 75 ↓ | 35 ↓ |
| Mean | 26.4 ↑ | 8.8 ↓ | 6.2 ↓ | 36.1 ↑ | 56.9 ↑ | 26.5 ↑ |
| Median | 27 ↑ | 9 = | 6 ↓ | 36 ↑ | 59 ↑ | 27 ↑ |
| Standard Deviation | 7.58015 ↓ | 2.66 ↓ | 1.83 ↓ | 12.80 ↑ | 16.37 ↑ | 7.95 ↑ |
| DS-8 Plot Summary Statistics | | | | | | |
| Minimum | 8 ↑ | 2 = | 1 = | 5 = | 13 ↑ | 6 = |
| Maximum | 50 ↓ | 19 ↓ | 12 ↓ | 67 ↑ | 87 ↑ | 43 ↓ |
| Range | 42 ↓ | 17 ↓ | 11 ↓ | 62 ↑ | 74 ↓ | 37 ↓ |
| Mean | 21.6 ↓ | 7.5 ↓ | 5.5 ↓ | 31.4 ↑ | 54.3 ↑ | 23.7 ↓ |
| Median | 20 ↓ | 7 ↓ | 5 ↓ | 30 ↑ | 56 ↑ | 23 ↓ |
| Standard Deviation | 6.83 ↓ | 2.54 ↓ | 1.61 ↓ | 11.03 ↓ | 12.36 ↓ | 6.55 ↓ |
| DS-9 Plot Summary Statistics | | | | | | |
| Minimum | 4 ↓ | 1 = | 1 = | 4 ↑ | 12 ↑ | 4 ↑ |
| Maximum | 38 ↓ | 17 ↓ | 14 ↓ | 60 ↓ | 78 ↓ | 38 ↓ |
| Range | 34 ↓ | 16 ↓ | 13 ↓ | 56 ↓ | 66 ↓ | 34 ↓ |
| Mean | 20.4 ↑* | 7.2 ↓ | 5.3 ↓ | 28.2 ↑ | 47.3 ↑ | 21.3 ↑ |
| Median | 20 ↑ | 7 = | 5 ↓ | 29 ↑ | 49 ↑ | 22 ↑ |
| Standard Deviation | 6.95 ↓ | 2.81 ↓ | 2.14 ↓ | 11.50 ↓ | 14.70 ↓ | 7.33 ↓ |
| DS-10 Plot Summary Statistics | | | | | | |
| Minimum | 13 ↑ | 3 ↑ | 2 ↑ | 14 ↑ | 28 ↑ | 12 ↑ |
| Maximum | 43 ↓ | 17 ↓ | 16 ↓ | 60 ↓ | 84 ↓ | 40 ↓ |
| Range | 30 ↓ | 14 ↓ | 14 ↓ | 46 ↓ | 56 ↓ | 28 ↓ |
| Mean | 24.4 ↓* | 8.3 ↓ | 6.0 ↓ | 33.6 ↑ | 53.7 ↑ | 24.8 ↑ |
| Median | 24 ↑ | 8 = | 6 = | 32 ↑ | 52 ↑ | 24 = |
| Standard Deviation | 5.70 ↓ | 2.29 ↓ | 1.67 ↓ | 9.47 ↓ | 10.67 ↓ | 5.56 ↓ |

↑ denotes that value in plot sample is greater than found in the random sample
↓ denotes that value in plot sample is less than found in the random sample
= denotes that value in plot sample is equal to that found in the random sample
* denotes that mean value in plot sample is not significantly different from random sample (at a 95% level of significance)

### 7.2.2. Generation of Getis Statistic

The computation of the normalized Getis statistic (Formula 9, p. 78) is based on the assessment of the sum of pixel values within a given distance of a pixel of interest in relation to the sum expected for that distance based upon global mean and variance values. As a result, knowledge of the global mean and variance values, generated using each pixel in the image for computation, provides an increased understanding of the resultant $G_i^*$ values (Table 7.3). As the global mean and variance values where computed from all image pixels slight differences are found in comparison to the random sample. The values in Table 7.3 are presented to allow for the verification of $G_i^*$ results. Knowledge of the global mean and variance values allows for the comparison of individually computed results to the computer generated results. (In verification of results it is important to consider the computation window size.) Global mean and variance relate to the context of where the $G_i^*$ values are derived from, such as an image dominated by a lake or roads, which may have an influence upon the values generated for the region of interest, in this case the plot areas. Spatial information which may be generated for a spectral feature that is within the centre of the complete range of spectral values may be obscured by features such as roads or lakes. As the $G_i^*$ values are standardized and normal, this allows for the comparison of Z-scores generated for each pixel location. The total number of pixels present in the sample images and the total number of pixels utilized in the computation of $G_i^*$ values is not equal due to masking out an edge border of 9 pixels in width and the non-inclusion in processing of image areas which only include zero values. Generation of $G_i^*$ upon a variety of images has demonstrated the detriment of including large areas of zero values (Wulder and Boots, 1998a; Derksen, *et al.*, 1998a). With inclusion of non-data values, the global mean and variance values are

suppressed and the richness of the spatial information generated is diminished through inflation of the sample size with zero values.

**Table 7.3. Summary of distribution of spectral values within each channel for each image containing a ground sample plot. The global mean, variance, and number of pixels are included in $G_i^*$ computation as the global expectation to be compared to local characteristics. (each image is 300 pixels by 400 lines = 120,000 pixels possible total)**

| | *casi*-1 | *casi*-2 | *casi*-3 | *casi*-4 | *casi*-5 | *casi*-PAN |
|---|---|---|---|---|---|---|
| DS-5 | | | | | | |
| Global mean | 18 | 6 | 5 | 25 | 45 | 19 |
| Global variance | 38 | 7 | 4 | 110 | 226 | 47 |
| # of pixels | 119700 | 119679 | 119680 | 119700 | 119700 | 119700 |
| DS-6 | | | | | | |
| Global mean | 25 | 15 | 13 | 31 | 43 | 25 |
| Global variance | 143 | 188 | 196 | 163 | 243 | 111 |
| # of pixels | 119700 | 119700 | 119700 | 119700 | 119700 | 119700 |
| DS-7 | | | | | | |
| Global mean | 24 | 11 | 9 | 29 | 44 | 23 |
| Global variance | 68 | 55 | 47 | 131 | 227 | 61 |
| # of pixels | 119589 | 119589 | 119589 | 119589 | 119589 | 119589 |
| DS-8 | | | | | | |
| Global mean | 25 | 11 | 9 | 32 | 47 | 24 |
| Global variance | 88 | 65 | 63 | 152 | 249 | 70 |
| # of pixels | 119422 | 119422 | 119422 | 119422 | 119422 | 119422 |
| DS-9 | | | | | | |
| Global mean | 21 | 11 | 10 | 26 | 38 | 21 |
| Global variance | 149 | 158 | 159 | 173 | 216 | 120 |
| # of pixels | 119700 | 119700 | 119694 | 119700 | 119700 | 119700 |
| DS-10 | | | | | | |
| Global mean | 25 | 13 | 11 | 32 | 44 | 25 |
| Global variance | 138 | 172 | 179 | 164 | 243 | 109 |
| # of pixels | 119700 | 119700 | 119700 | 119700 | 119700 | 119700 |

### 7.2.3. Spatial Data Summary

The distribution of $G_i^*$ values are first presented as summary values extracted randomly to represent the entire image and then in terms of what characteristics are present in the plot area. In Table 7.4 we present the distribution of $G_i^*$ values generated for each spectral channel within each sample image. Within the red wavelength range, the expected reflectance for vegetation is low, and for non-vegetation features it is high. As a result, the $G_i^*$ values for the red spectral wavelengths demonstrate a range of data that is of marginal interest in assessment

of vegetation. The presence of anthropogenic features such as roads and exposed soil of cut-blocks result in an high $G_i^*$ with a large range, yet for the vegetated features the spatial information is less expansive. A possible means to maximize the spectral information in the red wavelengths is to apply a mask to remove non-vegetation pixels. This may be accomplished through assessment of the infrared and red wavelength; if the red reflectance exceeds the infrared, remove the pixel from consideration. As the purpose of this investigation is to assess the behavior of the Getis statistic in a variety of image spectral conditions masking has not been undertaken.

The distribution of $G_i^*$ in each channel, in each image, are found to approximate a normal distribution with a mean of 0 and a standard deviation of 1 (Table 7.4). Whereas, the distribution of $G_i^*$ demonstrated in Table 7.5, are not approaching normality relating unique conditions being captured in the plot area versus the image area. The field plots, with the sample restricted to a single area, have a distribution of values which relate the spatial characteristics found within each plot area. The mean values relate to the distribution of the vegetation in the plots, therefore an increase in the magnitude of clustering is found for most channels. The sample image DS7 is difficult to assess due to the presence of a dense conifer stand, cut blocks, and roads, while the plot area of interest is a mixed forest stand (Figure 6.5c).

**Table 7.4. Distribution of random sample Getis Statistic values by sample image denoted by which image channels were used for computation (n=400)**

| | *casi*-1 | *casi*-2 | *casi*-3 | *casi*-4 | *casi*-5 | *casi*-PAN |
|---|---|---|---|---|---|---|
| DS-All Summary Statistics | | | | | | |
| Minimum | -2.35 | -2.06 | -1.83 | -2.11 | -2.77 | -2.40 |
| Maximum | 4.97 | 5.27 | 5.27 | 3.78 | 3.07 | 4.91 |
| Range | 7.32 | 7.33 | 7.09 | 5.89 | 5.84 | 7.31 |
| Mean | -0.01 | 0.00 | 0.01 | -0.03 | -0.02 | -0.02 |
| Median | -0.29 | -0.41 | -0.41 | -0.15 | -0.14 | -0.20 |
| Standard Deviation | 0.97 | 0.97 | 0.97 | 0.91 | 0.92 | 0.94 |
| DS-5 Summary Statistics | | | | | | |
| Minimum | -2.35 | -2.06 | -1.83 | -2.11 | -2.39 | -2.40 |
| Maximum | 2.83 | 3.86 | 4.87 | 2.48 | 2.13 | 2.31 |
| Range | 5.18 | 5.92 | 6.70 | 4.58 | 4.52 | 4.70 |
| Mean | -0.01 | -0.01 | 0.00 | 0.00 | 0.00 | -0.01 |
| Median | -0.16 | 0.01 | -0.09 | -0.12 | 0.11 | -0.07 |
| Standard Deviation | 0.89 | 0.84 | 0.83 | 0.85 | 0.88 | 0.87 |
| DS-6 Summary Statistics | | | | | | |
| Minimum | -1.57 | -0.90 | -0.83 | -2.07 | -2.23 | -1.89 |
| Maximum | 4.97 | 5.15 | 5.02 | 3.78 | 2.29 | 4.91 |
| Range | 6.54 | 6.05 | 5.85 | 5.85 | 4.51 | 6.80 |
| Mean | 0.02 | 0.07 | 0.08 | 0.00 | -0.04 | 0.02 |
| Median | -0.34 | -0.50 | -0.52 | 0.04 | -0.04 | -0.20 |
| Standard Deviation | 1.05 | 1.09 | 1.08 | 0.95 | 0.94 | 1.03 |
| DS-7 Summary Statistics | | | | | | |
| Minimum | -2.10 | -1.28 | -1.14 | -2.11 | -2.77 | -2.33 |
| Maximum | 3.16 | 4.66 | 4.78 | 2.55 | 2.29 | 2.82 |
| Range | 5.26 | 5.93 | 5.92 | 4.66 | 5.06 | 5.16 |
| Mean | 0.00 | 0.00 | 0.00 | -0.01 | -0.02 | -0.01 |
| Median | -0.25 | -0.39 | -0.42 | 0.06 | -0.26 | 0.03 |
| Standard Deviation | 1.00 | 0.98 | 0.97 | 0.94 | 0.94 | 0.96 |
| DS-8 Summary Statistics | | | | | | |
| Minimum | -2.10 | -1.28 | -1.14 | -2.11 | -2.77 | -2.04 |
| Maximum | 3.16 | 4.66 | 4.78 | 2.55 | 2.29 | 4.01 |
| Range | 5.26 | 5.93 | 5.92 | 4.66 | 5.06 | 6.05 |
| Mean | 0.00 | 0.00 | 0.00 | -0.01 | -0.02 | 0.01 |
| Median | -0.25 | -0.39 | -0.42 | 0.06 | -0.26 | -0.18 |
| Standard Deviation | 1.00 | 0.98 | 0.97 | 0.94 | 0.94 | 0.93 |
| DS-9 Summary Statistics | | | | | | |
| Minimum | -1.31 | -0.78 | -0.68 | -1.63 | -2.27 | -1.56 |
| Maximum | 4.78 | 5.24 | 5.27 | 3.53 | 2.59 | 4.48 |
| Range | 6.09 | 6.02 | 5.95 | 5.16 | 4.86 | 6.04 |
| Mean | -0.08 | -0.05 | -0.05 | -0.10 | -0.06 | -0.09 |
| Median | -0.36 | -0.38 | -0.39 | -0.31 | -0.19 | -0.31 |
| Standard Deviation | 0.92 | 0.91 | 0.91 | 0.90 | 0.93 | 0.91 |
| DS-10 Summary Statistics | | | | | | |
| Minimum | -1.58 | -0.84 | -0.75 | -2.06 | -2.34 | -1.93 |
| Maximum | 4.93 | 5.27 | 5.14 | 3.62 | 3.07 | 4.81 |
| Range | 6.51 | 6.11 | 5.89 | 5.68 | 5.41 | 6.74 |
| Mean | -0.02 | -0.01 | 0.00 | -0.03 | 0.00 | -0.03 |
| Median | -0.33 | -0.45 | -0.46 | -0.24 | -0.08 | -0.29 |
| Standard Deviation | 0.98 | 1.02 | 1.02 | 0.90 | 0.89 | 0.95 |

**Table 7.5. Summary statistics of Getis statistic values computed upon each *casi* spectral channel**

| | *casi*-1 | *casi*-2 | *casi*-3 | *casi*-4 | *casi*-5 | *casi*-PAN |
|---|---|---|---|---|---|---|
| DS-5 Getis statistic values (n=400) | | | | | | |
| Minimum | -1.64 ↑ | -1.55 ↑ | -1.56 ↑ | -1.49 ↑ | -1.49 ↑ | -1.61 ↑ |
| Maximum | 2.32 ↑ | 3.99 ↑ | 4.76 ↑ | 2.07 ↑ | 2.27 ↑ | 2.05 ↑ |
| Range | 3.96 ↑ | 5.54 ↑ | 6.32 ↑ | 3.57 ↑ | 3.76 ↑ | 3.65 ↑ |
| Mean | 0.45 ↓ | 0.16 ↓ | 0.09 ↓* | 0.61 ↓ | 0.96 ↓ | 0.70 ↓ |
| Median | 0.61 ↓ | 0.22 ↑ | 0.06 ↑ | 0.82 ↓ | 1.11 ↓ | 0.90 ↓ |
| Standard Deviation | 0.80 ↑ | 0.92 ↑ | 0.98 ↓ | 0.79 ↑ | 0.79 ↑ | 0.80 ↑ |
| DS-6 Getis statistic values (n=380) | | | | | | |
| Minimum | -1.31 ↑ | -0.82 ↑ | -0.74 ↑ | -1.54 ↑ | -1.32 ↑ | -1.40 ↑ |
| Maximum | 0.74 ↑ | -0.30 ↑ | -0.26 ↑ | 1.52 ↑ | 2.40 ↓ | 1.07 ↑ |
| Range | 2.05 ↑ | 0.51 ↑ | 0.48 ↑ | 3.06 ↑ | 3.72 ↑ | 2.47 ↑ |
| Mean | -0.39 ↓ | -0.58 ↓ | -0.57 ↓ | -0.09 ↓* | 0.85 ↓ | -0.18 ↓ |
| Median | -0.40 ↓ | -0.56 ↓ | -0.56 ↓ | -0.10 ↑ | 1.01 ↓ | -0.18 ↓ |
| Standard Deviation | 0.40 ↑ | 0.09 ↑ | 0.07 ↑ | 0.63 ↑ | 0.78 ↑ | 0.52 ↑ |
| DS-7 Getis statistic values (n=400) | | | | | | |
| Minimum | -1.64 ↓ | -1.18 ↓ | -0.97 ↓ | -1.72 ↑ | -1.59 ↑ | -1.86 ↑ |
| Maximum | 2.03 ↑ | 0.30 ↑ | 0.21 ↑ | 2.45 ↑ | 2.34 ↓ | 2.08 ↑ |
| Range | 3.67 ↑ | 1.48 ↑ | 1.18 ↑ | 4.18 ↑ | 3.93 ↑ | 3.95 ↑ |
| Mean | 0.37 ↑ | -0.39 ↓ | -0.48 ↓ | 0.66 ↓ | 0.96 ↓ | 0.50 ↓ |
| Median | 0.55 ↓ | -0.37 ↑ | -0.44 ↑ | 0.85 ↓ | 1.15 ↓ | 0.70 ↓ |
| Standard Deviation | 0.82 ↑ | 0.27 ↑ | 0.15 ↑ | 0.91 ↑ | 0.89 ↑ | 0.86 ↑ |
| DS-8 Getis statistic values (n=441) | | | | | | |
| Minimum | -1.56 ↑ | -0.98 ↑ | -0.81 ↑ | -1.87 ↑ | -1.73 ↑ | -1.89 ↑ |
| Maximum | 2.11 ↑ | 0.66 ↑ | 0.14 ↑ | 2.31 ↑ | 2.12 ↑ | 1.88 ↑ |
| Range | 3.66 ↑ | 1.64 ↑ | 0.95 ↑ | 4.18 ↑ | 3.85 ↑ | 3.77 ↑ |
| Mean | -0.37 ↓ | -0.47 ↓ | -0.45 ↓ | -0.13 ↓ | 0.51 ↓ | -0.13 ↓ |
| Median | -0.57 ↓ | -0.50 ↓ | -0.45 ↓ | -0.34 ↓ | 0.58 ↓ | -0.27 ↓ |
| Standard Deviation | 0.63 ↑ | 0.23 ↑ | 0.11 ↑ | 0.72 ↑ | 0.61 ↑ | 0.64 ↑ |
| DS-9 Getis statistic values (n=441) | | | | | | |
| Minimum | -1.23 ↑ | -0.75 ↑ | -0.67 ↑ | -1.53 ↑ | -1.65 ↑ | -1.37 ↑ |
| Maximum | 1.04 ↑ | -0.08 ↑ | -0.20 ↑ | 1.69 ↑ | 2.20 ↑ | 1.18 ↑ |
| Range | 2.27 ↑ | 0.67 ↑ | 0.47 ↑ | 3.21 ↑ | 3.85 ↑ | 2.55 ↑ |
| Mean | -0.06 ↓* | -0.38 ↓ | -0.39 ↓ | 0.23 ↓ | 0.70 ↓ | 0.05 ↓ |
| Median | -0.09 ↑ | -0.36 ↑ | -0.37 ↑ | 0.35 ↓ | 0.85 ↓ | 0.16 ↑ |
| Standard Deviation | 0.49 ↑ | 0.12 ↑ | 0.08 ↑ | 0.70 ↑ | 0.82 ↑ | 0.56 ↑ |
| DS-10 Getis statistic values (n=441) | | | | | | |
| Minimum | -0.85 ↑ | -0.68 ↑ | -0.62 ↑ | -0.96 ↑ | -0.56 ↑ | -0.94 ↑ |
| Maximum | 1.13 ↑ | -0.19 ↑ | -0.28 ↑ | 1.55 ↑ | 2.20 ↑ | 1.01 ↑ |
| Range | 1.98 ↑ | 0.49 ↑ | 0.34 ↑ | 2.51 ↑ | 2.76 ↑ | 1.95 ↑ |
| Mean | -0.05 ↑* | -0.42 ↓ | -0.44 ↓ | 0.18 ↓ | 0.71 ↓ | 0.01 ↑ |
| Median | -0.13 ↑ | -0.41 ↓ | -0.44 ↓ | 0.22 ↓ | 0.71 ↓ | -0.06 ↑ |
| Standard Deviation | 0.40 ↑ | 0.08 ↑ | 0.06 ↑ | 0.54 ↑ | 0.47 ↑ | 0.41 ↑ |

↑ denotes that value in plot sample is greater than found in the random sample
↓ denotes that value in plot sample is less than found in the random sample
= denotes that value in plot sample is equal to that found in the random sample
* denotes that mean value in plot sample is not significantly different from random sample (at a 95% level of significance)

### 7.2.4. Integrated Consideration of the Spectral and Spatial Data

The previous data summaries have illustrated that the distributions of the *casi* spectral and spatial data are independent of one another. Consideration of the spectral data in reference to the spatial data provides insights into where the spectral information is occurring in image space. When computing $G_i^*$ the distance value, which relates the distance around the pixel of consideration at which the autocorrelation is maximized, is also collected. A distance value of 1 relates that a 3x3 window surrounding a pixel is the spatial region at which spectral response is found to be most similar. In contrast, a distance value of 4 relates that the spatial dependence around a pixel is maximized within a 9x9 window. Consideration of the distribution of reflectance and $G_i^*$ values in terms of the distance at which spatial association is maximized provides insights into the spatial distribution of image spectral values (maximum Getis distance: MGD).

The integrated distribution of spectral and spatial data presents the manner in which the spectral data are spatially distributed in the imagery. To enable the demonstration of the integrated distribution of spectral and spatial data, the following distributions are presented following a short introduction:

1. original spectral reflectance, in aggregate and in terms of MGD,
2. $G_i^*$ values computed within static sized window,
3. overall distribution of $G_i^*$ values plotted as a function of MGD,
4. count of the proportion of occurrence of each distance value, and
5. proportion of distance occurrence as a function of $G_i^*$ range.

Distribution 1 demonstrates that the original spectral reflectance values are normally distributed, both in terms of all image pixels and when the distribution of spectral response is considered as a function of MGD. Distribution 2 illustrates the frequency of occurrence of $G_i^*$ values when computed within static sized windows. Yet, distribution 2 operates on the

assumption that all processes are occurring at the same scale. The frequency of occurrence of each MGD in reference to where these values occur, in terms of $G_i^*$ value, relates that each computation distance is generating different information. To illustrate the dependence of scale upon the resultant $G_i^*$ values, distribution 3 presents the $G_i^*$ values as a function of associated MGD. Distribution 3 deconstructs the MGD to include distance values and associated $G_i^*$ values. As each MGD has an associated $G_i^*$ value these numbers may be plotted to demonstrate the composition of the aggregate MGD. The aggregate values relate to the $G_i^*$ values utilized for analysis in this thesis. Distribution 4 presents the frequency of occurrence of each MGD for the entire image, and is included to provide further insights into the spatial dependence characteristics of the imagery, and the scale at which the dominant spatial processes in the imagery are operating. The proportional occurrence of MGD values may also be considered in terms of the $G_i^*$ range. Distribution 5 presents the proportion of each distance value which comprises each $G_i^*$ range. The dominant spectral characteristics, related to the spatial structure of the imagery, plots of MGD as a function of $G_i^*$ range, which relate the manner in which the original spectral values are distributed spatially in the imagery.

The spectral and spatial values of red (C2), infrared (C5), and panchromatic reflectance, MGD, and $G_i^*$, are assessed with the aforementioned distributional series upon sample image DS7. The image encompassing the plot DS7 was selected to due the complex conditions present. Selection of a simple image may lead to observations particular to a single case, the choice to utilize DS7 for further analysis is intended to present a variable spectral scenario with elements of the other study plots also included. Such analysis of the spectral and spatial dependencies with unique values for each pixel in an image is unusual in the remote sensing literature. The red spectral channel was selected to represent the visible wavelengths and the behavior of spectral and spatial information with a limited range of

values. Figure 7.1 is presented to illustrate the original distribution of red spectral response which is skewed towards the higher reflectance values. The dominance of low reflectance values relates the dominance of vegetation in the study image. The skew towards higher reflectance values is due to the non-vegetation features present in the image. The combined value relates the complete distribution of spectral values to be compared to the what is occurring at each MGD. At each MGD the distribution of reflectance values vary in frequency, yet all are found to be relatively normal with the skew towards high reflectance values.

Figure 7.2 is presented to illustrate the distribution of $G_i^*$ values computed within static sized windows. The dominance of low reflectance values results in a high frequency of moderate negative $G_i^*$ values for all distances. The frequent occurrence of distance 1 (3x3 window) at the $G_i^*$ range near zero is an indication of lack of sensitivity of $G_i^*$ with values at the middle of the full range of processed values. The frequent occurrence of $G_i^*$ values near zero indicates the variety of spatial dependency characteristics which may be related within a 3x3 window. The high count of $G_i^*$ occurrence near zero at distance 1 may be the result of a distinct spatial regime with a high value computed for distance 1, or may represent an area of weak spatial dependence which is maximized within distance 1. As a result, caution must be exercised when interpreting the image spatial dependency values which are represented by $G_i^*$ values that are near zero.

Figure 7.3 is presented to illustrate that when $G_i^*$ is extracted at MGD, the frequency of values at the $G_i^*$ range near zero are reduced in importance. The distribution of $G_i^*$ values at MGD for the red spectral channel are mildly bi-modal. A bi-modal distribution to $G_i^*$ values indicates the presence in the imagery of a spatial dependence between the magnitude of reflectance values and location within the image. At a spatial resolution of 1m, the

interpretation of the distribution of $G_i^*$ at MGD indicates the clustering of low red reflectance values associated with vegetation and a clustering of higher red reflectance values related to the non-vegetated features. The dominance of vegetation in the sample scene processed for this demonstration resulted in the greater prevalence of values centered about a $G_i^*$ of -0.7.

In Table 7.6 we present the frequency of each MGD over the entire image. The counts for each distance relate the frequency at which the spatial dependence in the sample image is maximized. The frequent occurrence of distance 1 indicates that neighbouring pixels are most often the region in which a spatial process is best summarized. Yet, 45% of the occurrences indicate that the region of spatial dependency is best described within a larger region. Figure 7.4 relates the relationship between MGD frequency and $G_i^*$, the prevalence of distance 1 in the low range of $G_i^*$ values relates the strong spatial association between the tree object reflectance values. The high proportion of distance 1 values at a $G_i^*$ may indicate a region of high spatial association, or that in regions of low association the spatial dependence found to be maximized in the immediate neighbourhood, with a distance of 1, may be due to the $G_i^*$ value being the highest of a series of low values. The roughly equal occurrence of distance proportions above zero indicates the lack of strong spatial dependency between the higher red reflectance values found in a 1m spatial resolution image of a forest.

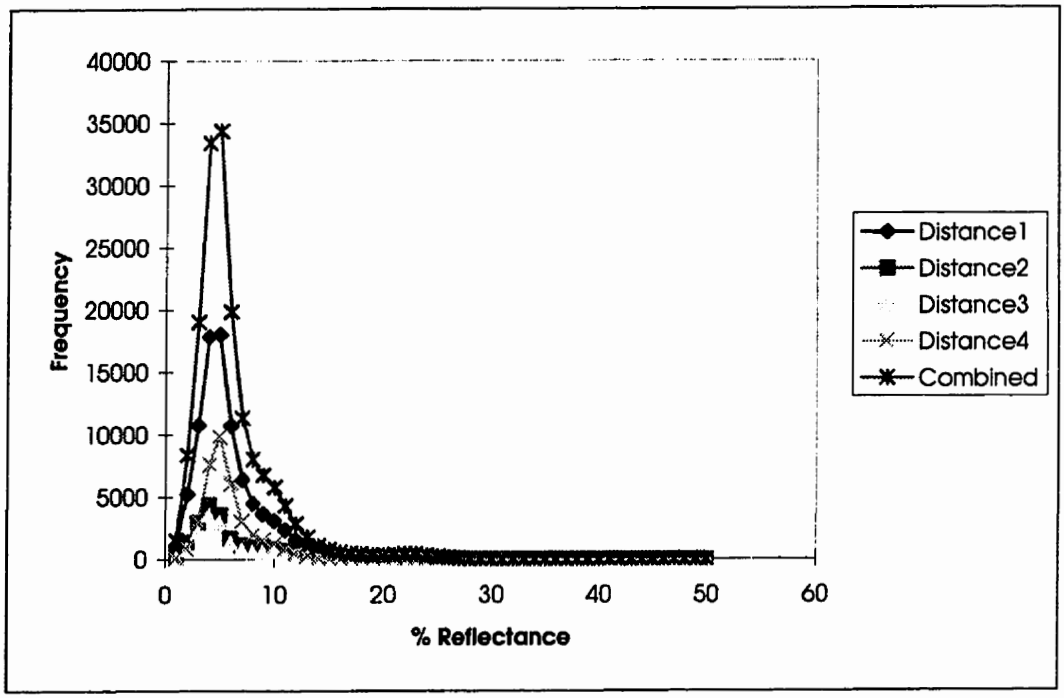


**Figure 7.1. Original distribution of red spectral response (combined) and as a function of the distance at which the maximum Getis statistic is computed.**

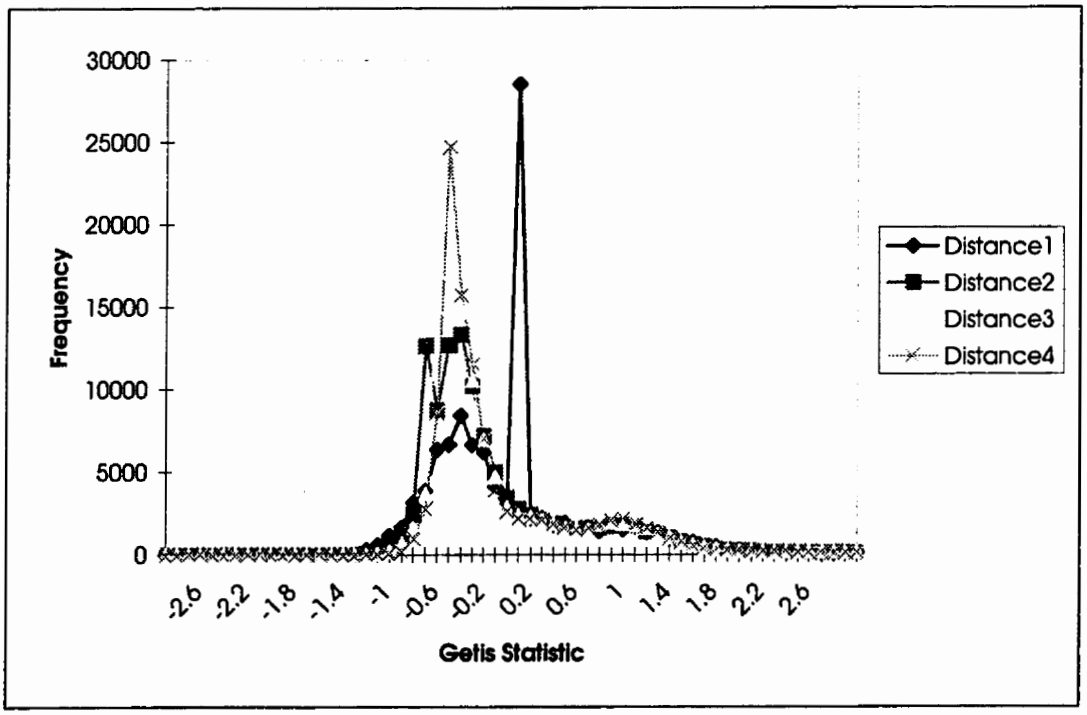


**Figure 7.2. Distribution of Getis statistic values when computed on the red spectral channel for a single distance.**

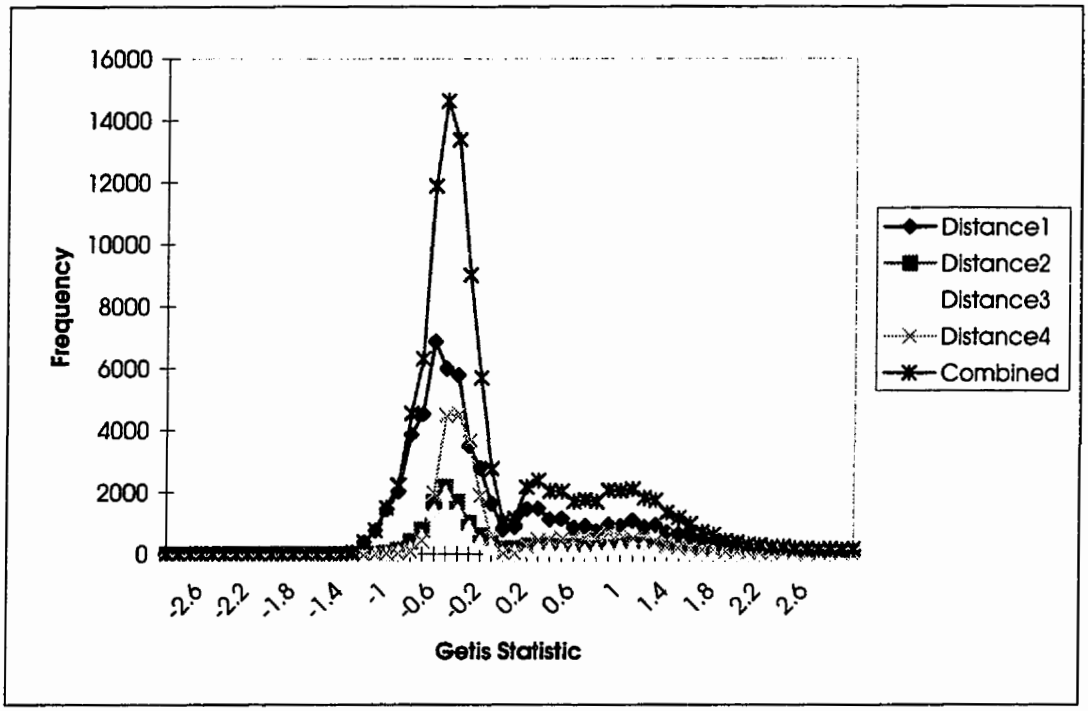


**Figure 7.3. Overall distribution of red channel Getis statistic values (combined) and as a function of distance at which the maximum Getis statistic value is computed.**

**Table 7.6. Frequency of distance selection at maximized red Getis statistic location (n=108772)**

| Distance | Count | Percentage |
|---|---|---|
| 1 | 59917 | 55 |
| 2 | 13621 | 13 |
| 3 | 9926 | 9 |
| 4 | 25308 | 23 |

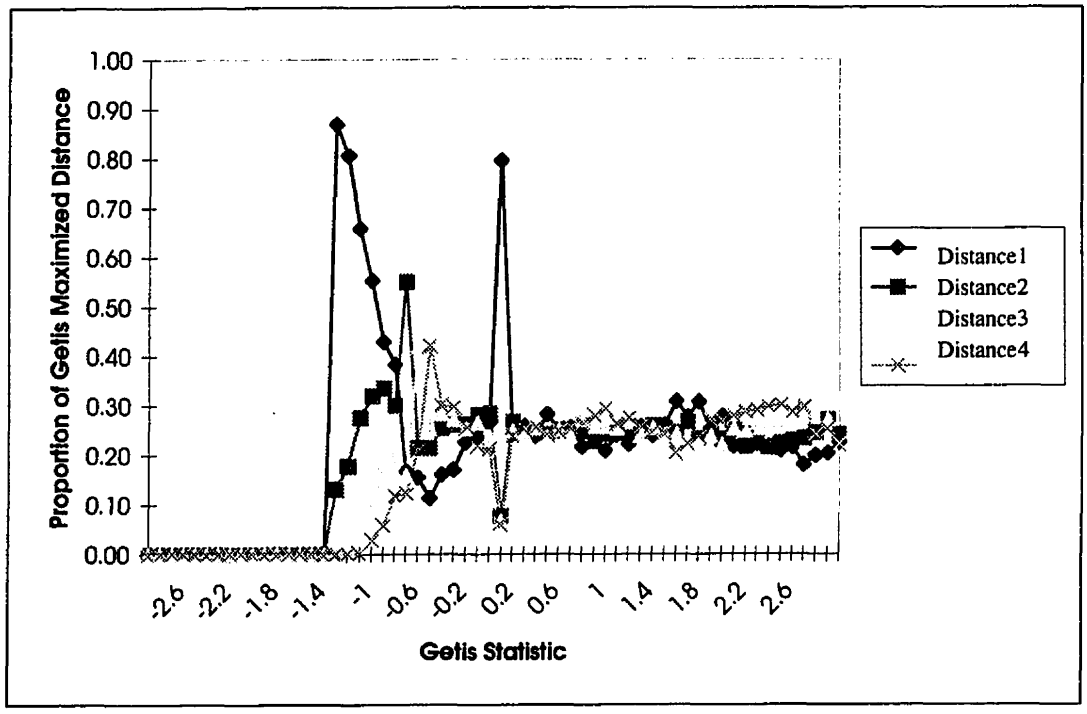


**Figure 7.4. Proportion of MGD value frequency for the red channel by Getis statistic location.**

As illustrated (in Table 7.4 and 7.5), red reflectance values for vegetation are low and are of a limited range; whereas, infrared reflectance values are high for vegetation, and occupy a larger range of potential values. In Figure 7.5 we present the large range of infrared reflectance values found on the sample image. The infrared reflectance values approach normality for the entire image, and also when considered as a function of MGD. The strong association of neighbouring pixel values is illustrated here with the frequent occurrence of distance 1 as the MGD.

Figure 7.6 is presented to illustrate the distribution of $G_i^*$ values computed within static sized windows. The distribution of the $G_i^*$ for distance 1, 2, and 3, with prevalence at a negative $G_i^*$ near -0.5 may indicate the low infrared values which occur in shadows created by the trees. The high count of distance 1 $G_i^*$ values indicates the frequent occurrence of

unrelated values within a 3x3 window. Yet, when considering the $G_i^*$ values at MGD these low associations are no longer included.

Figure 7.7 is presented as an illustration of the bi-modal distribution of $G_i^*$ values for the infrared reflectance values on the sample image DS7. The bi-modal distribution to the $G_i^*$ values at MGD indicates the low infrared reflectance values related to image shadow features and the high infrared reflectance values are related to vegetation. The range of spectral values which may be found in a shadow are limited resulting in the peaked distribution of negative $G_i^*$ values. The greater potential range of vegetation infrared reflectance results in a less peaked distribution. The spatial dependence is maximized within a 3x3 window 62% of the potential instances (Table 7.7). Yet, in 38% of the instances a static window would not capture the spatial structure present in the imagery. As the image spatial structure is a function of the forest vegetation structure, the use of a series of windows to characterize the spatial dependence characteristics maximizes the information extraction potential.

In Figure 7.8 we present the relationship between the MGD frequency as a function of $G_i^*$. Distance 1, which relates a strong spatial dependence within a 3x3 pixel window is capturing a variety of information. At low $G_i^*$ the proportion of $G_i^*$ accounted for within distance 1 appears related to the constrainment of dark objects and shadow features, at $G_i^*$ near zero the regions of low association are accounted for, and at high $G_i^*$ values a strong spatial dependence between high infrared values is demonstrated. The distribution of the distances 2 and 3 appear to account for transitional areas between regions of high and low spatial association. Distance 2 appears to indicate a moderate level of larger regions of association of low and high infrared reflectance values. As expected, distance 4 is most prevalent in regions of low association in the centre of the distribution.

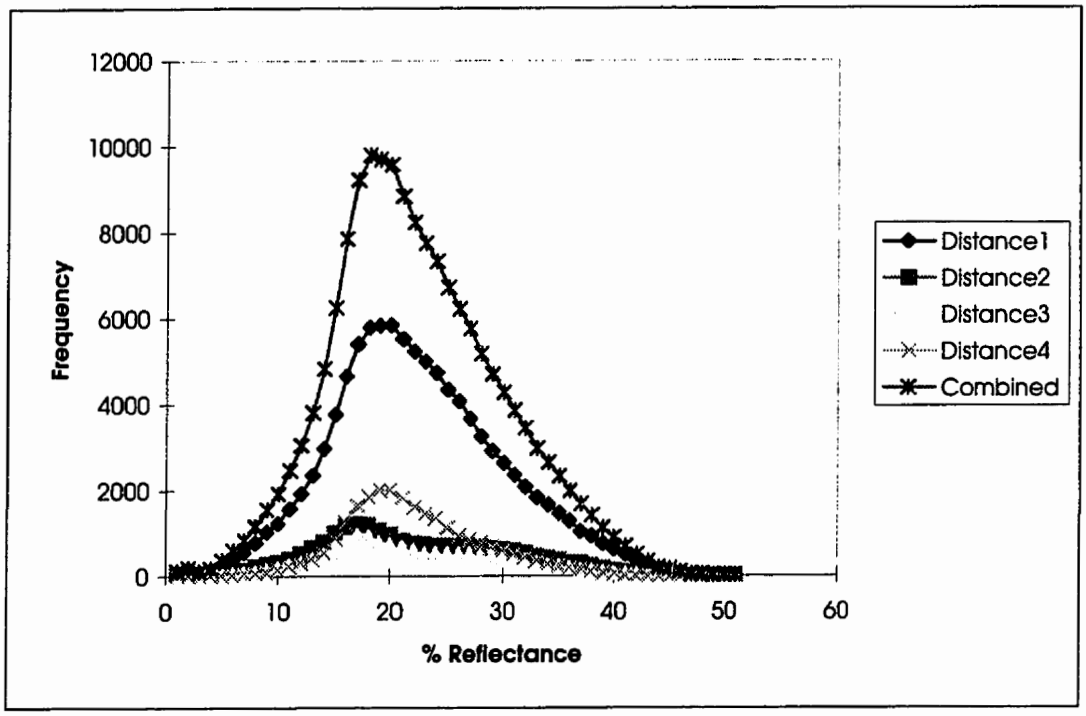


**Figure 7.5. Original distribution of infrared spectral response (combined) and as a function of the distance at which the maximum Getis statistic is computed.**

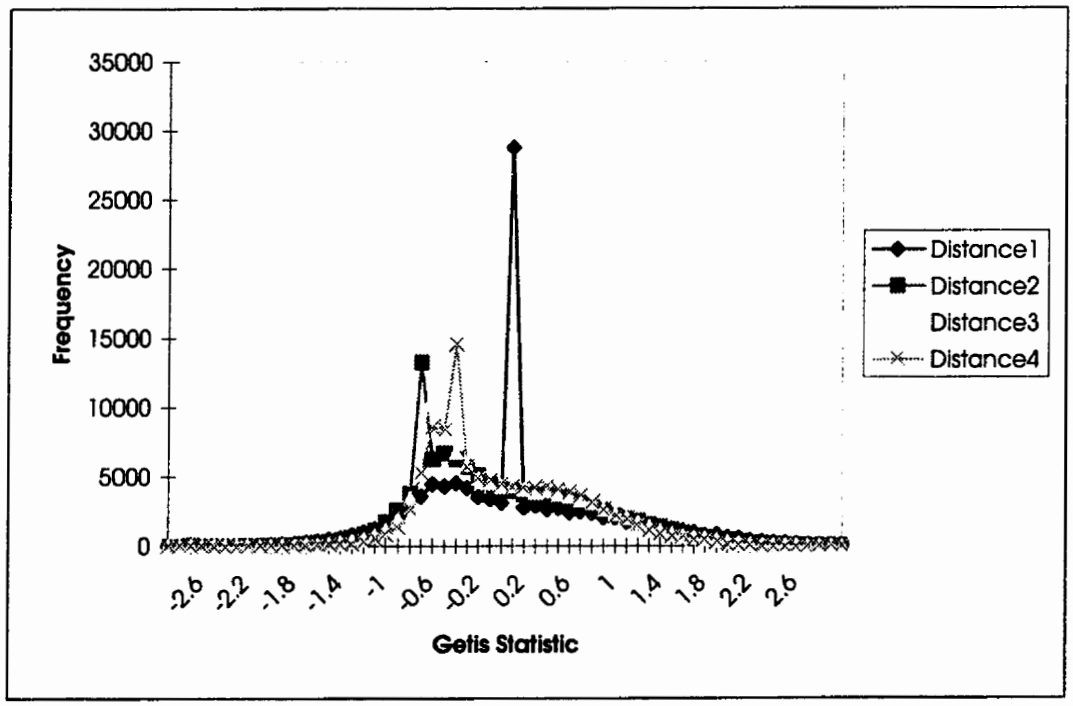


**Figure 7.6. Distribution of Getis statistic values when computed on the infrared channel for a single distance.**

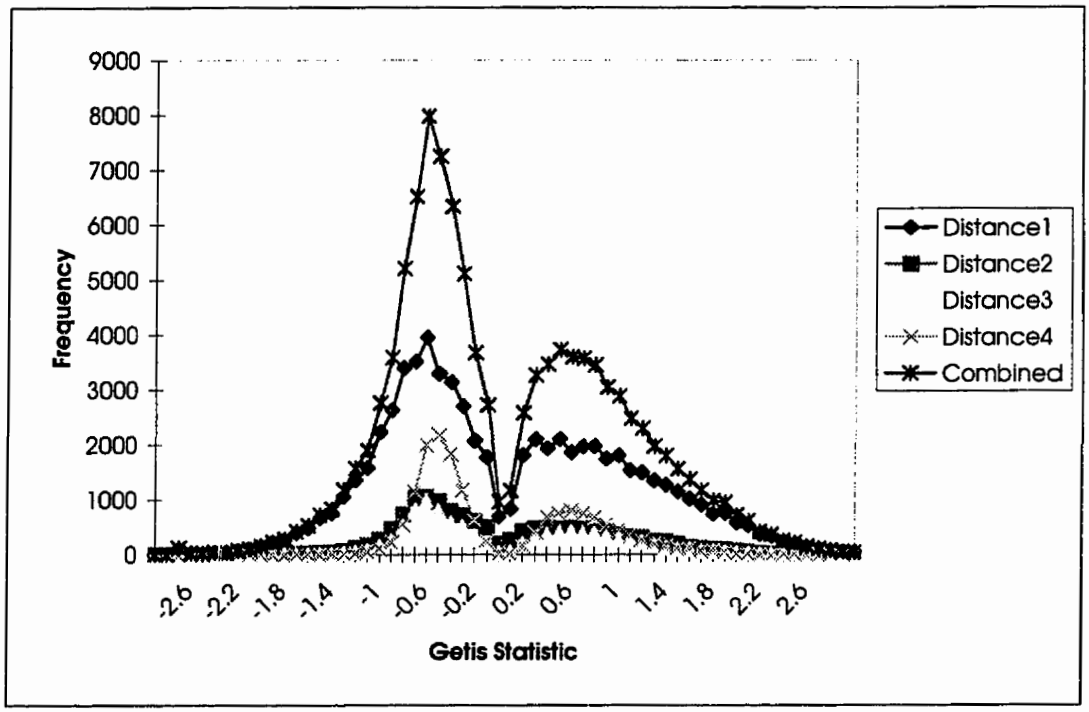


**Figure 7.7. Overall distribution of infrared Getis statistic values (combined) and as a function of the distance at which the maximum Getis is statistic computed.**

**Table 7.7. Frequency of distance selection at maximized infrared Getis statistic location (n=108772)**

| Distance | Count | Percentage |
|---|---|---|
| 1 | 67844 | 62 |
| 2 | 14282 | 13 |
| 3 | 9774 | 09 |
| 4 | 16872 | 16 |

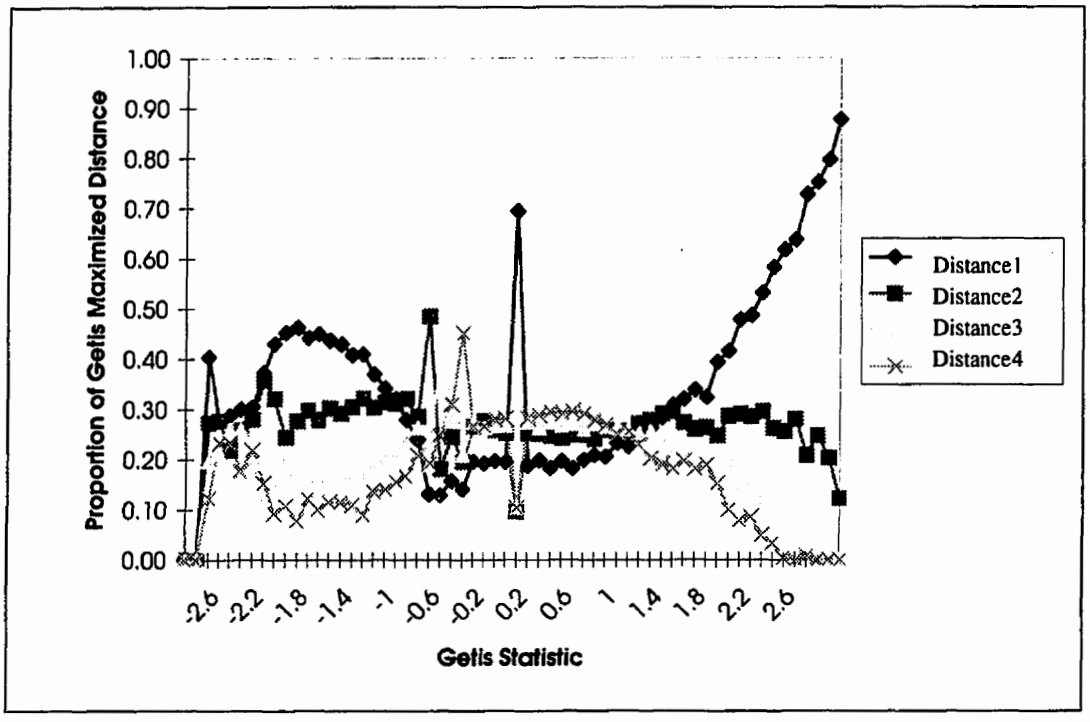


**Figure 7.8. Proportion of MGD value frequency for the infrared channel by Getis statistic location.**

The panchromatic spectral response is a function of the spectral response in both visible and infrared wavelengths. The distribution of panchromatic spectral values approximates the normal distribution over the entire image as well as when considered as a function of MGD (Figure 7.9). The wide spectral bandwidth of the panchromatic channel is illustrated in the moderated spectral response.

We present in Figure 7.10 the distribution of $G_i^*$ values computed within static sized windows. A familiar distribution emerges with a high occurrence of $G_i^*$ near zero in a 3x3 window related to the lack of spatial dependence often found within a 3x3 window. The frequent occurrences of distances 2, 3, and 4, at mild negative $G_i^*$ is a function of the constrained range of low panchromatic values.

Figure 7.11 is a presentation of the $G_i^*$ frequency as a function of the distance at which $G_i^*$ is maximized. The distribution of $G_i^*$ at MGD for the panchromatic spectral information found in sample image DS7 is bi-modal. This bi-modal distribution relates the tendency of high values to be found with high values, low values to be found with low values, and for a smaller number of transitional values to be found between these more dominant spectral objects. The frequent occurrence of distance 1 as the MGD indicates a tendency for the spatial association of the panchromatic reflectance data to be maximized within a 3x3 window (Table 7.8). The spatial dependence is maximized at Distance 1 in the sample image in the neighbourhood for ≈ 61% of image pixels. Yet, ≈ 39% of the image local spatial dependence occurs within a window larger than 3x3.

The distribution of the spatial dependence regions in terms of $G_i^*$ values is presented as a proportion of distance occurrence in Figure 7.12. Distance 1 accounts for a range of strengths in spatial dependency, including clusters of low panchromatic values, mid-range low spatial association regions, and clusters of high panchromatic values. The $G_i^*$ values in the centre of the distribution likely relate areas where the spatial dependence between pixels at any of the four distance values is low, $G_i^*$ is merely maximized with a low value in the 3x3 window. The larger distances, 3 and 4, are consistent through the moderate $G_i^*$ range accounting for regions of moderate, yet broad association. The consistent proportion of distance 2 as the MGD indicates image spatial processes in operation within a 5x5 pixel window, including both low and high panchromatic reflectance values.

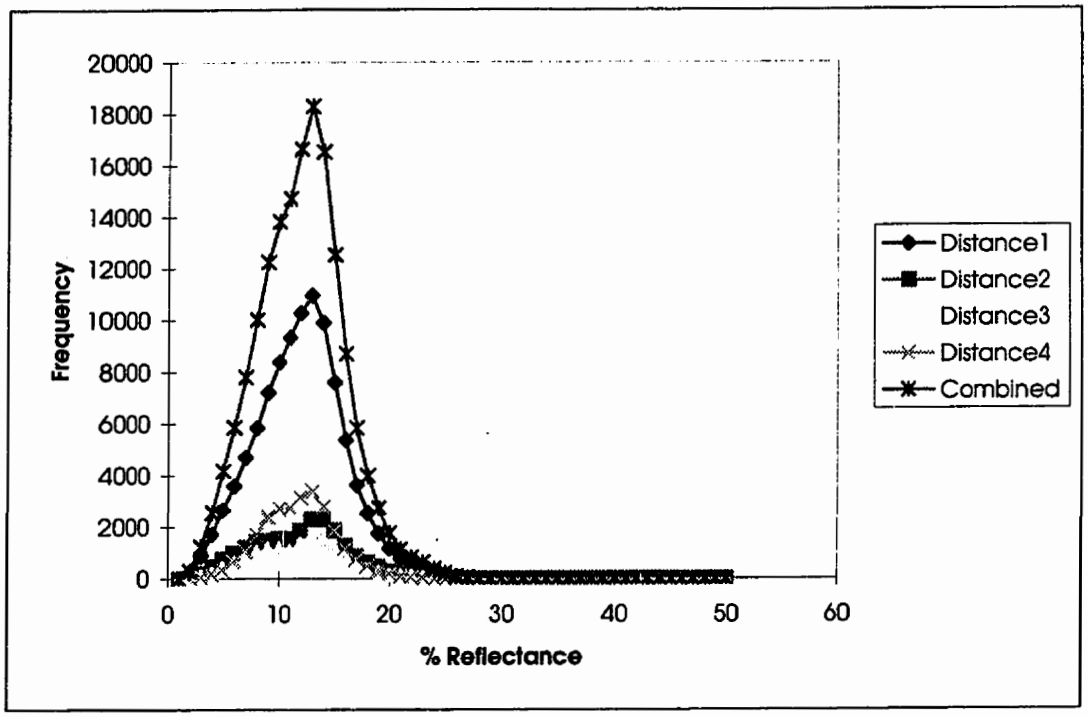


**Figure 7.9. Original distribution of panchromatic spectral response (combined) and as a function of distance at which the maximum Getis statistic is computed.**

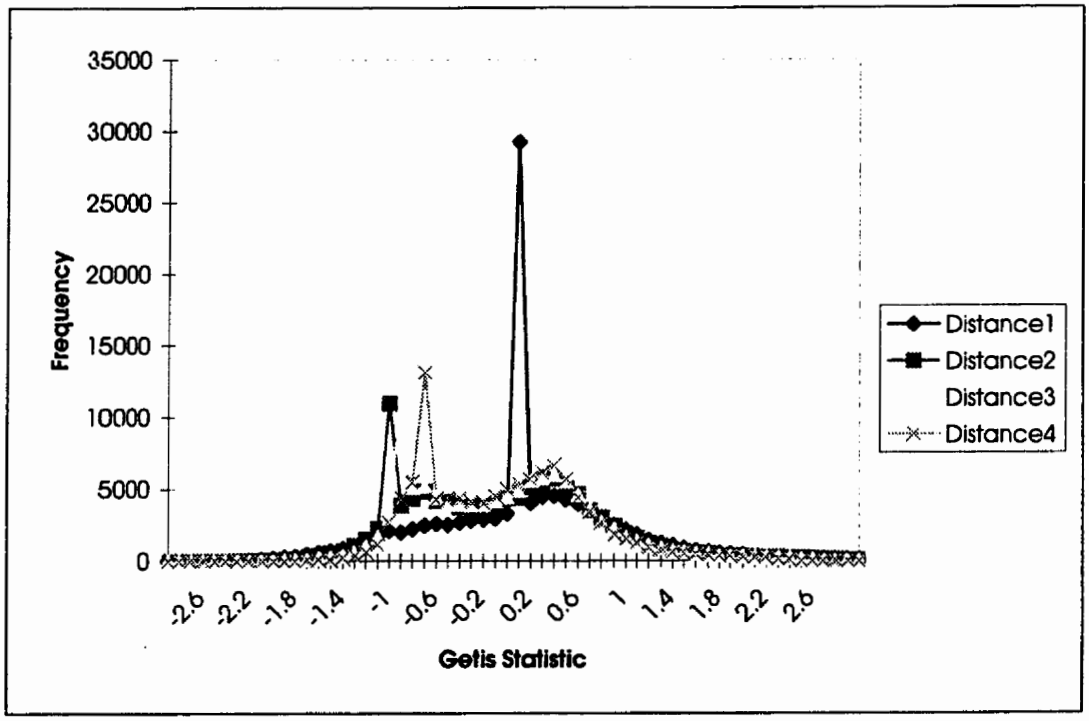


**Figure 7.10. Distribution of Getis statistic values when computed on the panchromatic channel for a single distance.**

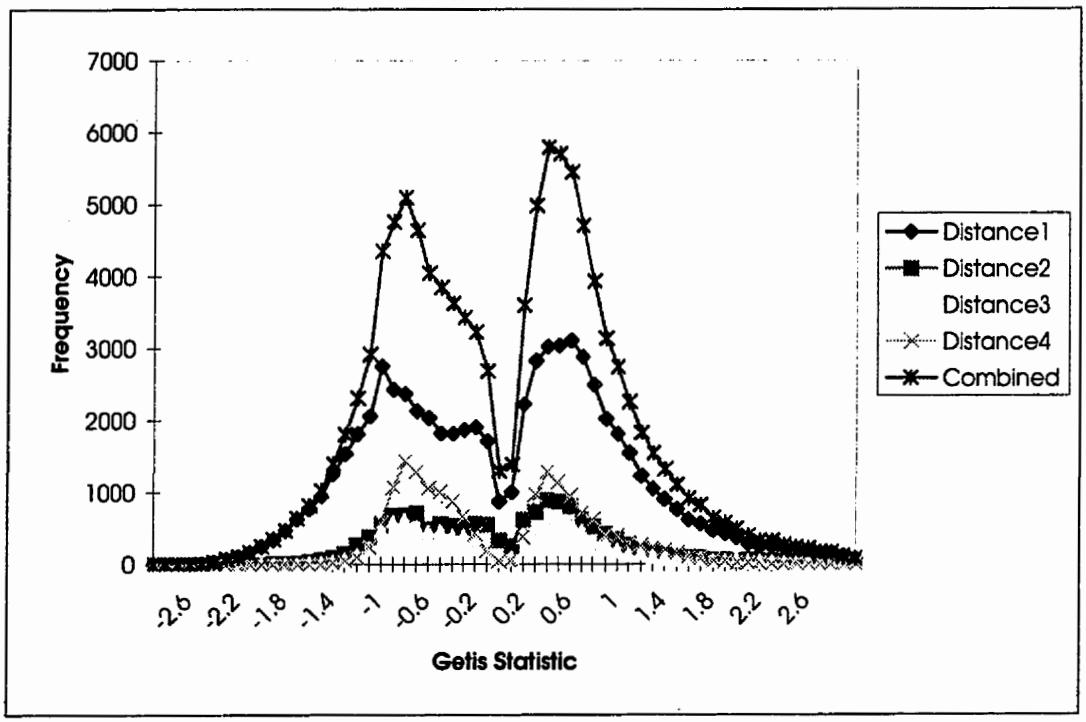


**Figure 7.11. Overall distribution of panchromatic Getis statistic values (combined) and as a function of the distance at which the maximum Getis statistic is computed.**

**Table 7.8. Frequency of distance selection at maximized panchromatic Getis statistic location (n=108772)**

| Distance | Count | Percentage |
|---|---|---|
| 1 | 66631 | 61 |
| 2 | 14728 | 14 |
| 3 | 9970 | 9 |
| 4 | 17442 | 16 |

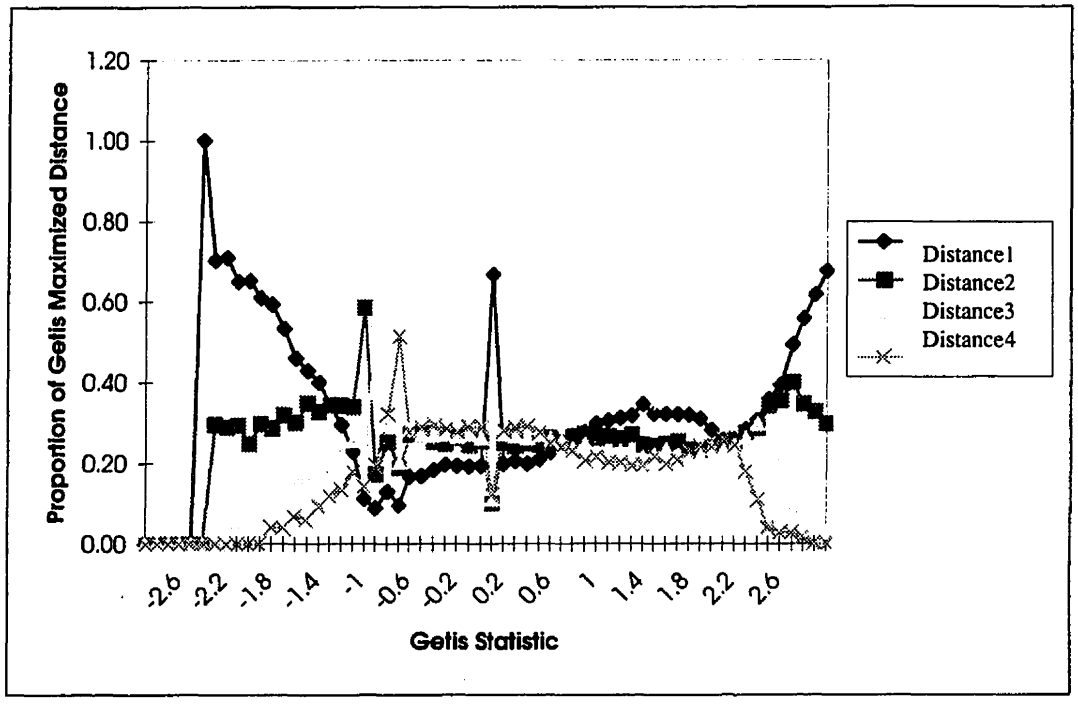


**Figure 7.12. Proportion of MGD value frequency for the panchromatic channel by Getis statistic location.**

### 7.2.4.1. Section Summary

The preceding consideration of the spectral reflectance values in reference to the spatial data generated from the spectral data exposed many interesting relationships, such as:

- image spatial structure relates to the size of objects found in forest imagery which is also related to the spatial resolution,
- image spectral values have a unique distribution in the spatial domain, and
- image spatial processes are not all operating at the same scale.

The ability to detect patterns of spatial dependency as a function of original spectral characteristics enables extraction of unique information relating to the forest structure. Further investigation on the range of $G_i^*$ values between the minimum and maximum may be a means to reveal the nature of the spatial dependence in homogeneous regions. The demonstration of the spatial distribution of spectral values in image space reveals that the

image structure is capturing unique information based on the relationship between image spatial resolution and the size of the objects remotely sensed.

### 7.2.5. Selection of Spectral Channels for Analysis

To reduce unnecessary duplication in the following analyses, the inter-relationships between the spatial and spectral data are investigated. In Table 7.9 the correlations between the *casi* spectral data and $G_i^*$ values are presented. High correlations indicate a dependence between the spectral values found at the same pixel locations. Low correlations between the spectral channels indicate the presence of unique spectral information in comparison to the other spectral channels. The NIR spectral channel (*casi*-5), has the lowest correlations to all other channels, indicating an independence of spectral information. The *casi* visible channels are all strongly interrelated. The *casi* visible channels are also strongly related to the panchromatic channel. Sensors which have the ability to collect narrow band visible spectral information normally also have the capability to collect near infrared information (Anger, *et al.*, 1996; Aplin, *et al.*, 1997). Yet, sensors which collect panchromatic information normally lack the ability to collect other spectral information. As a result, for further analyses in this thesis, the NIR channel (*casi*-5), and the panchromatic channel will be utilized. The $G_i^*$ data generated from *casi*-5 and *casi*-PAN are weakly correlated.

**Table 7.9. Correlations between *casi* spectral and $G_i^*$ spatial data (random sample, n=400)**

| | *casi*-1 | *casi*-2 | *casi*-3 | *casi*-4 | *casi*-5 | *casi*-PAN | GETIS -1 | GETIS -2 | GETIS -3 | GETIS -4 | GETIS -5 |
|---|---|---|---|---|---|---|---|---|---|---|---|
| *casi*-2 | 0.87 | | | | | | | | | | |
| *casi*-3 | 0.83 | 1.00 | | | | | | | | | |
| *casi*-4 | 0.90 | 0.67 | 0.61 | | | | | | | | |
| *casi*-5 | 0.39 | -0.01 | -0.08 | 0.68 | | | | | | | |
| *casi*-PAN | 0.85 | 0.73 | 0.70 | 0.83 | 0.47 | | | | | | |
| GETIS-1 | 0.91 | 0.79 | 0.75 | 0.82 | 0.35 | 0.74 | | | | | |
| GETIS-2 | 0.81 | 0.88 | 0.87 | 0.62 | 0.02 | 0.64 | 0.88 | | | | |
| GETIS-3 | 0.77 | 0.88 | 0.87 | 0.57 | -0.04 | 0.61 | 0.84 | 0.99 | | | |
| GETIS-4 | 0.87 | 0.63 | 0.58 | 0.90 | 0.60 | 0.75 | 0.92 | 0.70 | 0.64 | | |
| GETIS-5 | 0.34 | -0.06 | -0.12 | 0.58 | 0.92 | 0.39 | 0.36 | -0.01 | -0.07 | 0.62 | |
| GETIS-PAN | 0.78 | 0.67 | 0.64 | 0.73 | 0.40 | 0.91 | 0.81 | 0.69 | 0.66 | 0.81 | 0.41 |

## 7.3. SEGMENTATION OF GETIS STATISTIC VALUES INTO TREE CLUSTERS

There are many techniques for the extraction of information from digital images (Rosenfeld, 1984). A method of grouping related pixels is through image segmentation (Reed and Du Buff, 1993). There is a wide variety of image segmentation techniques; yet, the selection of an appropriate technique for a particular image type and objective is not a trivial task (Pal and Pal, 1993). Image segmentation is an art and science. For successful segmentation, the art is to consider physical characteristics of how the imagery was created and what the data represent, while also developing a consistent and rigorous technique to process the data. Based upon the image spatial resolution and the forest composition in the study area, the goal of the segmentation of $G_i^*$ values is to group together, or cluster, high near infrared and panchromatic reflectance values. For example, high near infrared reflectance values are expected for trees based on an understanding of the reflectance

properties of vegetation (Gausman, 1977). $G_i^*$ values are generated from the reflectance values to enable such clustering.

The selection of threshold values to partition the $G_i^*$ values into image based objects is not possible due the local computation of $G_i^*$ values (Pal and Pal, 1993). A threshold value which may successfully create clusters in one image section may not work in another section due to changes in forest structure. As a result, a measurement guided spatial clustering technique is needed to group the $G_i^*$ values into clusters based upon local characteristics. The generation of tree clusters is undertaken from the segmentation of $G_i^*$ values. The $G_i^*$ values are well prepared for segmentation as each pixel has a value which indicates the strength of the relationship between neighbouring pixels.

The $G_i^*$ values computed from the reflectance imagery provide information relating the strength of the relationship between pixels and the magnitude of the reflectance values which are found in association. The segmentation approach developed for this study utilizes both the strength and the magnitude of the $G_i^*$ to form tree clusters. The following steps are undertaken to cluster the $G_i^*$ values:

- select reflectance imagery for analysis
- assess the spectral reflectance characteristics of the selected wavelength(s):
    - near infrared and panchromatic; high reflectance ≈ vegetation
    - visible, such as red wavelengths, low reflectance ≈ vegetation
- generate $G_i^*$ from the image data
- process the $G_i^*$ values to find local minima and maxima for use as seed points (minima are pixels which are found to be the lowest value within a 3x3 window; maxima are the greatest value found within a 3x3 window)
- label each seed point (seed labels are used to populate each pixel or the resultant objects)

- merge seed points which are directly adjacent; this implemented to avoid equal values resulting in multiple adjacent seed points.
- initiate iterative grouping from each minima and maxima seed point
    - omni-directional clustering based upon $G_i^*$ similarity
    - place the pixels in clusters where similarity is maximized
    - similarity is calculated as minimum difference between pixels

The resultant clusters are labeled representations of groups of similar reflectance characteristics. The labels enable the extraction of the original spectral values which comprise a spatially dependent cluster. In the following section we will assess the ability to match the image spatial structure generated clusters with ground measured forest characteristics.

## 7.4. COMPARISON OF FIELD DATA WITH IMAGE CLUSTERS

A complete consideration of the field data and the $G_i^*$ clusters to assess the relationship between forest inventory and biophysical parameters is undertaken in dedicated chapters. This section is intended to allow for a discussion of the problems in matching the field data to the image data. In Figure 7.13 we present a sub-image of raw infrared data and the $G_i^*$ data which were computed from the raw values. As the image data is geocoded and the field data have been oriented with a GPS in the field, co-registration of the field and image data may be undertaken for analysis.

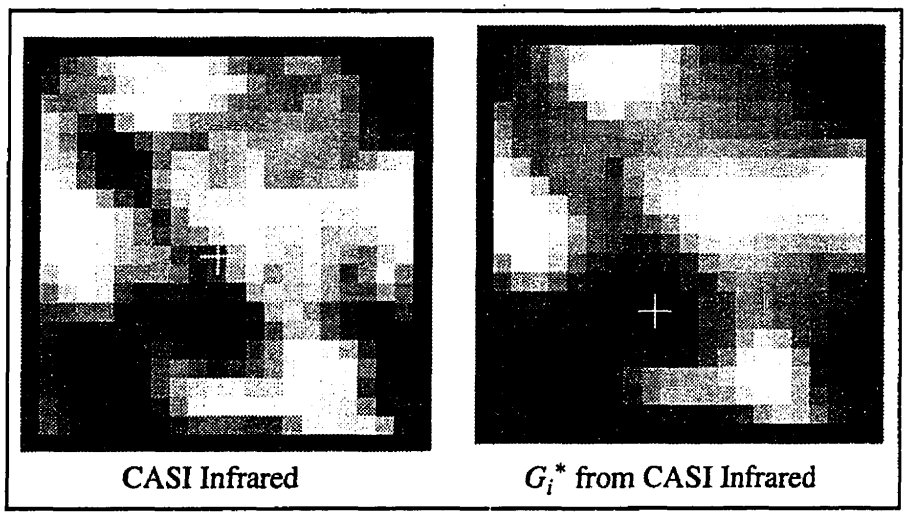


**Figure 7.13. Comparison of image spectral and spatial data (DS7)**

As the tree locations are known, and stored in a GIS, the crown dimensions for each tree have been computed (see Figure 6.3) and have enabled the generation of plot maps based upon ground survey data. The ground measured and delineated stand maps are a reasonable representation of the tree distribution within the sample plot based upon ground measurements taken from below the canopy (Figure 7.14). As may be expected, the forest stand appears much different from above, and this difference in representation hampers the ability to match ground data to remotely sensed data. An exact match of the ground measured plot map with the representation derived from image spatial information is unlikely based upon the aforementioned errors. Yet, if the image derived plot map contains similar distribution characteristics to the field derived plot map some assumptions may be made. The analyst may assume, based upon confidence in the ground control and the ability to locate a plot, that the variability between plot maps is largely a function of error in relating the field collected data to the image data. The ability to "line-up" each of the datum is indeed a difficult proposition.

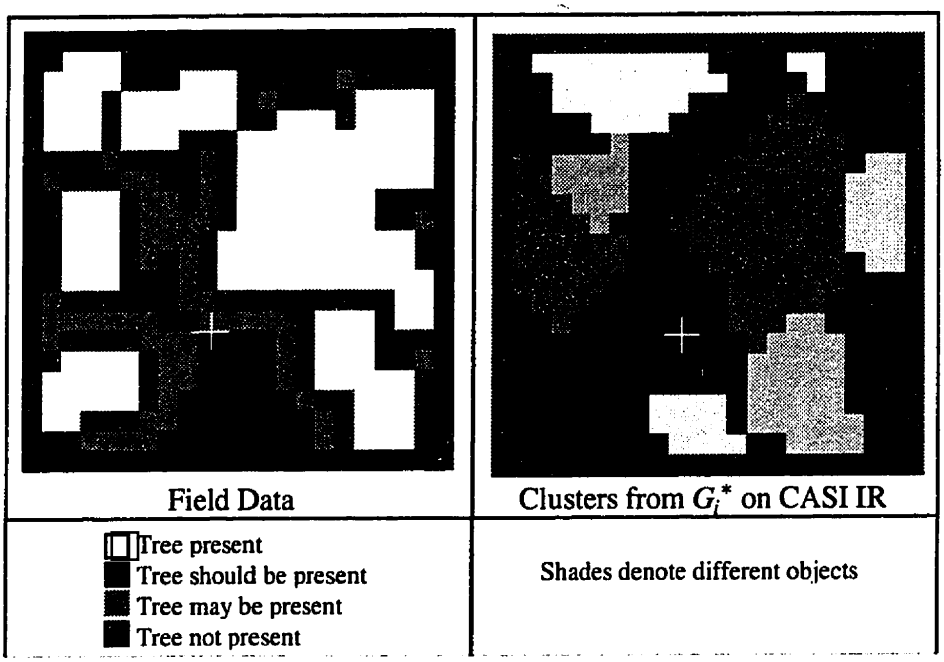


**Figure 7.14. Comparison of field data and clusters generated from $G_i^*$ on *casi* NIR channel (from image DS7)**

The image derived plot maps and distribution characteristics may be understood as the "remote truth", or the best fit data according to the limitations of spatial resolution and data scaling. The concept of a "remote truth" versus ground truth is an acknowledgment that remote sensing instruments, collecting data from above, are unable to record the surface of the canopy in the same manner as mensuration data which are measured from below. Likewise, factors such as spatial and spectral resolution, view angles, and illumination conditions will invariably result in a remotely sensed canopy which varies from ground mensuration data. Figure 7.15 presents the clusters generated for each of the plots studied, which may be compared to the field plots (Figure 6.3).

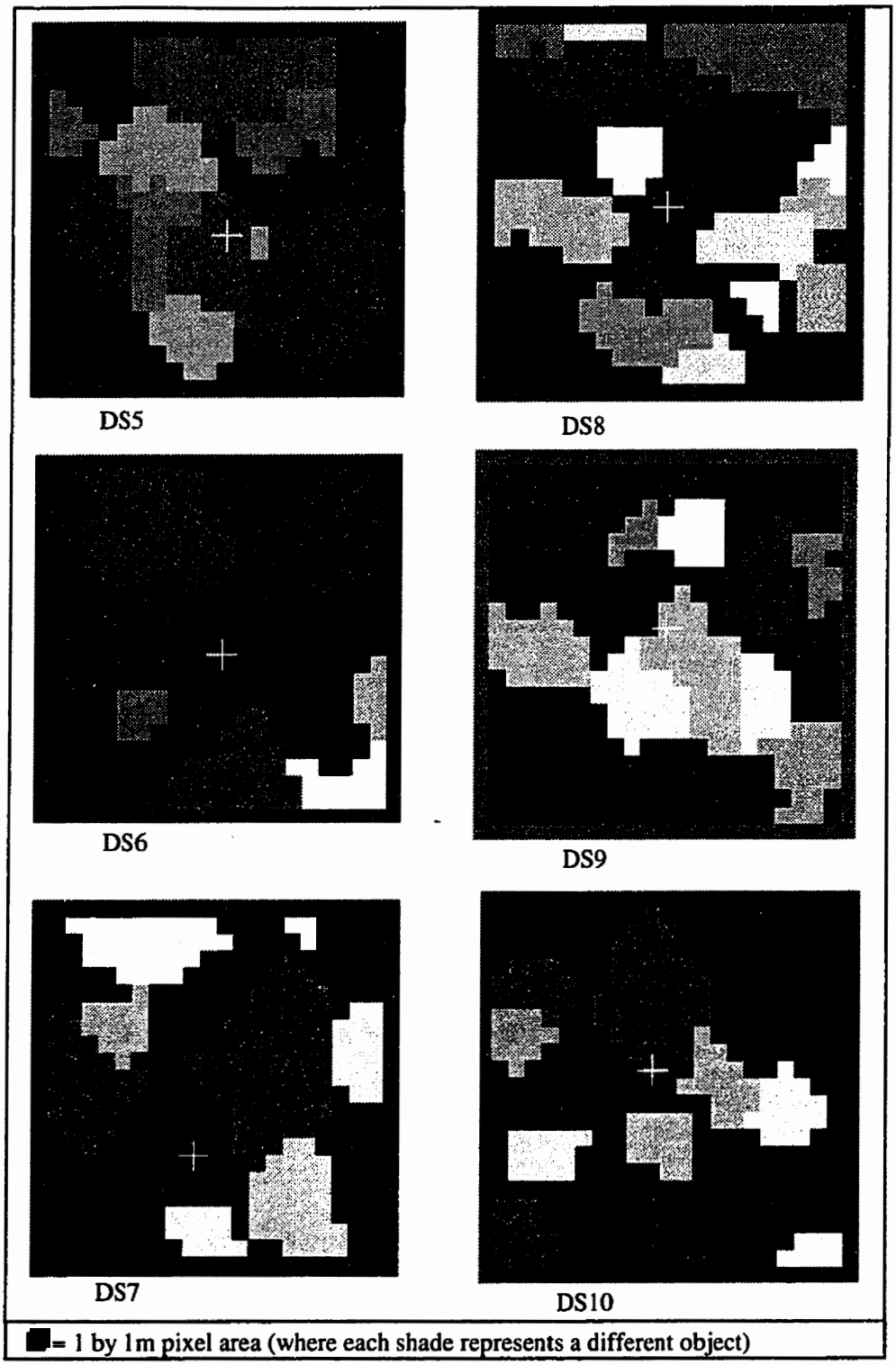


**Figure 7.15. Image spatial dependency generated clusters**

## 7.5. CHAPTER SUMMARY

The investigation of the spectral and spatial properties of the imagery has presented new insights into the spatial distribution of reflectance in image space. The technique of assessing the distance at which spatial dependency is maximized in relation to spectral reflectance provides new clues to the physical link between a forest landscape and image spatial structure. The spatial dependence measure of $G_i^*$ is capturing image spatial structure which is related to forest structure. Subsequently, further analysis to investigate the relationship between the image spatial structure and forest inventory and biophysical parameters is appropriate.

The visual agreement between the clusters and the field data is promising. The spatial resolution of 1m in consideration of deciduous and mixed forests results in a difficulty in the cross recognition of image objects to forest objects. Confidence in the match between the field data and the image generated clusters is based upon image geocorrection, the plot based GPS measures, and field site visits. Further analysis in the estimation of forest inventory and structural parameters will provide a means of quantification of the match between the image clusters and field data.

# 8. ESTIMATION OF FOREST INVENTORY PARAMETERS

***Chapter Objective:*** *Develop and test a methodology to combine existing information extraction techniques with the Getis statistic to allow for estimation of forest inventory parameters.*

## *8.1. INTRODUCTION*

The relationship between the forest inventory parameters of crown closure, stand density, and tree species classification with spatially derived image vegetation clusters is investigated in this chapter. The relationships between forest inventory parameters and the $G_i^*$ clusters will be limited due to the nature of the clusters. A single tree cluster may contain a number of trees resulting in a limited ability to estimate the number of stems in a particular area. Yet, clusters as a spatially derived entity are appropriate for relating the extent of vegetation within an area, enabling the estimation of crown closure. As a cluster may be composed of a number of trees, there is difficulty in labeling the cluster with a single species. Cover classes, based on the broad groupings of deciduous, coniferous, and mixed forest, are measurable from the spectral information found within clusters. Cover class information is valuable for the provision of model inputs and to relate the general characteristics of a stand. The investigation undertaken in this chapter will allow for further insights regarding the type of forest inventory information that may be collected from the spatial and spectral information available from 1m spatial resolution airborne and forthcoming satellite remotely sensed data.

## 8.2. ESTIMATION OF STAND DENSITY

Stand density is a quantitative measure of the number of trees found within a unit area of forest. Stand density may be expressed in absolute or relative terms. Absolute measures of stand density are derived directly from measurements in the stand whereas relative measures are comparisons between stands (Avery and Burkhart, 1994). For example, the number of trees per hectare is an absolute measure of density, while relative measures of stand density are based upon comparison to a known or ideal density.

As clusters are composed of 1 or more trees in close association, the ability to estimate the number of stems per a unit of area is difficult. The nature of the forest growth through a succesional series results in an ever changing forest structure over time, such as the variability in stand stratification based upon dominance. Forest structure may change through situations such as suppressed trees replacing aging dominant or co-dominant trees. Figure 8.1 illustrates situations from co-dominance in an even-aged stand through to a complex situation of dominance, co-dominance, intermediate, and suppressed trees found in association in an un-even aged stratified mixture. The difficulty in the remote sensing of deciduous and mixed forest stand density is apparent in such illustrations. At a 1m spatial resolution, with the forest type present in the Acadian forest region, the ability to discern individual stems is unlikely. Yet, a relationship between stand stratification, based upon dominance, and clustering information may exist.

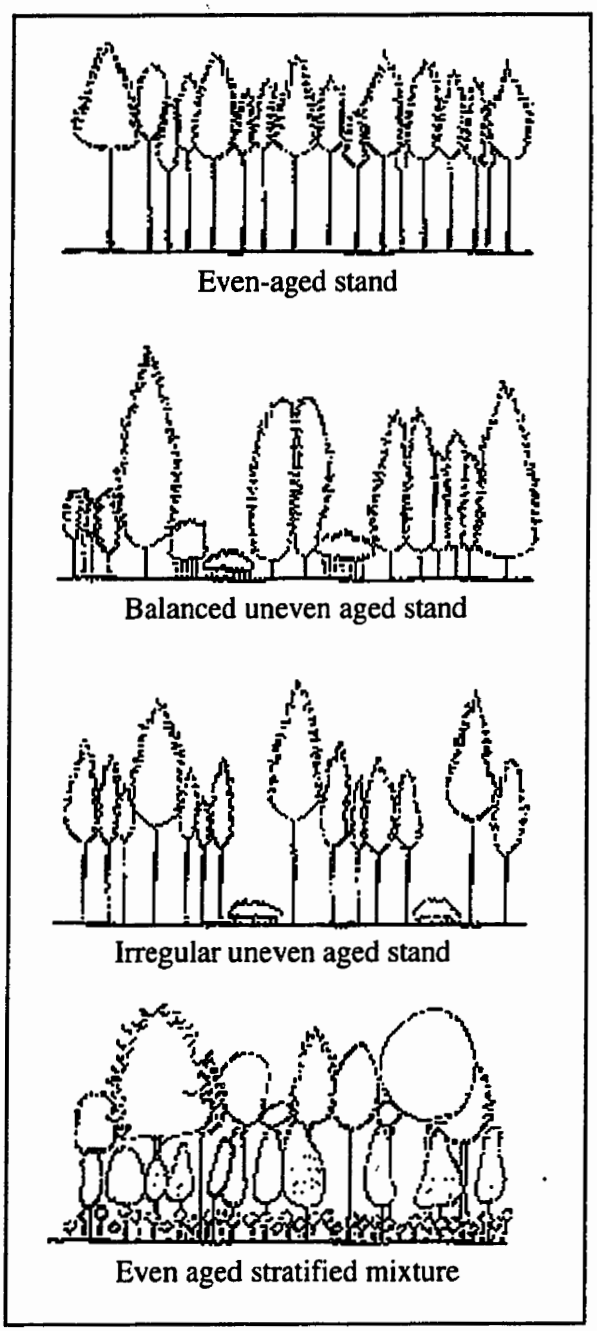


**Figure 8.1. Variation in structure of forest stands. The first three stands (from the top) consist of the same species. The forth is composed of several species of the same age (after Kozlowski, *et al.*, 1991).**

The counts of tree crown class levels, such as dominant, co-dominant, suppressed, and intermediate, relate the structure found in each stand (Table 8.1). Crown classes are determined as follows: dominant trees are those which have crowns which extend above the general level of the crown cover and receive full light from above and partially from the sides and are larger than the average trees within the stand; co-dominant trees are those which form the general level of the crown cover and receive full light from above but relatively little from the sides; intermediate trees are those which are shorter than dominant or co-dominant trees and may extend into the crown cover formed by dominant or co-dominant trees and are crowded and receive little light from the top and almost none from the sides; suppressed trees are found entirely below the general level of the canopy and receive no direct light (Avery and Burkhart, 1994). Counts of tree crown class are selected to relate to the image cluster data as the stratification of the trees present within the study areas is taken from the crown class information. Clusters are expected to develop between dominant and trees in a suppressed situation. Clearly dominant trees are relatively infrequent in comparison to co-dominant trees, relating the age structure and succesional characteristics of the sample plots. Further, within a 20x20 m sample plot area, the number of clearly dominant trees is limited. By definition, intermediate and suppressed trees are found in association with more dominant trees. The multi-layered characteristics of the study plots relates the structural complexity present.

**Table 8.1. Counts of tree crown class levels, trees within plots, and cluster derived parameters**

| | Dominant | Suppressed | Intermediate | Co-dominant | Tree Total | Pixels/ cluster | No. of clusters | Total pixels |
|---|---|---|---|---|---|---|---|---|
| DS5 | 6 | 17 | 21 | 23 | 67 | 22.5 | 13 | 293 |
| DS6 | 4 | 8 | 12 | 17 | 41 | 18.3 | 13 | 238 |
| DS7 | 6 | 8 | 11 | 14 | 39 | 24.3 | 9 | 219 |
| DS8 | 6 | 13 | 15 | 20 | 54 | 11.8 | 23 | 272 |
| DS9 | 2 | 7 | 8 | 10 | 27 | 14.9 | 17 | 253 |
| DS10 | 3 | 7 | 10 | 30 | 50 | 15.6 | 11 | 172 |

As an investigation of the potential density information that may be available from image clusters three parameters are extracted (Table 8.1). The number of pixels per cluster (pixels/cluster) is a mean value generated from the number of pixels found within each cluster for each sample plot. The number of clusters (No. of clusters) is a count of the number of clusters found within each sample plot. To provide an indication of the coverage of the plot by the image derived clusters, the total number of pixels which are expected to be included within a plot is generated from the multiplication of the number of clusters by the mean number of pixels per cluster (Total pixels).

Table 8.2 presents the relationships between the field collected tree crown class data and the image generated cluster information. Inspection of the correlations between the field collected crown class data indicates a relationship between dominant, suppressed, and intermediate trees. Suppressed and intermediate trees, by definition, are most often found in conjunction with dominant trees. The weak negative relationship between dominant and suppressed trees with co-dominant trees is indicative of the stand structure which resulted in the categorization of the trees. Co-dominant trees are categorized based upon similarity of characteristics of neighbouring trees. Co-dominance often includes local characteristics such as even age and height, which results in scant opportunity for growth of intermediate or suppressed trees.

**Table 8.2. Correlations between tree crown class, number of trees, and cluster derived values for all six plots combined**

| | Dominant | Suppressed | Intermediate | Co-dominant | Tree Total | Pixels/ cluster | No. of clusters | Total pixels |
|---|---|---|---|---|---|---|---|---|
| Dominant | 1.00 | | | | | | | |
| Suppressed | 0.78 | 1.00 | | | | | | |
| Intermediate | 0.82 | 0.96 | 1.00 | | | | | |
| Co-dominant | -0.22 | -0.12 | 0.07 | 1.00 | | | | |
| Tree Total | 0.43 | 0.59 | 0.74 | 0.73 | 1.00 | | | |
| Pixels/cluster | 0.59 | 0.17 | 0.35 | -0.16 | 0.11 | 1.00 | | |
| No. of clusters | -0.06 | 0.34 | 0.07 | -0.39 | -0.19 | -0.75 | 1.00 | |
| Total pixels | 0.54 | 0.73 | 0.53 | -0.74 | -0.13 | 0.02 | 0.64 | 1.00 |

Dominant, suppressed, and intermediate tree counts appear to be accounting for similar variance when compared to the cluster summary information. The physical association of dominant, suppressed, and intermediate trees in the field results in the generation of image clusters due to the proximity of the trees and the image 1m spatial resolution utilized in this analysis. The strong relationship between dominant trees and the total number of trees found within each plot is likely a function of the consistent representation of dominant trees in the imagery. The negative relationship between co-dominant trees and cluster derived information is due to generation of more clusters as the level of co-dominance increases, as the association between objects is more clearly defined. Co-dominant trees often possess a discrete space in the field, which results in the generation of an increasing number of small clusters as co-dominance increases. As the sample space is limited (20 x 20m field plot) the size of the clusters generated from the co-dominant trees in the imagery decreases as the level of co-dominance increases. Conversely, as the number of dominant trees increases, the clusters increase in size. The increase in cluster size for dominant trees is the increased potential for the presence of intermediate and suppressed trees in association with the dominant trees. In the field plots, the intermediate and suppressed trees will often share pixel space with the dominant trees resulting in an undefined delimitation between trees and an opportunity for inclusion of intermediate and suppressed trees in clusters spectrally dominated by the dominant trees. For example, the strong positive relationship ($r=0.73$) between the count of pixels included in image generated clusters and the field count of suppressed trees indicates the role of suppressed trees in the occupation of pixels along with dominant trees at a spatial resolution of 1m. Manual stem count extraction from aerial photographs also finds the greatest success when seeking dominant species (Needham and Smith, 1987).

### 8.2.1. Section Results and Discussion

The relationships between the field collected crown class data and the image generated cluster data indicate complementary information content. Knowledge of the stand crown class regime provides a variety of insights to the clusters that are generated from the image data. Based upon the complex stand structure, due to the presence of deciduous and coniferous trees, individual stem counting at a 1m spatial resolution is limited. The cluster data shows promise for the extraction of relative density information, yet based upon the use of clusters which are composed of one or more trees, exact stem counts will be elusive. While absolute stem counts may not be possible, relative density changes within an image area may be an alternative approach. Areal based parameters, such as crown closure, which do not require the delineation of single trees may be more successfully addressed.

## *8.3. ESTIMATION OF CROWN CLOSURE*

Crown closure, also referred to as canopy closure, is a measure of the percentage of a forest area accounted for within a vertical projection of the tree crowns (Avery and Burkhart, 1994), with the maximum amount of crown closure being 100 percent. Crown closure can be an indicator of stand volume, density, and basal area. As crown closure is the vertical projection of vegetation over an area it is well suited to measurement with remote sensing techniques. Crown closure estimates are problematic to compare between field, photo, and digitally interpreted methods. Field estimates of crown closure are commonly generated from the measurement of crown extent in two perpendicular directions that provides a mean radius which may then be used to compute individual crown areas that may be aggregated to represent a plot area (Cole, 1995), resulting in a ratio value of crown closure. Optical methods based upon hemispherical photography may also be utilized (Chan, *et al.*, 1986) to measure crown closure in the field from below the canopy. Estimates of crown closure from aerial

photographs are often derived from placing a clear plastic sheet over the photograph with dots drawn on the plastic at a known interval, allowing for estimates of crown closure to be estimated by the amount of crown foliage area found beneath the dots (Avery and Burkhart, 1994). Estimates of crown closure based upon photo interpretation are often placed into closure classes, which are commonly 10% intervals, yet in particular instances may be further aggregated to 30% interval classes (Gillis and Leckie, 1993). Digital estimates of crown closure are also related in ratio values based upon the automated computation.

In this study, the crown closure estimates are based upon field measurements after Cole (1995) which generated ratio values of crown closure. These crown closure values, although likely of a false precision, are preferred over the placement of the crown closure values into 10% class intervals. The placement of the crown closure values generated from the field collected data into 10% classes for comparison to image based estimates of crown closure would make comparison difficult. Placement of the field estimates and image based estimates of crown closure into 10% classes for comparison would not allow for the full potential of the data to be explored. When placing values into 10% classes the actual similarity of closure estimates is obscured. Placement of a crown closure estimate of 13 into the 10% class interval of 10 to 20% would result in the appearance of 13% as a better estimate of crown closure of 19% than 21% which would be placed in the next greater crown closure range.

In this section, crown closure as measured in the field is compared to the area of the plot accounted for by image clusters. The clusters are generated from $G_i^*$ values generated upon infrared and panchromatic image data. For further comparison, the clusters formed from image segmentation are compared to a simple threshold of $G_i^*$ values. The threshold limit was zero, with values above zero assumed to be canopy foliage related. Table 8.3 presents the

results of the comparison between field estimates of crown closure and closure estimates derived from image spatial dependency.

**Table 8.3. Crown closure estimates from image threshold and cluster data. The difference between the estimate and the field data is noted in parenthesis. (Critical $t = \pm 2.228$, DF = 10, $\alpha = 0.05/2$, * denotes statistical significance of difference to field data)**

| Plot/Image | Field Data | Threshold IR | Threshold PAN | Cluster IR | Cluster PAN |
|---|---|---|---|---|---|
| DS5 | 0.82 | 0.58 (-0.24) | 0.83 (+0.01) | 0.73 (-0.09) | 0.64 (-0.19) |
| DS6 | 0.59 | 0.51 (-0.09) | 0.42 (-0.17) | 0.62 (+0.03) | 0.38 (-0.21) |
| DS7 | 0.69 | 0.57 (-0.12) | 0.75 (+0.06) | 0.55 (-0.14) | 0.56 (-0.12) |
| DS8 | 0.74 | 0.14 (-0.60) | 0.38 (-0.36) | 0.62 (-0.12) | 0.48 (-0.25) |
| DS9 | 0.59 | 0.39 (-0.20) | 0.57 (-0.02) | 0.57 (-0.02) | 0.43 (-0.16) |
| DS10 | 0.54 | 0.23 (-0.30) | 0.47 (-0.06) | 0.38 (-0.16) | 0.36 (-0.18) |
| Absolute difference from field data | | 1.55 | 0.68 | 0.56 | 1.11 |
| StDev. difference from field data | | 0.18 | 0.15 | 0.07 | 0.04 |
| *t*-statistic | | 2.97* | 1.06 | 1.30 | 3.00* |

An underestimation of crown closure results occurs in most instances. The underestimation of crown closure with the image based information is likely related to shadowing within the stand. For the six plots available to this study, an ability to estimate crown closure to within $\approx 10\%$ is demonstrated for estimates from a threshold of $G_i^*$ generated on panchromatic image data and clusters generated from infrared image data. The crown closure estimates from Threshold IR and Cluster PAN are found to be significantly different from the field based estimates of canopy closure. Insignificant *t*-statistic values for Threshold PAN and Cluster IR do not allow for the rejection of the null hypothesis, indicating a similarity between the field based and remotely sensed estimates of crown closure. Although the Threshold IR values are significant, the provision of a threshold value is not sensitive to spatial dependency variations found within the images and is accordingly unreliable with a large absolute difference combined with a large standard deviation indicating the high variability of the estimates. The estimates of crown closure with the cluster information have a small absolute error with a low standard deviation indicating a lower range to the estimates.

The under-estimation of the cluster based crown closure estimates on plot 7, 8, and 10 may be related to the stand structure and resultant shadow regime within the stand. The underestimation of crown closure with panchromatic image data may be related to the lower dynamic range of the data in comparison to the infrared image data. The larger dynamic range of the infrared image data allows for greater variability between neighbouring pixel values for the generation of clusters.

## 8.4. ASSIGNMENT OF COVER CLASS

This section is a demonstration of a technique for assigning species cover classes to the image generated clusters. As the 1m spatial resolution will not allow for regular separation of individual trees the clusters are subject to spectral dilution by the inclusion of a variety of species within each cluster. As a result, the assignment of a general cover class is undertaken, which is broader than individual species and is comprised of hardwood (HW), softwood (SW), and mixed wood (MW). It should be noted, however, that softwood clusters are an uncommon occurrence in this study. Cover classes may be utilized as an input to predictive equations of LAI from high spatial resolution digital remotely sensed imagery (Wulder, *et al.*, 1996a; 1998). The cover classes predicted for the clusters are applied in Chapter 9 to estimate LAI.

The procedure to generate cover classes for the clusters is as follows;

- $G_i^*$ spatial dependence values generated (Section 7.2.2)
- data segmented based upon spatial dependence (Section 7.3)
- mean spectral values extracted for each polygon
- Ward's method of clustering undertaken to group the clusters based upon the spectral information within each cluster (Davis, 1986).[1]

[1] Clustering techniques generally create groups based upon within and between group variance. Pixels are placed into a cluster based upon having more in common with one group than another, through minimization of internal variation while maximizing variation between groups. Homogeneous and distinct groups are delineated

- The groups generated from the clustering are compared to standard spectra to be placed in the appropriate cover class. (Once clusters are generated, the spectral values which compose the clusters may be investigated to assist in assignment of each cluster in a cover class. A wide range of input spectral values results in an assignment of MW, a small range of spectral values with spectral characteristics similar to conifer spectra collected in the field will be assigned SW. While a small range of spectral values similar to hardwood spectra collected in the field will be assigned to HW. This process was implemented with the assistance of the dendrograms generated from each plot through the clustering process.)
- the cover classes assigned are compared to field data stored in a raster GIS.

Appendix 2 contains tables presenting the mean spectral reflectance values for each extracted cluster within each sample plot. To assess the success of the assignment of cluster labels, tables for each plot have been created which present the class assigned utilizing a statistical clustering technique to the trees which are expected based upon the ground data. The image data generated cover class is compared to the tree species which have been noted for the field plots in the same locations. The portion of the stand that is not grouped into a cluster is characterized as understory (US). The success of the labeling of the image clusters is based upon the inclusion of related species from the ground data found for the image derived clusters. For instance, an image cluster cover class of hardwood (HW) must have hardwood species within the cluster to be labeled as matching. Although more complex schemes may be developed, such as those which may utilize the areal contribution of each tree in the cluster to adjust the labels, these methods assume a less complex situation than is actually present. The complexity of the situation is based upon the 3-dimensional distribution of forest elements in the field and how remote sensing instruments collect these data. The estimation method applied in this study provides for an indication of the ability to classify

---

based upon assessment of distances between group centroids, or in the case of Ward's method, an F-test. The ability to select a statistical tolerance led to the selection of Ward's method.

clusters of a complex forest environment. Also recorded for each sample plot is the number of trees which are recorded in the field data and the number which are accounted for within the image generated clusters.

Sample plot DS5 is characterized as having an intolerant and tolerant hardwood overstory (Table 6.2). The clusters generated for the sample image DS5, produce classes that are correct 9 of 13 times (Table 8.4). Clusters, such as 3497 and 3622, may have been classed as MW based upon a strong conifer reflectance signal from the understory. The large number of trees found within a single cluster relates the difficulty in differentiation between image objects, with similar spectral characteristics, at a 1m spatial resolution.

**Table 8.4. Summary of DS5 image cluster data and field collected cluster data. Cluster from segmentation, class from reflectance, number of pixels in clusters from image data, trees per cluster and total trees per cluster from fusion with GIS data (where * denotes matching class, ^denotes non-matching class; n=67, n in clusters=52)**

| Cluster | Class | # Pixels in Cluster | Trees / Cluster | Total trees / Cluster |
|---|---|---|---|---|
| 0 | US | 108 | NA | NA |
| 3427 | HW* | 24 | rM(3) | 3 |
| 3444 | HW* | 27 | rM(4), Be, sM, yB | 7 |
| 3495 | HW^ | 8 | 0 | 0 |
| 3497 | MW^ | 19 | rM(5), yB(2) | 7 |
| 3523 | HW* | 2 | yB | 1 |
| 3534 | HW* | 24 | yB(2), rM(3) | 5 |
| 3563 | HW* | 32 | wB, rM | 2 |
| 3579 | HW* | 21 | sM | 1 |
| 3622 | MW^ | 24 | rM(2), stM, yB(2) | 5 |
| 3623 | HW* | 25 | yB(3), Be(2) | 5 |
| 3646 | HW* | 29 | rM(4), yB, Be, sM | 7 |
| 3700 | HW^ | 40 | stM, rS, rM(4), yB | 7 |
| 3714 | HW* | 18 | yB(2), rM(2) | 4 |

Sample plot DS6 is characterized as having a mixed wood overstory and a light hardwood understory (Table 6.2). The complex composition of this sample plot, with contrasting spectral features in the overstory and understory layers, diminished the ability to spectrally classify the image generated clusters to match the field collected data, and resulted in a low

success rate of 2 of 13 correct matches (Table 8.5). Table A2.2, in Appendix 2, denotes the low variability in mean spectral values extracted, which may have reduced the ability to correctly classify the clusters. A greater problem appears to be the lack of trees found to be present in five of the image generated clusters. The lack of field values where there are image generated clusters may be related to the difficulty in matching the image data to the field data. An additional cause for the generation of ghost clusters may be that spectrally significant portions of understory vegetation in an open canopy situation are generating clusters based upon spatial dependence characteristics.

**Table 8.5. Summary of DS6 image cluster data and field collected cluster data. Cluster from segmentation, class from reflectance, number of pixels in clusters from image data, trees per cluster and total trees per cluster from fusion with GIS data (where * denotes matching class, ^denotes non-matching class; n=42, n in clusters=37)**

| Cluster | Class | # Pixels in Cluster | Trees / Cluster | Total trees / Cluster |
|---|---|---|---|---|
| 0 | US | 143 | NA | NA |
| 3056 | HW^ | 22 | 0 | 0 |
| 3068 | HW* | 13 | rM | 1 |
| 3071 | HW^ | 28 | bF(2), wB(2) | 4 |
| 3099 | MW* | 50 | rM(2), bF(5), wA, wB(2) | 10 |
| 3125 | MW^ | 9 | rS | 2 |
| 3176 | HW^ | 51 | rM(6), wB, bF(2) | 9 |
| 3242 | MW^ | 8 | 0 | 0 |
| 3263 | MW^ | 8 | 0 | 0 |
| 3296 | HW^ | 15 | rM(3), rS(3) | 6 |
| 3320 | HW^ | 5 | rM, bF | 2 |
| 3321 | HW^ | 18 | rS, rM(2) | 3 |
| 3338 | MW^ | 4 | 0 | 0 |
| 3339 | MW^ | 7 | 0 | 0 |

Sample plot DS7 is characterized as having a mixed-wood overstory and a light mixed-wood understory (Table 6.2). Table 8.6 presents the agreement between the image generated estimates of cover class and the field collected tree data. Agreement between the image generated classified clusters and the field data is found in 5 of 9 instances, with 2 clusters failing to have any trees present. Tree shadows, from both trees within the sample plot and

outside, may cause a reduction in spectral information available for the development of clusters. For example, in DS7 a count of 31 or 40 trees are accounted for within the clusters. As a result, clusters are being generated where there may be no tree, or there may be a lack of a cluster where there is a tree. The sample plot is dominated by HW species with the SW species making a small contribution to the spectral values derived for some clusters resulting in mis-labeling.

**Table 8.6. Summary of DS7 image cluster data and field collected cluster data. Cluster from segmentation, class from reflectance, number of pixels in clusters from image data, trees per cluster and total trees per cluster from fusion with GIS data (where * denotes matching class, ^denotes non-matching class; n=40, n in clusters=31)**

| Cluster | Class | # Pixels in Cluster | Trees / Cluster | Total trees / Cluster |
|---|---|---|---|---|
| 0 | US | 182 | NA | NA |
| 3332 | MW* | 3 | rM(2), rS, Be, wB | 5 |
| 3352 | HW^ | 29 | 0 | 0 |
| 3390 | HW* | 15 | Be | 1 |
| 3427 | MW^ | 13 | wB, rM | 2 |
| 3442 | HW* | 16 | Be, stM | 2 |
| 3459 | HW^ | 31 | wB(2), rS, rM | 4 |
| 3460 | MW* | 69 | Be(5), wB(4), rS(2), stM | 13 |
| 3560 | MW* | 31 | rS(2), rM(2) | 4 |
| 3586 | HW^ | 12 | 0 | 0 |

Sample plot DS8 is characterized as having a hardwood/softwood overstory and a hardwood softwood understory (Table 6.2). DS8 has the largest number of clusters generated in this study with 23 (Table 8.1). Table 8.7 presents the agreement between the image generated estimates of cover class and the field collected tree data. Agreement between the image generated classified clusters and the field data is found in 15 of 23 instances, with 4 clusters failing to have any trees present. Equal success is found in matching field data to image data for both HW and MW cover classes. A low count of trees outside of any cluster, with 49 of 55 trees being found within a cluster, relates a strong geometric match between the image data and the field data stored in a raster GIS.

**Table 8.7. Summary of DS8 image cluster data and field collected cluster data. Cluster from segmentation, class from reflectance, number of pixels in clusters from image data, trees per cluster and total trees per cluster from fusion with GIS data (where * denotes matching class, ^denotes non-matching class; n=55, n in clusters=49)**

| Cluster | Class | # Pixels in Cluster | Trees / Cluster | Total trees / Cluster |
|---|---|---|---|---|
| 0.0 | US | 170 | NA | NA |
| 2929 | HW* | 5 | wB, rM | 2 |
| 2960 | HW* | 7 | rM(2) | 2 |
| 2973 | HW* | 10 | wB(3) | 3 |
| 2974 | HW* | 32 | wB(2), rM | 3 |
| 2991 | HW^ | 28 | rM, wB(2), bF | 4 |
| 3005 | HW* | 9 | rM | 1 |
| 3040 | HW* | 5 | wB | 1 |
| 3041 | MW* | 8 | wB(2), rS | 3 |
| 3058 | HW* | 23 | rM(2), wB(4), bF | 7 |
| 3069 | MW* | 14 | rS, rM | 2 |
| 3086 | HW* | 7 | wB, rM | 2 |
| 3114 | HW* | 3 | wB | 1 |
| 3115 | HW* | 26 | wB(5) | 5 |
| 3117 | MW^ | 8 | wB | 1 |
| 3158 | MW* | 13 | wB, rS | 2 |
| 3161 | MW^ | 8 | 0 | 0 |
| 3175 | MW^ | 4 | 0 | 0 |
| 3192 | MW* | 7 | rS(2), wB | 3 |
| 3213 | MW^ | 12 | stM, Be | 2 |
| 3237 | MW^ | 6 | wB | 1 |
| 3260 | MW* | 17 | rS(2), wB(2) | 4 |
| 3261 | MW^ | 10 | 0 | 0 |
| 3307 | MW^ | 10 | 0 | 0 |

Sample plot DS9 is characterized as having a hardwood overstory and a softwood understory (Table 6.2). Table 8.8 presents the agreement between the image generated estimates of cover class and the field collected tree data. Agreement between the image generated classified clusters and the field data is found in 11 of 17 instances, with 3 clusters failing to have any trees present. Matching between image clusters classified as MW and the field data appears problematic, which may be based upon the contrast between overstory and understory vegetation. All 27 trees recorded in the field are found within image generated clusters, although 3 clusters are found to have no trees present. The presence of all 27 trees

within clusters for this low density sample plot relates a good geometric match between the image and field collected data.

**Table 8.8. Summary of DS9 image cluster data and field collected cluster data. Cluster from segmentation, class from reflectance, number of pixels in clusters from image data, trees per cluster and total trees per cluster from fusion with GIS data (where * denotes matching class, ^denotes non-matching class; n=27, n in clusters=27)**

| Cluster | Class | # Pixels in Cluster | Trees/Cluster | Total trees / Cluster |
|---|---|---|---|---|
| 0 | US | 189 | NA | NA |
| 4021 | HW* | 34 | rM(3), wB | 4 |
| 4022 | HW* | 7 | rM | 1 |
| 4067 | HW* | 14 | rM(3) | 3 |
| 4089 | MW^ | 7 | rS | 1 |
| 4097 | HW* | 10 | wB | 1 |
| 4111 | HW* | 23 | rM | 1 |
| 4113 | HW^ | 1 | 0 | 0 |
| 4153 | HW^ | 5 | 0 | 0 |
| 4167 | HW* | 10 | wB, rM | 2 |
| 4183 | HW* | 18 | rM(2) | 2 |
| 4184 | MW^ | 1 | 0 | 0 |
| 4186 | HW* | 34 | rM(3) | 3 |
| 4206 | MW^ | 15 | ltA, rM | 2 |
| 4215 | HW* | 25 | rM(2) | 2 |
| 4266 | HW* | 17 | rM | 2 |
| 4275 | HW* | 28 | ltA, rM | 3 |
| 4309 | MW^ | 4 | rM | 1 |

Sample plot DS10 is characterized as having a hardwood overstory and a softwood understory (Table 6.2). Table 8.9 presents the agreement between the image generated estimates of cover class and the field collected tree data. Agreement between the image generated classified clusters and the field data is found in 9 of 11 instances, with no clusters failing to have any trees present. Yet, although there are no clusters with no trees present, there are 17 trees which are in the sample plot which are not accounted for in an image based cluster. The geometric match between the image and the field data may be sub-optimal, with

the homogeneity of the sample plot vegetation allowing for the strong matching between the image and field data.

**Table 8.9. Summary of DS10 image cluster data and field collected cluster data. Cluster from segmentation, class from reflectance, number of pixels in clusters from image data, trees per cluster and total trees per cluster from fusion with GIS data (where * denotes matching class, ^denotes non-matching class; n=51, n in clusters=34)**

| Cluster | Class | # Pixels in Cluster | Trees / Cluster | Total trees / Cluster |
|---|---|---|---|---|
| 0 | US | 270 | NA | NA |
| 1706 | HW* | 14 | wB(3), stM | 4 |
| 1718 | HW* | 43 | rM(3), wB(3) | 6 |
| 1734 | HW^ | 11 | rM, wB, sP | 3 |
| 1782 | MW^ | 16 | rM(2), wB | 3 |
| 1789 | HW* | 2 | wB | 1 |
| 1798 | HW* | 14 | rM(3) | 3 |
| 1836 | HW* | 14 | wB(2) | 2 |
| 1854 | HW* | 13 | wB, rM(3) | 4 |
| 1925 | HW* | 19 | wB(4) | 4 |
| 1937 | HW* | 14 | rM | 1 |
| 1958 | HW* | 12 | wB(3) | 3 |

### 8.4.1. Section Results and Discussion

In general the matching between the trees present in the image generated clusters and the field collected data was good considering the limitations of the study. This statement of efficacy is based upon limitations of the method, such as the wide spectral range eligible for inclusion in a particular cluster and the complex mixed forest composition present. The method described is not one which is intended to be automated and implemented at the current stage of development, it is more intended as an investigation of the utility of a cluster based approach to object grouping. Both the spatial and spectral data available at an image spatial resolution of 1m are providing information to enable the generation and classification of image based clusters. The results demonstrated here indicate promise in the technique and a need for further investigation. A future investigation would benefit from utilization of a forest of simple structure with an exact knowledge of tree locations, based upon ground or tree markers. The ability to classify and distinguish objects at 1m spatial resolution is limited; a cluster based approach acknowledges the complexity of the forest and the limitations imposed through remote sensing instrumentation. The provision of a cover class to vegetation objects may prove useful as a model input, such as in the estimation of leaf area index.

# 9. ESTIMATION OF FOREST LAI

***Chapter Objective:*** *Develop and test a methodology to combine existing information extraction techniques with the Getis statistic to allow for estimation of the forest biophysical parameter leaf area index (LAI).*

## *9.1. INTRODUCTION*

The ability to estimate LAI from spectral response is strong up to an LAI of approximately 3 (Gong *et al.*, 1992), after which an asymptote is normally encountered (Wulder *et al.*, 1996a). The flattening of the relationship is due to the inability of NDVI, generated from a nadir remote sensing instrument, to sense increases in foliage overlap (Baret and Guyot, 1991) as forest complexity increases. As a result, additional information is required which still undergoes change as the forest increases in complexity. Forest spatial structure varies through levels of forest development (Waring and Schlesinger, 1985). Image spatial information may capture some of the variability in forest structure (St-Onge and Cavayas, 1997). Digital image processing provides spatial measures which characterize the spatial neighbourhood of a pixel, such as, digital image texture (Wulder, *et al.*, 1998) and image semivariance (Cohen, *et al.*, 1990; Franklin and McDermid, 1993) capture information relating to the variability around a pixel related to the forest structure.

In this research an alternate approach is presented to the estimation of LAI. Clusters generated based upon spatial dependence characteristics are composed of regions of image spatial structural similarity. This image spatial structural similarity is understood to be related to the forest structure that is being sensed with the remote sensing instrument. Generation of clusters allows for an increase in the likelihood that the pixels selected for incorporation in the empirical estimation of LAI are indeed the foliage unit suspected. Image spectral response in

the clusters was compared to field collected spectral information which allowed for a broad image object classification into general cover classes, such as deciduous, coniferous, and mixed, for inclusion in the computation of LAI. The image spatial information dictates the regions from which pixels are selected for spectral data, while the textural information is collected to represent the region around the pixel, not merely within the object. This allows for the characteristics of the local region to be incorporated in the empirical estimation of LAI.

## 9.2. ESTIMATION OF LAI FROM THE SPECTRAL RESPONSE WITHIN TREE CLUSTERS

The previous studies have demonstrated the synergy between spatial and spectral information present in remotely sensed imagery of forests. In this section we will further explore the role of spatial and spectral information in the estimation of LAI. Two techniques will be demonstrated with the first using both spatial and spectral information, and the second utilizing knowledge of the local maximum LAI and spatial information. The first technique is related to previous works (Wulder, *et al.*, 1996a; 1998), while the second technique is based upon the hypothesis that the foliage extent present in an area, as indicated with canopy closure, may be used to scale maximum LAI to that present in a particular area.

The prediction of LAI for clusters based upon spectral and spatial information requires the following steps:

- $G_i^*$ spatial dependence values generated (Section 7.2.2)
- generation of tree clusters from spatial information (Section 7.3)
- mean spectral values extracted for each polygon (Section 8.4)
- assign cover classes to the clusters (Section 8.4),
- estimate the leaf area for each cluster,
- rate LAI estimate based upon the size of the cluster, and
- sum the leaf areas for each cluster to generate a LAI for the plot.

In Table 9.1 we present the results of the estimation of LAI for the study plot DS5. The results for the remaining plots may be found in Appendix 3. The leaf area for each cluster is estimated through the generation of a mean NDVI to represent each cluster which is then used as an input to a LAI predictive equation. The predictive equations for LAI are based upon a study of the regional LAI of the Fundy Model Forest (Wulder, 1998a), where,

Hardwood LAI = (2.99 * NDVI) + 5.34
Mixed Wood LAI = (2.47 * NDVI) + 5.94
Softwood LAI = (-5.05 * NDVI) + 11.44

The NDVI values are found to be of limited range, resulting in regression results that are also of a limited range. The use of the spectral values from within vegetation clusters appears to have further limited the range of NDVI values. The size of the cluster is valuable information that enables the spatial information relating the proportion of the stand occupied by the cluster to be included in the estimation of LAI.

**Table 9.1. Computation of leaf area for sample plot DS5, from cluster mean NDVI and cluster spatial extent (total number of pixels = 400)**

| Cluster | Cluster NDVI | Class | Pixels/Cluster | LA | Pixels per cluster/ Total | LA/Cluster | Plot LAI |
|---|---|---|---|---|---|---|---|
| 0 | 0.81 | US | 108 | | 0.27 | | |
| 3427 | 0.79 | HW | 24 | 7.69 | 0.06 | 0.46 | |
| 3444 | 0.81 | HW | 27 | 7.76 | 0.07 | 0.52 | |
| 3495 | 0.81 | HW | 8 | 7.75 | 0.02 | 0.15 | |
| 3497 | 0.77 | MW | 19 | 7.85 | 0.05 | 0.37 | |
| 3523 | 0.85 | HW | 2 | 7.87 | 0.01 | 0.04 | |
| 3534 | 0.81 | HW | 24 | 7.78 | 0.06 | 0.47 | |
| 3563 | 0.81 | HW | 32 | 7.75 | 0.08 | 0.62 | |
| 3579 | 0.63 | HW | 21 | 7.21 | 0.05 | 0.38 | |
| 3622 | 0.75 | MW | 24 | 7.59 | 0.06 | 0.46 | |
| 3623 | 0.82 | HW | 25 | 7.80 | 0.06 | 0.49 | |
| 3646 | 0.79 | HW | 29 | 7.70 | 0.07 | 0.56 | |
| 3700 | 0.81 | HW | 40 | 7.76 | 0.10 | 0.78 | |
| 3714 | 0.80 | HW | 18 | 7.74 | 0.05 | 0.35 | **5.6** |

The above procedure for estimating LAI from the NDVI values found within the spatial dependence generated clusters is undertaken for all forest plots. Table 9.2 presents a

comparison of the field based estimates of LAI with those computed from the spectral characteristics found within clusters. The difference between the field and image based estimates of LAI are found to be statistically insignificant. Yet, as the mean difference and deviation demonstrate the estimates are variable.

**Table 9.2. Comparison of field based to image cluster estimates of LAI. (Critical $t = \pm 2.23$, DF = 10, $\alpha = 0.05/2$)**

| Plot | Field LAI | Image Cluster LAI | Difference between field and cluster LAIs |
|---|---|---|---|
| DS5 | 4.93 | 4.93 | 0.72 |
| DS6 | 5.87 | 5.87 | -1.05 |
| DS7 | 6.88 | 6.88 | -2.71 |
| DS8 | 5.25 | 5.25 | -0.52 |
| DS9 | 3.28 | 3.28 | 1.07 |
| DS10 | 4.30 | 4.3 | -1.38 |
| | | average absolute deviation | 1.40 |
| | | *t*-statistic | 0.31 |

The ability to estimate crown closure provides an indication of the areal extent of the vegetation. Knowledge of the proportion of an area which is vegetated may allow for the estimation of LAI through rating of the maximum expected LAI. In the previous examples where LAI was estimated from a species specific equation utilizing NDVI as an input, the input range of NDVI is small. The NDVI range within clusters is found to be small resulting in small alterations of the computed LAI. Rather than use an LAI estimation model based upon NDVI, the proportion of area within clusters may be multiplied by the maximum expected regional LAI of 7.75 for the FMF region, that is based upon a deciduous-mixed wood species composition (Wulder, 1998a). Table 9.3 presents for comparison to Table 9.1 the LAI estimation results based upon a static leaf area of 7.75. The remainder of the tables demonstrating the estimation of LAI from image spatial information and a standardized LAI are found in Appendix 4.

**Table 9.3. Computation of leaf area for sample plot DS5, from a standardized leaf area and cluster spatial extent (total number of pixels = 400)**

| Cluster | Cluster NDVI | Class | Pixels/Cluster | LA | Pixels per cluster/ Total | LA/Cluster | Plot LAI |
|---|---|---|---|---|---|---|---|
| 0 | 0.81 | US | 108 | | 0.27 | | |
| 3427 | 0.79 | HW | 24 | 7.75 | 0.06 | 0.47 | |
| 3444 | 0.81 | HW | 27 | 7.75 | 0.07 | 0.52 | |
| 3495 | 0.81 | HW | 8 | 7.75 | 0.02 | 0.16 | |
| 3497 | 0.77 | MW | 19 | 7.75 | 0.05 | 0.37 | |
| 3523 | 0.85 | HW | 2 | 7.75 | 0.01 | 0.04 | |
| 3534 | 0.81 | HW | 24 | 7.75 | 0.06 | 0.47 | |
| 3563 | 0.81 | HW | 32 | 7.75 | 0.08 | 0.62 | |
| 3579 | 0.63 | HW | 21 | 7.75 | 0.05 | 0.41 | |
| 3622 | 0.75 | MW | 24 | 7.75 | 0.06 | 0.47 | |
| 3623 | 0.82 | HW | 25 | 7.75 | 0.06 | 0.48 | |
| 3646 | 0.79 | HW | 29 | 7.75 | 0.07 | 0.56 | |
| 3700 | 0.81 | HW | 40 | 7.75 | 0.10 | 0.78 | |
| 3714 | 0.80 | HW | 18 | 7.75 | 0.05 | 0.35 | **5.7** |

Table 9.4 presents a comparison of proportional LAI with the aforementioned image cluster LAI estimates which required knowledge of cover class for input of NDVI into the proper LAI estimation equation. As related in the comparison of the average difference and deviation from the field data, the LAI estimates for both the "Image Cluster" spectral and the "Proportional" LAI estimation techniques are similar. Both of the estimation techniques are not found to be significantly different from the estimate of LAI made from the field data.

**Table 9.4. Comparison of image cluster generated LAI with proportional LAI. The difference between the estimate and the field data is noted in parenthesis. (Critical $t = \pm 2.228$, DF = 10, $\alpha = 0.05/2$)**

| Plot | Field LAI | Image Cluster LAI | Proportional LAI |
|---|---|---|---|
| DS5 | 4.93 | 5.6 (0.67) | 5.7 (0.77) |
| DS6 | 5.87 | 4.8 (-1.07) | 4.8 (-1.07) |
| DS7 | 6.88 | 4.2 (-2.68) | 4.2 (-2.68) |
| DS8 | 5.25 | 4.7 (-0.55) | 4.8 (-0.45) |
| DS9 | 3.28 | 4.3 (1.02) | 4.4 (1.12) |
| DS10 | 4.30 | 2.9 (-1.4) | 3.0 (-1.3) |
| average absolute deviation | | 1.39 | 1.41 |
| *t*-statistic | | 0.103 | 0.962 |

The LAI values predicted with structural information alone, the proportional LAI values, are nearly identical to the image cluster LAI estimates which required a cover class specific input of NDVI. Yet, similar deviations from the field LAI estimates are found for both estimation methods. This may be due to the spatial component, as a function of the clusters, being included in both estimation techniques. Due to the similarity of the results, the Proportional LAI estimation technique shows promise for further analysis. The estimation of LAI from spatial data indicates potential for estimation of LAI from panchromatic data, and as a parsimonious solution to the estimation of LAI from spatial information.

## 9.3. CHAPTER SUMMARY

After a review of previous work in the estimation of LAI from spectral and spatial information, two new methods for the estimation of LAI are presented. The first method demonstrates the estimation of LAI based upon spectral and spatial information. In the second example $G_i^*$ clusters generated to represent image spatial dependency are classified for cover class and then processed with an appropriate equation to estimate LAI. The estimates of LAI from both techniques are found to be within approximately ±1.4. As all field estimates of LAI are greater than 3, the results are promising, yet not of sufficient accuracy for addressing ecological issues or for up-scaling. The ability to estimate LAI based on vegetation spatial extent and knowledge of regional LAI indicates that estimates of LAI may be made from satellite collected panchromatic data.

# 10. DISCUSSION

***Chapter Objective:*** *Discuss issues raised through the presentation of the thesis to provide a context for the conclusions.*

## *10.1. Introduction*

The goal of this thesis is to:

> *investigate alternate methods for the estimation of forest inventory and biophysical parameters based upon spatial information extraction through digital image processing of high spatial resolution multispectral imagery.*

The investigation of alternate methods for the estimation of forest inventory and biophysical parameters both acknowledges the variety of existing methods while also attempting to address potential shortcomings. Currently, there is a rich "tool box" of image analysis tools and techniques available for forest information extraction, yet often situations exist where algorithm performance is weak. The investigation and development of additional, or complementary, "tools" is intended to enhance the existing suite of methods. As has been demonstrated in the review of existing image processing techniques there is no one analysis procedure that can be universally or routinely applied. The relationship between forest complexity and the ability to capture this complexity from digital imagery for analysis is a problematic pursuit requiring the union of an appropriate match between image spatial resolution and analysis technique. As a result, additional tools for the analysis of forest structural parameters are a valuable remote sensing research pursuit. The following sub-sections are intended to provide depth to the preceding chapters with a discussion of key topics grouped as following, spatial dependence processing, measures of spatial dependence, a comparison of spatial and spectral approaches, and a discussion of research limitations accompanied with recommendations.

## 10.2. Spatial Dependence Processing

Following the introduction of the necessary statistical background is a discussion of spatial dependence characteristics and context. Initially the characteristics will be presented generically and then in the context of remotely sensed data. A statistical process is understood to be stationary if the distribution function is not altered when the distance is altered. The distance is the area around an individual point which is included in the assessment. Stationary processes are also said to be spatially homogeneous, as the space process-homogeneity is related to the distance between the values under consideration (Bailey and Gatrell, 1995). It follows that spatial dependence is a special case of spatial homogeneity as identifiable spatial units are related and found to be similar to data for other neighbouring spatial units in a spatially identifiable way (Getis, 1994). Measures of spatial autocorrelation are often used to provide an indication of spatial dependence (Ord and Getis, 1995).

The exploration of spatial dependence has been identified as a critical area for future research upon spatially representative GIS data (Sinton, 1992). This statement is based upon the conception of the spatial dependence between entities as providing additional and valuable information. This concept may be extended to remotely sensed data as both site and situation indicate unique spatial characteristics. The site, or pixel, has a location, and at that location the pixel is found in a particular situation. Each pixel may have an associated attribute which describes it's spatial dependence characteristics. Spatial dependence information may accordingly be generated to indicate the site and situation of an individual pixel (Getis, 1994). The processing of remotely sensed data to generate spatial dependence information is related to kernel approaches for density estimation (Bailey and Gatrell, 1995). In consideration of remotely sensed data individual points are pixels. The distance of consideration may be

thought of as the size of a kernel around an individual pixel. Remotely sensed data are commonly found to be non-stationary, that is, the distribution characteristics change with changing areas of consideration. As a result, variability of spatial dependence is expected as a characteristic of remotely sensed data.

Autocorrelation characteristics of remotely sensed imagery are summarized in Section 5.2 and the pertinent literature is presented in Table 5.1. A variety of techniques to characterize remotely sensed image spatial characteristics have been developed, such as image co-occurrence (Haralick, 1973, 1979), scanline techniques (Labovitz and Masuoka, 1984), and semivariograms (Curran and Atkinson, 1998). In the body of spatial statistical literature, not commonly applied to remotely sensed imagery, there may be found an alternate approach to the assessment of spatial dependence. The approaches generally have an understood statistical distribution and an associated suite of assumptions. Examples of these approaches are measured by Moran's *I*, Geary's *c*, and the suite of *G* statistics. Moran's *I* and Geary's *c* were initially developed as global statistics but have been adapted to allow for local computation (Anselin, 1994). A discussion of the rationale for the selection of $G_i^*$ for further investigation is presented in the following.

The suite of *G* statistics (Getis and Ord, 1992; Ord and Getis, 1995) were developed for the investigation of local patterns potentially present in spatial data. Getis (1994) subsequently applied an unstandardized version of $G_i^*$ in conjunction with an analysis of variance measure to characterize the spatial dependence trends exhibited. The value of such an approach was noted by Wulder and Boots (1998b) who altered a standardized version of $G_i^*$ to process remotely sensed imagery. Subsequent investigations were undertaken upon Landsat TM data (Wulder and Boots, 1998a), and SSM/I passive microwave data (Derksen, *et al.*, 1998ab). This current study allowed for an unprecedented investigation of the spatial

dependence of spectral values of high spatial resolution imagery with a direct measure of local spatial dependence. Understanding of the spatial dependence characteristics of remotely sensed data allows for the attachment of an attribute relating information about the site and situation of an individual pixel, which is useful supplementary image information. Through the development and computation of $G_i^*$ the investigation of the local spatial dependence characteristics on a per-pixel basis presented in the thesis is unique. The application of $G_i^*$ to investigate forest structural parameters is undertaken to assess the characteristics and utility of spatial dependence information. (A discussion of limitations and recommendations related to the estimation of forest structural characteristics in this thesis is presented in the Section 10.5.)

## 10.3. Measures of Spatial Dependence

Spatial dependence describes the relationship between neighbouring pixels. Characterization of the relationship between pixels has led to the development of a variety methods to measure spatial dependence, such as second-order statistical co-occurrence, image semivariance, and more recently, local indicators of spatial association. In this section, a selection of measures of spatial dependence are described. Following the description of the range of measures of spatial dependence, the rationale for development and introduction of the measure of spatial dependence $G_i^*$ to the remote sensing and forestry communities is presented.

Second-order statistical co-occurrence (Haralick, 1973, 1979) and image semivariance (Curran and Atkinson, 1998) are the most common methods for characterizing image spatial characteristics. Second-order statistical co-occurrence provides an indication of the relationship between digital numbers in a feature space which is then used as a measure of local characteristics. Second-order statistical co-occurrence is valuable for the description of image textural features. A second-order statistical measure is so defined as it is not made

directly upon the numbers under consideration. In the computation of co-occurrence values, pixel digital numbers are placed into a co-occurrence matrix from which the actual second-order statistical co-occurrence measure is derived. The placement of values into the co-occurrence matrix is undertaken by defining a set of parameters to indicate the pixel interrelationships. The parameters required are window size, angle for comparison, direction, quantization level, and step size. Once the parameters are defined each pixel in the image is consistently assessed. Within the predefined window, each pixel is compared based upon the *user defined rules for angle of comparison, direction, and step size. Co-occurrence is said to* happen and an increment is added to the co-occurrence matrix relating the numbers which are found together at the location within the window based upon the comparison rules. The quantization level is important as it defines the bounds of the co-occurrence matrix, for example 8 bit data may have a range of co-occurrence from $2^8$, or the 256 values from 0 to 255. Once the pixel inter-relationships have been processed based upon the defined co-occurrence rules the values within the co-occurrence matrix are processed to provide an indication of possible relationships such as entropy, homogeneity, contrast, dissimilarity, mean, and standard deviation (Haralick 1979). Differing results may be expected from co-occurrence based upon changes may to any of the rules for inclusion in the co-occurrence matrix. The selection of window size is particularly problematic (Franklin, *et al.*, 1996). An additional short coming of co-occurrence processing is the inability of the statistical representations of the co-occurrence matrix to indicate the actual spatial relationships measured. The co-occurrence relationships are computed upon the entire matrix resulting in an inability to relate what spatial inter-relationships are occurring between the input digital numbers.

Semivariance is a measure of the variance found between pixels of a remotely sensed image. A description of semivariance computation and application is presented in Section 4.7. In summary, the spatial domain found at a pixel location may be computed based upon changes in the variance found around a particular pixel location. The ability to characterize the region of spatial dependence around a pixel has been a valuable addition to the remote sensing tool box. As summarized, studies using semivariance may compute semivariance along a single transect (Woodcock, *et al.*, 1988b) or in multiple directions around a pixel (Wulder, *et al.*, 1998). A shortcoming with semivariance is that it is a positive valued function that indicates a region of spatial dependence without reference to the values processed. Yet, semivariance and the structurally based information derived is unique and versatile in remote sensing studies (Curran and Atkinson, 1998). The versatility and utility of semivariance for providing image structural information related to the structure of the remotely sensed surfaces leads researchers to either enhance semivariance analysis or to seek complementary measures. Local indicators of spatial association (Anselin, 1995) and the suite of *G* statistics (Getis and Ord, 1992) provide information that describes the relationship between an observation and the values around that observation and are seen as a logical complement to semivariance and a research opportunity worthy of further investigation.

According to the characterization by Anselin (1995, p. 94) a local indicator of spatial association (LISA) is a statistic that meets the following requirements,

1. the LISA for each observation gives an indication of the extent of significant spatial clustering of similar values found around that observation;
2. the sum of LISAs for all observations is proportional to a global indicator of spatial association.

While a measure of spatial association, the suite of $G$ statistics are not a considered as a LISA in the terminology due to the lack of a relationship to a global statistic of spatial association. The requirement of a relationship to a global measure of association is not problematic in the identification of significant local clusters. Moran's $I$, and Geary's $c$ can be transformed to meet the LISA criteria and this is demonstrated in an application and compared to $G_i^*$ by Anselin (1995). The local Moran's $I$ is a standardized normal value, with positive values representing a spatial cluster of similar values and negative values indicating a clustering of dissimilar values. In comparison, positive $G_i^*$ values indicate an association of high values, while negative $G_i^*$ values indicate a clustering of low values (Ord and Getis, 1994). Based upon the information inferred from the statistics, and in the context of processing of remotely sensed imagery, $G_i^*$ initially appeared more applicable to the generation of information from remotely sensed imagery than a local Moran's $I$. As neither has been applied in a per-pixel basis upon high spatial resolution remotely sensed data, algorithm development and programming was required. The utility of $G_i^*$ in a remote sensing context has indicated the potential for adaptation of the local Moran's $I$ to enable processing of remotely sensed imagery.

The $G_i^*$ statistic is a means of generating information to characterize the level of spatial dependence associated with a location. In the case of remotely sensed imagery the locations are pixels. A full description of the background, computation, and application of $G_i^*$ comprises Chapter 5. Applying the method presented by Wulder and Boots (1998b), an image of spatial dependence values may be computed from original image spectral values. The result is that for each pixel the strength of spatial association (or spatial autocorrelation) and the magnitude of the input values is quantified. Clusters of high values are noted with a positive sign while clustering of low values is denoted with a negative sign. Also stored is

information indicating the distance at which $G_i^*$ is maximized, previously noted as MGD – the Maximized Getis Distance. The absolute maximum value of $G_i^*$ indicates the size of the spatial domain found around a particular pixel.

Provision of each pixel in an image with a value relating the strength of association to its neighbours while also indicating the magnitude of input values allow techniques to be developed which exploit both spectral and spatial characteristics of the imagery. As noted earlier, computation of image semivariance is a useful image processing technique to generate a value, such as the range, which indicates the size of the region of spatial dependence through consideration of the relationship between values along a transect. The computation of $G_i^*$ is undertaken to indicate the strength of the association, or the level of autocorrelation, found within the range. Comparison of the links between $G_i^*$ and the semivariance range is problematic based upon factors such as how each is computed and what is being measured. $G_i^*$ is computed within a square kernel and represented by the absolute maximum value, while semivariance is computed along a transect and is by nature a positive valued function. Further, visual plot comparisons between proportional values and direct data measures illustrate relationships of little spatial meaning.

A unique feature of $G_i^*$ is the underpinnings of a statistical distribution. As presented in Section 5.3, $G_i^*$ is based upon knowledge of a known mean and variance. While $G_i^*$ is based upon global mean and variance values, global stationarity is not required for computation. The $G_i^*$ values generated for an entire image are not necessarily normally distributed; it is at the individual location, or pixel level, that normality occurs. A minimum of 8 values are required at a location for the assumption of normality to hold (Griffith, *et al.*, 1996). In comparison to other measures of spatial dependence, such as second-order spatial co-occurrence, this is unique. Second-order statistical co-occurrence requires the user

intervention for a number of parameters, such as angle, step size, direction, quantization level, window size, and choice of which statistic to compute from the co-occurrence matrix to represent the relationships. For one-off studies this is likely not too large an issue, but in cases when attempting to characterize the spatial relationships between multiple image dates, the second-order statistical co-occurrence settings may no longer hold. Small changes in spectral values may alter the co-occurrence results. In comparison to $G_i^*$, it is postulated that small changes in digital number values are minimized, as the spatial relationships still hold *although the relative values of the digital numbers may have changed.*

When processing $G_i^*$ the relationship between the input digital numbers and resultant $G_i^*$ values is strong. The high correlation's are due to the nature of the computation of $G_i^*$. Consider what $G_i^*$ relates; the strength of spatial dependence, and the magnitude of the values found to be dependent. The provision of a sign to the $G_i^*$ values to represent the magnitude of the association results in the fact that high digital numbers have positive signs that may also be high values, conversely, low digital numbers have negative signs that may also be low numbers. This situation results in high correlation's between the spectral and $G_i^*$ values. The result is that computation of $G_i^*$ acts as a moving proportion filter transforming the original spectral values to relate both the character of the initial spectral features while also providing information related to the level of spatial association present at a particular location. The data transformation indicates the potential of building clusters from spatial objects generated out of the spectral data. For example, a shortcoming noted for the well developed and successful valley following techniques is the erroneous division of individual objects that contain spectral variability (Gougeon, 1995a). To reduce this problem the imagery is often preprocessed with a mean filter, or additional rules are added to the crown delineation procedures based upon factors such as inter-pixel curvature (Held and Billings, 1998). The

availability of a smoothing function based upon spatial dependence may also aid in future development of rules for influencing crown delineation. The work presented in this thesis may provide some insights to researchers implementing valley following techniques upon deciduous forest cover.

## 10.4. Comparison of Information Extraction Approaches

Measures of forest structure may be estimated based upon spectral or spatial information extraction approaches. The estimation of forest structure characteristics based upon spectral relationships implies a meaningful relationship between the spectral response and forest structure. Spatial information extraction approaches to the extraction of forest structural information are based upon the spatial inter-relationships of the pixel values. Further, approaches which acknowledge the complexity of remotely sensed representation of forests have resulted in hybrid approaches to information extraction. The clustering approach, based upon spatial dependence, demonstrated in this thesis may be considered a new and separate approach. In this sub-section, an overview and comparison of the varied approaches to forest structural information extraction from remotely sensed data are presented. A variety of outstanding issues, such as the effect of the modifiable areal unit problem and the effect of different cover types, especially hardwoods, are also presented.

### 10.4.1. Spectral Approaches

Spectral approaches to the estimation of forest inventory and biophysical parameters, are commonly empirical in nature, and use the spectral values found at a location to relate to the ground measured properties at the same location. These spectral approaches to the estimation of forest inventory and biophysical parameters are based upon an understanding of the reflectance characteristics of vegetation. For example, vegetation absorbs visible electromagnetic radiation while scattering near infrared radiation (Curran, 1980). This is a

result of pigments, especially chlorophyll, which absorb visible wavelengths, while the air-water interfaces between the intercellular spaces and cell walls cause multiple refraction, resulting in high net reflectance values in the near-infrared wavelengths (Gausman, 1977). The reflectance characteristics are generally distinct for each surface cover type and are thought of as spectral signatures (Avery and Berlin, 1992).

In the estimation of forest stand parameters, relationships may be developed empirically or deterministically. Empirical approaches are based upon relating, often through regression, field measured parameters to the spectral response found at the same location. There are a variety of examples using mid-resolution imagery, pixels greater than 10m spatial resolution, for the empirical estimation of forest inventory (Franklin, 1986; Danson, 1987; De Wulf, *et al.*, 1991) and biophysical parameters (Spanner, *et al.*, 1990; Fassnacht, *et al.*, 1997). In the case of forest inventory parameters, success is generally limited by the low resolution of the sensors utilized. The estimation of biophysical parameters, such as LAI, is hindered by both low spatial resolution and an asymptote of the relationship between LAI and spectral information at approximately 3 (Peterson, *et al.*, 1987).

Landsat TM has a spatial resolution of 30m which allows for regional estimation of forest stand parameters. A standard full scene measures 185 x 175 km resulting in regional coverage of approximately 31,450 $km^2$ (Avery and Berlin, 1992). The trade-off for the regional coverage, is the spatial resolution, which results in estimates of forest stand parameters which are often of too low an accuracy for operation forest management. The interpretation of the suitability of a particular accuracy level depends on the goals of a particular analysis. In comparing spectral values to basal area and biomass, Franklin *et al.* (1986) found that correlations are strongly dependent upon the spectral channel, with the strongest relationships found in TM 1, 2, and 3. Danson (1987) applied SPOT-1 HRV imagery to correlate digital

numbers to a suite of forest stand parameters. Significant correlations were found for density, mean DBH, mean height, and age, but not for canopy closure. One of the findings of this study was that variation in efficacy in the estimation of forest stand parameters is not a function of vegetation amount, but is due to the amount of shadow found within the canopy. De Wulf *et al.* (1990), also using SPOT imagery, found moderate relationships between forest stand parameters and both infrared and panchromatic spectral response. Model inversion was also undertaken to estimate the suite of forest stand parameters. The stand parameters with the greatest influence upon shadowing within the canopy, stand density and canopy height, are reported to have reasonable accuracies of between 60 to 70 percent. Estimation of forest biophysical parameters, such as volume (Gemmel, 1995), biomass (Franklin, 1986), and LAI (Spanner, *et al.*, 1990), all reach an asymptote, where the digital information changes little while the parameter still increases. Fassnacht *et al.* (1997) found in regression relationships between LAI and image spectral response variability in success related to species composition. The LAI of conifer species was measured within a range of $r^2$ from 0.69 to 0.73, while the best relationship found for hardwoods was an $r^2$ of 0.35.

Empirical estimation of forest parameters with high resolution imagery of less than 10m spatial resolution is a less established methodology with differing limitations. The lower resolution techniques consider the forest in terms of multiple objects within a single pixel, whereas the higher resolution techniques deal with a higher variance environment. In the high variance environment abrupt changes in digital numbers can occur as the pixel contents change from tree to between tree reflectance. In the lower variance environment, the changes in pixel contents occur more slowly as the transition areas are often contained within pixels. As a result, new techniques have been developed to address the variance rich environment present with high resolution imagery. The estimation of forest parameters with high spatial

resolution imagery spectral values is an active research area. Techniques have been investigated which utilize the spectral information present in high spatial resolution imagery for the estimation of forest inventory (Baulies and Pons, 1995) and biophysical parameters (Smith, *et al.*, 1991b; Spanner, *et al.*, 1994; Seed and King, 1997). In acknowledgement of the difficulties inherent in undertaking a forest inventory with high spatial resolution multispectral data Leckie *et al.* (1995) present a methodology which prepares digital data for visual interpretation. Baulies and Pons (1995) attempt a spectral approach to forest inventory parameter extraction and cover type mapping. The spatial resolution of the *casi* data for the study by Baulies and Pons was 5 x 5m with a dominant vegetation cover type of coniferous pines. Multiple regression relationships developed from one flight line were applied to an adjacent flight line. A discussion of the results of the application of the relationships to the adjacent flight line illustrates a correlation of 0.87 for crown closure ($p = 0.01$), while for density an insignificant correlation is found. Based upon the study parameters, such as cover type and image spatial resolution, Baulies and Pons indicate that spectral response can only be related to forest structural parameters when there is a homogeneous spatial distribution. The homogeneous spatial distribution desired may be related to image spatial resolution, 5m data is an L-resolution environment with each pixel containing a variety of objects. An increase in spatial resolution allows for the imaging of an H-resolution environment, where each object is composed of a number of pixels. The availability of H-resolution data has not led to a variety of studies based upon empirical spectral estimation of inventory parameters. The variance rich H-resolution data has more commonly been approached spatially or with combined spatial and spectral analyses.

Forest biophysical parameters have seen more success with spectral estimation with high spatial resolution data. An early empirical study by Smith *et al.* (1991b) related optically

collected LAI values to pixels with a spatial resolution of either 1.58 to 2.34m on a side, over an LAI range of 2.6 to 9.5. The straight empirical relating of digital numbers to LAI values were found to corroborate lower the spatial resolution results reported by Peterson *et al.* (1987) and Spanner *et al.* (1990), that correlations may be found but are limited by an asymptotic relationship. In an empirical study based upon the spectral characteristics of shadow, rather than tree spectral features, Seed and King (1997) report promising results. The shadows between trees are broken into three components based upon user defined thresholds and are used to develop multivariate regression relationships with LAI as the dependant variable. Undertaking image analysis upon 0.25m spatial resolution digital camera data, over an LAI range of 1.12 to 4.92, an $R^2$ of 0.90 with a standard error of 0.34 is reported, with a sample size of 15 plots.

### 10.4.2. Spatial Approaches

While information extraction from spectral data is often undertaken, the use of spatial information to determine forest structural parameters is becoming increasingly common. Information extraction approaches based upon spatial data are based upon the premise that forest structural information is captured in the image spatial structure. The image spatial structure refers to the way in which pixels are related to one-another, not solely on the magnitude of the actual pixel digital numbers. In a spatial approach, it is the way pixels are found together, not merely the digital number that is important. As a result, the knowledge of the relationship between image spatial resolution in relation to the size of the image object of interest is often required.

Spatial information extraction approaches generally require a greater level of processing than spectral approaches as a greater number of pixels are involved. Mid-resolution imagery has a been processed for forest inventory and biophysical estimates based upon techniques

such as texture (Kushwaha, *et al.*, 1994), and image semivariance (Cohen, *et al.*, 1990). Kushwaha *et al.* (1994), following the efforts of Peddle and Franklin (1991) integrate texture to improve the results of multispectral image classifications. These results demonstrate the relationship between forest structure and cover type. Semivariance is a means by which the link between forest structure and cover type may be further explored. Cohen *et al.* (1990) applied image semivariance to a set of image spatial resolutions including 1, 10, and 30m. The spatial variability of coniferous forest cover varied in relation to the image spatial resolution. At a spatial resolution of 1m the semivariogram ranges were best related to mean tree canopy size. At a spatial resolution of 10m the semivariance indicated only whether tree canopy sizes were less than 10m or between 10 and 20m. With a spatial resolution of 30m only the sills of the semivariograms related any forest structural information, even though the differences between the sills were small. Based upon these results, the potential for semivariance processing of high spatial resolution imagery is indicated. The low variance environment present in mid-resolution imagery hampers the efficacy of textural and semivariance processing. Examples of the utility of semivariance processing of high spatial resolution imagery are provided by Lévesque and King (1996) and St-Onge and Cavayas (1995). Lévesque and King (1996) present a multi-scale analysis illustrating the relationship between information content and image semivariance. Lévesque and King (1996) indicate that individual tree crown closure and the semivariance range have a 0.80 correlation when processing 0.25 metre resolution imagery, while a decrease in correlation between semivariance range and crown closure to –0.16 occurs with 0.5 metre resolution imagery. St-Onge and Cavayas (1995) have utilized the information inherent in the directional variogram as a method to estimate the stocking and height of forest stands. St-Onge and Cavayas (1995) found that the relationship between actual and predicted stand level values changed little with

a change in image spatial resolution from 0.36 to 2.16m. The robust nature of the directional semivariance technique for characterizing forest structure indicated the possibility for creation of absolute spatial signatures, as the spatial structure is not hampered by radiometric factors. High spatial resolution imagery has enabled the development of a variety of spatial information extraction techniques.

High spatial resolution imagery provides an image environment rich in spatial information. The spatial structure contained in high spatial resolution digital imagery is a function of the size and distribution of objects within the imagery. The availability of high spatial resolution imagery has allowed for the investigation of the utility of spatial information in the estimation of forest stand parameters. The most common approaches to extract forest inventory and biophysical parameters from high spatial resolution imagery based upon spatial information are, texture (Gougeon and Wong, 1986; Section 4.3), image semivariance (Lévesque and King, 1996; Section 4.7), local maxima filtering (Hay, *et al.*, 1996; Walsworth and King, 1997; Section 4.4), and valley following (Gougeon, 1995a; Section 4.4). In an early study of the relationship between texture and forest stand parameters, Gougeon and Wong (1986) present a segmentation approach based upon texture segmentation and region growing. Local maxima filtering is considered as a spatial information extraction approach as it is based upon the spatial context of where a pixel is found. Local maxima filtering may indicate tree locations for the development of object specific textural classifications (Hay, *et al.*, 1996), to indicate stem locations to estimate density (Burnett, *et al.*, 1998), or to provide seed points for the generation of tree objects (Walsworth and King, 1998). Walsworth and King (1998) applied a radiance peak filter to isolate individual tree locations, with further steps taken to ensure the accuracy of these locations. The transitions between stems, computed from automata and Markov transition matrices, demonstrate differing forest

structural information content for pixel based and neighborhood based estimates. Changes in forest composition over time are captured in the neighbourhood based estimates of forest structure.

### 10.4.3. Hybrid Approaches

This sub-section on hybrid approaches is intended to present combinations of spatial and spectral information extraction. The two previous sections described the nature of both spectral and spatial information content in the context of a remotely sensed image. In short, the spectral approaches tend to attempt to account for characteristics related to vegetation content, while spatial approaches tend to relate structural information. As a result, the combination of both spectral and spatial information appears desirable in attempting to explain forest structure.

In Section 4.3.1, a summary of the union of spectral and spatial information is presented. Described is the work of Wulder *et al.* (1996a, 1998), which is an investigation of the relationship between LAI, NDVI, and texture. Wulder *et al.* (1996a) assessed the change in variance explained with empirical estimation equations with LAI as the dependant variable. The independent variables were combinations of NDVI and first- and second-order texture variables generated upon 2m spatial resolution *casi* imagery. The ability to estimate LAI based solely upon spectral information generated a bivariate $r^2$ value of 0.67 with a standard error of 0.70 over an LAI range of 2.39 to 7.05. For the same range of LAI, texture alone only accounted for an $r^2$ of 0.56 and a standard error of 0.77. The combination of the spectral and textural information for the complete range of LAI, resulted in a multivariate $R^2$ of 0.92 with a standard error of 0.68. Stratification by species demonstrated the association of accuracy with LAI range. The deciduous stands in the study occupied a limited LAI range of 2.39 to 3.70 and had a larger proportion of the variance in the empirical relationships explained than for

conifers which occupied a larger LAI range from 3.45 to 7.05. While not as large an amount of the variance was explained for the conifers, the results are nevertheless encouraging as the entire range of LAI values is above the usual asymptote of 3. Shortcomings with this study were identified as sub-optimal texture measures and small sample size. As a result, a follow-up study was undertaken upon deciduous mixed-woods with 1m spatial resolution *casi* imagery (Wulder, *et al.*, 1998). In this study the range of deciduous LAI spans from ≈1.5 to 7, resulting in weaker relationships than were found in the previous study. The initial bivariate relationship between LAI and spectral data resulted in an $r^2$ of 0.42, which increased to an $R^2$ of 0.61 with the integration of texture. The computation and selection of texture measures is often problematic. First-order texture measures, those computed directly from the image spectral values, best improved regression relationships involving homogeneous surfaces. Second-order texture measures, those computed from a transformation of spectral values (such as co-occurrence), explained the greatest amount of variance when involving heterogeneous surfaces. In an attempt to integrate the proven ability of semivariance to differentiate subtleties in forest structure, a new texture measure was developed based upon discrete locations extracted from variograms. Semivariance moment texture measures are sensitive to the spatial characteristics of the stand such as crown closure and density and as a result are useful in the estimation of a variety of cover types.

An additional exploration of the relationship been forest stand LAI and textural information is presented by Olthof and King (1997). Imagery of a high spatial resolution of 0.25m, over an LAI range of 1.2 to 4.9, sensed over a stand dominated by hardwood species were used in this study. Correlation relationships were developed with and without texture, with more of the model variance explained when including texture. For example, the following correlation relationships are present between LAI and the dependant variables: near

infrared reflectance (r = 0.56), texture from measure of co-occurrence contrast (r = 0.64), near infrared reflectance and texture (0.79). These results corroborate those of Wulder *et al.*, (1996a, 1998) further demonstrating the utility of the combination of spectral and spatial information.

Yuan *et al.* (1991) investigated changes in the structure of sugar maples based upon spectral and textural analysis of multispectral aerial videography. Spectral and textural features computed for individual trees were compared through correlation to manually interpreted colour and colour infrared photography. Indices were developed from the imagery and photos to relate forest decline. These results were also found to be compatible with ground surveys. As a result, the authors stated that the aerial video data is appropriate for analysis of maple decline on a single tree basis.

### 10.4.4. Clustering Approaches

Clustering is an approach by which pixels identified as representing a single discernable object are joined. The single discernable object, in the context of this research, may be characterized by a situation such as, a single large tree sensed with high spatial resolution imagery, a group of trees that are layered by dominance, or trees that are close together but undiscernable in lower resolution imagery. As a result, image spatial resolution is an important consideration when undertaking a clustering approach. The conceptual frame of clustering, as opposed to segmentation, is that it is a process of building image objects from seed points based upon similarity, rather than splitting objects found to be dissimilar. Clustering approaches are complementary to existing segmentation and image processing techniques. In a forestry context, clustering acknowledges forest complexity and limitations based upon image resolution.

In this thesis a clustering approach based upon statistically generated spatial dependence is developed (Chapter 7). This clustering approach was developed to account for the spatial structure of forest canopies composed of both coniferous and deciduous trees as represented by 1m spatial resolution multi-spectral imagery. Factors such as the large size, irregular shapes, and overlapping that occur within and between deciduous crowns indicated a need for investigation of alternate approaches to delineate crowns than those developed for coniferous tree species. This clustering approach based upon spatial dependence does not require the user input of threshold values for qualification of a given pixel to a cluster, the clustering is based upon the similarity of neighbouring pixels. A key component of this research is the development of a statistically robust clustering approach. The derivation of forest inventory and structural parameters faced a variety of limitations, which will be discussed in a following section (Section 10.5). Despite the study limitations, several observations are made: the clusters generated represent unique spatial information; the clusters are related to the size and distribution of trees within the imagery; the clusters are related to the amount of crown closure present; density is difficult to measure with clusters; leaf area index may be computed from the combination of spatial and spectral information, as well as, from spatial information alone. In this research the cluster development was based upon as little user intervention as possible, allowing for local spatial similarity to dictate the size, shape, and number of clusters. Intervention of additional rules, such as size and shape limits, or threshold specifications, may allow for an improved cluster integrity in relation to the field measured data. Following is a summary of the primary findings of the spatial dependence clustering approach to object determination for estimation of forest structural parameters.

Section 7.2.4 presents the data to support the statement that clusters generated represent unique spatial information. The spatial distribution of spectral values is illustrated through a series of tables and plots. For example, it is shown that,

- image spatial structure relates to the size of objects found in forest imagery which is also related to the spatial resolution,
- image spectral values have a unique distribution in the spatial domain, and
- image spatial processes are not all operating at the same scale.

These statements provide a context for research through indication of the complexity present in the spatial dependence characteristics present in a forested area. A related study undertaken to generate spatial dependence information, represented by $G_i^*$, upon Landsat TM data produced clusters which explored stand level characteristics (Wulder and Boots, 1998b). In contrast, the clusters generated in this present study, as a function of the image spatial resolution, grouped pixels representing individual or groups of trees.

As mentioned, cluster generation is a function of image spatial resolution and the forest structure under investigation. As a result, the forest characteristics present and represented at a spatial resolution of 1m result in mixed pixels and clusters composed of more than one tree. The presence of more than one tree within a cluster results in a limited ability to estimate forest stand density (Section 8.2). Crown closure, in contrast, is represented moderately well with tree objects based upon spatial dependence (Section 8.3). The small sample size limits the confidence in relating the results, which found for clusters generated upon infrared data, an absolute difference of 0.56 to the field data, with a standard deviation 0.07. In general, the cluster based estimates of crown closure are found within approximately 10 percent of field based estimates. These accuracies must be weighted against the small possible range of crown closures and the large relative error.

A statistical clustering approach was undertaken to place each tree object into a cover type class (Section 8.4). The typing of cover class varied in success by plot. The method used to place objects in clusters was good considering the limitations of the study but would not be repeated in a subsequent analysis.

Leaf area index was estimated using two techniques, one which required an input of cover type to aid in the selection of the most appropriate LAI estimation equation, while the second used a regional stand for maximum LAI and rated the estimate based upon areal contribution of the objects within the plot area (Chapter 9). The caveats of the previously mentioned interpretation based upon sample size are also present for this analysis. The estimates of LAI from both techniques are found to be within approximately ±1.4. As all field estimates of LAI are greater than 3, the results are promising, yet not of sufficient accuracy for addressing ecological issues or for up-scaling. The ability to estimate LAI based on vegetation spatial extent and knowledge of regional LAI indicates that estimates of LAI may be made from satellite collected panchromatic data.

In reference to the field data available for this study, the relationships between the image generated clusters and forest inventory and structural parameters are not conclusive, nevertheless a worthwhile approach appears to be under development. The spatial dependence data may be used to generate clusters or be used as attribute data to describe pixels to be utilized by techniques such as valley following or threshold based approaches. The use of spatial dependence information in concert with valley following methods will allow for increased knowledge of the pixel inter-relationships to be integrated as a possible qualification rule. In threshold based clustering approaches, spatial dependence information may be used as a rule to allow for relaxation of threshold boundaries.

In a recent work, Culvenor *et al.* (1998) present a threshold clustering approach based upon 2m spatial resolution digital multi-spectral video data. The rationale for the clustering approach is based upon the forest structural characteristics found to occur in Australian native forests. The clustering approach was developed to account for low foliage density and complex crown structure and to allow for a minimization of crown segmentation. The approach developed is referred to as the Tree Identification and Delineation Algorithm (TIDA). The generation of tree clusters from TIDA is based upon identification of maxima and minima pixels, of an infrared image channel, to represent crown centroids and crown edges. A user defined parameter is used to calculate a threshold value for acceptance or rejection of a pixel's membership to the crown under consideration. Pixels are clustered into a given crown object if the reflectance present is greater than the defined threshold value and is not already identified as a boundary pixel. This process is repeated for all pixels until all have been added to a crown or have been found spectrally invalid. A sensitivity analysis was undertaken to assess the efficacy of the approach by comparing a stand constructed from geometrical optical properties to the remotely collected imagery. The maximum number of trees identified by TIDA was 92% at an off-nadir viewing angle of 2 degrees. The optimum crown delineation was achieved at mid-day with the average crown area reported as $61m^2$ for the imagery and $67m^2$ for the simulated data. It is noted, however, that in this case no attempt is made to distinguish between vegetation and non-vegetation pixels; therefore, improved results may be possible for this procedure.

The utility of the TIDA clustering approach has been identified as appropriate for the characterization of Australian forest cover types and is the subject of further investigation. The TIDA tree clustering results have been compared to forest type and structure maps produced through the interpretation of 1:25,000 colour air photos (Preston, *et al.*, 1998). In

this study a comparison of estimates of species, tree size and density, tree development index, and height, among others, from multispectral video are compared to the values determined from air photo interpretation. The estimates made from the digital multispectral video incorporating the TIDA clusters explained approximately 20% more variance than the parameter estimates determined from air photo interpretation. The success of this methodology prompted the authors to state in their conclusions,

> Despite these operational constraints the research presented in this paper is sufficient to indicate that an entirely new approach to forest mapping is becoming available. Mapping of detailed forest attributes, based on tree clusters and high resolution imagery, will require a major rethink of procedures for mapping, monitoring, and field assessment of forests (Preston, *et al.*, 1998).

The cluster based approach to looking at forests is seen to incorporate the importance of both forest species and structural characteristics. As a result, the clustering approach needs to be assessed over a variety of forest cover types, and an assessment of costs and timing is also necessary to determine a measure of model reliability.

### 10.4.5. Comparison of Approaches

In discussion of some of the factors which affect the remote sensing of forests, the most appropriate image analysis technique is shown to be related to cover type (Section 3.4). In summary, Strahler *et al.* (1986) present some of the primary concepts in remote sensing, which is then built upon by Woodcock and Strahler (1987) through illustration of the importance of scale in selection of image analysis approach. Single pixel based approaches may be appropriate for homogeneous entities, while methods that account for spatial pattern are suitable for more heterogeneous surfaces, such as forests. As a result, the image analysis approach is related to surface cover and heterogeneity, which limits the universal application of any methodology. The selection of an image processing approach should be based upon an

understanding of the relationship between image spatial resolution, tree species, tree size, and tree distribution. In the previous sections, addressing the efficacy of a variety of spatial, spectral, hybrid, and clustering approaches for forest structural information extraction, the relationship between image spatial resolution, tree species, tree size, and tree distribution is demonstrated. The direct comparison between studies is problematic, as the conditions present in each study vary. The variation may not be primarily a function of the approach undertaken, but due to differences in conditions resulting from differing spatial resolution, spectral resolution, temporal resolution, forest cover type, crown closure, or stand density.

### 10.4.6. Information Extraction from Mixed- and Hardwood Forests

This section will summarize the utility of the previously presented approaches in reference to cover type. As presented by Fassnacht *et al.* (1997) the ability to characterize softwoods is greater than that of hardwoods. Much of the previous research has focused upon softwoods, with the more difficult to characterize hardwoods subject to fewer research initiatives.

Hardwood tree species are characterized by large and overlapping crowns. The presence of large and overlapping crowns is problematic for construction of methods for parameter estimation from remotely sensed data. For example, Fassnacht *et al.* (1997) found in regression relationships between LAI and image spectral response, accuracy related to species composition, with the LAI of conifer species measured within a range of $r^2$ from 0.69 to 0.73, while the best relationship found for hardwoods was an $r^2$ of 0.35. A variety of detailed calibration projects have been undertaken to assess the nature of deciduous spectral response based upon vegetation indices and particular spectral locations (Vogelmann, et at., 1993), seasonal variability (Blackburn and Milton, 1995), spectral directionality (Milton, *et al.*, 1994), and in relation to the local ecology (Blackburn and Milton, 1995-568). Multi-date *casi* imagery was collected to produce a map of canopy gaps which was used to quantify the

character of the canopy gaps and tree canopy (Blackburn and Milton, 1995). This information was used to assess the relative ecological status of the different forests.

A variety of approaches have been applied to extract deciduous forest structural information from high spatial resolution remotely sensed imagery. A number of the approaches have been presented in previous sections, and will be described here. Following is also a selection of additional research undertaken to relate the structural characteristics of deciduous forests. The accuracy generated from the classification of 2.5m spatial resolution *casi* data has been shown to be sensitive to view angle geometry and terrain effects (Franklin, *et al.*, 1991). Aerial videography has also been applied in the classification of deciduous forests (Slaymaker, *et al.*, 1996). This classification of deciduous forests, flown in transects to characterize a sub-sample of the larger area, was undertaken to provide validation for a Landsat TM based classification program. The increased spatial resolution of the aerial video data over the Landsat TM allowed for the re-labeling of classes generated upon the Landsat TM data.

Following is a summary of the previously mentioned studies to use image processing of high spatial resolution imagery to assess forest structure. Spectral estimation of the LAI of deciduous forests is reported on by Seed and King (1997) in an empirical study based upon the spectral characteristics of shadow, rather than tree spectral features. Image analysis of 0.25m spatial resolution digital camera data, over an LAI range of 1.12 to 4.92, an $R^2$ of 0.90 with a standard error of 0.34 was reported, with a sample size of 15 plots. Spatial estimation of crown closure, utilizing semivariance is presented by Lévesque and King (1996). Individual tree crown closure and the semivariance range have a 0.80 correlation when processing 0.25 metre resolution imagery, while a decrease in correlation between semivariance range and crown closure to –0.16 occurs with 0.5 metre resolution imagery.

Radiance peak filtering exploits the spatial relationship to indicate tree crown locations. Walsworth and King (1998) applied a radiance peak filter applied to isolate individual tree locations, with further steps taken to ensure the accuracy of these locations. Changes in forest composition over time are captured in the neighbourhood based estimates of forest structure. The estimation of LAI from spectral information alone, and including textural information is undertaken by Wulder *et al.* (1996a, 1998) and Olthof and King (1997). In Wulder *et al.* (1996a) the deciduous stands in the study occupied a limited LAI range of 2.39 to 3.70 and had a larger proportion of the variance in the empirical relationships explained than for conifers which occupied a larger LAI range from 3.45 to 7.05. A follow-up study was undertaken upon deciduous mixed-woods with 1m spatial resolution *casi* imagery (Wulder, *et al.*, 1998) with a range of deciduous LAI from ≈1.5 to 7, resulting in weaker relationships than were found in the previous study. The initial bivariate relationship between LAI and spectral data resulted in an $r^2$ of 0.42, which increased to an $R^2$ of 0.61 with the integration of texture. An additional exploration of the relationship been forest stand LAI and textural information is presented by Olthof and King (1997). Imagery of a high spatial resolution of 0.25m over an LAI range of 1.2 to 4.9 sensed over a stand dominated by hardwood species were used in this study. The following correlation relationships are present between LAI and the dependant variables: near infrared reflectance (r = 0.56), texture from measure of co-occurrence contrast (r = 0.64), near infrared reluctance and texture (0.79). These results corroborate those of Wulder *et al.*, (1996a, 1998) further demonstrating the utility of the combining of spectral and spatial information. Using a different approach, Yuan *et al.* (1991) investigate changes in the structure of sugar maples based upon spectral and textural analysis of multispectral aerial videography. Indices are developed from the imagery and photos to successfully relate forest decline. These approaches demonstrate the variety of methods

which may be undertaken to assess the structure of deciduous forests. Radar data has also been utilized to assess the structure of deciduous forests (Ustin, *et al.*, 1991; Mead and McIntosh, 1991; Wu, 1987).

### 10.4.7. Modifiable Areal Unit Problem

In discussion of the factors which affect the remote sensing of forest canopies (Section 3.4), the following issues are discussed: spectral response of forest canopies (Section 3.4.1), scale in remote sensing (Section 3.4.2), the nature of models in remote sensing (Section 3.4.3), and scale and the representation of geographic data (Section 3.4.4). In the dicussion of scale and the represtation of geographic data, the issue of the modifiable areal unit problem, or MAUP, is introduced. In brief the MAUP is comprised of two key issues,

- a variety of different results may be computed for the same data as it is increasingly aggregated (scale problem), and
- the data may also be aggregated in a variety of ways (aggregation problem).

The scale problem refers to the variation of results that can be obtained when the same areal data are combined into progressively larger units of analysis, and indicates a failure to discriminate the objects of geographical inquiry. The aggregation problem arises from the large number of ways in which these areal units can be combined, and reflects a failure to understand the processes at work between scales. The integrity of the analysis is dependent upon the knowledgeable integration of the data during analysis through an understanding of the geographical phenomenon taking place and the scale of the initial data collection.

The MAUP is deserving of further disccusion due to the effects of spatial aggregation and scale upon what information is represented by remotely sesend imagery at different scales. In the context of this thesis, spatial information is applied to generate objects, yet the compostition of the objects is a function of the image spatial resolution. The information

content that is available from the image processing of remotely sensed imagery is related to the spatial resolution of the data. This point can be best illustrated using the results of Cohen, *et al.* (1990) and Lévesque and King (1996).

Cohen *et al.* (1990) applied image semivariance to a set of image spatial resolutions including 1, 10, and 30m. The spatial variability of coniferous forest cover varied in relation to the image spatial resolution. At a spatial resolution of 1m the semivariogram ranges were best related to mean tree canopy size. At a spatial resolution of 10m the semivariance indicated only whether tree canopy sizes were less than 10m or between 10 and 20m. With a spatial resolution of 30m only the sills of the semivariograms related any forest structural information, even though the differences between the sills were small. In a multi-scale study undertaken by Lévesque and King (1996), a strong correlation of 0.80 is evident between individual tree crown closure and the semivariance range upon 0.25m resolution imagery, yet when the imagery is degraded to a spatial resolution of 0.50 there is a decrease in correlation between semivariance range and crown closure to –0.16. In contrast to the individual tree based predictions, St-Onge and Cavayas (1995) found that the relationship between actual and predicted values of stand based measures changed little with a change in image spatial resolution from 0.36 to 2.16m. The robust nature of the directional semivariance technique for characterizing forest stand structure indicated to the authors the possibility for creation of absolute spatial signatures, as the spatial structure is not hampered by radiometric factors. These results indicate the complex nature of forest structure and the current lack of a single commonly accepted approach.

In applying spatial dependence to generate objects, the effects of the MAUP must be considered. In this thesis, based upon 1m spatial resolution imagery, the spatial dependence characteristics of the imagery resulted in the generation of objects representing individual or

groups of trees. Using the same techniques upon Landsat TM data, the objects generated represent forest stands (Wulder and Boots, 1998b).

### 10.4.8. Context of Thesis Research in Field

The intention of this sub-section is to indicate where the research presented in this thesis fits in the larger context of high spatial resolution remote sensing of forest structure. No single study can be expected to answer all the outstanding issues in the high spatial resolution remote sensing of forest structure, but each study can act to make small but significant contributions. The body of work cited in the previous sections are all important in clarifying the complex interpretation of high spatial resolution imagery. The interpretation of high spatial resolution imagery to address issues in forestry has been likened to the programming of an artificial intelligence,

> Photointerpretation is an art as well as a science, so teaching a computer to recognize individual trees successfully is akin to teaching Deep Blue to play competitive chess – not impossible, but not easy either (McGraw, *et al.*, 1998).

The complexity of the digital interpretation of high spatial resolution imagery, while not impossible, requires flexibility. The ability to adapt to changing conditions, related to factors such as differing image spatial resolutions, cover types, densities, etc., requires an understanding of a variety of approaches. Often the image characteristics dictate the information content, requiring the analyst to either choose the image specification carefully beforehand or to be able to adapt to the resultant image spatial structure. The growing toolbox of image processing approaches appropriate for high spatial resolution imagery is indicative of a maturing application area. The work undertaken in this thesis allows for a new way of understanding the relationships found in high spatial resolution imagery. The ability to characterize a pixel location with attribute information relating the spatial dependence of that

pixel is useful information. In this thesis, the spatial dependence information was used to generate objects which were subsequently related to forest structural parameters. The limited field data hampers the interpretation of object relationships to the forest structural parameters, yet it is evident that spatial dependence, with little user intervention, is sensitive to forest structural information represented by image spatial structure.

## 10.5. Research Limitations and Recommendations

To address the objectives stated in the introduction of this thesis, a variety of tasks were undertaken. To investigate the forest structural issues of importance in this thesis, an understanding and implementation of a wide array of subject areas was necessary, such as computer programming, image processing, field spectroscopy, airborne multispectral scanning, spectral physics, global positioning systems, spatial statistics, geographic information systems, and forest mensuration. Forests are varied and complex ecosystems. The ability to measure and/or estimate characteristics related to forests faces a variety of limitations. The key limitations present in this research are presented in this sub-section accompanied with recommendations on how improvements may be made. The primary limitations of the research undertaken in this thesis are, number of plots, image spatial resolution, and other potential sources of error.

### 10.5.1. Number of Plots

The number of plots available for analysis in this study is a key limitation. The available six plots may be considered not sufficient for full statistical validation of the relationships found. Recommendations for future research efforts are an increased number of plots for ground validation. To enable a greater number of plots, field sampling techniques utilized may be improved upon. The mensuration of plots for inventory parameters is a time consuming process due to the intensity and rigour of the sampling. The measurement of LAI

for this study required the generation of new allometric relationships between leaf area and sapwood cross sectional area at breast height. In a subsequent study these new locally appropriate equations could be used without the need for the expensive and time consuming development. Also, optical approaches to the estimation of LAI have improved allowing for an alternate LAI sampling technique.

### 10.5.2. Image Spatial Resolution

The image spatial resolution available for the analysis undertaken in this study was 1 x 1m. As has been presented through the discussion, the information content that is available is a function of the relationship between image spatial resolution and the size and distribution of the tree crowns. The pixel based representation of tree crowns is also limited by the irregular shape of the tree crowns and the differing tree heights. In this study, the 1m spatial resolution pixels were found to be both spectrally mixed and pure. The cluster based approach undertaken in this study was intended to account for the spectral situation of both mixed and pure pixels. A clustering based approach is an attempt to extract the most information possible from the 1m spatial resolution data, found at the threshold between H- and L-resolution. The difficulty to delineate individual trees in this study location with 1m spatial resolution data indicates some possible limitations for 1m spatial resolution satellites. Further, forest structure generated from tree clusters is likely unable to account for the variability occurring within tree crowns. Higher spatial resolution imagery may allow for forest structure to be derived from the clustering found within an individual tree crown.

### 10.5.3. Potential Sources of Error

In a large and integrated project the sources of error are plentiful. The strategy employed in this thesis to avoid aggregation of error is to minimize the error at each stage of analysis. In the previous discussion section, the time and monetary expenses associated with the

collection of field validation data was discussed. A particularly expensive process is the generation of allometric equations between sapwood cross-sectional area and leaf area. For this study we developed new allometric equations for the most common species in the study area. For species which occurred less often we relied upon allometric equations found in the peer reviewed literature. While the estimates of LAI made from these equations are good, the intensity of the field data collection to derive sapwood cross-sectional areas limited the extent of the field data campaign. In some instances the bivariate regressions between the intensive and summary field data sample may have produced sub-optimal LAI results for a particular tree within a plot. The difficulty and expense associated with the application and development of allometric equations spawned the development of optical methods for the estimation of LAI (Section 3.3.1.2).

The matching of clusters to the field plots is also a problematic area (Section 7.4). The variability of tree heights and the complex dominance regimes result in overlap of foliage as well as shadowing of trees. Mixed pixels add to this problem through the obscuring of the edges between where a tree begins and ends. Further, the construction of a digital plot map accentuates the problems with relating the field and image data. Analog approaches permit analysis with more flexibility in the comparison of the field and image data. The spatial relationships between pixels processed with an algorithm that generates $G_i^*$ values for each pixel provides an indication of the distribution of vegetation in an area. A prediction of forest objects is made from the $G_i^*$ values and is tested for agreement with ground collected data representing the canopy. Problems are found in the matching of the continuous ground data to the discrete objects. The compiling of errors which occurs when converting continuous ground measurements to a discrete pixel based mask hampers the ability for comparison. The physical characteristics which govern the spectral reflectance of a stand result in a differing

vision of the stand than is expected from ground data. The remotely sensed mosaic of shadow and reflectance is difficult to compare to the ground data. High spatial resolution data may aid in improving the ability to match the field data precisely to the image data. A vector based approach to the development of a ground validation tree map may also reduce the errors introduced by gridding the tree data. An understanding of the clusters not as tree objects, but as radiometric objects may also improve the interpretation. Understanding of the clusters as radiometric objects, subject to view angle effects as a function of the forest structure and imaging geometry, may allow for interpretation of the clusters as relating the structure over plots and stands, and not necessarily of individual trees. View angle effects may have also contributed to introduction of error in the data. In designing the study an attempt was made to have the plots well centred in the flight line. Flight path navigation errors may have caused plots to be less than perfectly centred. For future satellite borne instruments, view angle effects should be kept to a minimum through the high orbit altitudes (≈500 km depending on the sensor) resulting in small angular differences.

The plots selected for measurement in this study had a limited range of values. The conditions present in the study forest region are indicative of the common forest types present yet not of a sufficient range conducive to extensive modeling. When selecting plots, the final conditions are estimated, but not exactly known until measurement is complete. As there is a short window of opportunity for measurement of the field validation sites, in concert with the airborne data acquisition, the resultant sample may not be exactly as desired. Long term analysis of sites within a single region would allow for an increased knowledge based from which to select plots. Plots which meet desired conditions may be re-measured on subsequent imaging campaigns, while plots found as undesirable may be dropped in favour of a more representative sample.

## 10.6. Potential Modifications to $G_i^*$

As stated earlier in this thesis, the application of local spatial statistics to remotely sensed data is a nascent approach. Accordingly, there are still many questions remaining to the utility of local spatial statistics in the processing of remotely sensed data. The implementation of $G_i^*$ in this thesis is not an exclusive form. Changes may be made to the manner in which $G_i^*$ is computed and implemented. Following is a variety of modifications that may be made to alter the information content offered through the computation of the local spatial statistic of $G_i^*$. Examples of potential modifications to the computation of $G_i^*$ are alterations such as, allowing for distances of greater than four, customization of the weights matrix, non-square windows, image sub-setting, and implementation in concert with semivariance. Further research would also be appropriate to compare $G_i^*$ to another measure of local spatial association, such as Moran's *I*. Investigation of $G_i^*$ with through a range of image spatial resolutions and on a variety of surface cover types is also of interest.

Allowing for distances larger than 4, which in the current context is a 9x9 window, would allow for discrimination of larger regions of association. Larger regions of association may indicate the presence of different spatial processes. Non-square windows may also allow for the integrity of the pixel of interest to be better maintained. Any assumptions that dictate an altered window shape will alter the spatial associations indicated and may create a bias. Further, customization of the weights matrix is also a possibility. Currently the weights matrix is binary, which allows a pixel either to be included in computation or not. The weights in the diagonals may be altered to better represent the physical ground distances that are being incorporated. The weights matrix may also be altered to either accentuate or diminish the effect of pixels at a particular location in reference to the central pixel of interest. As the computation of $G_i^*$ is based upon global measures of variability, an image pre-

segmentation may be undertaken to dictate regions of homogeneity to be considered as the population for the generation of the global statistics to enable a maximization of the values. The notion of an image pre-segmentation indicates the potential to compute $G_i^*$ in concert with semivariance. The approach of St-Onge and Cavayas (1995), utilizing directional semivariance, illustrates a structurally sensitive image segmentation procedure. Computation of $G_i^*$ within the segmented regions would allow for the range of standardized $G_i^*$ values to be related to similar structural characteristics. An additional exercise that would provide insights into the values generated by $G_i^*$ would be a comparison to a local measure of spatial dependence such as Moran's *I*. The link between local Moran's *I* values measured at the first lag and global Moran's *I* could through comparison to $G_i^*$ enable an investigation of local spatial statistics within different levels of non-stationarity.

# 11. CONCLUSIONS

***Chapter Objective:*** *Synthesize the results of the combination of spectral and spatial information extraction techniques on forests of complex multi-species structure and relate these findings back to the primary thesis objective*

Globally, forests are the most widely distributed ecosystem which, as a result, affect the lives of most humans daily, either as an economic good or an environmental regulator. Approximately 40% of Earth is forested, of which 10% is in Canada, accounting for 51% of the Canadian landscape. The diversity of the interests upon which the presence or absence of forests has an effect indicates the need for responsible stewardship of forests. The number of high spatial resolution optical remote sensing satellites that are soon to be launched will increase the availability of imagery for the monitoring of forest structure. This technological advancement is timely as current forest management practices have been altered to reflect the need for sustainable ecosystem level management. The findings presented in this thesis, based upon an analysis of 1m spatial resolution data, provide a variety of insights to the type of data that will be collected with the forthcoming high spatial resolution satellites.

In the initial thesis chapters we provide a summary of the methods by which remote sensing may be applied in forestry while also indicating the various limitations that are faced. The application of spatial statistics to high spatial resolution imagery is explored as a means of increasing the information which may be extracted from digital images. The Getis statistic is presented as a means to extract information which relates the strength of pixel inter-dependence and the magnitude of the values which are present. The Getis statistic also enabled the extraction of the spatial distribution of spectral values within image space. The spatial dependence information is then applied as a means to generate clusters representing groups of similar vegetation. The image structure at the high spatial resolution of 1m is

capturing a representation of the actual forest structure which enables the estimation of forest inventory and biophysical parameters.

The low accuracy level with which forest structural parameters have often been estimated in the past is partly due to low image spatial resolution, such as for the 30m Landsat. A large pixel is often composed of a number of surface features, resulting in a spectral value which is due to the reflectance characteristics of all surface features within that pixel. In the case of small pixels, a portion of a surface feature may be represented by a single pixel. When a single pixel represents a portion of a surface object, the potential to isolate distinct surface features exists. At the 1m spatial resolution analyzed in this thesis, the image objects of interest are of a variety of sizes. The variability in size of the image objects, in this case the trees, is important as few of the trees are large enough to enable digital reconstruction with a number of pixels. As a result, techniques suitable for either high or low spatial resolution data are not universally applicable. Spatial statistics, such as the Getis statistic, allow for an image processing means to isolate distinct surface features, such as the generation of distinct image objects into clusters, representing individual or groups of trees.

Tree clusters are a means to deal with the inevitable foliage overlap which occurs within complex mixed and deciduous forest stands. The generation of image objects, clusters, is necessary to deal with the presence of spectrally mixed pixels. The ability to estimate forest inventory and biophysical parameters from image clusters generated from spatially dependent image features is tested in this thesis. The inventory parameter of crown closure is successfully estimated from image clusters, yet the grouping of trees into clusters causes mixed results when estimating stem counts. The assignment of a cover class of each cluster is also undertaken. The knowledge of cluster cover class has enabled the estimation of leaf area index. Further, spatial information alone may be used to estimate LAI with knowledge of the regional maximum LAI. The ability to use image spatial information to assist in the selection of pixels appropriate for the extraction of spectral information improved the reliability of the empirical models through the input of consistently derived data.

Based upon the primary thesis objective to,

> *Investigate alternate methods for the estimation of forest inventory and biophysical parameters based upon spatial information extraction through digital image processing of high spatial resolution multispectral imagery*

the following material is presented to summarize the thesis contents, results, and accomplishments. An initial presentation of the importance of forests globally and in Canada illustrated the vast coverage and the importance of forests in the regulation of the atmosphere and climate to provide context for the thesis. Analysis of forest structure, either in the context of forest inventory or biophysical parameters, is a means for the characterization of forests to allow for monitoring.

Techniques for the measurement of forest structure may be undertaken at the field level or from remotely sensed imagery. Measurement techniques from remotely sensed data are often based upon either image spectral or spatial data. In this thesis we presented the use of spatial information, as measured with the Getis statistic, as a means to extract forest structural information. In consideration of the limitations present in this study, the Getis statistic results provided an illustration of the spatial distribution of spectral values in image space. The spatial dependence information generated from the image spectral values enabled the generation of vegetation clusters. The spatial dependence information generated with the Getis statistics appears complementary to spatial techniques which have been previously applied to remotely sensed imagery, such as semivariance. The spatial dependence clusters are a representation of the forest structure as a function of the spatial resolution of the imagery. The clusters generated from the spatial dependence clusters are also suitable for labeling with a forest cover-type. In general, the matching between the trees present in the image generated clusters and the field collected data was good. Based upon both the spatial and spectral data

available, at an image spatial resolution of 1m, information is present to enable the generation and classification of image based clusters.

In this thesis, in the context of the issues presented in the discussion chapter, we also estimated the forest inventory parameters of crown closure and stand density. The areal extent of the spatial dependence generated clusters allowed for estimates of crown closure to within ±10% of field based closure measures. The same level of success was not found in the estimation of stand density, due to the stratified multilevel forest present in the study area. Yet, the relationship between the field collected crown class data and the image generated cluster data indicate complementary information content. Knowledge of the stand crown class regime provided a variety of insights to the clusters that are generated from the field data. Based upon the complex stand structure, and due to the presence of deciduous and coniferous trees, individual stem counting at a 1m spatial resolution is problematic.

As a representation of forest biophysical structural in this thesis we estimated leaf area index (LAI). Through the application of two new methods we are able to estimate LAI to within ±1.4, for a range of field measured LAI from ≈3.28 to 6.88. The estimation of LAI is undertaken from a combination of spectral and spatial data, as follows:

1. extraction of spectral information, in the form of the vegetation index NDVI, from within spectrally classified $G_i^*$ clusters as an input to a species specific LAI estimation equation.
2. combination of crown closure information relating the areal extent of local vegetation extent with maximum regional LAI. This is the most parsimonious technique, which also shows potential for estimation of LAI with high spatial resolution satellite sensors.

This research focused upon which forest inventory and biophysical parameters may be extracted from 1m spatial resolution imagery of deciduous and mixed forests. The complexity

of the digital image data collected with remote sensing instruments, as a result of the landscape cover and spatial resolution, requires the availability of a number of methods to approach a problem. Analysis of the potential of $G_i^*$ spatial dependence information has served to identify an additional method for the estimation of forest inventory and biophysical parameters based upon spatial information extraction through digital image processing of high spatial resolution multispectral imagery. The results presented in this thesis indicate a valuable information source available from the analysis of the spatial information inherent to remotely sensed data. Spatial and spectral characteristics extracted from digital remotely sensed imagery are a rich and complementary information source, resulting in many opportunities for both pure research and applications development.

# 12. FUTURE RESEARCH

***Chapter Objective:*** *proposition of a future research agenda based upon the results generated and discussed in this thesis.*

The future composition of forests that may result due to the effects of climate variability can currently only be hypothesized upon. The ability to monitor changes in forest structure will provide the ability to assess forests from a measurement baseline and monitor changes against this baseline. The techniques made possible through the collection of remotely sensed data and image processing improve the ability to evaluate changes in forest structure. The incorporation of techniques and methods from forest science and inventory with H-resolution imagery is providing for unique approaches to unsolved problems. The spatial distribution of Canadian forests in terms of species and related structure is complex at the local scale. Improvements at the local scale translate to an increased accuracy of data scaled to represent a region. Due to the economic and scientific importance of Canadian forests, any effort to improve upon the ability to characterize forests is worthwhile.

Based upon continuation of the primary thesis objective, to develop improved methods for assessing forest inventory and biophysical parameters with remotely sensed data, the following research potential is evident:

- further investigation, with improved field data, will attempt to address the ability to partition forest layers of overstory and understory with a spatial dependence clustering technique
- data collection above a forest which has had the understory removed to enable calibration of understory contribution to forest spectral response
- crown delineation of deciduous and mixed stands on H-resolution imagery utilizing spatial information

- using fine resolution, aerial images as training for analyzing satellite imagery to estimate LAI
- estimates of mean crown size may be used as an input to the inversion of geometrical optical models (Woodcock, *et al.*, 1997)
- spatial autocorrelation as ancillary data in both H- and L-resolution image classification
- use of spatial dependence information to create fuzzy boundaries around L-resolution image objects
- scale dependency of spatial autocorrelation assessed on multi-scale imagery of conifer, deciduous and mixed forests, with *casi*, SPOT, Landsat TM, and AVHRR.
- assessing the impact of spatial resolution on LAI estimation using remote sensing data
- the relationship between spatial resolution and forest structure properties affecting LAI estimation
- application of landscape ecology techniques to high spatial resolution image objects
- invert the approach of this study, which clustered high pixel values, and generate clusters to estimate the extent and spectral characteristics of stand shadow fractions.

The utility of image based spatial information is not limited to high spatial resolution imagery. The discretization of a continuous surface into a grid of regularly sized and shaped pixels will result in spatial dependence between neighbouring pixels regardless of the scale. As a result, spatial information such as the Getis statistic, may prove to be valuable as an information source at a variety of scales in a remote sensing context.

# REFERENCES


Aldred, A., and I. Alemdag, 1988; *Guidelines for forest biomass inventory*, (Petawawa National Forestry Institute, Canadian Forest Service, Information Report PI-X-77, 134p.)

Aplin, P., P. Atkinson, and P. Curran, 1997; Fine spatial resolution satellite sensors for the next decade, *International Journal of Remote Sensing*, Vol. 18, No. 18, pp. 3873-3881.

Apps, M., J. Cihlar, B. Goodison, F. Hall, B. Harriss, D. Leckie, E. LeDrew, P. Matson, S. Running, and P. Sellars, 1995; BOREAS: Global change and biosphere-atmosphere interactions in the boreal forest, In LeDrew, E. F., M. Strome and F. Hegyi (eds.), *The Canadian Remote Sensing Contribution to Understanding Global Change*, Department of Geography Publication Series, No. 38, University of Waterloo, pp. 237-258.

Analytical Spectral Devices, Inc., 1993; *Personal Spectroradiometer: Procedures Reference*, (ASD, Inc., 4760 Walnut St., Suite 105, Boulder, CO, USA).

Anger, C., S. Achal, T. Ivanco, S. Mah, R. Price, and J. Busler, 1996; Extended operational capabilities of the *casi*, *In Proceedings of the Second International Airborne Remote Sensing Conference and Exhibition*, San Francisco, United States, 24-27 June, Vol. I, pp. 124-133.

Anselin, L., 1995; Local indicators of spatial association - LISA, *Geographical Analysis*, Vol. 27, No. 2, pp. 93-115.

Asrar, G., M. Fuchs, E. Kanemasu, and J. Hatfield, 1984; Estimating absorbed photosynthetic radiation and leaf area index from spectral reflectance in wheat, *Agronomy Journal*, Vol. 76, pp. 300-306.

Atkinson, P., and P. Curran, 1997; Choosing an appropriate spatial resolution for remote sensing investigations, *Photogrammetric Engineering & Remote Sensing*, Vol. 63, No. 12, pp. 1345-1351.

Avery, T., and G. Berlin, 1992; *Fundamentals of Remote Sensing and Airphoto Interpretation*, (5th Edition, Maxwell Macmillan, Toronto, 472p).

Avery, T., and H. Burkhart, 1994; *Forest Measurements*, (McGraw-Hill, Toronto, 408p.)

Bailey, T., and A. Gatrell, 1995; *Interactive Spatial Data Analysis*, (Addison Wesley Longman Ltd., Essex, UK, 413p.)

Baulies, X., and X. Pons, 1995; Approach to forest inventory and mapping by means of multi-spectral airborne data, *International Journal of Remote Sensing*, Vol. 16, No. 1, pp. 61-80.

Barbezat, V., and J. Jacot, 1998; The CLAPA project: Automated classification of forest with aerial photographs, *Proceedings of the International Forum on Automated Interpretation of High Spatial Resolution Digital Imagery for Forestry*, Natural Resources Canada, Forestry Canada, Pacific Forestry Centre, Victoria, BC, Feb. 10-12, *In press.*

Baret, F., and G. Guyot, 1991; Potentials and limits of vegetation indices for LAI and APAR assessment, *Remote Sensing of Environment*, Vol. 35, pp. 161-173.

Baret, F., G. Guyot, A. Begue, P. Maurel, and A. Podaire, 1988; Complementarity of middle-infrared with visible and near-infrared reflectance for monitoring wheat canopies, *Remote Sensing of Environment*, Vol. 26, pp. 213-225.

Beaubien, J., 1994; Landsat TM satellite images of forests: From enhancement to classification, *Canadian Journal of Remote Sensing*, Vol. 20, No. 1, pp. 17-26.

Blackburn, G., and E. Milton, 1995; Ecology through spectrometry: the detection and classification of canopy gaps in deciduous woodlands, From: *TERRA 2 - Understanding the Terrestrial Environment, Remote Sensing Data Systems and Networks*, Chapter 15, Ed. P. Mather, John Wiley and Sons, pp. 175-187.

Blackburn, G., and E. Milton, 1995; Seasonal variations in the spectral reflectance of deciduous tree canopies, *International Journal of Remote Sensing*, Vol. 16, No. 4, pp. 709-720.

Bonham, C., 1989; Measurements for terrestrial vegetation, (John Wiley & Sons, New York, 338p.)

Bowers, W., S. Franklin, J. Hudak, and G. McDermid, 1994; Forest structural damage analysis using image semivariance, *Canadian Journal of Remote Sensing*, Vol. 20, No. 1, p. 28-36.

Brand, D., 1990; Advances in Canadian forest research: an introduction, *Canadian Journal of Forest Research*, Vol. 20, pp. 373-374.

Brandtberg, T., 1997; Towards structure-based classification of tree crowns in high spatial resolution aerial images, Scandinavian Journal of Forest Research, Vol. 12, pp. 89-96.

Brown, D., and T. Bara, 1994; Recognition and reduction of systematic error in elevation and derivative surfaces from 71/2-minute DEMs, *Photogrammetric Engineering & Remote Sensing*, Vol. 60. No. 2, p. 189-194.

Bruniquel-Pinel, V., and J. Gastellu-Etchegorry, 1998; Sensitivity of texture of high resolution images of forest to biophysical and acquisition parameters, *Remote Sensing of Environment*, Vol. 65, pp. 61-85.

Bryant, E., A. Dodge, and S. Warren, 1980; Landsat for practical forest type mapping: A test case, *Photogrammetric Engineering & Remote Sensing*, Vol. 46, No. 12, pp. 1575-1584.

Burnett, C., M. Wulder, N. Daley, O. Niemann, and D. Goodenough, 1998; Comparison of generalized and scale-sensitive windows for the estimation of tree crown position using local maximum filters, *Presented at the International Workshop on Scaling and Modeling In Forestry: Applications in Remote Sensing and GIS*, Université de Montréal, Québec, Canada, March 19-21, 6p.

Canadian Council of Forest Ministers (CCFM), 1995; *Defining sustainable forest management: A Canadian approach to criteria and indicators*, (Ottawa, Natural Resources Canada, 22p.)

Campbell, J., 1981; Spatial correlation effects upon accuracy of supervised classification of land cover, *Photogrammetric Engineering & Remote Sensing*, Vol. 47, No. 3, pp. 355-363.

Carr, J., and D. Myers, 1984; Application of the theory of regionalized variables to the spatial analysis of Landsat data, *Proceedings of the Pecora 9 Spatial Information Technologies for Remote Sensing Today and Tomorrow, IEEE Computer Society Press*, pp. 55-61.

Chan, S., R. McCreight, J. Walstad, and T. Spies, 1986; Evaluating forest vegetative cover with computerized analysis of fisheye photographs, Forest Science, Vol. 32, No. 4, pp. 1085-1091.

Chavez, P., 1992; Comparison of spatial variability in visible and near-infrared spectral images, *Photogrammetric Engineering & Remote Sensing*, Vol. 58, Mo. 12, pp. 957-964.

Chen, J., 1996; Evaluation of vegetation indices and a modified simple ratio for boreal applications, *Canadian Journal of Remote Sensing*, Vol. 22, No. 2, pp. 229-242.

Chen, J., and T. Black, 1992; Foliage area and architecture of plant canopies from sunfleck size distribution, *Agricultural and Forest Meteorology*, Vol. 60, pp. 249-266.

Chen, J., and J. Cihlar, 1995; Quantifying the effect of canopy architecture on optical measurements of leaf area index using two gap size analysis methods, *IEEE Transactions on Geoscience and Remote Sensing*, Vol. 33, No. 3, pp. 777-787.

Chen, J., and M. Guilbeault, 1996; Examination of vegetation indices for retrieving biophysical parameters of boreal conifer forests, *Proceedings of the 26th International Symposium on Remote Sensing of the Environment and 18th Annual Symposium of the Canadian Remote Sensing Society*, Vancouver, pp. 168-171.

Chen, J., and J. Cihlar, 1996; Retrieving leaf area index of boreal conifer forests using Landsat TM images, *Remote Sensing of Environment*, Vol. 55, pp. 153-162.

Chen, J., T. Black, and R. Adams, 1991; Evaluation of hemispherical photography for determining plant area index and geometry of a forest stand, *Agricultural and Forest Meteorology*, Vol. 56, pp. 129-143.

Civco, D., Topographic normalization of Landsat Thematic Mapper digital imagery, *Photogrammetric Engineering & Remote Sensing*, Vol. 55, No. 9, pp. 1303-1309.

Cohen, W., T. Spies, and G. Bradshaw, 1990; Semivariograms of digital imagery for analysis of conifer canopy structure, *Remote Sensing of Environment*, Vol. 35, pp. 167-178.

Cole, W., 1995; Hardwood tree crown measurement guide, (Sault Ste. Marie, ON, Ontario Forest Research Institute, Ontario Ministry of Natural Resources, 18p.)

Congalton, R., 1988; Using spatial autocorrelation analysis to explore the errors in maps generated from remotely sensed data, *Photogrammetric Engineering & Remote Sensing*, Vol. 54, No. 5, pp. 587-592.

Congalton, R., 1991; A review of assessing the accuracy of classifications of remotely sensed data, *Remote Sensing of Environment*, Vol. 46, pp. 35-46.

Cosandier, D., T. Ivanco, and S. Mah, 1992; The geocorrection and integration of the global positioning system with the compact airborne spectrographic imager, *Presented at the Canadian Symposium on Remote Sensing*, June 1992, pp. 385-390.

Culvenor, D., N. Coops, R. Preston, and K. Tolhurst, 1998; A spatial clustering approach to automated tree crown delineation, *Proceedings of the International Forum on Automated Interpretation of High Spatial Resolution Digital Imagery for Forestry*, Natural Resources Canada, Forestry Canada, Pacific Forestry Centre, Victoria, BC, Feb. 10-12, *In press.*

Curran, P., 1980; Multispectral remote sensing of vegetation amount, *Progress in Physical Geography*, Vol. 4, pp. 315 to 341.

Curran, P., 1988; The semivariogram in remote sensing: an introduction, *Remote Sensing of Environment*, Vol. 24, pp. 493-507.

Curran, P., J. Dungan, and H. Gholz, 1992; Seasonal LAI in slash pine estimated with Landsat TM, *Remote Sensing of Environment*, Vol. 39, pp. 3-13.

Curran, P., and P. Atkinson, 1998; Geostatistics and remote sensing, *Progress in Physical Geography*, Vol. 22, No. 1, pp. 61-78.

Craig, R., 1979; Autocorrelation in Landsat data, *Presented at the Thirteenth International Symposium on Remote Sensing of Environment*, pp. 1517-1524.

Craig, R., 1981; Precision in the evaluation of Landsat autocorrelation: The terrain effect, *Presented at the Fifteenth International Symposium on Remote Sensing of Environment*, Ann Arbor, MI, May 1981, pp. 1305-1314.

Craig, R., 1984; The spatial structure of terrain: a process signal in satellite digital images, *Proceedings of the 9th Annual Pecora Symposium*, Sioux Falls, S.D., pp. 51-54.

Craig, R., and M. Labovitz, 1980; Sources of variation in Landsat autocorrelation, *Presented at the Fourteenth International Symposium on Remote Sensing of Environment*, pp. 1755-1767.

Cushnie, J., 1987; The interactive effect of spatial resolution and degree of internal variability within land-cover types on classification accuracies, *International Journal of Remote Sensing*, Vol. 8, No. 1, pp. 15-29.

Danson, F., 1987; Preliminary evaluation of the relationship between SPOT-1 HRV data and forest stand parameters, *International Journal of Remote Sensing*, Vol. 8, No. 10, 1571-1575.

Davis, J., 1986; *Statistics and data analysis in geology*, (John Wiley & Sons, New York, 646p.)

Davis, M., and D. Botkin, 1985; Sensitivity of cool temperate forests and their fossil pollen to rapid climate change, *Journal of Quaternary Research*, Vol. 22, pp. 327-340.

Davis, F., and D. Simonett, 1991; *GIS and remote sensing, Volume 1, Principles In Geographical Information Systems*, Edited by Maguire, D., M. Goodchild, and D. Rhind, (Longman Scientific and Technical, New York, pp. 191-213).

Daley, N., C. Burnett, M. Wulder, K. Niemann, and D. Goodenough, 1998; Comparison of fixed-size and variable-sized windows for the estimation of tree crown position, *IGARSS'98*, Seattle, WA, USA, July 6-10, 1323-1325.

De Wulf, R., R. Goossens, B. De Roover, and F. Borry, 1990; Extraction of forest stand parameters from panchromatic and multispectral SPOT-1 data, *International Journal of Remote Sensing*, Vol. 11, No. 9, pp. 1571-1588.

Dean, T., and J. Long, 1986; Variations in sapwood area-leaf area relations within two stands of Lodgepole Pine, *Forest Science*, Vol. 32, No. 3, 749-758.

Dean, T., J. Long, and F. W. Smith, 1988; Bias in leaf area - sapwood area ratios and its impact on growth analysis in *Pinus contorta*, *Trees*, Vol. 2, pp. 104-109.

Derksen, C., M. Wulder, E. LeDrew, and B. Goodison, 1998a; Application of the Getis statistic to hemispheric and regional scale passive microwave derived snow water equivalent imagery, Presented at *IGARSS '98*, Seattle, WA, July 6-10, 3p.

Derksen, C., M. Wulder, E. LeDrew, and B. Goodison, 1998b; The association between spatially autocorrelated patterns of SSM/I derived Prairie snow cover and atmospheric circulation, Presented at the *55th Eastern Snow Conference*, 15p.

Dralle, K., and M. Rudemo, 1997; Stem number estimation by kernel smoothing of aerial photos, *Canadian Journal of Forest Research*, Vol. 26, pp. 1228-1236.

Dymond, J., 1992; Nonparametric modeling of radiance in hill country for digital classification of aerial photographs, *Remote Sensing of Environment*, Vol. 39, pp. 95-102.

Ehlers, M., G. Edwards, and Y. Bédard, 1989; Integration of remote sensing with geographic information systems: A necessary evolution, *Photogrammetric Engineering & Remote Sensing*, Vol. 55, No. 11, pp. 1619-1627.

Falinski, J., 1989; Differentiation and integration of community structure in the course of forest secondary succession and regeneration, Edited by E. Sjögren, *Forests of the world, diversity and dynamics, Studies in plant ecology*, Vol. 18, Uppsala, 295p.

Fassnacht, K., and S. T. Gower, 1997; Interrelationships among the edaphic and stand characteristics, leaf area index, and aboveground net primary production of upland forest ecosystems in north central Wisconsin, *Canadian Journal of Forest Research*, Vol. 27, pp. 1058-1067.

Fassnacht, K., S. Gower, J. Norman, and R. McMurtrie, 1994; A comparison of optical and direct methods for estimating foliage surface area index in forests, *Agricultural and Forest Meteorology*, Vol. 71, pp. 183-207.

Fassnacht, K., S. Gower, M. MacKenzie, E. Nordheim, and T. Lillesand, 1997; Estimating the leaf area index of north central Wisconsin forests using the Landsat thematic mapper, Remote Sensing of Environment, Vol. 61, pp. 229-245.

Fisher, P., 1997; The pixel: A snare and a delusion, *International Journal of Remote Sensing*, Vol. 18, No. 3, pp. 679-685.

Fournier, R., G. Edwards, N. Eldridge, 1995; A catalogue of potential spatial discriminators for high resolution digital images of individual tree crowns, *Canadian Journal of Remote Sensing*, Vol. 21, No. 3, pp. 285-298.

Frank, T., 1984; The effect of change in vegetation cover and erosion patterns on albedo and texture of Landsat images in a semiarid environment, *Annals of the Association of American Geographers*, Vol. 74, No. 3, pp. 393-407.

Franklin, J., 1986; Thematic mapper analysis of coniferous forest structure and composition, *International Journal of Remote Sensing*, Vol. 7, No. 10, pp. 1287-1301.

Franklin, J., 1995; Predictive vegetation mapping: geographic modeling of biospatial patterns in relation to environmental gradients, *Progress in Physical Geography*, Vol. 19, No. 4, pp. 474-499.

Franklin, J., and J. Stephenson, 1996; Integrating GIS and remote sensing to produce regional vegetation databases: attributes related to environmental modeling, from the *Proceedings of the Third International Conference/Workshop on Integrating Geographic Information Systeme and Environmental Modeling*, January 21-25, 15p.

Franklin, J., T. Logan, C. Woodcock, and A. Strahler, 1986; Coniferous forest classification and inventory using Landsat and digital terrain data, *IEEE Transactions on Geoscience and Remote Sensing*, Vol. GE-24, No. 1, pp. 139-149.

Franklin, S., 1994; Discrimination of subalpine forest species and canopy density using digital *casi*, SPOT PLA, and Landsat TM data, *Photogrammetric Engineering & Remote Sensing*, Vol., 60. No. 10, pp. 1233-1241.

Franklin, S., and D. Peddle, 1990; Classification of SPOT HRV imagery and texture features, *International Journal of Remote Sensing*, Vol. 11, No. 3, pp. 551-556.

Franklin, S., and G. McDermid, 1993; Empirical relations between digital SPOT HRV and *casi* spectral response and lodgepole pine (*Pinus contorta*) forest stand parameters, *International Journal of Remote Sensing*, Vol. 14, No. 12, pp. 2331-2348.

Franklin, S., and P. Giles, 1995; Radiometric processing of aerial and satellite remote-sensing imagery, *Computers and Geosciences*, Vol. 21, no. 3, pp. 413-423.

Franklin, S., M. Lavigne, B. Wilson, and E. Hunt Jr., 1994; Empirical relations between Balsam Fir (*Abies balsamea*) forest stand conditions and ERS-1 SAR data in western Newfoundland, *Canadian Journal of Remote Sensing*, Vol. 20, No. 2, pp. 124-130.

Franklin, S., C. Blodgett, S. Mah, C. Wrightson, 1991; Sensitivity of *casi* data to anisotropic reflectance, terrain aspect, and deciduous forest species, *Canadian Journal of Remote Sensing*, Vol. 17, No. 4, pp. 314-321.

Franklin, S., M. Wulder, and M. Lavigne, 1996; Automated derivation of geographic windows for use in remote sensing digital image texture analysis, *Computers and Geosciences*, Vol. 22, No. 6, pp. 665-673.

Franklin, S., M. Lavigne, M. Deuling, M. Wulder, and E. Hunt, 1997a; Estimation of forest leaf area index using remote sensing and GIS data for modeling net primary production, *International Journal of Remote Sensing*, Vol. 18, No. 16, pp. 3459-3471.

Franklin, S., M . Lavigne, M. Deuling, M. Wulder, and R. Hunt, 1997b; Landsat derived forest covertypes for modeling net primary productions, *Canadian Journal of Remote Sensing*, Vol. 23, No. 3, pp. 243-251.

Franklin, S., M. Wulder, and M. Lavigne, 1996; Automated derivation of geographic windows for use in remote sensing digital image analysis, *Computers and Geosciences*, Vol. 22, No. 6, pp. 665-673.

Freemantle, J. R., R. Pu, J. R. Miller , 1992; Calibration of Imaging spectrometer Data to Reflectance Using Pseudo-Invariant Features, *Proceedings of the 15th Canadian Symposium on Remote Sensing*, Toronto, Ontario, June 1-4th, pp. 452-455.

Fritz, L., 1996; The era of commercial Earth observation satellites, *Photogrammetric Engineering & Remote Sensing*, Vol. 62, No. 1, pp. 39-45.

Gates, D., 1990; Climate change and the response of forests, *International Journal of Remote Sensing*, Vol. 11, No. 7, pp. 1095-1107.

Gausman, H., 1977; Reflectance of leaf components, *Remote Sensing of Environment,* Vol. 6, pp. 1-9.

Gemmel, F., 1995, Effects of forest cover, terrain, and scale on timber volume estimation with thematic mapper data in a rocky mountain site, *Remote Sensing of Environment*, Vol. 51, pp. 291-305.

Getis, A., 1994; Spatial dependence and heterogeneity and proximal databases, Chapter 2, In *Spatial Analysis and GIS*, Ed. S. Fotheringham and P. Rogerson, (Taylor & Francis, London, 281p.)

Getis, A., and J. Franklin, 1987; Second-order neighbourhood analysis of mapped point patterns, *Ecology*, Vol. 68. pp. 473-477.

Getis, A., and J. Ord, 1992; The analysis of spatial association by distance statistics, *Geographical Analysis*, Vol. 24, No. 3, pp. 189-206.

Gibbons, G., 1992; The global positioning system as a complementary tool for remote sensing and other applications, *Photogrammetric Engineering & Remote Sensing*, Vol. 58. No. 8, pp. 1255-1257.

Gillis, M. and D. Leckie, 1993; *Forest inventory mapping procedures across Canada*, (Natural Resources Canada, Petawawa National Forestry Institute - Information Report PI-X-122, 192p.)

Gillis, M., and D. Leckie, 1996; Forest inventory update in Canada, *The Forestry Chronicle*, Vol. 72, No. 2, pp. 138-156.

Gholz, H., 1982; Environmental limits on above ground net primary production, leaf area, and biomass in vegetation zones of the Pacific Northwest, *Ecology*, Vol. 54, pp. 152-159.

Goodchild, M., 1986; Spatial autocorrelation, *Concepts and Techniques in Modern Geography*, Vol. 47, Geo Books, Norwich.

Gong, P., Ruiliang Pu, John R. Miller, 1992; Correlating Leaf Area Index of Ponderosa Pine with Hyperspectral *casi* Data, *Canadian Journal of Remote Sensing*, Vol. 18, No. 4, October 1992, pp. 275-282.

Gong, P., J. Miller, and M. Spanner, 1994; Forest canopy closure from classification and spectral unmixing of scene components- multisensor evaluation of an open canopy, *IEEE Transactions on Geoscience and Remote Sensing*, Vol. 32, No. 5, pp. 1067-1079.

Gougeon, F., 1993; Individual tree identification from high resolution MEIS images, Pages 117-128 *in* Leckie, D.; Gillis, M.D., eds. *Proceedings of the International Forum on Airborne Multispectral Scanning for Forestry and Mapping (with Emphasis on MEIS).* 13-16 April 1992, Val Morin, Quebec. Forestry Canada Information Report PI-X-113.

Gougeon, F., 1995a; A crown-following approach to the automatic delineation of individual tree crowns in high spatial resolution aerial images, *Canadian Journal of Remote Sensing*, Vol. 21, No. 3, pp. 274-284.

Gougeon, F., 1995b; Comparison of possible multispectral classification schemes for tree crowns individually delineated on high spatial resolution MEIS images, *Canadian Journal of Remote Sensing*, Vol. 21, No. 1, pp. 1-9.

Gougeon, F., and A. Wong, 1986; Spectral and textural segmentation of multispectral aerial images, *Proceedings, 10th Canadian Symposium on Remote Sensing, May 5-8, 1986, Edmonton, AB*, pp. 291-300.

Gougeon, F., 1998; Automatic individual tree crown delineation using a valley-following algorithm and rule-based system, *Proceedings of the International Forum on Automated Interpretation of High Spatial Resolution Digital Imagery for Forestry*, Natural Resources Canada, Forestry Canada, Pacific Forestry Centre, Victoria, BC, Feb. 10-12, *In press.*

Gower, S., and J. Norman, 1991; Rapid estimation of leaf area index in conifer and broad-leaf plantations using the Li-Cor LAI-2000, *Ecology*, Vol. 72, pp. 1896-1900.

Gray, S., 1995; *A descriptive forest inventory of Canada's forest regions*, (Natural Resources Canada, Petawawa National Forestry Institute - Information Report PI-X-122, 192p.)

Grier, C., and R. Waring, 1974; Conifer foliage mass related to sapwood area, *Forest Science*, Vol., 20, No., 3, pp. 205-206.

Griffith, P., A. Getis, and E. Griffin, 1996; Regional patterns of affirmative action compliance costs, *The Annals of Regional Science*, Vol. 30, pp. 321-340.

Guyot, G., D. Guyon, and J. Riom, 1989; Factors affecting the spectral response of forest canopies: a review, *Geocarto International*, Vol. 3, pp. 3-18.

Hall, F., Y. Shimabukuro, and K. Huemmrich, 1995; Remote sensing of forest biophysical structure using mixture decomposition and geometric reflectance models, *Ecological Applications*, Vol. 5, No. 4., pp. 993-1013.

Haralick, R., K. Shanmugam, and I. Dinstein, 1973; Textural features for image processing, *IEEE Transactions on Systems, Man, and Cybernetics*, Vol. SMC-3, No. 6, pp. 610-621.

Hay, G., and K. Niemann, 1994; Visualizing 3-D texture: a three-dimensional approach to model forest texture, *Canadian Journal of Remote Sensing*, Vol. 20, No. 2, pp. 89-101.

Hay, G., K. Niemann, and G. McLean, 1996; An object-specific image texture analysis of H-resolution forest imagery, *Remote Sensing of Environment*, Vol. 55, pp. 108-122.

Held, A., and S. Billings, 1998; Automatic tree crown recognition and counting from high resolution casi data, CD-ROM Proceedings of the 9th Australasian Remote Sensing and Photogrammetry Conference, July 20-24, Sydney, Australia.

Hoekman, D., 1985; Radar backscatter of forest stands, *International Journal of Remote Sensing*, Vol. 6, No. 2, pp. 325-343.

Hoffman-Wellenhof, B., H. Lichtenegger, and J. Collins, 1992; *Global Positioning Systems: Theory and Practice*, (Springer-Verlag, New York, 326p.)

Horler, D., and F. Ahern, 1986; Forestry information content of Thematic Mapper data, *International Journal of Remote Sensing*, Vol. 7, No. 3, pp. 405-428.

Huete, A., 1988; A soil-adjusted vegetation index, *Remote Sensing of Environment*, Vol. 25, pp. 295-309.

Hungerford, R., 1987; Estimation of foliage area in dense Montana lodgepole pine stands, *Canadian Journal of Forest Research*, Vol. 17.

Hyppanen, H., 1997; Spatial autocorrelation and optimal spatial resolution of optical remote sensing data in the boreal forest environment, *International Journal of Remote Sensing*, Vol. 17, No. 17, pp. 3441-3452.

Irons, J., B. Markham, R. Nelson, D. Toll, D. Williams, R. Latty, and M. Stauffer, 1985; The effects of spatial resolution of the classification of Thematic Mapper data, *International Journal of Remote Sensing*, Vol. 6, No. 8, pp. 1385-1403.

Jarvis, P., and R. Dewar, 1993; Forest in the global carbon balance: From stand to region, (chapter 12) from, *Scaling Physiological Processes: Leaf to Globe*, Edited by, J. Ehleringer and C. Field, (Academic Press, Inc., Toronto, pp. 191-221.)

Jensen, J., 1986; *Introductory Digital Processing: A Remote Sensing Perspective*, (Prentice-Hall; Englewood Cliffs, NJ, 379p).

Johnson, D., and P. Howarth, 1987; The effects of spatial resolution on land cover/land use theme extraction from airborne digital data, Canadian Journal of Remote Sensing, Vol. 13, No. 2, pp. 68-74.

Jupp, D., A. Strahler, and C. Woodcock, 1988; Autocorrelation and regularization in digital images: I. Basic theory, *IEEE Transactions on Geoscience and Remote Sensing*, Vol. 26, No. 4, pp. 463-473.

Jupp, D., A. Strahler, and C. Woodcock, 1989; Autocorrelation and regularization in digital images: II. Simple image models, *IEEE Transactions on Geoscience and Remote Sensing*, Vol. 27, No. 3, pp. 463-473.

Kasischke, E., L. Bourgeau-Chavez, N. Christensen, Jr., E. Haney, 1994; Observations on the sensitivity of ERS-1 SAR image intensity to changes in aboveground biomass in young loblolly pine forests, *International Journal of Remote Sensing*, Vol. 15, No. 1, pp. 3-16.

Kaufmann, M., and C. Troendle, 1981; The relationship of leaf area and foliage biomass to sapwood conducting area in four subalpine forest tree species, *Forest Science*, Vol. 27, No. 3, pp. 477-482.

Keeling, C., R. Bacastow, A. Carter, *et al.*, 1989; A three dimensional model of atmospheric $CO_2$ transport based on observed winds: 1. Analysis of observed data. In Peterson, D. H. (ed.), *Aspects of Climate Variability in the Pacific and the Western Americas*, Geophysical monograph 55, American Geophysical Union, Washington, D.C., pp. 167-182.

King, D., 1995; Airborne multispectral digital camera and video sensors: A critical review of system designs and applications, *Canadian Journal of Remote Sensing*, Vol. 21, No. 3, pp. 245-273.

Kozlowski, T., P. Kramer, and S. Pallardy, 1991; *The physiological ecology of woody plants*, (Academic Press Inc., Toronto, 657p.)

Kushwaha, S., S. Kuntz, and G. Oesten, 1994; Applications of image texture in forest classification, International Journal of Remote Sensing, Vol. 15, No. 11, pp. 2273-2284.

Kuuluvainen, T. and T. Pukkala, 1989; Simulation of within-tree and between-tree shading of direct radiation in a forest canopy: effect of crown shape and sun elevation, *Ecological Modeling*, Vol. 49, pp. 89-100.

Labovitz, M., and E. Masuoka, 1984; The influence of autocorrelation in signature extraction - an example from a geobotanical investigation of Cotter Basin, Montana, *International Journal of Remote Sensing*, Vol. 5, No. 2, pp. 315-332.

Lacaze, B., S. Rambal, and T. Winkel, 1994; Identifying spatial patterns of Mediterranean landscapes from geostatistical analysis of remotely-sensed data, *International Journal of Remote Sensing*, Vol. 15, No. 12, pp. 2437-2450.

Landry, R., R. Fournier, F. Ahern, and R. Lang, 1997; Tree vectorization: A methodology to characterize fine tree architecture in support of remote sensing models, *Canadian Journal of Remote Sensing*, Vol. 23, No. 2, pp. 91-107.

Landsburg, J., and S. T. Gower, 1997; *Applications of physiological ecology to forest management*, (Academic Press, New York, 354p.)

Lark, R., 1996; Geostatistical description of texture on an aerial photograph for discriminating classes of land cover, *International Journal of Remote Sensing*, Vol. 17, No. 11, pp. 2115-2133.

Larson, M., 1998; Finding an optimal match window for spruce top detection based on an optical tree model, *Proceedings of the International Forum on Automated Interpretation of High Spatial Resolution Digital Imagery for Forestry*, Natural Resources Canada, Forestry Canada, Pacific Forestry Centre, Victoria, BC, Feb. 10-12, *In press.*

Lavigne, M., J. Luther, S. Franklin, and E. Hunt, 1996; Comparing branch biomass prediction equations for *Abies balsamea*, *Canadian Journal of Forest Research*, Vol. 26, pp. 611-616.

Law, B., and R. Waring, 1994; Remote sensing of leaf area index and radiation intercepted by understory vegetation, *Ecological Applications*, Vol. 4, pp. 272-279.

Leckie, D., 1990; Advances in remote sensing technologies for forest survey and management, *Canadian Journal of Forest Research*, Vol. 20, pp. 464-483.

Leckie, D., and A. Dombrowski, 1984; Enhancement of high resolution MEIS II data for softwood species discrimination, *In proceedings, 9th Canadian Symposium on Remote Sensing*, St. John's, Newfoundland, pp. 617-626.

Leckie, D., and M. Gillis, 1995; Forest inventory in Canada with an emphasis on map production, *The Forestry Chronicle*, Vol. 71, No. 1, pp. 74-88.

Leckie, D., J. Beaubien, J. Gibson, N. O'Niell, T. Piekutowski, and S. Joyce, 1995; Data processing and analysis for MIFUCAM: A trial for MEIS imagery for forest inventory mapping, *Canadian Journal of Remote Sensing*, Vol. 21, No. 3, pp. 337-356.

Leckie, D., and D. Hill (editors), 1998; *International Forum on Automated Interpretation of High Spatial Resolution Digital Imagery for Forestry*, Natural Resources Canada, Forestry Canada, Pacific Forestry Centre, Victoria, BC, Feb. 10-12, *In press.*

Leckie, D., M. Gillis, F. Gougeon, M. Lodin, J. Wakelin, and X. Yuan, 1998; Computer-assisted photointerpretation aids to forest inventory mapping: Some possible

approaches, Proceedings of the *International Forum on Automated Interpretation of High Spatial Resolution Imagery for Forestry*, Canadian Forest Service, Pacific Forestry Centre, Victoria, British Columbia, Feb. 10-12, *In press*.

LeDrew, E., 1995; The role of remote sensing in understanding the effects of sea ice on global change, (In LeDrew, E., M. Strome and F. Hegyi (eds.), 1995: *The Canadian Remote Sensing Contribution to Understanding Global Change*. Department of Geography Publication Series, No. 38, University of Waterloo, 434 p.)

Lévesque, J., and D. King, 1995; The use of airborne digital camera image semivariance in the evaluation of forest damage at an acid mine site, *Proceedings of the 15th Biennial Workshop on Color Photography and Videography in Resource Assessment*, Terre Haute, IN, May 1-3, pp. 270-279.

Lévesque, J., and D. King, 1996; Semivariance analysis of tree crown structure in airborne digital camera imagery. *Proceedings of the 26th International Symposium on Remote Sensing of Environment / 18th Canadian Symposium on Remote Sensing*, Vancouver, BC. March 23-26. pp. 275-278

Levin, S., 1993; Concepts of scale at the local level, (Chapter 2) In, *Scaling Physiological Processes: Leaf to Globe*, Edited by, J. Ehleringer and C. Field, (Academic Press, Inc., Toronto, pp. 7-19.)

Li, X., and A. Strahler, 1985; Geometric-optical modeling of a conifer forest canopy, *IEEE Transactions on Geoscience and Remote Sensing*, Vol. GE-23, No. 5, pp. 705-721.

Li, X. and A. H. Strahler, 1992: Geometric-optical bidirectional reflectance modeling of the discrete crown vegetation canopy: effect of crown shape and mutual shadowing, IEEE *Transactions on Geoscience and Remote Sensing*, Vol. 30, No. 2, pp. 276-292.

Li, X., A. H. Strahler and C. E. Woodcock, 1995: A hybrid geometric optical-radiative transfer approach for modeling albedo and directional reflectance of discontinuous canopies, *IEEE Transactions on Geoscience and Remote Sensing*, Vol. 33 No. 2, pp. 466-480.

Li., Z., and L. Moreau, 1996; A new approach for remote sensing of canopy-absorbed photosynthetically active radiation. I. Total surface absorption, *Remote Sensing of Environment*, Vol. 55, pp. 179-191.

Long, J., and F. W. Smith, 1988; Leaf area - sapwood area relations of lodgepole pine as influenced by stand density and site index, *Canadian Journal of Forest Research.*, Vol. 18.

Loveland, T., J. Merchant, D. Ohlen, and J. Brown, 1991; Development of a land-cover characteristics database for the conterminous U.S., *Photogrammetric Engineering & Remote Sensing*, Vol. 57. No. 11, pp. 1453-1463.

McGraw, J., T. Warner, T. Key, and W. Lamar, 1998; High spatial resolution remote sensing of forest trees, *Trends in Ecology & Evolution*, Vol. 13, No. 8, 300-301.

Milton, T., G. Blackburn, E. Rollin, and F. Danson, 1994; Measurement of the spectral directional reflectance of forest canopies: A review of methods and a practical application, *Remote Sensing Reviews*, Vol. 10, pp. 285-308.

Miranda, F., and J. Carr, 1994; Application of the semivariogram textural classifier (STC) for vegetation discrimination using SIR-B data of the Guiana Shield, northwestern Brazil, *Remote Sensing Reviews*, Vol. 10, pp. 155-168.

Miranda, F., J. MacDonald, J. Carr, 1992; Application of the semivariogram textural classifier (STC) for vegetation discrimination using SIR-B data of Borneo, *International Journal of Remote Sensing*, Vol. 13, pp. 2349-2354.

Miranda, F., L. Fonseca, J. Carr, and J. Taranik, 1996; Analysis of JERS-1 (Fuyo-1) SAR data for vegetation discrimination in northwestern Brazil using the semivariogram textural classifier (STC), *International Journal of Remote Sensing*, Vol. 17, No. 17, pp. 3523-3529.

Matheron, G., 1963; Principles of geostatistics, *Economic Geology*, Vol. 58, p. 1246-1266.

Marceau, D., P. Howarth, D. Gratton, 1994a; Remote sensing and the measurement of geographical entities in a forested environment. 1. The scale and spatial aggregation problem, *Remote Sensing of Environment*, Vol. 49, pp. 93-104.

Marceau, D., D. Gratton, R. Fournier, and J. Fortin, 1994b; Remote sensing and the measurement of geographical entities in a forested environment. 2. The optimal spatial resolution, *Remote Sensing of Environment*, Vol. 49, pp. 105-117.

Mead, J., and R. McIntosh, 1991; Polarimetric backscatter measurements of deciduous and coniferous trees at 225 GHz, *IEEE Transactions on Geoscience and Remote Sensing*, Vol. GE-29, No. 1, pp. 21-28.

Meentemeyer, V., 1989; Geographical perspectives of space, time, and scale, *Landscape Ecology*, Vol. 3, No. 3/4, pp. 164-173.

Milton, E., 1987; Principles of field spectroscopy, *International Journal of Remote Sensing*, Vol. 8, No. 12, pp. 1807-1827 .

Myneni, R., F. Hall, P. Sellers, and A. Marshak, 1995; The interpretation of spectral vegetation indexes, *IEEE Transactions on Geoscience and Remote Sensing*, Vol. 33, No. 2, pp. 481-486.

Natural Resources Canada, 1994; Model Forests: *An International Network Of Working Models Of Sustainable Forest Management*, (Ottawa, 43p.)

Natural Resources Canada, 1995; *The State of Canada's Forests*, (Ottawa, 113p.)

Niemann, O., 1995; Remote sensing of forest stand age using airborne spectrometer data, *Photogrammetric Engineering & Remote Sensing*, Vol. 61, No. 9, pp. 1119-1127.

Niemann, K. O., and S. Adams, 1998; Automated tree crown identification using digital orthophoto mosaics, *Proceedings of the International Forum on Automated Interpretation of High Spatial Resolution Digital Imagery for Forestry*, Natural Resources Canada, Forestry Canada, Pacific Forestry Centre, Victoria, BC, Feb. 10-12, *In press.*

Needham, T., and J. Smith, 1987; Stem count accuracy and species determination in loblolly pine plantations using 35-mm aerial photography, *Photogrammetric Engineering & Remote Sensing*, Vol. 53, No. 12, pp. 1675-1678.

Nel, E., and C. Wessman, 1993; Canopy transmittance models for estimating forest leaf area index, *Canadian Journal of Forest Research*, Vol. 23, pp. 2579-2586.

Nemani, R., L. Pierce, S. Running, and L. Band, 1993; Forest ecosystem processes at the watershed scale: sensitivity to remotely-sensed leaf area index estimates, *International Journal of Remote Sensing*, Vol. 14, No. 13, pp. 2519-2534.

Norman, J, 1993; Scaling processes between leaf and canopy levels, (Chapter 4) from, *Scaling Physiological Processes: Leaf to Globe*, Edited by, J. Ehleringer and C. Field, (Academic Press, Inc., Toronto, pp. 41-76.)

Oker-Blom, P. and S. Kellomaki, 1983, Effect of grouping of foliage on the within-stand and within-crown light regime: comparison of random and grouping canopy models, *Agricultural Meteorology*, Vol. 28, pp. 143-155.

Olthof, I. and D. King, 1997; Evaluation of textural information in airborne CIR digital camera imagery for estimation of forest stand leaf area index, *Proceedings of the 1st North American Symposium on Small Format Aerial Photography*, Cloquet, MN, Oct. 14-17, pp. 154-164.

Oliver, M., R. Webster, and J. Gerrard, 1989; Geostatics in physical geography. Part I: theory, *Transactions of the Institute of British Geographers*, N.S., Vol. 14, pp. 259-269.

Openshaw, S., 1984; *The modifiable areal unit problem, concepts and techniques in modern geography*, (CATMOG Series, GeoBooks, Regency House, Norwich, Vol. 38, 40p.)

Ord, J., and A. Getis, 1995; Local spatial autocorrelation statistics: Distributional issues and an application, *Geographical Analysis*, Vol. 27, No. 4, pp. 286-306.

Pal, N., and S. Pal, 1993; A review on image segmentation techniques, Pattern Recognition, Vol. 26, No. 9, pp. 1277-1294.

Peddle, D., H. White, R. Soffer, J. Miller, and E. LeDrew, 1995; Reflectance processing of field spectrometer data in BOREAS, presented at *the 17th Canadian Symposium on Remote Sensing*, June 13-15, 1995, Saskatoon, Saskatchewan, vol. I, pp. 189-194.

Peddle, D., F. Hall, E. LeDrew, 1997; Spectral mixture analysis and geometric optical reflectance modeling of boreal forest biophysical structure, *Remote Sensing of Environment, In press.*

Peterson, D., and S. Running, 1989; Applications in forest science and management, *In Theory and Applications of Optical Remote Sensing*, edited by, G. Asrar, (John Wiley and Sons, New York, 733p.)

Peterson, D. L. and R. H. Waring, 1993: Overview of the Oregon transect ecosystem project, *Ecological Applications*, Vol. 4, pp. 211-225.

Peterson, D., M. Spanner, S. Running, and K. Teuber, 1987; Relationship of Thematic Mapper simulator data to leaf area index of temperate coniferous forests, *Remote Sensing of Environment*, Vol. 22, pp. 323-341.

Pierce, L., and S. Running, 1988; Rapid estimation of coniferous forest leaf area index using a portable integrating radiometer, *Ecology*, Vol. 69, No. 6, pp. 1762-1767.

Pinz, A., 1998; Tree isolation and species classification, *Proceedings of the International Forum on Automated Interpretation of High Spatial Resolution Digital Imagery for Forestry*, Natural Resources Canada, Forestry Canada, Pacific Forestry Centre, Victoria, BC, Feb. 10-12, *In press.*

Pollock, R, 1998; Individual tree recognition based on a synthetic tree crown image model, *Proceedings of the International Forum on Automated Interpretation of High Spatial Resolution Digital Imagery for Forestry*, Natural Resources Canada, Forestry Canada, Pacific Forestry Centre, Victoria, BC, Feb. 10-12, *In press.*

Price, R., D. Davison, S. Mah, D. Trudeau, and C. Anger, 1996; Utilization of *casi* as a forest management tool, *In Proceedings of the Second International Airborne Remote Sensing Conference and Exhibition*, San Francisco, United States, 24-27 June, Vol. III, pp. 514-523.

Preston, R., D. Culvenor, and N. Coops, 1998; Modeling of tree species and structural attributes from high resolution multi-spectral imagery using decision tree analysis for east coast eucalypt forests of Australia, *Proceedings of the International Forum on Automated Interpretation of High Spatial Resolution Digital Imagery for Forestry*, Natural Resources Canada, Forestry Canada, Pacific Forestry Centre, Victoria, BC, Feb. 10-12, *In press.*

Qi, J., A. Huete, M. Moran, A. Chehbouni, and R. Jackson, 1993; Interpretation of vegetation indices derived from multi-temporal SPOT images, *Remote Sensing of Environment*, 44: 89-101.

Ramstein, G. and M. Raffy, 1989; Analysis of the Structure of Radiometric Remotely Sensed Images, *International Journal of Remote Sensing*, Vol. 10, No. 6, 1049-1073.

Reed, T., and J. Du Buf, 1993; A review of recent texture segmentation and feature extraction techniques, *Computer Vision, Graphics, and Image Processing: Image Understanding*, Vol. 57, No. 3, pp. 359-372.

Ripple, W., S. Wang, D. Isaacson and D. Paine, 1991; A preliminary comparison of Landsat Thematic Mapper and SPOT-1 HRV multispectral data for estimating coniferous forest volume, *International Journal of Remote Sensing*, Vol. 12, No. 9, pp. 1971-1977.

Robichaud, E., and I. Methven, 1992; The applicability of the pipe model theory for the prediction of foliage biomass in trees from natural, untreated black spruce stands, *Canadian Journal of Forest Research*, Vol. 22, pp. 1118-1123.

Robinove, C., 1981; The logic of multispectral classification and mapping of land, *Remote Sensing of Environment*, pp. 231-342.

Robinson, A., and G. Wood, 1994; Individual tree volume estimation: A new look at new systems, *Journal of Forestry*, December, pp. 25-29.

Rosenfeld, A., 1984; Image analysis: Problems, progress, and prospects, *Pattern Recognition*, Vol. 17, No. 1, pp. 3-12.

Rossi, R., J. Dungan, and L. Beck, 1994, Kriging in the shadows: geostatistical interpolation for remote sensing, *Remote Sensing of Environment*, Vol. 49, p. 32-40.

Rowe, J., 1977; *Forest regions of Canada*, (Ottawa, Canada Forest Service, 172p.)

Running, S., and E. Hunt, Jr., 1993, Generalization of a forest ecosystem process model for other biomes, BIOME-BGC, and an application for global scale models, (Chapter 8) from, *Scaling Physiological Processes: Leaf to Globe*, Edited by, J. Ehleringer and C. Field, (Academic Press, Inc., Toronto, pp. 141-157.)

Running, S., D. Peterson, M. Spanner, and K. Teuber, 1986; Remote sensing of coniferous forest leaf area, *Ecology*, Vol. 67, No. 1, pp. 273-276.

Running, S., T. Loveland, and L. Pierce, 1994; A vegetation classification logic based on remote sensing for use in global biogeochemical models, *AMBIO*, Vol. 23, No. 1, 77-81.

Sayn-Wittenstein, L., 1978; *Recognition of tree species on aerial photographs*, (Canada Forest Service Information Report FMR-X-118, Ottawa, Ontario, 97p.)

Schaaf, C., X. Li, and A. Strahler, 1994; Topographic effects on bidirectional and hemispherical reflectances calculated with a geometric-optical canopy model, *IEEE Transactions on Geoscience and Remote Sensing*, Vol. 32, No. 6, pp. 1186-1193.

Schlesinger, W., 1991; *Biogeochemistry: An Analysis of Global Change*, (Academic Press, Toronto, 443p.)

Schowengerdt, R., 1997; *Remote sensing: Models and methods for image processing*, (Academic Press, San Diego, 522p.)

Schroeder, P., S. Brown, J. Mo, R. Birdsey, and C. Cieszewski, 1997; Biomass estimation for temperate broadleaf forests of the United States using inventory data, *Forest Science*, Vol. 43, No. 32, pp. 424-434.

Schwarz, K., M. Chapman, M. Cannon, and P. Gong, 1993; An integrated INS/GPS approach to the georeferencing of remotely sensed data, *Photogrammetric Engineering & Remote Sensing*, Vol. 59. No. 11, pp. 1667-1674.

Seed, E. and D. King, 1997; Determination of mixed boreal forest stand biophysical structure using large scale airborne digital camera imagery, Proceedings of GER '97, The 19th Canadian Symposium on Remote Sensing, Ottawa, Ontario, May 26-29, CD-ROM, paper #75, 8p.

Sellers, P., 1985; Canopy reflectance, photosynthesis and transpiration, *International Journal of Remote Sensing*, Vol. 6, No. 8, pp. 1335-1372.

Sellers, P., F. Hall, H. Margolis, B. Kelly, D. Baldocchi, G. den Hartog, J. Cihlar, M. Ryan, B. Goodison, P. Crill, K. Ranson, D. Lettenmaier, and D. Wickland, 1995; The Boreal Ecosystem-Atmosphere Study (BOREAS): An Overview and Early Results from the 1994 Field Year, *Bulletin of the American Meteorological Society*, Vol. 76, No. 9, pp. 1549-1577.

Sellers, P., 1989; Vegetation-canopy spectral reflectance and biophysical processes, *In Theory and Applications of Optical Remote Sensing*, edited by, G. Asrar, (John Wiley and Sons, New York, 733p.)

Sharpe, G., C. Hendee, and S. Allen, 1976; *Introduction to forestry*, (McGraw-Hill Book Company, Montreal, 544p.)

Singh, T., 1982; *Biomass equations for ten major tree species of the prairie provinces*, (Information Report NOR-X-242, Northern Forest Research Centre, Canadian Forestry Service, Environment Canada.)

Sinton, D., 1992; Reflections on 25 years of GIS, *GIS World*, February, pp. 1-8.

Slaymaker, D., K. Jones, C. Griffin and J. Finn. 1996. Mapping deciduous forests in Southern New England using aerial videography and hyperclustered multi-temporal Landsat TM imagery. Pages 87-101 in *Gap Analysis: A Landscape Approach to Biodiversity Planning*, J. Scott, T. Tear and F. Davis (eds.). American Society of Photogrammetry and Remote Sensing, Bethesda, MD, USA.

Smith, F., D. Sampson, and J. Long, 1991a; Comparison of leaf area index estimates from tree allometrics and measured light interception, *Forest Science*, Vol. 37, No. 6, pp. 1682-1688.

Smith, N., G. Borstad, D. Hill, and R. Kerr, 1991b; Using high-resolution airborne spectral data to estimate forest leaf area and stand structure, *Canadian Journal of Forest Research*, Vol. 21, pp. 1127-1132.

Spanner, M., L. Pierce, D. Peterson, and S. Running, 1990; Remote sensing of temperate coniferous forest leaf area index: the influence of canopy closure, understory vegetation and background reflectance, *International Journal of Remote Sensing*, Vol. 11, No. 1, pp. 95-111.

Spanner, M., L. Johnson, J. Miller, R. McCreight, J. Freemantle, J. Runyon, and P. Gong, 1994; Remote sensing of seasonal leaf area index across the Oregon Transect, *Ecological Applications*, Vol. 4, No. 2, pp. 258-271.

Spencer, R., and R. Hall, 1988; Canadian Large-Scale Aerial Photographic Systems (LSP), *Photogrammetric Engineering and Remote Sensing*, Vol. 54, No. 4, pp. 475-482.

Spurr, S., 1952; *Forest Inventory*, (The Ronald Press Company, New York, 476p.)

Spurr, S., and B. Barnes, 1980; *Forest Ecology*, (John Wiley and Sons, Toronto, 687p.)

Steven, M., 1987; Ground truth: An underview, *International Journal of Remote Sensing*, Vol. 8, No. 7, pp. 1033-1038.

Strahler, A., C. Woodcock, and J. Smith, 1986; On the nature of models in remote sensing, *Remote Sensing of Environment*, Vol. 20, pp. 121-139.

St-Onge, B., and F. Cavayas, 1995; Estimating forest stand structure from high resolution imagery using the directional variogram, *International Journal of Remote Sensing*, Vol. 16, No. 11, pp. 1999-2021.

St-Onge, B., and F. Cavayas, 1997; Automated forest structure mapping from high resolution imagery based on directional semivariogram estimates, *Remote Sensing of Environment*, Vol. 61, pp. 82-95.

Sun, G., D. Simonett, and A. Strahler, 1991; A radar backscatter model for discontinuous coniferous forests, *IEEE Transactions on Geoscience and Remote Sensing*, Vol. GE-29, No. 4, pp. 639-650.

Tiefelsdorf, M. and Boots, B., 1997. A note on the extremities of local Moran's $I_i$'s and their impact on global Moran's *I*. *Geographical Analysis*, Vol. 29, pp. 248-257.

Toman, M., and P. Ashton, 1995; Sustainable forest ecosystems and management: A review article, *Forest Science*, Vol. 42, No. 3, pp. 366-377.

Townshend, J., C. Justice, W. Li, C. Gurney, and J. McManus, 1991; Global land cover classification by remote sensing: present capabilities and future possibilities, *Remote Sensing of Environment*, Vol. 35, pp. 243-255.

Treitz, P., P. Howarth, R. Suffling, and P. Smith, 1992; Application of detailed ground information to vegetation mapping with high spatial resolution digital imagery, *Remote Sensing of Environment*, Vol. 42, pp. 65-82.

Trotter, C., 1991; Remotely-sensed data as an information source for geographical information systems in natural resource management: a review, *International Journal of Geographical Information Systems*, Vol. 5, No. 2, pp. 225-239.

Tucker, C., 1977; Spectral estimation of grass canopy variables, *Remote Sensing of Environment*, Vol. 6, pp. 11-26.

Turner, M., R. O'Neill, R. Gardner, and B. Milne, 1989; Effects of changing spatial scale on the analysis of landscape pattern, *Landscape Ecology*, Vol. 3, No. 3/4, pp. 153-162.

UBC, 1983; *Forestry Handbook for British Columbia*, (University of British Columbia, Faculty of Forestry, Forestry Undergraduate Society, 611p.)

Ustin, S., S. Martens, and V. Vanderbilt, 1991; Canopy architecture of a walnut orchard, *IEEE Transactions on Geoscience and Remote Sensing*, Vol. GE-29, No. 6, pp. 843-851.

van Martin, A., 1984; Forests and Forestry in National Life, In: Hummel, F., *Forest Policy: A Contribution to Resource Development*, (Kluwer Academic Publishers Group, The Hague, pp. 1-19)

Vane, G., and A. Goetz, 1993; Terrestrial imaging spectrometry: current status, future trends, *Remote Sensing of Environment*, Vol. 44, pp. 117-126.

Vogelmann, J., B. Rock, and D. Moss, 1993; Red edge spectral measurements from sugar maple leaves, *International Journal of Remote Sensing*, Vol. 14, No. 8, pp. 1563-1575.

Votour, G.,1998; personal communication, Clark Labs Technical Support, The Clark Labs, Worcester, MA, USA.

Wald, L., 1989; Some examples of the use of structure functions in the analysis of satellite images of the ocean, *Photogrammetric Engineering & Remote Sensing*, Vol. 55, No. 10, pp. 1487-1490.

Walsworth, N., and D. King, 1997; Image modeling of forest changes associated with acid mine drainage using a cellular automata transition model - KamKotia mine site, Timmins, Ontario, *Proceedings of GER '97 / 19th Canadian Symposium. on Remote Sensing*, Ottawa, Ontario, May 26-29, CD-ROM, paper #74, 8p.

Walsworth, N., and D. King; 1998; Comparison of two tree apex delineation techniques, *Proceedings of the International Forum on High Resolution Remote Sensing in Forestry* (Canadian Forest Service), Victoria BC, Feb. 9-12. *In press.*

Waring, R., and W. Schlesinger, 1985; *Forest Ecosystems: Concepts and Management,* (Academic Press, Inc., Toronto, 340p.)

Waring, R., Schroeder, and R. Oren, 1982; Application of the pipe model theory to predict canopy leaf area, *Canadian Journal of Forest Research*, Vol. 12.

Waring, R., J. Runyon, S. Goward, R. McCreight, B. Yoder, and M. Ryan, 1993; Developing remote sensing techniques to estimate photosynthesis and annual forest growth across a steep climatic gradient in western Oregon, USA, In: Management of structure and productivity of boreal and subalpine forests (ed. S. Linder, and S. Kellomaki), *Studia Forestalia Suecica 191*, 1994, pp. 33-42.

Watts, S., 1983; *Forestry handbook for British Columbia*, (D. W. Friesen & Sons, Cloverdale, B.C., 611p.)

Welch, R., 1982; Spatial resolution requirements for urban studies, *International Journal of Remote Sensing*, Vol. 3, No. 2, pp. 139-146.

Welles, J., 1990; Some indirect methods of estimating canopy structure, *Remote Sensing Reviews*, Vol. 5, No. 1, pp. 31-43.

Werle, D., 1989; *Radar remote sensing for application in forestry: A literature review for investigators and potential users of SAR data in Canada*, ( Commissioned by: Canada Centre for Remote Sensing, Technology Transfer Program/Applications Division, 42p.)

Westoby, J., 1989; *Introduction to World Forestry*, (Basil Blackwell Ltd., Oxford, 228p.)

Whitehead, D., J. Grace and M. Godfrey, 1990; Architectural distribution of foliage in individual *Pinus radiata* D. Don crowns and the effects of clumping on radiation interception, *Tree Physiology* , Vol. 7, pp. 135-155.

Wong, A., and M. Vogel, 1977; Resolution dependent information measures for image analysis, *IEEE Transactions on Systems, Man, and Cybernetics*, Vol. SMC- 7, No. 1, pp. 49-61.

Woodcock, C., and A. Strahler, 1987; The factor of scale in remote sensing, *Remote Sensing of Environment*, Vol. 21, pp. 311-322.

Woodcock, C., A. Strahler, and D. Jupp, 1988a; The use of variograms in remote sensing: I. scene models and simulated images, *Remote Sensing of Environment*, Vol. 25, p. 323-348.

Woodcock, C., A. Strahler, and D. Jupp, 1988b; The use of variograms in remote sensing: II. real digital images, *Remote Sensing of Environment*, Vol. 25, p. 323-348.

Woodcock, C., J. Collins, V. Jakabhazy, X. Li, S. Macomber, and Y. Wu, 1997; Inversion of the Li-Strahler canopy reflectance model for mapping forest structure, IEEE Transactions on Geoscience and Remote Sensing, Vol. 35, No. 2, pp. 405-414.

Woods, K., A. Feiveson, and Botkin, 1991; Statistical error analysis for biomass density and leaf area index estimation, *Canadian Journal of Forest Research*, Vol. 21, pp. 974-989.

Wu, Shih-Tseng, 1987; Parametric analysis of synthetic aperture radar data for characterization of deciduous forest stands, Remote Sensing, ASPRS Technical Papers, 1987 ASPRS -ACSM Annual Convention, Vol. 1, pp. 320-328.

Wu, Y., and A. Strahler, 1994; Remote estimation of crown size, stand density, and biomass on the Oregon transect, *Ecological Applications*, Vol. 4, No. 2, pp. 299-312.

Wulder, M., M. Lavigne, and Franklin, 1995; Empirical relations between forest stand parameters and ERS-1 SAR imagery in northwestern New Brunswick, *Presented at the 17th Canadian Symposium on Remote Sensing*, June 13-15, 1995, Saskatoon, Saskatchewan, Vol. 2, pp. 663-668.

Wulder, M., 1996; *Airborne remote sensing of forest structure: Estimation of leaf area index*, (Unpublished Masters Thesis, University of Waterloo, Waterloo, Ontario, Canada, 101p.)

Wulder, M., Lavigne, M., and S. Franklin, 1996a; High spatial resolution optical image texture for improved estimation of forest stand leaf area index, *Canadian Journal of Remote Sensing*, Vol. 22, No. 4, pp. 441-449.

Wulder, M., S. Franklin, M. Lavigne, 1996b; Statistical texture properties of forest structure for improved LAI estimates from *casi*, *Presented at the 18th Annual Symposium of the Canadian Remote Sensing Society, and The 26th International Symposium on Remote Sensing of Environment*, March 25 to 29, 1996, Vancouver, BC, Canada, pp. 161-164.

Wulder, S. Franklin, M., Lavigne, M. Deuling, and E. Hunt, 1996c; Estimation of the net primary productivity of the Fundy Model Forest, *Presented at Eco-Informa '96*, November 4-7, Lake Buena Vista, FL, USA.

Wulder, M., S. Mah and D. Trudeau, 1996d; Mission planning for operational data acquisition campaigns with the *casi*, *Presented at the Second International Airborne Remote Sensing Conference and Exhibition*, San Francisco, CA, USA, June 24-27, Vol. III, pp. 53-62.

Wulder, M., B. Boots, M. Anstey, M. Lavigne, and E. LeDrew, 1997a; Spatial dependence characteristics of multi-scale remotely sensed imagery, *For presentation at GER'97, Canadian Remote Sensing Society Conference*, May 24 to 30, Ottawa, ON, Canada.

Wulder, M., E. LeDrew, M. Lavigne, and S. Franklin, 1997b; A comparison of texture measures in the estimation of LAI: Introduction of semivariance moment texture, *For presentation at GER'97, Canadian Remote Sensing Society Conference*, May 24 to 30, Ottawa, ON, Canada.

Wulder, M., M. Lavigne, S. Franklin, and E. LeDrew, 1997c; Refinement of GIS forest polygon content with classified remotely sensed image data, *For presentation at GER'97, Canadian Remote Sensing Society Conference*, May 24 to 30, Ottawa, ON, Canada.

Wulder, M., E. LeDrew, M. Lavigne, and S. Franklin, 1998; Aerial image texture information in the estimation of northern deciduous and mixed wood forest leaf area index (LAI), *Remote Sensing of Environment*, Vol. 64, pp. 64-76.

Wulder, M., 1998a; Forest polygon decomposition through the integration of remote sensing, GIS, UNIX, and C, *Computers & Geosciences*, Vol. 24, No. 2, pp. 151-157.

Wulder, M., 1998b; Image spectral and spatial information in the assessment of forest structural and biophysical data, *In the Proceedings of: The International Forum on Automated Interpretation of High Spatial Resolution Digital Imagery for Forestry, Natural Resources Canada, Forestry Canada, Pacific Forestry Centre, Victoria, BC, February 10-12, In press.*

Wulder, M., 1998c; A review of optical remote sensing techniques and applications for the assessment of forest inventory and biophysical parameters, *Progress in Physical Geography*, Vol. 22, No. 4, pp. 449-476.

Wulder, M., and B. Boots, 1998a; Local spatial autocorrelation characteristics of Landsat TM imagery of a managed forest area, *Canadian Journal of Remote Sensing, In review.*

Wulder, M., and B. Boots, 1998b; Local spatial autocorrelation characteristics of remotely sensed imagery assessed with the Getis statistic, *International Journal of Remote Sensing*, Vol. 19, No. 11, pp. 2223-2231.

Yuan, X., D. King, and J. Vlcek, 1991; Sugar maple decline assessment based on spectral and textural analysis of multispectral aerial videography, *Remote Sensing of Environment*, Vol. 37, pp. 47-54.

Zonneveld, I., 1989; The land unit - A fundamental concept in landscape ecology, and its applications, *Landscape Ecology*, Vol. 3, No. 2, pp. 67-86.

# APPENDIX

## *Appendix 1. Data Collection in Support of Airborne Remote Sensing*

The required needs of a particular mission will dictate the mode of operation to be utilized, the desired resolution, flight line azimuth and location, desired illumination conditions, and acceptable flight conditions (Wulder, *et al.*, 1996d). Once the mission parameters have been decided upon, data collection may begin. A typical mission is divided into pre-, during-, and post-flight portions to enable a summary of necessary mission components to be presented. Table 2.10 presents an outline of what to be aware of when contracting out an airborne multispectral scanner. The level of table detail would be greater if all the instrument operator concerns were also displayed.

**Table A1.1. General issues to address for successful image acquisition (from Wulder, *et al.*, 1996d)**

**Pre-flight**

Location of flight line(s)
- azimuth
- length

Survey GCPs and/or Markers

Resolution
- elevation (across track pixel size)
- aircraft velocity (along track pixel size)

Spatial mode:
- selection of bands and bandwidths

Spectral mode
- number of look directions
- where to locate the looks
- bandwidth of the scene recovery channel

Enhanced spectral mode
- spectral resolution (eg, 1.9nm, 3.8nm ... 11.4nm+)
- spatial coverage (eg, 101 adjacent looks, 203 ... 511)

**During flight**

Collection of atmospheric data
- collection of pseudo invariant features (PIFs)
- operation/monitoring of the Incident Light Sensor mounted on aircraft
- weather conditions (eg, calm, clear, solar position ...)

Dark data acquisition for improved radiometric quality (automatic with the motorized aperture lens)

Optimize Signal Levels
- 25 to 75% of full scale

Geometric positioning data
- GPS base station data collection, for possible differential correction

**Post flight**

Image Quality Assurance

Radiometric Corrections
- conversion to spectral radiance units (SRU)

Spectral reflectance determination
- processing of Incident Light Sensor (ILS) data
- incorporation of PIFs

Geometric Corrections and Bundle Adjustments
- differential correction of the airborne GPS data with the base station data
- GPS, aircraft attitude measurements and *casi* imagery time synchronization
- terrain height corrections using a digital elevation model
- remove sensor alignment offsets
- creation of a geocoded/orthorectified grid
- image resampling

## *Appendix 2. Within Cluster Spectral Values for Each Study Site (All Plots)*

**Table A2.1. Cluster ID, mean spectral values for each channel, and assigned class for sample plot DS5**

| Cluster | CASI1 | CASI2 | CASI3 | CASI4 | CASI5 | Class |
|---|---|---|---|---|---|---|
| 0 | 14.5 | 4.5 | 3.1 | 19.9 | 40.8 | US |
| 3427 | 22.5 | 7.3 | 5.3 | 33.0 | 60.3 | HW |
| 3444 | 21.1 | 7.0 | 5.3 | 33.7 | 65.6 | HW |
| 3495 | 22.8 | 6.9 | 4.9 | 33.9 | 62.4 | HW |
| 3497 | 26.0 | 8.7 | 6.0 | 40.3 | 68.0 | MW |
| 3523 | 17.0 | 4.5 | 3.0 | 25.0 | 53.5 | HW |
| 3534 | 19.8 | 6.5 | 4.8 | 31.5 | 62.0 | HW |
| 3563 | 22.8 | 6.9 | 4.8 | 34.2 | 63.5 | HW |
| 3579 | 25.3 | 12.2 | 10.2 | 33.6 | 52.9 | HW |
| 3622 | 26.1 | 8.7 | 6.1 | 37.2 | 60.0 | MW |
| 3623 | 21.0 | 6.7 | 4.7 | 33.2 | 67.4 | HW |
| 3646 | 23.4 | 7.7 | 5.7 | 34.1 | 63.6 | HW |
| 3700 | 23.0 | 7.1 | 5.2 | 35.8 | 68.2 | HW |
| 3714 | 22.3 | 7.0 | 5.1 | 34.9 | 63.6 | HW |

**Table A2.2. Cluster ID, mean spectral values for each channel, and assigned class for sample plot DS6**

| Cluster | CASI1 | CASI2 | CASI3 | CASI4 | CASI5 | Class |
|---|---|---|---|---|---|---|
| 0 | 16.1 | 5.7 | 4.4 | 21.9 | 40.1 | US |
| 3056 | 28.2 | 9.3 | 6.8 | 40.4 | 67.6 | HW |
| 3068 | 23.0 | 7.6 | 5.8 | 34.2 | 66.7 | HW |
| 3071 | 24.1 | 7.7 | 5.7 | 34.8 | 63.8 | HW |
| 3099 | 21.6 | 7.0 | 5.3 | 31.8 | 60.7 | MW |
| 3125 | 19.1 | 7.4 | 5.8 | 30.9 | 56.4 | MW |
| 3176 | 26.7 | 8.6 | 6.1 | 38.9 | 65.1 | HW |
| 3242 | 18.8 | 6.1 | 4.4 | 28.8 | 51.9 | MW |
| 3263 | 22.9 | 8.2 | 6.1 | 35.4 | 60.9 | MW |
| 3296 | 24.5 | 8.1 | 6.0 | 37.4 | 63.7 | HW |
| 3320 | 27.8 | 8.2 | 6.0 | 41.6 | 70.0 | HW |
| 3321 | 25.4 | 7.8 | 5.5 | 37.5 | 65.4 | HW |
| 3338 | 21.5 | 5.8 | 4.0 | 25.8 | 50.5 | MW |
| 3339 | 24.3 | 7.3 | 5.1 | 33.1 | 55.9 | MW |

**Table A2.3. Cluster ID, mean spectral values for each channel, and assigned class for sample plot DS7**

| Cluster | CASI1 | CASI2 | CASI3 | CASI4 | CASI5 | Class |
|---|---|---|---|---|---|---|
| 0 | 21.1 | 7.2 | 5.2 | 27.0 | 44.2 | US |
| 3332 | 21.3 | 8.0 | 6.0 | 33.7 | 56.0 | MW |
| 3352 | 33.3 | 11.1 | 7.5 | 46.4 | 71.4 | HW |
| 3390 | 31.1 | 10.1 | 6.7 | 42.9 | 64.5 | HW |
| 3427 | 26.4 | 8.0 | 5.2 | 31.8 | 46.5 | MW |
| 3442 | 33.6 | 11.0 | 7.2 | 50.6 | 75.1 | HW |
| 3459 | 35.4 | 11.3 | 7.5 | 50.5 | 72.3 | HW |
| 3460 | 28.4 | 9.4 | 6.7 | 40.3 | 67.3 | MW |
| 3560 | 30.3 | 10.1 | 6.8 | 44.6 | 68.1 | MW |
| 3586 | 30.7 | 11.7 | 8.7 | 42.1 | 63.7 | HW |

**Table A2.4. Cluster ID, mean spectral values for each channel, and assigned class for sample plot DS8**

| Cluster | CASI1 | CASI2 | CASI3 | CASI4 | CASI5 | Class |
|---|---|---|---|---|---|---|
| 0 | 17.3 | 6.1 | 4.6 | 24.3 | 44.7 | US |
| 2929 | 29.8 | 9.2 | 6.2 | 40.4 | 65.2 | HW |
| 2960 | 43.6 | 16.4 | 10.0 | 61.1 | 70.6 | HW |
| 2973 | 23.4 | 8.2 | 6.2 | 36.4 | 63.6 | HW |
| 2974 | 28.1 | 9.1 | 6.5 | 41.4 | 65.5 | HW |
| 2991 | 30.8 | 10.6 | 7.0 | 40.9 | 60.1 | HW |
| 3005 | 24.2 | 8.3 | 6.0 | 38.4 | 64.1 | HW |
| 3040 | 27.8 | 9.2 | 6.4 | 39.4 | 61.0 | HW |
| 3041 | 18.5 | 7.0 | 5.5 | 26.4 | 50.9 | MW |
| 3058 | 23.5 | 8.4 | 6.1 | 35.5 | 60.3 | HW |
| 3069 | 23.4 | 7.8 | 5.9 | 36.6 | 63.1 | MW |
| 3086 | 17.7 | 6.7 | 5.6 | 28.9 | 54.7 | HW |
| 3114 | 24.0 | 7.0 | 5.3 | 36.7 | 63.7 | HW |
| 3115 | 26.6 | 8.8 | 6.2 | 38.5 | 61.3 | HW |
| 3117 | 18.4 | 6.9 | 5.5 | 29.9 | 57.4 | MW |
| 3158 | 19.5 | 7.5 | 5.7 | 30.1 | 55.8 | MW |
| 3161 | 17.5 | 6.2 | 5.0 | 25.3 | 51.1 | MW |
| 3175 | 21.8 | 8.2 | 6.2 | 34.8 | 59.0 | MW |
| 3192 | 18.1 | 6.7 | 5.1 | 26.0 | 48.9 | MW |
| 3213 | 21.5 | 7.7 | 5.8 | 33.2 | 60.8 | MW |
| 3237 | 16.3 | 5.2 | 3.8 | 21.7 | 47.0 | MW |
| 3260 | 22.2 | 8.2 | 6.0 | 33.9 | 60.4 | MW |
| 3261 | 19.4 | 7.1 | 5.4 | 29.5 | 61.1 | MW |
| 3307 | 19.9 | 7.1 | 5.5 | 32.0 | 61.0 | MW |

**Table A2.5. Cluster ID, mean spectral values for each channel, and assigned class for sample plot DS9**

| Cluster | CASI1 | CASI2 | CASI3 | CASI4 | CASI5 | Class |
|---|---|---|---|---|---|---|
| 0 | 15.10 | 5.60 | 4.20 | 19.90 | 35.70 | US |
| 4021 | 28.60 | 9.80 | 6.80 | 39.80 | 59.90 | HW |
| 4022 | 26.00 | 10.70 | 8.30 | 36.30 | 54.60 | HW |
| 4067 | 20.90 | 7.80 | 5.60 | 31.70 | 53.90 | HW |
| 4089 | 17.10 | 5.10 | 3.90 | 21.00 | 41.40 | MW |
| 4097 | 28.30 | 10.20 | 7.00 | 39.90 | 59.60 | HW |
| 4111 | 25.30 | 8.30 | 5.90 | 34.30 | 55.00 | HW |
| 4113 | 28.00 | 10.00 | 7.00 | 37.00 | 60.00 | HW |
| 4153 | 22.80 | 8.80 | 6.40 | 35.40 | 55.60 | HW |
| 4167 | 25.50 | 9.00 | 6.40 | 36.50 | 59.80 | HW |
| 4183 | 21.60 | 8.50 | 6.70 | 31.00 | 57.60 | HW |
| 4184 | 17.00 | 6.00 | 5.00 | 25.00 | 49.00 | MW |
| 4186 | 24.70 | 8.30 | 5.90 | 37.00 | 60.50 | HW |
| 4206 | 19.50 | 6.30 | 4.60 | 25.30 | 43.90 | MW |
| 4215 | 25.60 | 8.90 | 6.30 | 35.60 | 59.10 | HW |
| 4266 | 21.80 | 7.20 | 5.10 | 31.60 | 53.10 | HW |
| 4275 | 25.60 | 8.60 | 6.10 | 35.60 | 55.30 | HW |
| 4309 | 17.30 | 6.80 | 4.50 | 24.00 | 41.80 | MW |

**Table A2.6. Cluster ID, mean spectral values for each channel, and assigned class for sample plot DS10**

| Cluster | CASI1 | CASI2 | CASI3 | CASI4 | CASI5 | Class |
|---|---|---|---|---|---|---|
| 0 | 21.6 | 7.6 | 5.6 | 29.1 | 47.9 | US |
| 1706 | 26.6 | 11.4 | 8.6 | 36.8 | 62.6 | HW |
| 1718 | 28.3 | 8.8 | 6.2 | 40.9 | 67.8 | HW |
| 1734 | 31.2 | 11.7 | 8.1 | 44.5 | 60.7 | HW |
| 1782 | 26.1 | 7.8 | 5.4 | 34.0 | 54.4 | MW |
| 1789 | 28.5 | 9.5 | 6.5 | 41.5 | 60.5 | HW |
| 1798 | 29.8 | 10.0 | 6.8 | 43.4 | 63.9 | HW |
| 1836 | 33.6 | 10.6 | 7.2 | 48.6 | 71.6 | HW |
| 1854 | 28.2 | 10.0 | 7.0 | 41.5 | 61.6 | HW |
| 1925 | 33.5 | 11.3 | 7.2 | 46.2 | 58.3 | HW |
| 1937 | 31.2 | 10.4 | 6.9 | 41.6 | 58.7 | HW |
| 1958 | 29.8 | 9.8 | 6.6 | 43.0 | 63.4 | HW |

# *Appendix 3. LAI from NDVI and Clusters, Plots DS6 to DS10*

**Table A3.1. Computation of leaf area for sample plot DS6, from cluster mean NDVI and cluster spatial extent (total number of pixels = 380)**

| Cluster | Cluster NDVI | Class | Pixels/Cluster | LA | Pixels per cluster/ Total | LA/Cluster | Plot LAI |
|---|---|---|---|---|---|---|---|
| 0 | 0.75 | US | 143 | | 0.38 | 0 | |
| 3056 | 0.76 | HW | 22 | 7.61 | 0.06 | 0.44 | |
| 3068 | 0.79 | HW | 13 | 7.72 | 0.03 | 0.26 | |
| 3071 | 0.78 | HW | 28 | 7.69 | 0.07 | 0.56 | |
| 3099 | 0.79 | MW | 50 | 7.90 | 0.13 | 1.04 | |
| 3125 | 0.77 | MW | 9 | 7.84 | 0.02 | 0.19 | |
| 3176 | 0.77 | HW | 51 | 7.63 | 0.13 | 1.02 | |
| 3242 | 0.79 | MW | 8 | 7.88 | 0.02 | 0.17 | |
| 3263 | 0.76 | MW | 8 | 7.82 | 0.02 | 0.16 | |
| 3296 | 0.77 | HW | 15 | 7.66 | 0.04 | 0.30 | |
| 3320 | 0.79 | HW | 5 | 7.71 | 0.01 | 0.10 | |
| 3321 | 0.79 | HW | 18 | 7.70 | 0.05 | 0.36 | |
| 3338 | 0.80 | MW | 4 | 7.91 | 0.01 | 0.08 | |
| 3339 | 0.77 | MW | 7 | 7.84 | 0.02 | 0.14 | **4.8** |

**Table A3.2. Computation of leaf area for sample plot DS7, from cluster mean NDVI and cluster spatial extent (total number of pixels = 400)**

| Cluster | Cluster NDVI | Class | Pixels/Cluster | LA | Pixels per cluster/ Total | LA/Cluster | Plot LAI |
|---|---|---|---|---|---|---|---|
| 0 | 0.72 | US | 182 | | 0.45 | 0 | |
| 3332 | 0.75 | MW | 3 | 7.79 | 0.01 | 0.06 | |
| 3352 | 0.73 | HW | 29 | 7.52 | 0.07 | 0.54 | |
| 3390 | 0.73 | HW | 15 | 7.53 | 0.04 | 0.28 | |
| 3427 | 0.71 | MW | 13 | 7.69 | 0.03 | 0.25 | |
| 3442 | 0.74 | HW | 16 | 7.57 | 0.04 | 0.30 | |
| 3459 | 0.73 | HW | 31 | 7.52 | 0.08 | 0.58 | |
| 3460 | 0.75 | MW | 69 | 7.80 | 0.17 | 1.34 | |
| 3560 | 0.74 | MW | 31 | 7.78 | 0.08 | 0.60 | |
| 3586 | 0.69 | HW | 12 | 7.41 | 0.03 | 0.22 | **4.2** |

**Table A3.3. Computation of leaf area for sample plot DS8, from cluster mean NDVI and cluster spatial extent (total number of pixels = 420)**

| Cluster | Cluster NDVI | Class | Pixels/Cluster | LA | Pixels per cluster/ Total | LA/Cluster | Plot LAI |
|---|---|---|---|---|---|---|---|
| 0 | 0.76 | US | 170 | | 0.38 | 0 | |
| 2929 | 0.75 | HW | 5 | 7.59 | 0.01 | 0.09 | |
| 2960 | 0.62 | HW | 7 | 7.20 | 0.02 | 0.11 | |
| 2973 | 0.77 | HW | 10 | 7.65 | 0.02 | 0.17 | |
| 2974 | 0.76 | HW | 32 | 7.61 | 0.07 | 0.55 | |
| 2991 | 0.71 | HW | 28 | 7.46 | 0.06 | 0.47 | |
| 3005 | 0.77 | HW | 9 | 7.64 | 0.02 | 0.16 | |
| 3040 | 0.74 | HW | 5 | 7.55 | 0.01 | 0.09 | |
| 3041 | 0.76 | MW | 8 | 7.82 | 0.02 | 0.14 | |
| 3058 | 0.76 | HW | 23 | 7.61 | 0.05 | 0.40 | |
| 3069 | 0.78 | MW | 14 | 7.87 | 0.03 | 0.25 | |
| 3086 | 0.78 | HW | 7 | 7.68 | 0.02 | 0.12 | |
| 3114 | 0.80 | HW | 3 | 7.74 | 0.01 | 0.05 | |
| 3115 | 0.75 | HW | 26 | 7.59 | 0.06 | 0.45 | |
| 3117 | 0.79 | MW | 8 | 7.89 | 0.02 | 0.14 | |
| 3158 | 0.77 | MW | 13 | 7.83 | 0.03 | 0.23 | |
| 3161 | 0.79 | MW | 8 | 7.88 | 0.02 | 0.14 | |
| 3175 | 0.76 | MW | 4 | 7.81 | 0.01 | 0.07 | |
| 3192 | 0.76 | MW | 7 | 7.81 | 0.02 | 0.12 | |
| 3213 | 0.78 | MW | 12 | 7.86 | 0.03 | 0.21 | |
| 3237 | 0.80 | MW | 6 | 7.93 | 0.01 | 0.11 | |
| 3260 | 0.76 | MW | 17 | 7.82 | 0.04 | 0.30 | |
| 3261 | 0.79 | MW | 10 | 7.90 | 0.02 | 0.18 | |
| 3307 | 0.79 | MW | 10 | 7.89 | 0.02 | 0.18 | **4.7** |

**Table A3.4. Computation of leaf area for sample plot DS9, from cluster mean NDVI and cluster spatial extent (total number of pixels = 420)**

| Cluster | Cluster NDVI | Class | Pixels/Cluster | LA | Pixels per cluster/ Total | LA/Cluster | Plot LAI |
|---|---|---|---|---|---|---|---|
| 0 | 0.73 | US | 189 | | 0.43 | 0 | |
| 4021 | 0.72 | HW | 34 | 7.49 | 0.08 | 0.58 | |
| 4022 | 0.68 | HW | 7 | 7.38 | 0.02 | 0.12 | |
| 4067 | 0.75 | HW | 14 | 7.58 | 0.03 | 0.24 | |
| 4089 | 0.78 | MW | 7 | 7.87 | 0.02 | 0.12 | |
| 4097 | 0.71 | HW | 10 | 7.46 | 0.02 | 0.17 | |
| 4111 | 0.74 | HW | 23 | 7.56 | 0.05 | 0.39 | |
| 4113 | 0.71 | HW | 1 | 7.48 | 0.00 | 0.02 | |
| 4153 | 0.73 | HW | 5 | 7.53 | 0.01 | 0.09 | |
| 4167 | 0.74 | HW | 10 | 7.56 | 0.02 | 0.17 | |
| 4183 | 0.75 | HW | 18 | 7.57 | 0.04 | 0.31 | |
| 4184 | 0.78 | MW | 1 | 7.87 | 0.00 | 0.02 | |
| 4186 | 0.76 | HW | 34 | 7.62 | 0.08 | 0.59 | |
| 4206 | 0.75 | MW | 15 | 7.79 | 0.03 | 0.26 | |
| 4215 | 0.74 | HW | 25 | 7.55 | 0.06 | 0.43 | |
| 4266 | 0.76 | HW | 17 | 7.62 | 0.04 | 0.29 | |
| 4275 | 0.73 | HW | 28 | 7.53 | 0.06 | 0.48 | |
| 4309 | 0.72 | MW | 4 | 7.72 | 0.01 | 0.07 | **4.3** |

**Table A3.5. Computation of leaf area for sample plot DS10, from cluster mean NDVI and cluster spatial extent (total number of pixels = 420)**

| Cluster | Cluster NDVI | Class | Pixels/Cluster | LA | Pixels per cluster/ Total | LA/Cluster | Plot LAI |
|---|---|---|---|---|---|---|---|
| 0 | 0.73 | US | 270 | | 0.61 | 0 | |
| 1706 | 0.69 | HW | 14 | 7.41 | 0.03 | 0.23 | |
| 1718 | 0.77 | HW | 43 | 7.64 | 0.10 | 0.74 | |
| 1734 | 0.67 | HW | 11 | 7.36 | 0.02 | 0.18 | |
| 1782 | 0.75 | MW | 16 | 7.80 | 0.04 | 0.28 | |
| 1789 | 0.73 | HW | 2 | 7.52 | 0.00 | 0.03 | |
| 1798 | 0.73 | HW | 14 | 7.53 | 0.03 | 0.24 | |
| 1836 | 0.74 | HW | 14 | 7.56 | 0.03 | 0.24 | |
| 1854 | 0.72 | HW | 13 | 7.50 | 0.03 | 0.22 | |
| 1925 | 0.68 | HW | 19 | 7.37 | 0.04 | 0.32 | |
| 1937 | 0.70 | HW | 14 | 7.43 | 0.03 | 0.24 | |
| 1958 | 0.74 | HW | 12 | 7.54 | 0.03 | 0.20 | **2.9** |

## *Appendix 4. LAI from Standardized LA and Clusters, Plots DS6 to DS10*

**Table A4.1. Computation of leaf area for sample plot DS6, from cluster mean NDVI and cluster spatial extent (total number of pixels = 380)**

| Cluster | Cluster NDVI | Class | Pixels/Cluster | LA | Pixels per cluster/ Total | LA/Cluster | Plot LAI |
|---|---|---|---|---|---|---|---|
| 0 | 0.75 | US | 143 | | 0.38 | 0 | |
| 3056 | 0.76 | HW | 22 | 7.75 | 0.06 | 0.45 | |
| 3068 | 0.79 | HW | 13 | 7.75 | 0.03 | 0.26 | |
| 3071 | 0.78 | HW | 28 | 7.75 | 0.07 | 0.57 | |
| 3099 | 0.79 | MW | 50 | 7.75 | 0.13 | 1.02 | |
| 3125 | 0.77 | MW | 9 | 7.75 | 0.02 | 0.18 | |
| 3176 | 0.77 | HW | 51 | 7.75 | 0.13 | 1.04 | |
| 3242 | 0.79 | MW | 8 | 7.75 | 0.02 | 0.16 | |
| 3263 | 0.76 | MW | 8 | 7.75 | 0.02 | 0.16 | |
| 3296 | 0.77 | HW | 15 | 7.75 | 0.04 | 0.31 | |
| 3320 | 0.79 | HW | 5 | 7.75 | 0.01 | 0.10 | |
| 3321 | 0.79 | HW | 18 | 7.75 | 0.05 | 0.37 | |
| 3338 | 0.80 | MW | 4 | 7.75 | 0.01 | 0.08 | |
| 3339 | 0.77 | MW | 7 | 7.75 | 0.02 | 0.14 | **4.8** |

**Table A4.2. Computation of leaf area for sample plot DS7, from a standardized leaf area and cluster spatial extent (total number of pixels = 400)**

| Cluster | Cluster NDVI | Class | Pixels/Cluster | LA | Pixels per cluster/ Total | LA/Cluster | Plot LAI |
|---|---|---|---|---|---|---|---|
| 0 | 0.72 | US | 182 | | 0.45 | 0 | |
| 3332 | 0.75 | MW | 3 | 7.75 | 0.01 | 0.06 | |
| 3352 | 0.73 | HW | 29 | 7.75 | 0.07 | 0.56 | |
| 3390 | 0.73 | HW | 15 | 7.75 | 0.04 | 0.29 | |
| 3427 | 0.71 | MW | 13 | 7.75 | 0.03 | 0.25 | |
| 3442 | 0.74 | HW | 16 | 7.75 | 0.04 | 0.31 | |
| 3459 | 0.73 | HW | 31 | 7.75 | 0.08 | 0.60 | |
| 3460 | 0.75 | MW | 69 | 7.75 | 0.17 | 1.33 | |
| 3560 | 0.74 | MW | 31 | 7.75 | 0.08 | 0.60 | |
| 3586 | 0.69 | HW | 12 | 7.75 | 0.03 | 0.23 | **4.2** |

**Table A4.3. Computation of leaf area for sample plot DS8, from a standardized leaf area and cluster spatial extent (total number of pixels = 420)**

| Cluster | Cluster NDVI | Class | Pixels/Cluster | LA | Pixels per cluster/ Total | LA/Cluster | Plot LAI |
|---|---|---|---|---|---|---|---|
| 0 | 0.76 | US | 170 | | 0.38 | 0 | |
| 2929 | 0.75 | HW | 5 | 7.75 | 0.01 | 0.09 | |
| 2960 | 0.62 | HW | 7 | 7.75 | 0.02 | 0.12 | |
| 2973 | 0.77 | HW | 10 | 7.75 | 0.02 | 0.18 | |
| 2974 | 0.76 | HW | 32 | 7.75 | 0.07 | 0.56 | |
| 2991 | 0.71 | HW | 28 | 7.75 | 0.06 | 0.49 | |
| 3005 | 0.77 | HW | 9 | 7.75 | 0.02 | 0.16 | |
| 3040 | 0.74 | HW | 5 | 7.75 | 0.01 | 0.09 | |
| 3041 | 0.76 | MW | 8 | 7.75 | 0.02 | 0.14 | |
| 3058 | 0.76 | HW | 23 | 7.75 | 0.05 | 0.40 | |
| 3069 | 0.78 | MW | 14 | 7.75 | 0.03 | 0.25 | |
| 3086 | 0.78 | HW | 7 | 7.75 | 0.02 | 0.12 | |
| 3114 | 0.80 | HW | 3 | 7.75 | 0.01 | 0.05 | |
| 3115 | 0.75 | HW | 26 | 7.75 | 0.06 | 0.46 | |
| 3117 | 0.79 | MW | 8 | 7.75 | 0.02 | 0.14 | |
| 3158 | 0.77 | MW | 13 | 7.75 | 0.03 | 0.23 | |
| 3161 | 0.79 | MW | 8 | 7.75 | 0.02 | 0.14 | |
| 3175 | 0.76 | MW | 4 | 7.75 | 0.01 | 0.07 | |
| 3192 | 0.76 | MW | 7 | 7.75 | 0.02 | 0.12 | |
| 3213 | 0.78 | MW | 12 | 7.75 | 0.03 | 0.21 | |
| 3237 | 0.80 | MW | 6 | 7.75 | 0.01 | 0.11 | |
| 3260 | 0.76 | MW | 17 | 7.75 | 0.04 | 0.30 | |
| 3261 | 0.79 | MW | 10 | 7.75 | 0.02 | 0.18 | |
| 3307 | 0.79 | MW | 10 | 7.75 | 0.02 | 0.18 | **4.8** |

**Table A4.4. Computation of leaf area for sample plot DS9, from a standardized leaf area and cluster spatial extent (total number of pixels = 420)**

| Cluster | Cluster NDVI | Class | Pixels/Cluster | LA | Pixels per cluster/ Total | LA/Cluster | Plot LAI |
|---|---|---|---|---|---|---|---|
| 0 | 0.73 | US | 189 | | 0.43 | 0 | |
| 4021 | 0.72 | HW | 34 | 7.75 | 0.08 | 0.60 | |
| 4022 | 0.68 | HW | 7 | 7.75 | 0.02 | 0.12 | |
| 4067 | 0.75 | HW | 14 | 7.75 | 0.03 | 0.25 | |
| 4089 | 0.78 | MW | 7 | 7.75 | 0.02 | 0.12 | |
| 4097 | 0.71 | HW | 10 | 7.75 | 0.02 | 0.18 | |
| 4111 | 0.74 | HW | 23 | 7.75 | 0.05 | 0.40 | |
| 4113 | 0.71 | HW | 1 | 7.75 | 0.00 | 0.02 | |
| 4153 | 0.73 | HW | 5 | 7.75 | 0.01 | 0.09 | |
| 4167 | 0.74 | HW | 10 | 7.75 | 0.02 | 0.18 | |
| 4183 | 0.75 | HW | 18 | 7.75 | 0.04 | 0.32 | |
| 4184 | 0.78 | MW | 1 | 7.75 | 0.00 | 0.02 | |
| 4186 | 0.76 | HW | 34 | 7.75 | 0.08 | 0.60 | |
| 4206 | 0.75 | MW | 15 | 7.75 | 0.03 | 0.26 | |
| 4215 | 0.74 | HW | 25 | 7.75 | 0.06 | 0.44 | |
| 4266 | 0.76 | HW | 17 | 7.75 | 0.04 | 0.30 | |
| 4275 | 0.73 | HW | 28 | 7.75 | 0.06 | 0.49 | |
| 4309 | 0.72 | MW | 4 | 7.75 | 0.01 | 0.07 | **4.4** |

**Table A4.5. Computation of leaf area for sample plot DS10, from a standardized leaf area and cluster spatial extent (total number of pixels = 420)**

| Cluster | Cluster NDVI | Class | Pixels/Cluster | LA | Pixels per cluster/ Total | LA/Cluster | Plot LAI |
|---|---|---|---|---|---|---|---|
| 0 | 0.73 | US | 270 | | 0.61 | 0 | |
| 1706 | 0.69 | HW | 14 | 7.75 | 0.03 | 0.25 | |
| 1718 | 0.77 | HW | 43 | 7.75 | 0.10 | 0.75 | |
| 1734 | 0.67 | HW | 11 | 7.75 | 0.02 | 0.19 | |
| 1782 | 0.75 | MW | 16 | 7.75 | 0.04 | 0.28 | |
| 1789 | 0.73 | HW | 2 | 7.75 | 0.00 | 0.04 | |
| 1798 | 0.73 | HW | 14 | 7.75 | 0.03 | 0.25 | |
| 1836 | 0.74 | HW | 14 | 7.75 | 0.03 | 0.25 | |
| 1854 | 0.72 | HW | 13 | 7.75 | 0.03 | 0.23 | |
| 1925 | 0.68 | HW | 19 | 7.75 | 0.04 | 0.33 | |
| 1937 | 0.70 | HW | 14 | 7.75 | 0.03 | 0.25 | |
| 1958 | 0.74 | HW | 12 | 7.75 | 0.03 | 0.21 | **3.0** |